UNIVERSITA' DEGLI STUDI DI TRIESTE

sede amministrativa del Dottorato di Ricerca

XXII ciclo della

Scuola di Dottorato di Ricerca in Scienze e Tecnologie Chimiche e Farmaceutiche

TESI DI DOTTORATO

Carbon Nanotubes and Neurons: Nanotechnology Application to the Nervous System.

(settore scientifico disciplinare CHIM/06)

Dottoranda:
Sara Cipollone

Direttore della Scuola:
Prof. Enzo Alessio - Università di Trieste

Relatore:
Prof. Maurizio Prato - Università di Trieste

Correlatore:
Prof. Laura Ballerini - Università di Trieste

anno accademico 2008-2009

Ulisse

Nella mia giovinezza ho navigato
lungo le coste dalmate. Isolotti
a fior d'onda emergevano, ove raro
un uccello sostava intento a prede,
coperti d'alghe, scivolosi, al sole
belli come smeraldi. Quando l'alta
marea e la notte li annullava, vele
sottovento sbandavano più al largo,
per fuggirne l'insidia. Oggi il mio regno
è quella terra di nessuno. Il porto
accende ad altri i suoi lumi; me al largo
sospinge ancora il non domato spirito,
e della vita il doloroso amore.

Umberto Saba
Trieste, 1946.

Table of Contents

Riassunto

I Nanotubi di Carbonio (CNT) sono una nuova forma allotropica del carbonio scoperta da Ijiima nel 1991, che li ha individuati nel materiale di scarto proveniente dalla produzione dei fullereni. Essi sono costituiti da un foglio di grafene arrotolato su se stesso a formare una struttura cilindrica chiusa alle estremità. I nanotubi di carbonio a parete singola (SWCNT) sono costituiti da un solo foglio di grafene, mentre i nanotubi di carbonio a parete multipla (MWCNT) sono formati da due o più fogli concentrici. Per via delle loro eccezionali proprietà chimico-fisiche, per esempio la forza meccanica superiore a quella di qualsiasi materiale conosciuto, la stabilità termica, la grande area superficiale, il basso peso specifico e le loro ottime proprietà di conduzione dell'elettricità; i CNT hanno trovato negli scorsi 20 anni un largo impiego nel campo delle scienze dei materiali, ma anche, alla luce della loro capacità precedentemente riportata di attraversare la membrana cellulare e della loro bassa citotossicità, nel campo della biomedicina, in applicazioni come il trasporto mirato di farmaci e la biosensoristica.

In questo lavoro di tesi, si riporta l'uso dei nanotubi di carbonio in neurobiologia/ neurofisiologia come substrato per lo studio dell'interazione tra cellule nervose e i nanotubi di carbonio stessi. In particolare, la loro struttura tubulare e le dimensioni nanometriche, associate con la loro conduttività elettrica e la loro biocompatibilità, li rendono un materiale ideale per l'associazione e l'integrazione con le cellule nervose, richiamandone sia la struttura che le proprietà. Questo potrebbe aprire la possibilità di usare i nanotubi di carbonio come materiale per la costruzione di nanoporotesi atte a riparare il tessuto nervoso dove danneggiato. I risultati ottenuti hanno dimostrato che cellule nervose cresciute su una superficie di nanotubi di carbonio mostrano un incremento della frequenza delle correnti sinaptiche spontanee e dei potenziali d'azione spontanei. Pù in dettaglio, i nanotubi di carbonio migliorano la risposta dei neuroni formando dei contatti molto intimi con la membrana della cellula nervosa. Questi contatti potrebbero favorire una facilità di comunicazione elettrica tra i vari compartimenti del neurone.

Al fine di interpretare meglio la natura dell'interazione fisica tra le cellule nervose e i nanotubi, abbiamo sviluppato un metodo per preparare superfici di vetro funzionalizzate covalentemente con nanotubi di carbonio con una morfologia definita e riproducibile. I nanotubi di carbonio sono stati purificati e processati opportunamente tramite funzionalizzazione organica per fornirli dei gruppi funzionali necessari all'ancoraggio sulla superficie del vetro mediato da organosilani come agenti di coupling. Inoltre i nanotubi sono stati funzionalizzati mediante un peptide RGD caratterizzato dalla sequenza amminoacidica arginina-glicina-acido aspartico, una sequenza che si ritrova normalmente *in vivo* nelle proteine di adesione e che rappresenta un substrato tipico per la promozione dell'adesione e lo sviluppo neurale. Anche questi nanotubi biofunzionalizzati sono stati attaccati covalentemente alla superficie del vetro mediante l'uso di organo-silani. Tutte le superfici preparate sono state caratterizzate con angolo di contatto, spettroscopia FT-IR, microscopia SEM e spettroscopia XPS. L'uso di questi substrati per lo studio della crescita e del comportamento neurale dovrebbe portare ad una valutazione più precisa degli

effetti che i nanotubi di carbonio hanno sulla rete neurale. Inoltre la definizione di un metodo efficiente e versatile per l'attacco covalente di nanotubi di carbonio su superfici inorganiche è di fondamentale importanza per la eventuale costruzione di superfici biocompatibili impiegabili nell'ingegneria tessutale.
Tra tutte le motivazioni che rendono i nanotubi un materiale eccellente per l'integrazione con le cellule nervose riportiamo anche uno studio sistematico in vitro su reti ibride di neuroni e MWCNTs. Abbiamo ottenuto la deposizione di un film sottile di CNTs sulla superficie elettrodica dei MEA, (microelectrode arrays), che sono supporti solidi forniti di una matrice di 60 elettrodi utilizzati comunemente in neurofisiologia per la stimolazione nervosa simultanea di molti siti contemporaneamente. Utilizzando questi MEA coperti da CNT come substrati per la crescita neuronale abbiamo avuto la possibilità di esaminare a livello di comunicazione sinaptica il modo in cui i CNT e le cellule nervose interagiscono in maniera direzionale con l'emergenza dell'attività sinaptica spontanea, come precendentemente osservato a livello della singola cellula.
Nell'appendice di questa tesi è riportato uno studio riguardante la funzionalizzazione di nanotubi di carbonio mediante una sonda fluorescente, e la relativa caratterizzazione dei derivati per lo studio della loro internalizzazione e distribuzione nelle cellule nervose. Risultati preliminari hanno mostrato che i CNT sono in grado di passare la membrana cellulare del neurone e si distribuiscono omogeneamente nel citoplasma ma non penetrano nel nucleo della cellula. Questo è un risultato molto importante perchè, nonostante sia stata precedentemente dimostrata la capacità dei nanotubi di attraversare la membrana cellulare, nulla ancora è stato detto a riguardo delle cellule nervose. La possibilità da parte dei nanotubi di carbonio di attraversare la membrana ematoencefalica potrebbe definire una nuova frontiera nell'uso dei CNT in neurofisiologia come sistemi di veicolazione mirata di farmaci nel sistema nervoso centrale e costituire, eventualmente, un importante strumento per le applicazioni terapeutiche riguardanti le malattie degenerative del sistema nervoso. Ulteriori sviluppi di questo studio potrebbero essere la verifica, *in vivo* della capacità dei CNT di attraversare la barriera ematoencefalica.

Abstract

Carbon nanotubes (CNT) are a novel allotropic form of carbon discovered in 1991 by Ijiima who observed their presence in the waste material coming from the production of fullerenes. They are constituted by a graphene aromatic layer rolled up to form a tubular shape, closed at the end. Single walled carbon nanotubes (SWCNT) are constituted by only one layer, while multi walled carbon nanotubes (MWCNT) are formed by two or more concentric layers. Due to their outstanding chemico-physical properties, such as mechanical strength superior to any known material, thermal stability, ultra-light weight, very large surface area and a good electrical conductivity; CNT found, during the past two decades, a large employ in the field of material science and also in the field of biomedicine, as drug delivery systems, or biosensor systems, since it has been reported their capability to cross the cell membrane and their low cytotoxicity.

In this thesis work, we report the use of carbon nanotubes as substrates in neurobiology/ neurophysiology to study the interaction between neural cells and nanotubes. In particular, the tubular shape and the nanometric size of carbon nanotubes, associated with the electrical conductivity and the previously tested biocompatibility, make them ideal materials for integration with neurons to possibly repair neural tissues where damaged. The results have shown that neurons grown on a carbon nanotubes layer display an increase in the frequency of synaptic responses together with an increase in firing frequency. More in detail the nanotubes improve the responsiveness of neurons by forming tight contacts with the cell membranes that might favor electrical shortcuts between the proximal and distal compartments of the neuron.

In order to better interpret the nature of the physical interaction between the cells and nanotubes we developed a method to build CNT functionalized glass surfaces with a defined and reproducible morphology. Carbon nanotubes were purified and suitably processed by organic functionalization to be anchored to the glass surface by silane coupling agents. Furthermore nanotubes were functionalized by an arginine-glycine-aspartic acid (RGD) peptide, a typical substrate promoting neuronal adhesion and development, and again covalently attached to glass surface by the use of silane coupling agents. All the surfaces where characterized by contact angle, FT-IR spectroscopy, SEM microscopy and XPS. This should lead to a precise evaluation of the effects of carbon nanotubes on the neuronal network. Moreover the definition of an efficient and versatile method to attach nanotubes to an inorganic surface is of fundamental importance for the costruction of biocompatible surfaces to be used for the future of tissue engineering.

Along all the motivation that makes carbon nanotubes an excellent material for neuroprosthetic devices, we also report a systematic study of hybrid MWCNTs-neuronal networks *in vitro*. We obtained thin-film depositions of MWCNTs over glass-substrate microelectrode arrays (MEAs), chronically coupled to cultured networks of postnatal hippocampal neurons. This allowed us for the first time to examine at the network-level, the way MWCTNs bidirectionally interacts with the spontaneous neuronal activity and its emergence *ex vivo*, as first observed at the single-cell level.

In the appendix of this thesis is also reported a study of the fluorescent functionalization and relative characterization of CNTs fluorescent derivatives for the study of their uptake and intracellular distribution in neural cells. Preliminary results have shown that CNT cross the nerve-cell membrane and distribute homogeneously in the cytoplasm, but not in the nucleus. This might be a very important result since in spite of the already demonstrated capability of nanotubes to pass the cellular membrane nothing has already been said about the capability of nanotubes to pass the blood brain barrier (BBB), which could define the possibility for CNT to be used as drug carriers for the central nervous system. Further development of this study might investigate *in vivo* the capability of functionalized CNT to pass the BBB and, therefore, individuate an important tool for the therapeutical applications that concern neural diseases.

Abbreviations

AcOEt ethyl acetate
ADP after-depolarization
AFM atomic force microscopy
AHP after-hyperpolarization
AMP adenosine monophosphate
AP MWNT as produced multiwalled nanotube
AuNP gold nanoparticle
BBB blood brain barrier
Boc tert-butyloxicarbonyl
C_h chiral vector
^{13}C NMR carbon nucler magnetic resonance
CNQX 6-cyano-7-nitroquinoxaline-2,3-dione
CNS central nervous system
CNT carbon nanotube
CSF cerebrospinal fluid
CVD chemical vapour deposition
Cys cysteine
DBU 1,8 diazobiciclo [5,4,0] undecene
DCM dichloro methane
DIEA diisopropyl ethyl ammine
DMF dimethyl formamide
DMSO dimethyl sulfoxide
DNA deoxyribonucleic acid
DOS density of states
DWCNT double walled carbon nanotube
DWNT double walled nanotube
ECM extracellular matrix
E_K potassium equilibrium voltage
E_{Na} sodium equilibrium voltage
ES-MS electrospray mass spectrometry
Et_2O diethyl ether
***f* DWNT** functionalized doublewalled nanotube
FITC fluorescein isotyocianate
***f* MWNT** functionalized multiwalled nanotube
FT IR Fourier transform infra-red

GFAP glia fiber acidic protein
HiPCO high pressure carbon monoxide
^{1}H NMR hydrogen nuclear magnetic resonance
IR infra-red
ITO indium tin oxide

KE kynetic energy
LBL layer by layer
Lys lysine
MAP2 microtubule-associated protein 2
MEA micro electtrode array
MeOH methanol
MW molecular weight
MW multi walled
MWCNT multi walled carbon nanotubes
MWNT multi walled nanotubes
NMP 1-methyl pirrolidinone
NMR nuclear magnetic resonance
NP nanoparticle
NR neutral response
NT nanotube
ODCB ortho-dichlorobenzene
OEG oligoethylene glycol
PEG polyethylene glycol
ppm parts per million
PSC post synaptic current
PSTH peristimulus time histogram
PTFE polytetrafluoroethylene (teflon)
RBM radial breathing mode
RGD arginine - glycine- aspartic acid
RNA ribonucleic acid
SAM self assembled monolayer
SEM scanning electron microscopy
siRNA small interfering ribonucleic acid
SPB surface plasmon band
SW single walled
SWCNT single walled carbon nanotubes
SWNT single walled nanotubes
TEM transmission electron microscopy
TFA trifluoroacetic acid
TGA thermogravimetric analysis
THF tetrahydrofurane
UHV ultra high vacuum
UV ultra violet
UV-Vis ultra violet/visible
UV-Vis-NIR ultra violet /visible / near infra-red
$\mathbf{V_{command}}$ command voltage
$\mathbf{V_m}$ membrane voltage
XPS X-ray photoelectron spectroscopy

Chapter 1: Introduction

1.1 The element Carbon

Carbon, [1] with symbol C and atomic number 6, is the most versatile element in the periodic table, owing to the large number of bonds of different type and strength that can form with many different elements.
There are six electrons in a carbon atom, arranged in the electronic configuration $1s^2 2s^2 2p^2$. In spite of the presence of only 2 electrons in the 2p orbitals, carbon can make up to four bonds, involving the electrons in both 2p and 2s orbitals. Covalent bonds are formed by promotion of the 2s electrons to one or more 2p orbitals. Since the s-orbital and the p-orbitals of carbon's second electronic shell have very similar energies they can hybridize and as a result carbon can adapt to form chemical bonds with different geometries.
In the first type of hybridization the 2s orbital pairs with one of the 2p orbitals form two hybridized sp^1 orbitals in a linear geometry separated by a 180° angle. In the second type of hybridization the 2s orbital hybridizes with two of the three p orbitals forming three sp^2 orbitals sharing 3 electron for covalent bonding, situated on the same plane with triangle geometry and a 120° angle separation. In the third and last type of hybridization the 2s orbital hybridizes with all the 2p orbitals forming four sp^3 orbitals that can establish four covalent bonds in the characteristic tetrahedric geometry, with a separation angle between each bond of 109,5° (fig. 1).

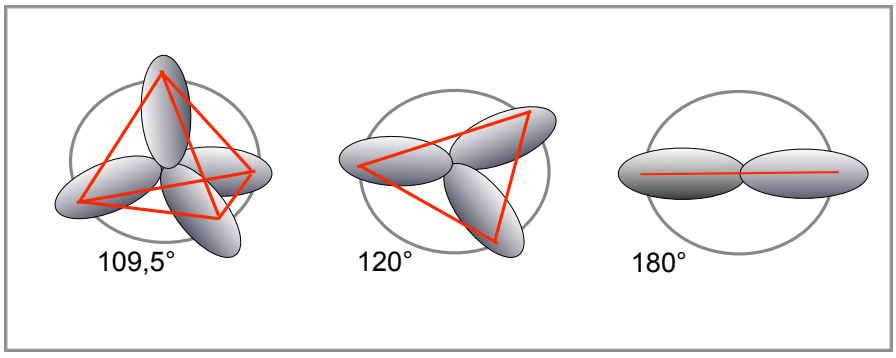

Fig 1: Hybridizations of Carbon

The diversity of bonds and the corresponding geometries are found in large, complex and diverse structures and allow for en endless variety of organic molecules. Carbon is in fact the fourth most abundant element in the universe by mass and it is the second in human body, after oxygen. This abundance and this versatility make this element the chemical basis of all known life.

1.2 Allotropes of Carbon

There are several allotropes of carbon of which the best known are graphite and diamond. The physical properties of carbon vary largely with the allotropic form.

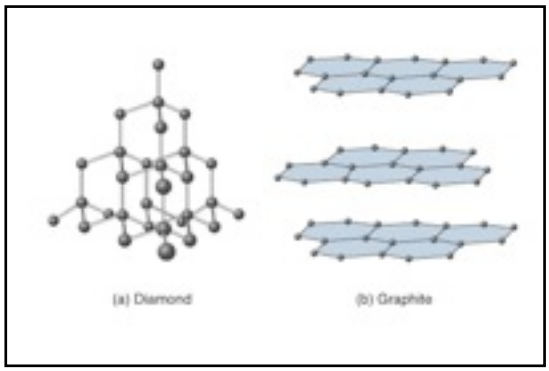

Fig. 2: Allotropes of Carbon

Diamond (fig. 2-a) is a transparent crystal of sp^3 carbon where each carbon atom is bonded to four others with a tetrahedral arrangement. The sp^3 crystalline network gives diamond the unique properties of hardness, excellent heat conduction, electric insulation and optical transparency.
Graphite (fig. 2-b) is made by layered planar sheets of sp^2 hybridized carbon, strongly bonded together in an hexagonal network. Each layer, called graphene, is weakly bonded and stacked trough Van Der Waals forces with other layers forming a pile-like structure. This gives graphite the typical softness and the cleaving properties: the sheets, in fact, slip easily past one another; because of the delocalization of the fourth electron of each atom in a 2p orbital, graphite conducts electricity on the plane of each covalently bonded sheet. The delocalization is also responsible for the higher thermodynamic stability over diamond at room temperature.
Besides diamond and graphite there are other ordered forms of carbon in nature [2] such as fullerenes (fig. 3) and nanotubes (fig. 4), which consist in a variety of spheroidal and cylindrical structures composed of sp^2 carbon. They have a graphite-like structure but instead of a pure hexagonal network they also contain pentagons which bend the sheets into spheres, ellipses and cylinders.

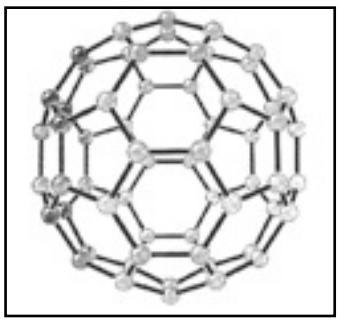

Fig. 3: C_{60} - buckminsterfullerene

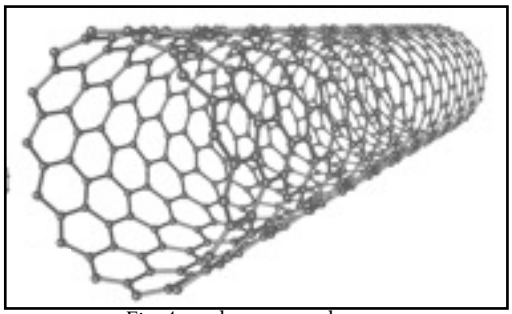

Fig. 4: carbon nanotube

The first fullerene to be discovered in 1985 by Kroto, Smalley and Curl [3] was the C_{60}, a truncated icosahedral cluster of 60 carbon atoms, bonded together in pentagons and hexagons, with 32 faces, 12 of which are pentagonal and 20 hexagonal. Because of the resemblance of the structure with the geodesic domes of the american architect Richard Buckminster Fuller it was named after him as an homage. The discovery of fullerenes, as many other scientific breakthroughs, was an accident: fullerenes happened to be found in the products of the vaporization of graphite by laser irradiation during experiments aimed at understanding the mechanism by which long-chain carbon molecules are formed in interstellar space and circumstellar shells. Since their discovery and their bulk production, [4, 5] fullerenes have been the subject of intense research both for their chemistry and for their technological applications, especially in material science, electronics and nanotechnology.

1.3 Carbon Nanotubes

Carbon nanotubes (CNT) were first introduced by R. Smalley in 1990 at a carbon - carbon composites workshop, who proposed the existence of a tubular shaped fullerene[6]. Their existence was experimentally confirmed in 1991 by S. Iijima[7] who noticed the presence of tubular shaped structures in the side products of fullerenes production. It's extremely difficult to give a unique definition of carbon nanotubes because of the large variety of structures, diameters and lengths, however the structure of a CNT can be conceptualized by wrapping a one layer of graphite (graphene) into a seamless cylinder.

It is possible to categorize the nanotubes in two great families (fig. 5): single-walled carbon nanotubes (SWCNT), composed by one layer of graphene and multi-walled carbon nanotubes (MWCNT), composed by two up to hundreds layer of graphene wrapped concentrically. Most SWCNT have a diameter close to 1 - 2 nanometers, with a tube length that can be many millions of times longer. The extremely high ratio between the two dimensions allows to consider SWCNT virtually mono-dimensional. MWCNT instead, depending on the number of layers, have a larger diameter, up to 200 nanometers. The interlayer distance in MWCNT is close to the distance between graphene layers in graphite, approximately 3,3 Å.

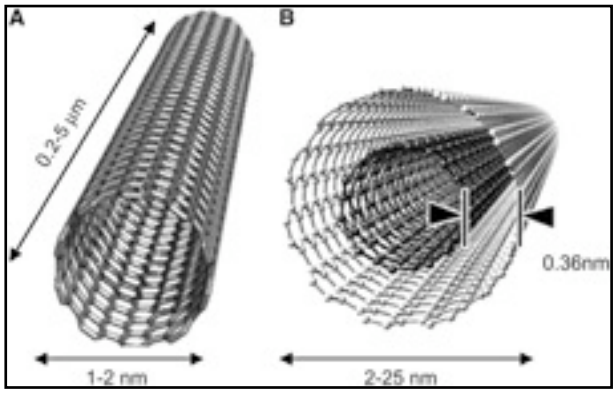

Fig. 5: Conceptual diagram of a SWCNT (A) and a MWCNT (B)

The surface of a SWCNT (fig. 6) is entirely constituted of sp^2 hybridized carbon atoms bonded together in an hexagonal pattern while the extremities are closed by two fullerene-like caps.

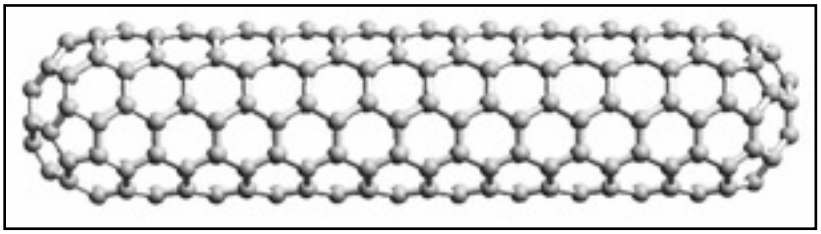

Fig. 6: Structure of an ideal SWCNT, with the graphene-like sidewall and the fullerenes-like terminal heads.

The presence of the pentagonal rings in the terminal fullerene caps justify the curvature and the closure of the tube heads.

A nanotube is univocally characterized by its diameter which greatly influences the properties of electrical conductivity as the smaller is the diameter the lower is the gap between the valence band and the conduction band. SWCNT consequentially are better conductor than MWCNT.

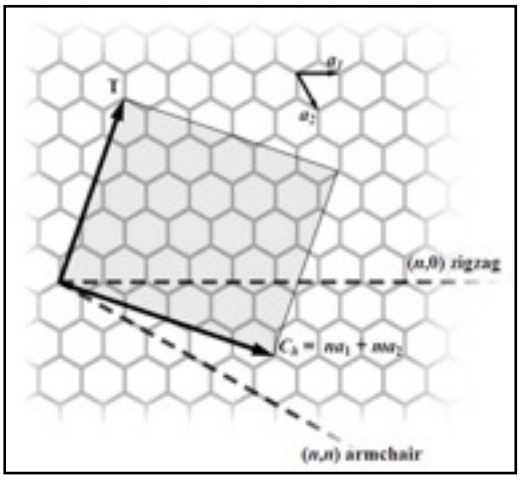

Fig. 7: Rapresentation of the chiral vector on the graphite plane.

Another important definition of the characteristic and the properties of a nanotube is the way the graphene sheet is wrapped to form the cylindrical shape.[8] The physical quantity that describes this is called Chiral Vector (C_h), or Elicity and is indicated by a pair of integers (n,m) and to versors (a_1,a_2) by the following vector equation (eq. 1):

$$C_h = na_1 + ma_2 \qquad \text{(eq. 1)}$$

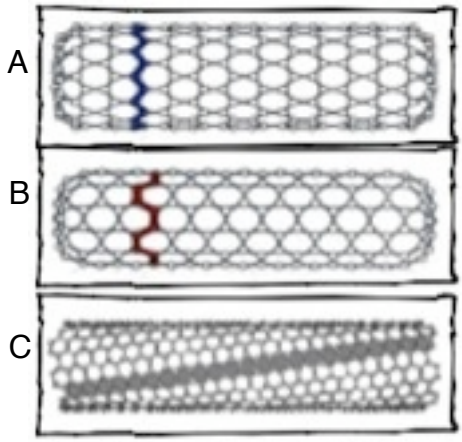

Fig. 8: The three conformational models of CNT: A) "zigzag"; B) "armchair"; C) "chiral"

The chiral vector is determined by the diagram at the left (fig. 7). Imagine that the nanotube is unravelled into a planar sheet. The dashed line individuates two directions in the graphene sheet: the "**armchair"** line, which travels across each hexagon, separating them into two equal halves, and the **"zigzag"** line. The wrapping angle θ (not shown) is formed between the chiral vector and the zigzag line.

If C_h lies along the zigzag line (θ=0°), then it is called a "zigzag" nanotube (fig.8 A). If θ=30°,

then the tube is of the "armchair" type (fig.8 B). Otherwise, if $0°<\theta<30°$ then it is a "chiral" nanotube (fig. 8 C).
The vector a_1 lies along the "zigzag" line. The other vector a_2 has a different magnitude than a_1, but its direction is a reflection of a_1 over the armchair line. When added together, they equal the chiral vector C_h.
The values of *n* and *m* determine the chirality, or "twist" of the nanotube. The chirality affects the conductance of the nanotube, its density, its lattice structure, and other properties. All armchair SWCNTs are metals. The nanotubes with *n* - *m* divisible by three are semiconducting, with a tiny band gap, the others are semiconducting with a band gap that inversely depends on the nanotube diameter. [8] Consequently, when tubes are formed with random values of *n* and *m*, we would expect that two-thirds of nanotubes would be semi-conducting, while the other third would be metallic. [8] Given the chiral vector *(n,m)*, the diameter of a carbon nanotube can be determined using the relationship (eq. 2):

$$d = (n^2 + m^2 + nm)^{1/2}\, 0.0783\ nm \qquad \text{(eq. 2)}$$

1.4 Production of Carbon Nanotubes

CNT synthesis has been shown to occur in a wide range of environments. The basic prerequisites for their production are an active catalyst, a source of carbon and adequate energy. Here are reported and described the fundamental methods:

- Arc discharge evaporation
- Laser ablation
- Solar Energy
- Electrolysis
- Chemical Vapor Deposition (CVD)
- High Pressure Carbon monoxide (HiPCO)

Arc Discharge Evaporation

Arc discharge [9] was the first recognized method for producing both SWCNT and MWCNT. The method was previously employed for the production of fullerenes and allowed the first observation of MWCNT which grew at the negative end of the electrode.[7] The process consists in operating a voltage of 20 V and a direct current of 150 A in a 1 to 4 mm wide gap between two graphite electrodes 6 to 12 mm in diameter that are installed in a water - cooled chamber filled with helium gas at sub-atmospheric pressure (500 Torr) (fig. 9).

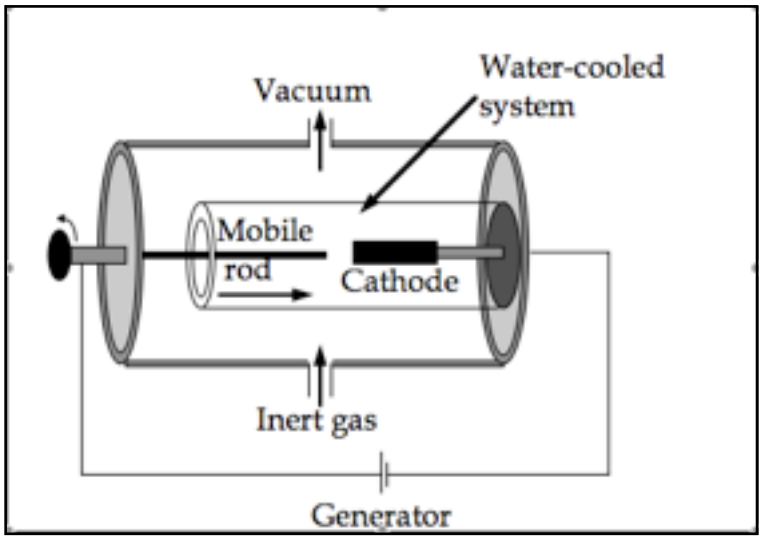

Fig. 9: Schematic rapresentation of an arc discharge device.

The temperature in the gap between the electrodes reaches 4000° C and allows the sublimation of carbon at the anode, which condenses at the cathode in the shape of carbon nanotubes, graphite particles, fullerenes and amorphous carbon.
The production of SWCNT is only observed by adding metal catalyst to the anode by drilling an hole in the centre of the electrode and filling it with a mixture of a metal and graphite. This element is co-evaporated with the carbon during the arc discharge process and this changes the microscopic and macroscopic characteristic of the formed products; Fe and Co were the first metals to be added by Iijima et al.[10] and Bethune et al.[11] The standard of the catalyst composition to produce SWCNT most widely used is a Y:Ni mixture that has been shown to yield up to 90% SWCNT. [9] Also, the gas composition in the chamber can be changed to tailor the arc discharge process. Currently most of the production is carried out in a mixture Ar:He. By tailoring the Ar:He gas ratio the diameter of the SWCNT formed can be controlled; the greater Ar yielding the smaller diameters.[12] Also the gas pressure has been shown to affect the weight percent yield of SWCNT.[12] In general, the nanotubes produced by this method need extensive purification before use. On the other hand this technique made possible the commercial availability of SWCNT and MWCNT at relatively inexpensive prices and helped to launch their massive use in research.[13]

Laser Ablation

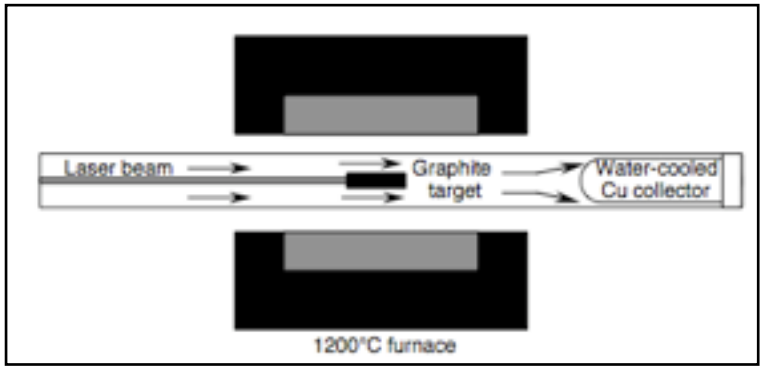

Fig.10: Schematic rapresentation of the oven laser-vaporization apparatus

A second method for the production of CNT is the laser ablation, a process introduced by Guo[14] in 1995 and optimized by Thess[15] in 1996. Carbon is vaporized from the surface of a solid disk of graphite into a high density helium or argon flow, using a focused pulsed laser.

The graphite target is placed in the middle of a long quartz tube mounted in a temperature-controlled furnace. The sealed tube is evacuated and then the furnace temperature is increased to 1200° C. The tube is then filled with a flowing inert gas and a scanning laser beam is focused onto the graphite target by a way of circular lens. The laser beam scans across the target surface to maintain a smooth, uniform face for vaporization (fig. 10). The laser vaporization produces carbon species which are swept from the high temperature zone and addressed to a conical water-cooled copper collector. Thess introduced as an improvement on this method, the presence of a second laser pulse after the first in order to minimize the amount of carbon deposited as soot and to break up the larger particles ablated by the first laser. The soot containing nanotubes is collected from the water-cooled support at the end of the apparatus, from the quartz tube and from the downstream face of the graphite target. This method allowed to obtain MWCNT formed with 4 to 24 graphitic layers and homogeneous length of 300 nm. The yield and quantity depend on the furnace temperature: at 1200° C all the observed nanotubes are free from defects and closed at the end. Decreasing the temperature it decreases the quality of the tubes.[16] SWCNT were also produced by adding a second target of a transition metal placed face to face with the graphitic target and irradiated simultaneously to this. [17] The as produced SWCNT have remarkably uniform diameters and self organize into ropes of 5 - 20 nm of diameter and tens to hundreds of microns length consisting of 100 - 500 nanotubes. The nature of the catalyst employed affects the yield: best yields are obtained with the use of Ni, Co or Ni:Co mixtures. The tubes obtained with this method are free from defects, with a low quantity of amorphous carbon and metallic impurities and present a prevalent armchair conformation.

Solar Energy

This method, comparable with the laser ablation one, consists in the use of a solar furnace to focus the sunlight on a graphite sample and vaporize carbon. The soot is then condensed in a cold dark zone of the reactor. The sunlight is collected by a system of mirrors and the target is placed at the centre of an experimental chamber which is firstly evacuated and then swept by argon or helium during the sublimation. In best condition the sample temperature can reach up to 3000 K. Until 1996 this process was only used to produce fullerenes but later with an improved set-up: by changing the target composition, adding metal catalyst to the graphite powder and adjusting the experimental conditions, either MW and SW nanotubes were produced.[18]

Electrolysis

The idea of this method is to produce carbon nanotubes by passing an electric current in a molten ionic salt between graphite electrodes. During the reaction, the cathode is consumed and a wide range of nanomaterials are formed.

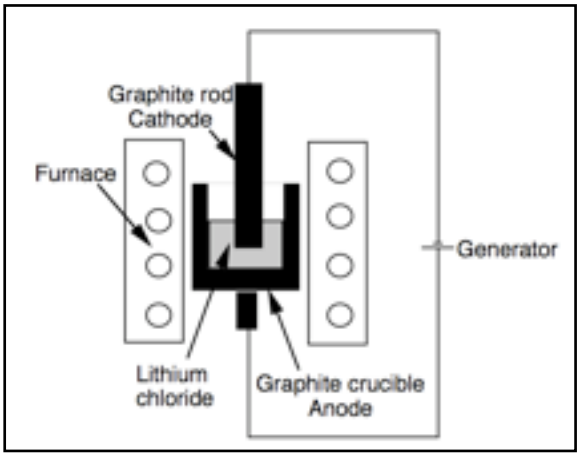

Fig. 11: Schematic representation of the electrolysis experimental set-up

A simple carbon crucible is made by drilling a hole in the centre of a high-purity graphite cylinder (fig. 11). This crucible acts as the anode of the electrolysis system. The cathode is formed by a high-purity carbon rod. The crucible is filled by lithium chloride and heated to the melting point under air or argon, then the cathode is immersed in the melt while a current between 1 and 30 A is maintained through the melt for at least one minute. During the process the immersed surface of the cathode is eroded and residues particles are dispersed into the melt. These particles are washed with water and the mixture is settled down for 4 hours, added to toluene, agitated, and the particles are extracted in the organic phase. In the obtained sample can be observed the presence of MWCNT with different morphologies and different diameters (2 - 20 nm) and length (up to 5 micron). It has been seen that nanotubes start to appear only between reaction times of 3 and 4 minutes and with currents between 3 and 5 A. [19]

Chemical Vapour Deposition

This method for the production of nanotubes exploits the catalytic decomposition of carbon-containing gas over metal surfaces for the formation of carbon filaments. It was firstly applied to the synthesis of nanotubes by Yacamàn et al.[20] Their method consisted in the catalytic decomposition of acetylene over iron particles at 700°C. With this method only the production of MWCNT is observed.

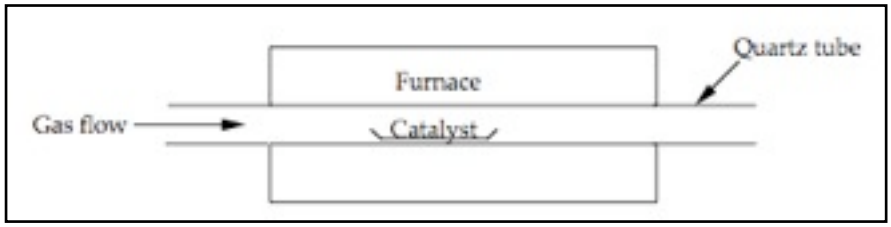

Fig. 12: schematic representation of the experiment set-up used for the catalytic decomposition of hydrocarbons.

The experiment is carried out in a flow furnace at atmospheric pressure. The catalyst particles are placed in a ceramic boat which is put in a

quartz tube (fig. 12). The reaction mixture, composed of 10% of carbon-based gas, and 90% of nitrogen, is passed over the catalyst bed for several hours at temperatures ranging from 500°C to 1500°C. The system is then cooled to room temperature.The tubes synthetized with this system are found to be hollow, consisting of concentric cylindrical graphene sheets. They often present an amorphous carbon coating and catalyst particles are sometimes found at the tips. By varying the active particles on the surface of the catalyst the nanotube diameter can be adjusted. The length of the tubes depends on the reaction time and very long tubes, up to 60 micron, can be produced. [21]

High Pressure Carbon Monoxide

The methods overviewed so far for the production of SWCNT are suitable for collecting milligrams to grams of material in a few hours. However, many potential applications of carbon nanotubes require kilogram to ton quantities. R. Smalley and co-workers at the Rice University[22] introduced a new method for the production of SWCNT based on the catalytic growth in a continuous-flow gas-phase process using carbon monoxide (CO) as the carbon feed-stock and $Fe(CO)_5$ as the iron containing catalyst precursor. The method is also known as HiPCO which stands for High Pressure CO.

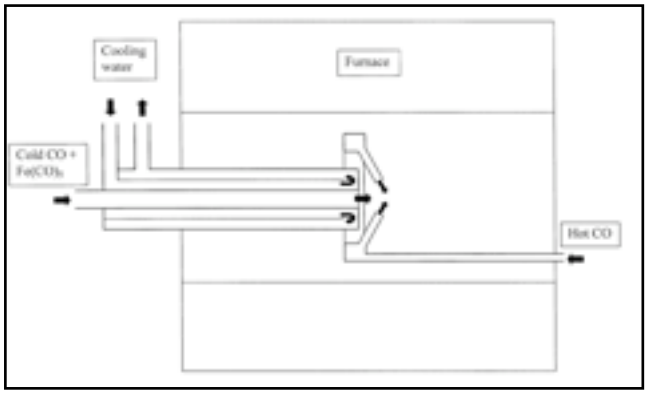

Fig. 13: Layout of CO flow-tube reactor

CO mixed with a small amount of $Fe(CO)_5$ is flown through a heated reactor (fig.13). The products of $Fe(CO)_5$ thermal decomposition (such as $Fe(CO)_n$, n=0-4) react to produce iron clusters in gas phase. These clusters grow as the iron particles collide, eventually reaching dimensions comparable to the SWCNT diameter (0,7 - 1,4 nm), acting as nucleation centers upon which SWCNT grow. Solid carbon is produced by CO disproportion (r.1) which occurs catalytically on the surface of the iron particles:

$$CO + CO \longrightarrow C(s) + CO_2 \qquad \text{(r. 1)}$$

The flow cell apparatus consist of quartz flow tube contained within a tube furnace through which reactant gases are flown. The tube section inside the furnace is maintained between 800 and 1200 °C while the tube entrance and exit are maintained at room temperature.

SWCNT will nucleate and grow from the catalytic particles by the "Yarmulke" mechanism. [23] That is, a hemifullerene cap forms on the partially carbon-coated particle, lifts off, and additional carbon atoms are continuously added to the edge of the cap, forming a hollow tube of constant diameter, closed at the tips, which grows away from the particle.
They found that both the yield of SWNT material and the diameters of the nanotubes produced can vary over a wide range, depending on the conditions and flow-cell geometry used such as temperature, pressure, heating velocity. The experimental conditions were found to be T=800 - 1200 °C; P= 1-10 atm; and allow to produce large quantities of SWCNT with an average diameter of 1,2 nm, almost free of amorphous carbon and metallic particles. Highest yield and narrower tubes are produced at the highest accessible temperature and pressure, 1200°C and 10 atm respectively. With this method it is possible to produce the expected smallest achievable chemically stable SWCNT with 0,7 nm of diameter.
The diameter of 0,7 nm corresponds to the size of a C_{60} molecule, the smallest stable fullerene. SWCNT cannot nucleate on smaller Fe particles because no stable end cap can form. Delays in cap formation and lift off will allow the Fe particles to accumulate more iron and grow larger so that if a SWCNT does eventually nucleate it will have a larger diameter. The higher CO pressure and experimental temperature, the narrower diameter distribution of nanotubes is observed. This is because high pressure and temperature lead to faster CO disproportionation giving more C atom on each Fe particle and faster SWCNT nucleation with respect to the particle growth. Higher CO pressure also leads to an higher yield of carbon to iron: the growth of the nanotubes lasts for a certain time and stops due to excess iron accretion followed by over-coating. Increasing the CO pressure one can reduce the relative amount of catalyst present and increase the rate of reaction, leading to higher yields.

1.5 Properties of Carbon Nanotubes

Electrical Properties

The unique electrical properties of Carbon nanotubes are derived to a large extent from the peculiar electronic structure of graphite , and their 1-D character.
Despite structural similarity to a single sheet of graphite, which is semiconductor with zero band gap, SWCNTs may be either metallic or semiconducting depending on the direction about which the graphite sheet is rolled to form the nanotube cylinder (paragraph 1.2). The electronic properties of perfect MWCNTs are rather similar to those of perfect SWCNTs because the coupling between the cylinders is weak in MWCNTs.

Carbon nanotubes have a very low electrical resistance. [24] Resistance occurs when an electron collides with some defect (an impurity atom, a defect in the crystal structure) of the material through which it is passing. Such collision deflects the electron from its path. Electrons inside a carbon nanotube are not easily scattered because of their very small diameter and huge ratio of length to diameter. In a 3-D conductor electrons have plenty of opportunity to scatter at any angle, and this gives rise to electrical resistance. In a 1-D conductor electrons can travel only backward and forward and only the mechanism of backscattering (the change in electron motion from backward to forward and vice versa) takes place. Since backscattering requires very strong collisions is less likely to happen and because of this nanotubes have a really low electrical resistance. In addition to this, they can carry the highest measured current density of any known material: 10^9 A/cm^2. [25]

Thermal Properties

The ballistic electronic transport in metallic SWCNTs and MWCNTs over long nanotube lengths enables the tubes to carry high currents with essentially no heating. The specific heat and thermal conductivity of carbon nanotube system are determined primarily by phonons. Because of their small size quantum effect are important and the low temperature specific heat and thermal conductivity show direct evidence of 1-D quantization of the phonon band structure. Before the discovery of carbon nanotube, diamond was the best known thermal conductor. CNT have been proofed to have a thermal conductivity at least twice that of diamond at room temperature. Berber et al.[26] have calculated the phonon thermal conductivity of isolated nanotubes measuring a maximum value of 37000 W/m K at 100 K, comparable to the highest thermal conductivity ever measured of 41000 W/m K for an isotopically pure diamond. Even at room temperature the thermal conductivity is quite high (6600 W/m K) exceeding the reported room temperature thermal conductivity on an isotopically pure diamond by almost a factor of two.
They also compared the thermal conductivity of SWCNT to the calculated thermal conductivity of a single plane of graphene and of 3-D graphite. In graphite the interlayer interactions quench the thermal conductivity by nearly an order of magnitude compared to graphene. It is likely that the same process occurs in nanotubes, it is significant that the thermal conductivity of an isolated nanotube highly overmatches the thermal conductivity of nanotubes in bundles. By analogy to the case of graphite, intertube interaction in bundles should depress the low-energy density of states.

Mechanical Properties

Carbon nanotubes are the strongest and stiffest materials yet discovered in terms of tensile strength and elastic modulus respectively. This strength results from the covalent sp^2 bonds formed between the individual carbon atoms [27]. Carbon fibers are widely used

to reinforce other materials because of their mechanical properties and their low density. It is known that the strength of the fibers increases with graphitization along the fiber axis. Therefore carbon nanotubes, which are formed of seamless cylindrical graphene layers, represent the ideal carbon fiber and exhibit the best mechanical properties.
The technical difficulties involved in the manipulation of these nano-scale structures make the direct determination of their mechanical properties a rather challenging task. In spite of these difficulties, a number of experimental measurements of the Young's modulus of carbon nanotubes have been reported. The first such study was that of Treacy et al.[28], who correlated the amplitude of the thermal vibrations of the free ends of anchored nanotubes as a function of temperature with the Young's modulus. Regarding a MWNT as a hollow cylinder with a given wall thickness, one can obtain a relation between the amplitude of the tip oscillations in the limit of small deflections and the Young's modulus. They quantified the amplitude of those oscillations by means of careful TEM observations of a number of nanotubes, they were able to obtain an average value of 1.8 TPa for the Young's modulus of MWCNTs and 1,4 TPa for SWCNTs. Although these numbers are subject to experimental errors, they are nevertheless indicative of the exceptional axial stiffness of these materials. For comparison the Young's modulus of high strength steel is around 200 GPa.

Defects

As with any material, the existence of a crystallographic defect affects the material properties. Defects can occur in the form of atomic vacancies. High levels of such defects can lower the tensile strength by up to 85%. Another form of carbon nanotube defect is the Stone Wales Defect, [29] that is the 90° rotation of two carbon atoms with respect to the midpoint of the bond (fig. 14), which creates a pentagon and heptagon pair by rearrangement of the bonds.

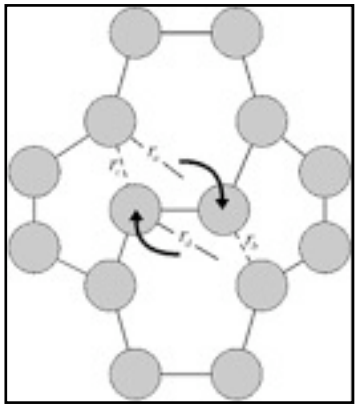

Fig. 14: Local density functional modelling of the Stone-Wales.

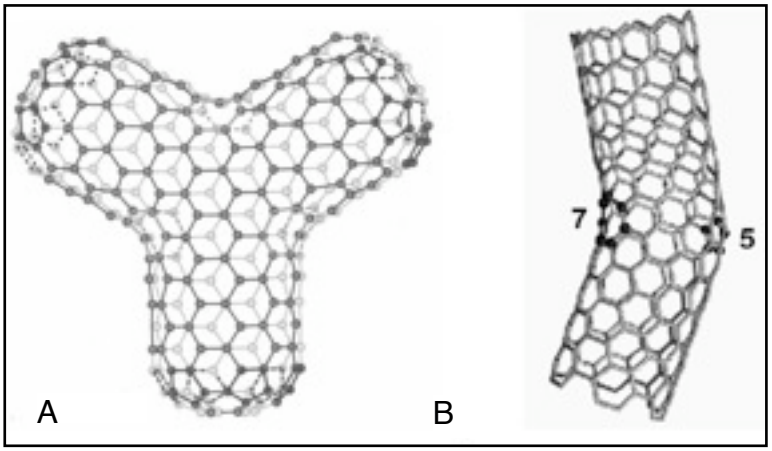

Fig 15: Examples of a Y-shaped nanotube (A) and a elbow-shaped nanotube (B).

The introduction of pentagon and heptagon rings in the structure of the tube modifies the shape of it introducing respectively positive or negative curvatures to the tube axis. Either Y - shaped (fig 15 - A) and elbow - shaped (fig. 15 - B) have been observed. [30]
High levels of such defects can lower the tensile strength by up to 85%. Because of the very small structure of CNTs, the tensile strength of the tube is dependent on its weakest segment in a similar manner to a chain, where the strength of the weakest link becomes the maximum strength of the chain.
Crystallographic defects also affect the tube's electrical properties. A common result is lowered conductivity through the defective region of the tube. Crystallographic defects strongly affect the tube's thermal properties. Such defects lead to phonon scattering, which in turn increases the relaxation rate of the phonons. This reduces the mean free path and reduces the thermal conductivity of nanotube structures. Phonon transport simulations indicate that substitutional defects such as nitrogen or boron will primarily lead to scattering of high-frequency optical phonons. However, larger-scale defects such as Stone Wales defects cause phonon scattering over a wide range of frequencies, leading to a greater reduction in thermal conductivity.

1.6 Chemistry of Carbon Nanotubes

Because of their outstanding properties CNT can be considered attractive candidates in many different nanotechnological and nanomedical applications. However, the total lack of solubility and the difficult manipulation in any solvents have imposed great limitations to the realistic application of pristine CNT in materials, devices and biology. In fact, as-produced CNT are insoluble in all organic solvents and aqueous solutions. They can be dispersed in few solvents by means of sonication, but precipitation immediately occurs when the process is interrupted. For this reason the fabrication of supramolecolar complexes, formed by CNT and different classes of organic compounds with which CNT have affinity, allows a better processing of CNT towards any application. In addition, chemical modification of CNT makes them more soluble for their integration into inorganic, organic and biological systems. [31] The chemistry of CNT is a current subject of intense research which produces continuous advances. However the controlled functionalization of CNT has not yet been fully achieved: despite of the great advances solubility remains still a matter, and the field is far to be fully explored but new advances are still needed.
As already highlighted, carbon nanotubes are constituted by a tubular shaped network of sp^2-hybridized carbon atoms. The strain in non planar conjugated organic molecules arises from two principal sources: **pyramidalization** of the conjugated carbon atoms and **p-orbital misalignment** between adjacent pairs of conjugated carbon atoms.
For an sp^2-hybridized carbon atom, planarity is strongly preferred and this implies a pyramidalization angle of 0°. On the other hand, an sp^3 hybridized carbon atom requires a pyramidalization angle of 19,5°. All the carbon atoms in the C_{60} buckminster fullerene

have a pyramidalization angle of 11,6°, which means that its geometry is more appropriate for tetrahedral than trigonal hybridization. Thus, the chemical conversion of any trivalent carbon atom in C_{60} to a tetravalent carbon atom relieves the strain at the point of attachment. [32] Reaction that serve to saturate the carbon atoms in C_{60} are accelerated by strain relief and this strongly favors fullerene addition chemistry. In the case of fullerenes the former source is the primarily involved in the strain explanation, in fact, the p-orbital alignment is perfect.
In the case of nanotubes, instead, either curvature induced pyramidalization and also misalignment of the p-orbitals induces a local strain and this makes carbon nanotubes generally more reactive of a flat graphene sheet. Conceptually is useful to divide the carbon nanotubes into two regions: the **end caps** and the **side wall**. The end caps of a carbon nanotube resemble a hemispherical fullerene and its reactivity: this means that the strain relief brought by the chemical conversion of the sp^2-hybridized carbon atoms into sp^3-hybridized ones is such to determine a consistent reactivity of the end caps with respect of the side wall, irrespectively of the diameter of the entire tube. The side wall, instead, presents carbon atoms with a lower pyramidalization angle, but in the mean time the p orbital misalignment is the major source of strain in that region and this represents a contrast with the fullerene chemistry which is translated in a different reactivity. Furthermore, a differentiation is expected between the reactivity of carbon nanotubes of different diameters: smaller CNTs present a more consistent reactivity due to the higher strain since the pyramidalization angles and the p-orbital misalignment of carbon nanotubes scale inversely with their diameter.
The main approaches for the modification of CNT can be grouped into four categories [31] (fig. 16):

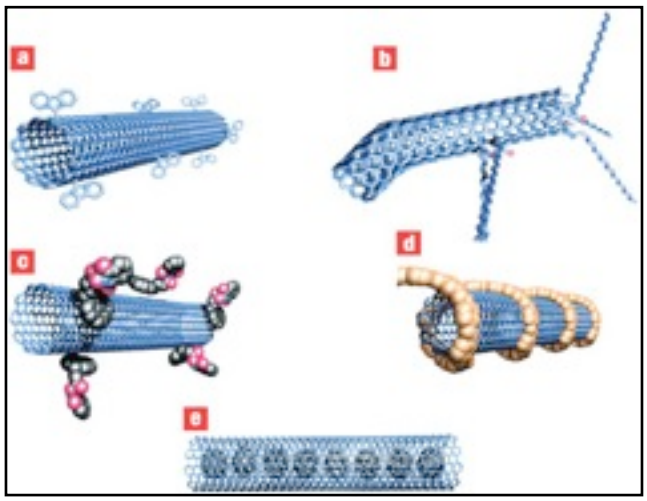

Fig. 16: (a,b), covalent side wall and open ends chemistry of CNT; (c,d), non-covalent encapsulation and polymer wrapping; (d), molecular insertion into a CNT cavity.

-covalent attachment of molecules on the p-conjugated skeleton (fig. 16-a).
-defect site chemistry (fig. 16-b).
-non covalent absorption or wrapping of various molecules (fig. 16-c/d).
-filling of the inner empty cavity (fig. 16-e).

Covalent Chemistry

1) Fluorination

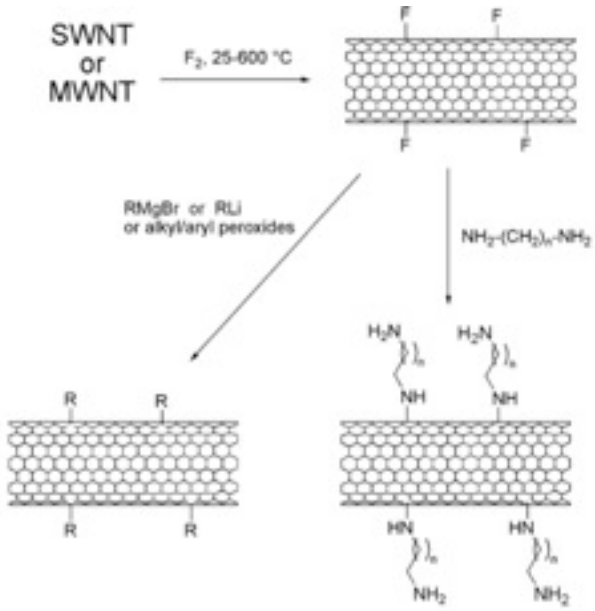

Fig.17: reaction scheme for fluorination of nanotubes

CNTs have been fluorinated by elemental fluorine and extensively characterized. The best range of temperature to achieve this functionalization was estimated to be between 150 and 400°C.[33] The structure of fluorinated CNT has been investigated and two favorable patterns of F addition onto the side walls have been identified. Kelly et al.[34] proposed two possible addition patterns: 1,2 addition or 1,4 addition. The small energy difference between the two patterns (4 Kcal/mol) implies that both type probably coexist. The side wall carbon atoms are tetrahedrally coordinated and adopt sp^3 hybridization.

This destroys the electronic band structure of CNT generating an insulating material. The highest degree of functionalization that was obtained was estimated to be C:F = 2:1. Fluorinated nanotubes were reported to have moderate solubility in alcoholic solvents. [35] The fluorination reaction is very useful because further functionalization can be accomplished:[36] alkyl groups can replace the fluorine atoms by Grignard or organolithium reagents and also several diamines and diols reacts with fluoronanotubes via nucleophilic substitution (fig. 17). The majority of fluorine atoms can be detached using hydrazine in 2-propanol and this effectively allows to recover pristine nanotubes. [33]

2)Cycloadditions

In a similar approach CNT were functionalized using azide photochemistry. The irradiation of the photoactive azothymidine in the presence of nanotubes was found to cause the formation of very reactive nitrene groups which in proximity of the carbon lattice couple the nanotubes and form aziridine adducts (fig.18- b2).[39]

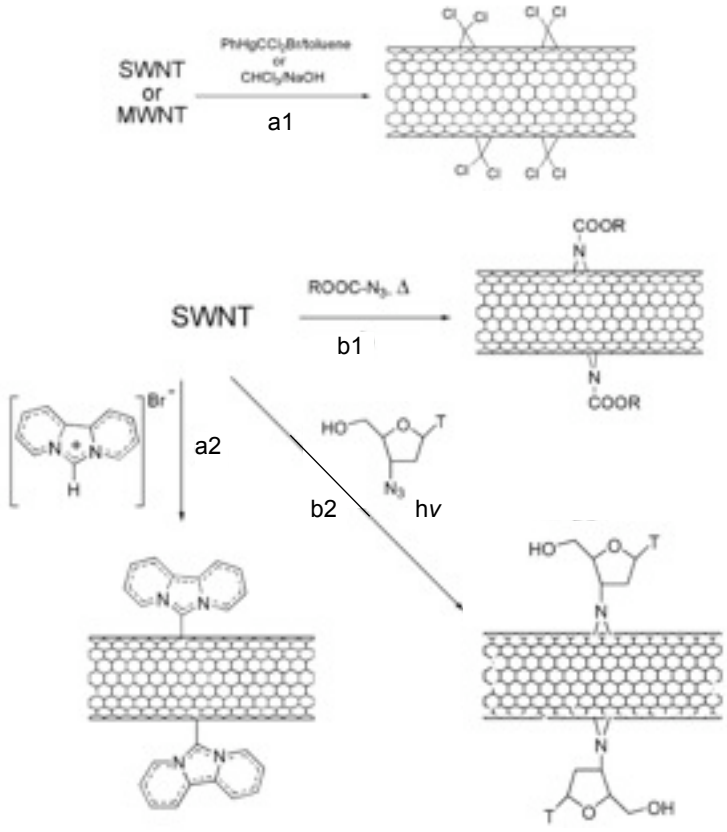

Fig. 18: (a 1-2) carbene additions; (b 1-2)nitrene additions

Carbene [2+1] cycloaddition to pristine CNT was first employed by Haddon's group.[37] Carbene was generated in situ using a chloroform/sodium hydroxide mixture and cyclopropane adducts were obtained (fig.18 - a1).
Carbene has also been nucleophilically additionated to CNT in a procedure reported by the Hirsch group[38] obtaining the formation of a zwitterionic 1:1 adduct (fig.18 - a2).
Nitrene was additionated to CNT[38] by the synthetical route illustrated in fig.18 - b1. The first step was the thermal decomposition of an organic azide which gives rise to alkoxycarbonylnitrene via nitrogen elimination; the second step consisted in the [2+1] cycloaddition of the nitrene to the side wall of CNT, which gives rise to alkoxycarbonylaziridino-CNT.

An efficient method for obtaining well functionalized CNT was developed by Prato's group.[40] The azomethine ylides, thermally generated in situ by condensation of an α-amino acid and an aldeyde, were successfully added to the graphitic surface via a 1,3 dipolar cycloaddition reaction, forming pyrrolidine fused rings (fig. 19).

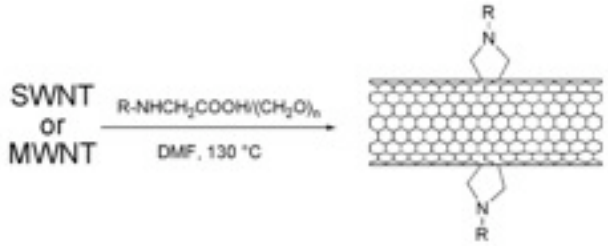

Fig. 19: 1,3 dipolar cycloaddition of azomethine

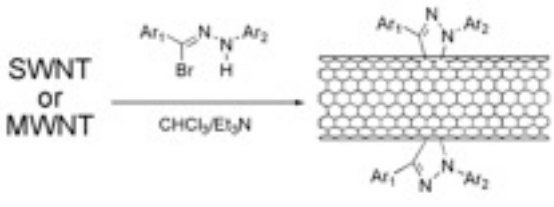

Fig. 20: 1,3 dipolar cycloaddition of nitrile imines

In a similar approach Alvaro et al.[41] modified nanotubes by thermal 1,3 dipolar cycloaddition of nitrile imines obtaining pyrazoline-modified tubes (fig.20)
Recently was reported the "Bingel" [2+1] cyclopropanation reaction by Coleman et al.[42] In this reaction biethylbromomalonate works as a formal precursor of carbene. The [2+1] addition of CNT dispersed in 1,8 diazobicyclo [5,4,0] undecene (DBU) afforded the modified material (fig.21).

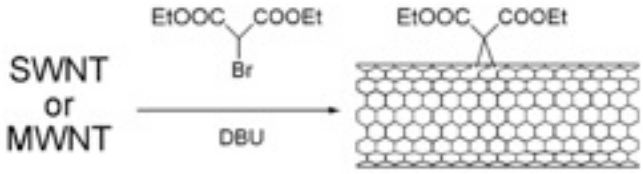

Fig. 21: Bingel reaction on Nanotubes

3) *Radical Additions*

It has been demonstrated by theoretical simulations that there is great probability of reaction of radicals on the walls of CNT.[43] A simple approach to covalent side-wall functionalization by radical species was developed via diazonium salts.

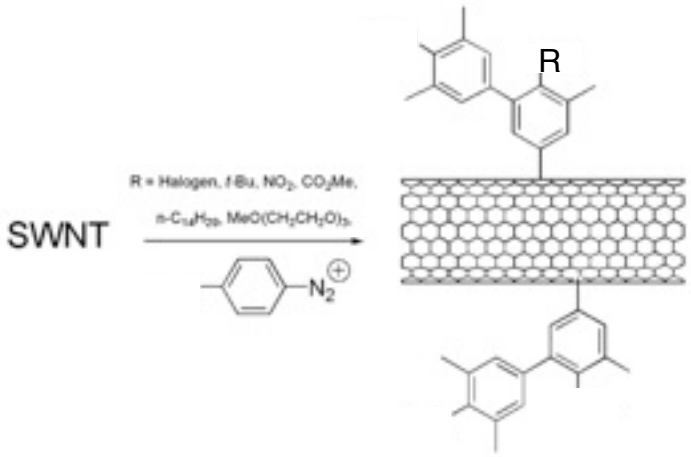

Fig. 22: Radical addition of aryl diazonium salts on nanotubes: general scheme.

Single wall carbon nanotubes (SWNT) have been functionalized with pendant aryl groups using diazonium salts under various conditions by Tour's group:[44] initially functionalization was achieved by **electrochemical reduction** of substituted aryl diazonium salts, where the reactive species was supposed to be an aryl radical. The formation of aryl radicals was triggered by electron transfer between CNT and the aryl diazonium salts in a self catalyzed reaction (fig. 22). A similar reaction [45] was later described utilizing **water-soluble** diazonium salts which have been shown to react selectively with metallic CNT.

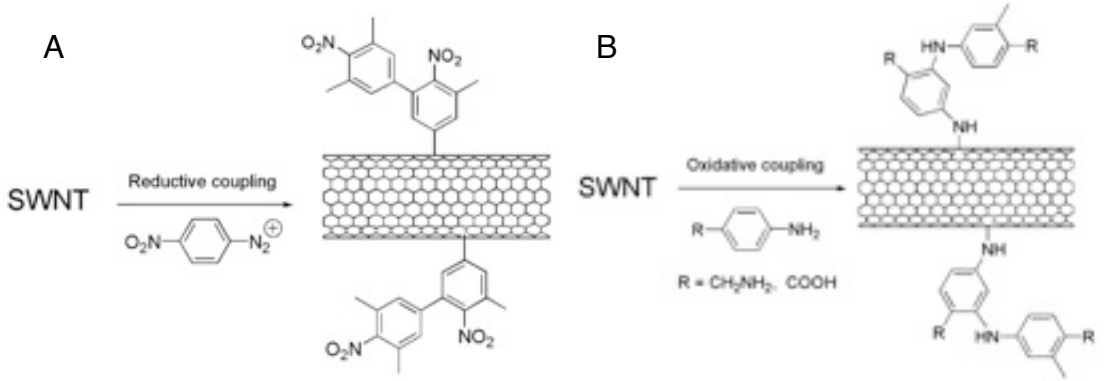

Fig 23: electrochemical functionalization resulting in C-C bond formation (a) and C-N

In situ chemical generation of the diazonium salts was found to be an efficient mean of functionalization:[46] the reaction uses aromatic amines which, in acidic conditions

or in presence of isopentyl nitrite, generate diazonium salts which are then transformed by bland heating in aryl radicals capable to react directly to the side walls of CNTs. The same reaction can also be performed under **solvent-free** conditions [47] offering the possibility of scaling-up with moderate volumes.
Electrochemical modification of individual CNT was demonstrated by the attachment of substituted phenyl groups. Two types of coupling reaction are proposed:[48] reductive coupling of aryl diazonium salts and oxidative coupling of aromatic amines. In the former case the reaction results in a C-C bond at the graphitic surface, in the latter case amines were directly attached to CNT (fig. 23 a-b).

4) Grafting of Polymers

Covalent reactions of CNT with polymers are important because the long polymer chains help a lot to dissolve the tubes into a wide range of solvents even at a low degree of functionalization. There are two main methods for the covalent attachment of polymeric substances to the surface of nanotubes which are defined "grafting to" and "grafting from" methods. [31]

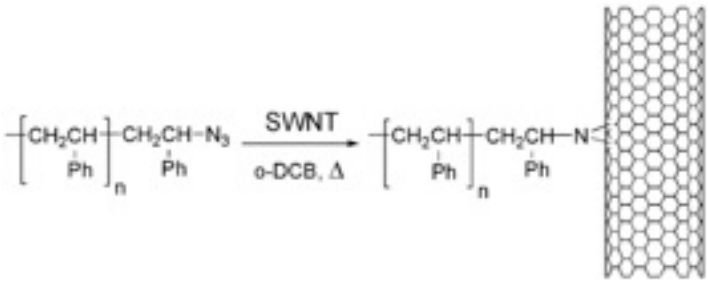

Fig. 24: "grafting to" approach for nanotube-polystirene composites.

In the **"grafting to" method** a polymer with a specific molecular weight is synthetized. The synthesis is followed by specific end-group transformation and subsequently this polymer chain is attached to the graphitic surface of CNT.

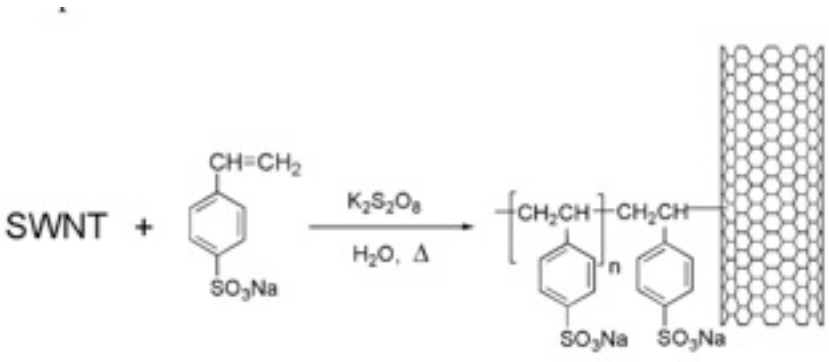

Fig. 25: "grafting from" approach for the attachment of a polyelectrolite on CNT by an *in situ* process.

The **"grafting from" method** is based on the covalent immobilization of the polymer precursor on the surface of CNT followed by the propagation of the polymerization in the presence of the monomeric species.Here we report few examples of both procedures.

Quin et al.[49] reported the grafting of functionalized polystirene to CNT via a cycloaddition reaction. An azido polystirene with a defined molecular weight was synthetized by atom transfer radical polymerization and then added to nanotubes (fig. 24).Quin et al. [50] still, reported the grafting of polystirene sulfunate by *in situ*

radical polymerization. Through the negative charges of the polymer chain the composite should be dispersed on water, whereas the impurities are eliminated by centrifugation (fig. 25).

Defect Site Chemistry

Up to now all the production methods of CNTs generate impurities like amorphous carbon and catalyst nanoparticles. There are techniques applied for the purification of the row material such acidic oxidation [51] by nitric acid or pirana solution, a mixture of sulfuric acid and hydrogen peroxide, which induce the opening of the tube caps as well as the formation of holes in the side-walls. The final products are nanotube fragments with lengths below 1 um, whose ends and side-walls are decorated by oxygenated functionalities, mainly carboxylic groups, which can be derivatized chemically according to their reactivity characteristics, playing the role of support for further functionalization (fig. 26).

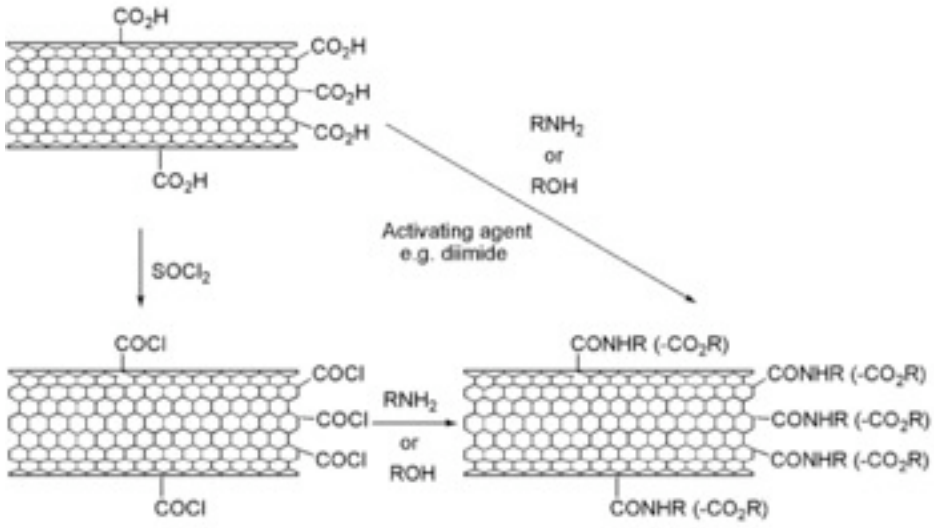

Fig. 26: derivatization reactions of acid-cut nanotubes through the defect sites

Chen et al.[52] treated for the first time oxidized nanotubes with long chain alkylamines via acylation, creating an amidic bond and made the material soluble in organic solvents. Amines of different chain length were employed to study the solubility of the tubes depending on the type of functionalization. Esterification is also possible by the use of long chain alcohols.[53] Exploiting these two possible types of bonds (amidic - esteric) many different functionalities can be attached to the nanotube skeleton, useful for several application i.e. dendrimers,[54] porphyrins,[55] various fluorescent probes,[56] crown ethers,[57] silanes,[58] gold nanoparticles[59] and gold substrates [60] by the use of a thiol derivative as cross linker. Also, intermolecular junctions between CNT are possible,[61] polymers can be grafted to oxidized nanotubes,[62] and various biomolecules [63] can be attached to the nanotubes which, in

this way, become potential carriers to transport and deliver various bioactive components into cells.

Noncovalent Interactions

One of the reasons why CNTs are very difficult to disperse homogeneously in solution is the formation of big bundles of tubes held strongly together by the p-p stacking of aromatic rings. One of the approaches that have been widely used to exfoliate bundles and prepare individual CNT is the noncovalent wrapping of the surface by various species of polymers, aromatic compounds, surfactants and biomolecules.
Noncovalent functionalization is based on van der Waals forces or p-p stacking and it is particularly interesting because it offers the possibility of attaching chemical moieties without affecting the electronic network of the tubes.
Different kind of polymers, for example, are largely used in noncovalent chemistry of nanotubes because, as nanotubes are considered ideal materials to reinforce fibers due to their excellent mechanical properties, the fabrication of high performance materials based on nanotube-polymers composites has many potential applications in many fields of technology. It is recognized that the material quality is higher the more efficient is the load transfer from the host matrix to the tubes. The load transfer requires homogeneous dispersion of the filler and strong interfacial bonding between the two components.[64] Many strategies have been developed to address this issue: physical mixing in solution, in situ polymerization of monomers in the presence of nanotubes, surfactant assisted processing of composites.

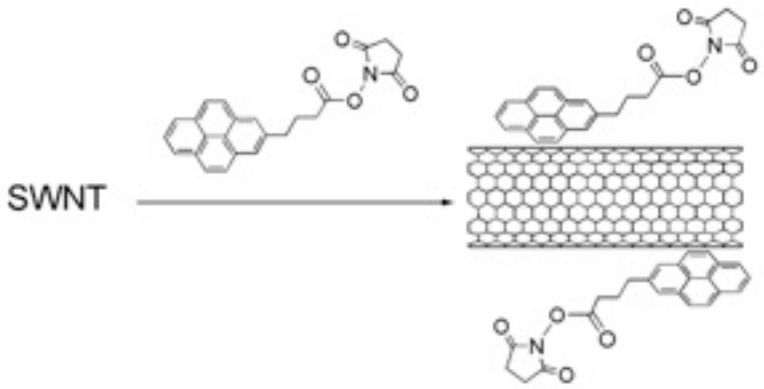

Fig. 27: interaction of nantubes with pyrene derivatives

Pyrene modified oxide surfaces have been employed for the patterned assembly of carbon nanotubes.[65] The method relies on distinct molecular recognition properties of pyrene functional group toward the carbon graphitic structure. Pyrenil groups interact with the aromatic structure of carbon nanotubes through a strong p-p stacking of the aromatic rings and this interaction is at the basis of the molecular recognition (fig. 27).
Surfactants were initially used in the purification protocols of carbon nanotubes as dispersing agents. [66] The interaction takes place between the hydrophobic aromatic structure of the tubes and the hydrophobic part of the molecules. Nanotubes can be

captured into the supramolecular amphiphilic aggregates of surfactants and dispersed in aqueous media. Solutions obtained with this method present high long-term stability. CNT can also interact with many biomolecules without forming a covalent conjugate. The electronic properties of CNT coupled with the specific recognition properties of the immobilized biosystem would therefore generate a miniaturized biosensor. Proteins for example are an important class of biosubstrates having high affinity with the graphitic network of nanotubes. They tend to absorb on the external sides of nanotubes walls presumably via interaction between the graphitic surface and the hydrophobic aminacidic domains, or even via charge-transfer.[67] For example, monoclonal fullerene-specific antibodies have been shown to specifically bind to the surface of carbon nanotubes. The binding cavity of the antibody consists of a cluster of specific hydrophobic amino acids. [68] A different approach to bind biomolecules to nantubes involves the use of bifunctional linkers based on pyrene moieties. The anchor molecule can adsorb irreversibly onto graphitic surface due to van der Waals interactions and various biomolecules can be covalently attached to the activated pyrene by nucleophilic attack of the basic aminoacid residues. [69] Amphiphilical helical peptides were found to fold around the graphitic surface of the nanotubes and to disperse them in aqueous solution by noncovalent interactions. [70] Also, synthetic single-chain lipids can interact with nanotubes by their hydrophobic part [71] and the polar part can be used in the selective immobilization of other biomolecules. Noncovalent interaction between carbon nanotubes and DNA are reported by several groups: DNA strands interact strongly with CNT to form stable hybrids that can be effectively dispersed in aqueous solutions.[72] Moreover, many applications are reported where the interaction of CNT with DNA strands of specific sequence made possible the separation between metallic and semiconducting tubes, and also a diameter dependent separation via ion-exchange chromatography.[73] Lastly, many groups explored the interaction of the graphitic surface of nanotubes with many different carbohydrate macromolecules of different size and chemistry and found also in this case an effective interaction and increment of dispersibility in water.

Filling of the Inner Cavity

Among the wide number of studies on CNT also their ability to fill their inner cavity was investigated. The group which firstly observed the filling of SWCNTs worked with C_{60} as encapsulated material. [74] The controlled synthesis of high amount of such structures was firstly achieved starting from oxidized SWCNT in the presence of added fullerenes under vacuum at high temperature (400 - 600°C) giving yields in the range of 50 - 100%.[75] Later, alternative strategies were developed, like alkali-fullerene plasma irradiation.[76] Also other order carbon spheres such as C_{70}, C_{80}, etc. were successfully encapsulated.[77] Beside fullerenes, other species were successfully introduced inside the nanotube cavity: metallic salts were introduced in solution, or in the molten form, to be then transformed in the oxidized metallic form by heating

in a second step (this is important to obtain metallic nanowires); metallocenes, like ferrocene, chromocene, cobaltocene etc. were efficiently introduced [78] and various electrolytes in solution.[79] Biomolecules of suitable size can be introduced in multi-walled nanotubes with open ends. It has been shown that small proteins, like lactamase, can be introduced, and the proteins remain catalytically active. [80] Also, single strand RNA was introduced into the cavity of tubes and it has been shown that it remains hydrophobically trapped into the graphitic wall despite the large entropic penalties of trapping a polyelectrolite into a non polar structure.[81] Transport process of liquids, like water, into the cavity of tubes was also explored: the transport is dependent on the ability of the solvent to wet the hydrophobic channel. The field was investigated theoretically by molecular dynamics simulations considering parameters such as the hydrogen bond network and the liquid pressure.[82]

1.7 Characterization Techniques of CNT

Production and as well chemical modification of carbon nanotubes encounter problems specifically due to the great variability that each methods brings in the resulting material. Each production method of CNT gives a product different for diameter distribution, length distribution, chirality, purity, nature of the catalyst, impurity species and defects. Also, the purification and functionalization methods increase the ratio of nanotubes in the sample with respect to the impurities but, in most of the cases, causes a degree of modification on the nanotubes themselves opening the ends, reducing the length, and introducing defects and functional groups on the side walls. In virtue of this it is needed to identify univocally all the properties of these tubes and fully characterize them. The common characterization techniques used to characterize any organic compounds like ^{1}H-NMR, ^{13}C-NMR, ES-MS, UV-Vis and IR are not enough to supply sufficient information and more methods are needed to get an exhaustive insight on structure, morphology, purity and chemical modification of CNT. Here we propose a review of the principal characterization techniques used in carbon nanotubes chemistry.

Optical Properties of Carbon nanotubes

The optical properties of carbon nanotubes refer specifically to the absorption, photoluminescence and Raman Spectroscopy. Spectroscopic methods offer the possibility of quick and non-destructive characterization of relatively large amounts of carbon nanotubes and allow a reliable characterization of nanotube "quality" in terms of amorphous carbon content, structure (chirality) of the produced nanotubes and structural defects.

UV-Vis-NIR spectroscopy

Optical properties of carbon nanotubes derive from electronic transitions within their density of states (DOS). Carbon nanotubes can be considered as one dimensional objects as they have a high ratio between length and diameter. A typical feature of one-dimensional nanomaterials is that their DOS is not a continuous function of energy, but it descends gradually and then increases in a discontinuous spike (fig. 28). In contrast, three-dimensional materials have continuous DOS. The sharp peaks found in one-dimensional materials electronic spectra are called Van Hove Singularities.

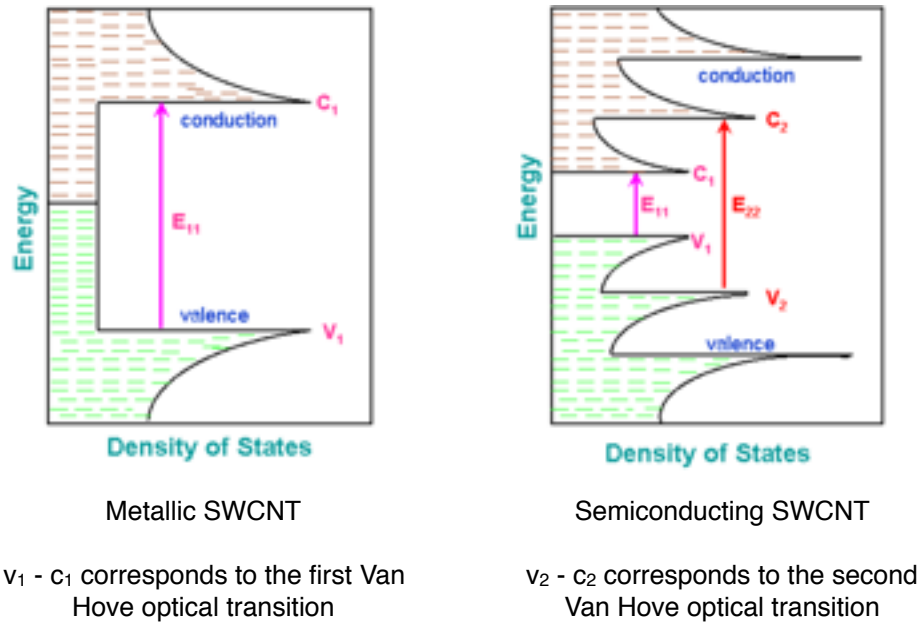

Fig. 28: Density of States diagram

Van Hove singularities results in the following remarkable optical properties of carbon nanotubes:

- Optical transitions occur between the v_1 - c_1, v_2 - c_2, etc., states of semiconducting or metallic nanotubes and are traditionally labeled as S_{11}, S_{22}, etc. for semiconducting tubes and M_{11} for metallic tubes. Crossover transitions c_1 - v_2, c_2 - v_1, etc., are dipole forbidden and thus are extremely weak. [83]
- The energies between the Van Hove singularities depend on the nanotube structure.
- Optical transitions are rather sharp (~10 meV) and strong. Consequently, it is relatively easy to selectively excite nanotubes having certain (n, m) indexes, as well as to detect optical signals from individual nanotubes.

In virtue of what just described, optical absorption spectra in carbon nanotubes differ from absorption spectra in conventional 3D materials for the presence of sharp peaks

instead of an absorption threshold followed by an absorption increase (which is the typical behavior of most 3D solids). Absorption in semiconducting nanotubes originates from electronic transitions from the v_2 to c_2 (energy S_{22}) or v_1 to c_1 (energy S_{11}) levels, etc., with bands included in the range of 800 - 1400 nm. For metallic nanotubes the transition between v_1 and c_1 (energy M_{11}) presents bands at 500 nm. The transitions are relatively sharp and can be used to identify nanotube types. The sharpness deteriorates with increasing energy, and since many nanotubes have very similar S_{22} or S_{11} energies, significant overlap occurs in absorption spectra. [84]

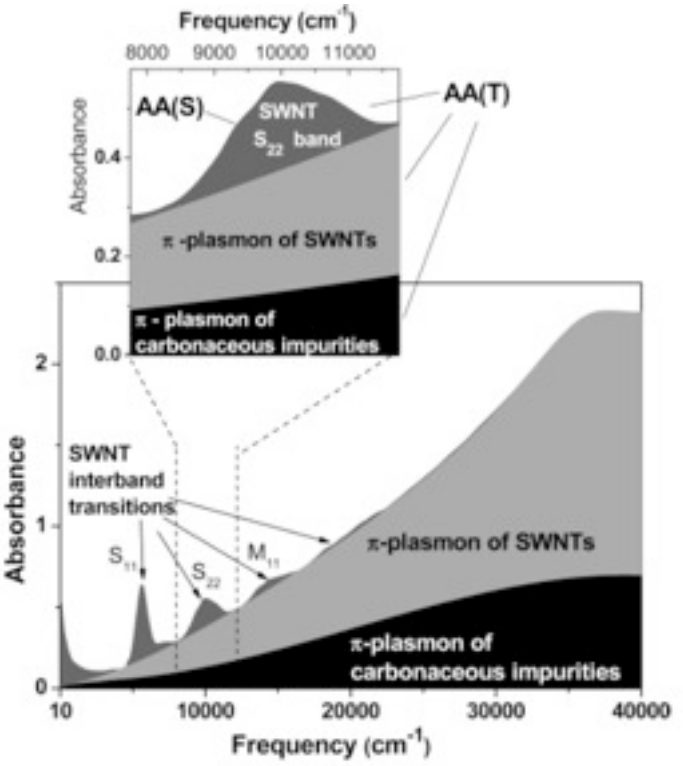

Fig. 29: schematic illustration of the electronic spectrum of a typical SWCNT sample.

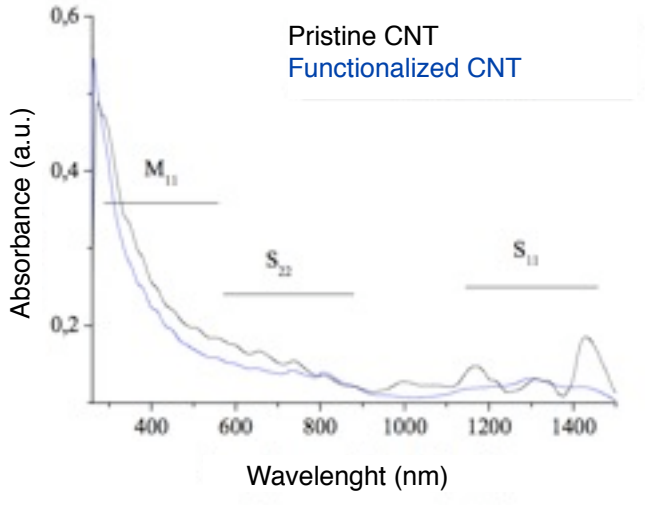

Fig. 30: UV-Vis spectrum of pristine-SWCNT(black) and generic functionalized SWCNT (blue).

Optical absorption is routinely used to quantify quality of the carbon nanotube powders. The spectrum is analyzed in terms of intensities of nanotube-related peaks (Van Hove singularities), p-plasmon of CNT and p-plasmon of carbonaceous impurities. Fig. 29 shows a schematic spectrum of a SWCNT sample in the spectral range between the far-IR to the UV (10 - 45000 cm^{-1}) with the three regions shown in different colors. The high energy part of the spectrum is dominated by the p-plasmon absorption of both CNT and carbonaceous impurities. The zone between 10 to 15000 cm^{-1} is instead dominated by the Van Hove singularities. The strength of the Van Hove singularities in comparison with the featureless baseline provides a measure of the purity of the sample. The purity is evaluated by considering the ratio between the area of one of the interband transition after linear baseline correction (AA(S)) and the total area under the spectral curve (AA(T)) with respect to the ratio AA(S)/AA(T) for an arbitrary sample of high-purity as produced CNT. This procedure of course gives rise to a relative purity evaluation because a 100% pure

reference is still not available. Moreover, there is the necessity of a different reference sample for each production method of nanotubes since different methods give rise to different quality and quantity of impurities. Other limitations to the use of this technique come from the difficulties in the formation of stable dispersion by nanotubes from some sources, and the different dispersion stability of CNT and impurities. [85]
Interactions between nanotubes, such as bundling, broaden optical lines. Thus, from UV-Vis spectra of CNT it is possible to extract information on the dispersibility of tubes since individual tubes will present a more defined spectrum.
Spectra of covalently functionalized carbon nanotubes show a significant loss of the van Hove singularities structure because the introduction of defects on the aromatic network of the tubes due to the chemical functionalization reduces significantly the electrical properties of CNT (fig. 30).

Raman Spectroscopy

Raman spectroscopy is one of the most powerful tools for characterization of carbon nanotubes. Without sample preparation, a fast and non-destructive analysis is possible. With Raman spectra we can provide information about the tube configuration, the diameter, the number of walls, the functionalization and the presence of crystalline or amorphous carbon. [86]
When a beam of light traverses a dust free transparent sample of a chemical compound, generally passes trough it unmodified or it is absorbed by the sample. A small fraction of the light emerges in directions other than that of the incoming beam. Most of this scattered light is of unchanged frequency (elastic scattering, Reileigh effect). However a small part of it (approximately 1 in 10 million photons) has a different frequency, usually lower, then the frequency of the incident light (unelastic scattering). Its presence is the result of the Raman effect. The Raman effect was first reported by C. V. Raman in 1928 and named after him. The importance of the discovery was such that he was vested of the Nobel Prize in physics in 1930.
The energy difference between the incident photons and the scattered photons corresponds to the energy gap between the vibrational energetic levels of the molecular species. The analysis of the shift of the spectral lines gives information on the chemical composition, the molecular structure and the intermolecular forces of the sample. The intensity is

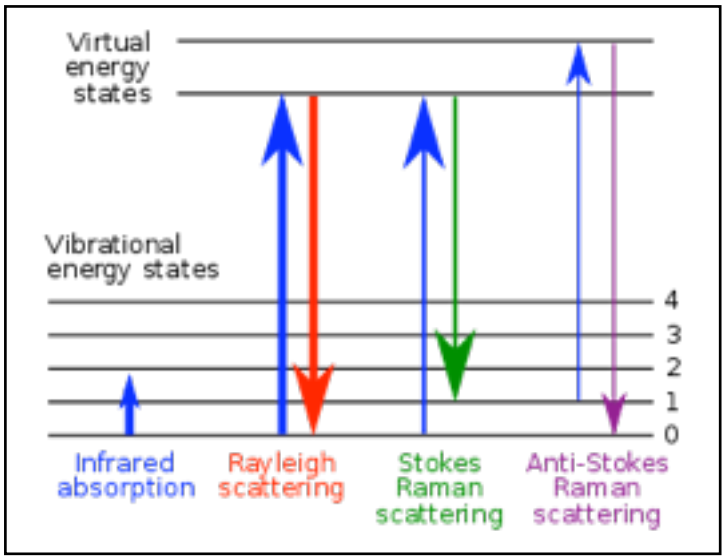

Fig 31: description of Raman effect

proportional to the number of scattering molecules in the path of light.
Raman effect can be described as an energy exchange between the incident photon and the molecule. A photon hν causes the excitation of the molecule from the fundamental vibrational energy state "0" (fig. 31) to a virtual energy state. If the molecule decades to the fundamental energy state, a photon with the same energy hν is reemitted (elastic scattering). If the molecule decades to an excited vibrational energy state (i.e. level "1") a photon $h(\nu - \nu_1)$ will be reemitted, with a lower energy than the incident light: in this case we have a Stokes Raman diffusion. If originally the molecule was on an excited vibrational state (i.e. level "1") and after excitation passes from the virtual energy state to the fundamental level, the reemitted photon will have energy $h(\nu + \nu_1)$, higher than that of the incident light and in this case we have anti-Stokes Raman diffusion. In normal condition Stokes diffusion is more intense of anti-Stokes, primarily because the lower vibrational states are more populated.
All allotropic forms of carbon are active in Raman spectroscopy: fullerenes, carbon nanotubes, amorphous carbon, graphite, etc. The position, width and relative intensity of bands are modified according to the carbon forms. Carbon nanotubes have a rich Raman spectrum. The parent material to carbon nanotubes is graphite, and we find in carbon nanotubes Raman spectra the typical pattern of the graphite modes. The most prominent modes in common with graphite are the G-band (G-graphite), the D-band (D-disorder) and the G' band. In addition to the graphite modes, carbon nanotubes have a unique, prominent, mode, which is called the radial breathing mode (RBM) (fig. 32).[87]

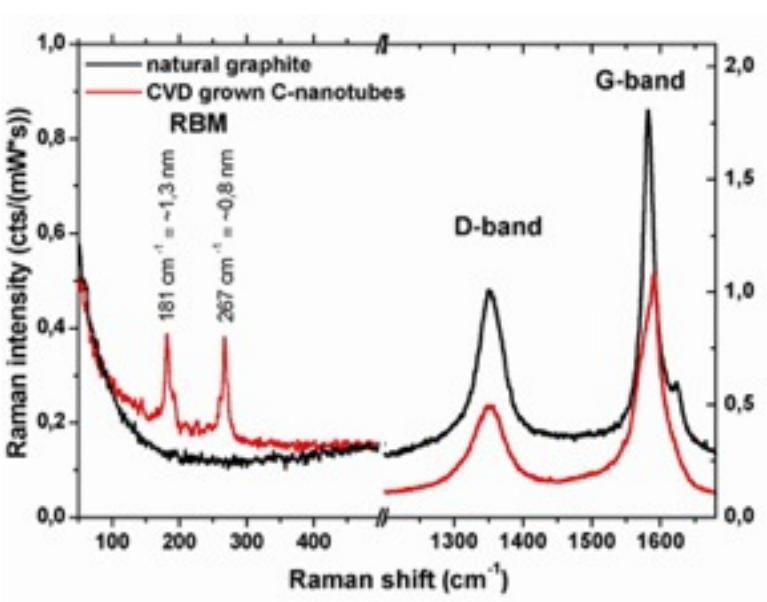

Fig. 32: Graphite and CNT Raman spectra

The RBM is situated in the spectral region from 160 to 300 cm^{-1} and is due to isotropic radial expansion of the tube. The RBM is the real signature of the presence of CNT in the sample since it is not present in graphite. The RBM frequency is inversely proportional to the diameter of the tube with the relation (eq. 3):

$$\omega(cm^{-1}) = A/\mathrm{dia}(nm) + B(cm^{-1}) \qquad \text{(eq.3)}$$

where the constants A and B have been determined experimentally with A= 223 cm^{-1}/nm and B=10 cm^{-1}. The RBM frequency is then an important feature for determining the

diameter distribution of a sample. The direct environment of the nanotubes causes a modification of the RBM mode. The formation of bundles in a nanotube sample, for example, can cause an up-shift of the RBM due to the van der Waals forces among the tubes of about 14 cm^{-1}. The tube/tube interaction is not the only one to be taken into account: the interaction between graphene sheets in the case of MWNTs also contributes to the RBM modification. [86]

The G mode is a tangential shear mode of the carbon atoms. In graphite, there is one single G mode at ≈ 1580 cm^{-1}. In carbon nanotubes, the single G-band transforms into several modes due to the confinement of wave-vectors along the circumference. Examples of G-band structure from different carbon-based materials are shown in figure 33. For semiconducting nanotubes the highest mode, G^+ (1590 to 1595) cm^{-1} is a longitudinal shear mode parallel to the axis of the nanotube. Transverse shear modes G^-, perpendicular to the tube axis, are lower the higher is the curvature of the tube, so they result more softened in tubes of smaller diameters. The metallic tubes instead are easily recognized from the broad and asymmetric "Breit-Wigner-Fano" line-shape of the G-band. The G^- band is particularly strong for metallic nanotubes, with down-shifts of the G^- mode of ≈ 100 cm^{-1} for tubes of small diameters. The G^- energy decreases with decreasing diameter faster than for semiconducting nanotubes while the G^+ remains essentially constant in frequency. [88]

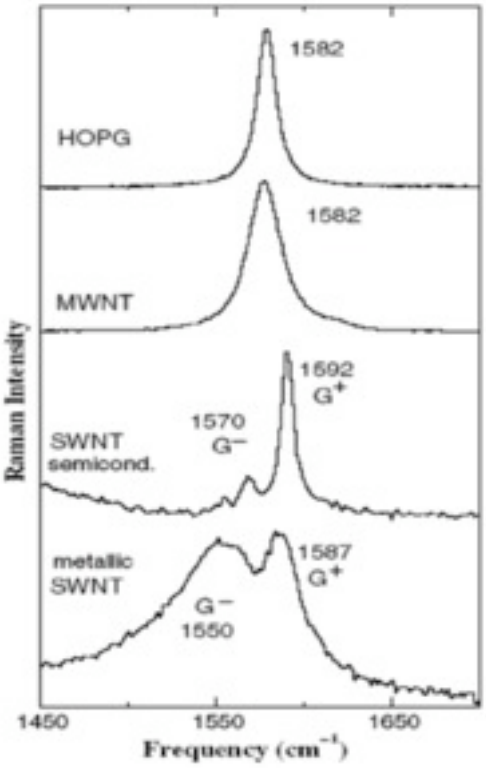

Fig. 33: G band for graphite, MWCNT, semiconducting SWCNT and metallic SWCNT.

The D-band, at 1350 cm^{-1}, is called defect mode. Its intensity is generally used to quantify the purity of pristine CNT. The D band is present in all carbon allotropes, including amorphous carbon. The D-band signal can originate from nanotubes with defects and/or from non-SWNT carbon. One way to identify the different contributions is by the line-shape of the D-band, where a broad peak (≈ 100 cm-1) is indicative of amorphous carbon. The D-band width for nanotube ensembles are ≈ (10 to 20) cm^{-1}. The quality of a sample is often evaluated by comparing the D to G band intensity. For high-quality samples, without defects and amorphous carbon, the D/G ratio is often below a couple of percent. The D-band is important also for the characterization of functionalized nanotubes because its intensity increases in the presence of sp^3 carbon, which is formed after the covalent bond to a side functional group. [89]

Lastly, in carbon nanotubes Raman spectra, there is an additional band at frequencies 2500 to 2900 cm^{-1} called G' band, which is an overtone of the D band. The G' band is an intrinsic property of nanotubes and graphite and it is present even in defect-free

nanotubes where the D-band is completely absent. The frequency of the G′ band is close to twice the D-band frequency. [87]

Imaging Techniques for the Characterization of CNT

As already mentioned, CNTs are commonly chemically processed in order to purify them and to bring appropriate functionalizations, that make them soluble and easy to hadle in organic solvents. This is necessary in order to take advantage of the outstanding properties of CNT in many useful applications, but in the mean time the functionalization process changes the structure and the intrinsic properties of the nanotubes. For example with the acidic purification treatments the caps at both ends of the CNTs are removed, the tubes are considerably shortened, and defects such as carboxylic acid groups on surface are revealed. Thus, the original structure of nanotubes is drastically modified. The properties of the nanotubes are influenced by these defects sites on the walls and at the ends. [86]
On the other hand the as-produced material is known to be inhomogeneous and contains a variety of impurities including carbon-coated metal clusters and amorphous carbon. The type and extent of these impurities change with the production method used. The production process also influences the length, diameter, chirality and surface moiety of the nanotubes.
To have a complete characterization of the nanotubes it is important to be able to visualize all this features in order to verify the efficiency of a functionalization method as well as that of a production method. Imaging techniques in the characterization of nanotubes are important for this reason. However, only few microscopical techniques are able to characterize CNTs at the individual level such as transmission electronic microscopy (TEM) and atomic force microscopy (AFM). Microscopical techniques are extremely important mainly because they allow the qualitative evaluation of the purity and the dispersibility on the nanotube sample.

AFM microscopy

The AFM apparatus consists of a cantilever with a sharp tip at its end that is used to scan the specimen surface. The cantilever is typically silicon or silicon nitride, the tip radius of curvature is on the order of nanometers. When the tip is brought into proximity of a sample surface, forces between the tip and the sample lead to a deflection of the cantilever according to Hooke's law. Depending on the situation, forces that are measured in AFM include mechanical contact force, van der Waals forces, capillary forces, chemical bonding, electrostatic forces, magnetic forces, solvatation forces, etc. Typically, the deflection is measured using a laser spot reflected from the top surface of the cantilever into an array of photodiodes (fig. 34).

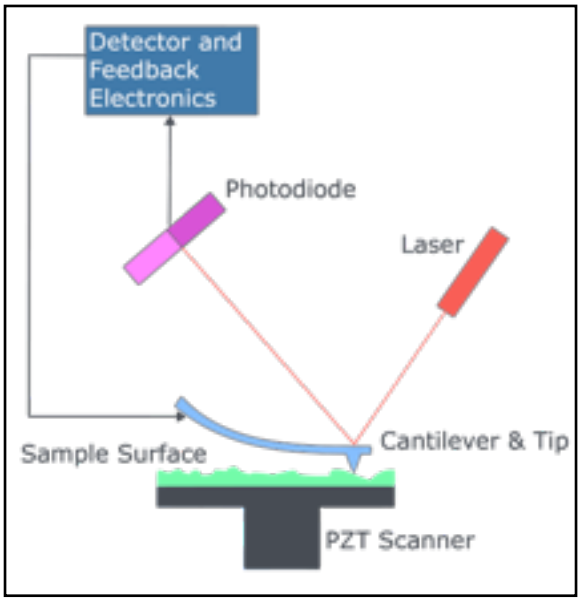

Fig. 34: Atomic Force Microscope: general scheme

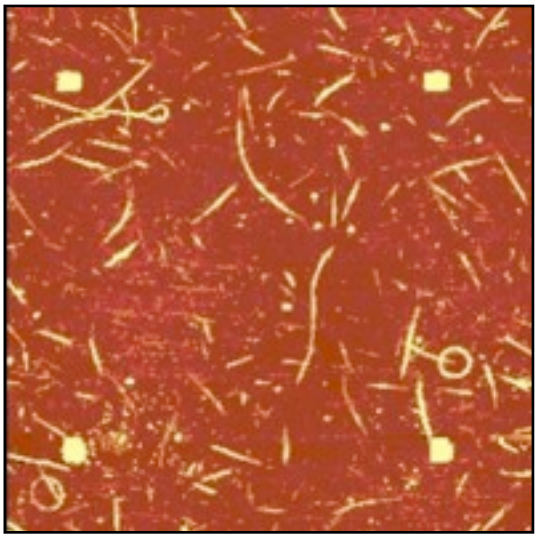

Fig 35: AFM image of a SWCNT sample

The atomic force microscopy is the most widely used instrument among scanning probe microscopy techniques. The widespread use of the AFM is attributed to the accurate three-dimensional reconstruction of the sample topography with atomic resolution for a relatively low cost and within a short time. Another important reason for using this characterization is that there is almost no restriction on the sample to be analyzed: Semiconductors, biotechnology, life sciences, materials, and surface characterizations are typical applications. In most of the cases, the morphological study is the main purpose of the AFM, since it provides almost real three dimensional topographic information. The AFM is considered a powerful tool for morphology analysis of nanoscale structures such as carbon nanotubes because it allows to realize a 3D nanotopography and morphologies profiles of the micro and nanomaterials/structures (fig. 35). With the AFM, the following characterizations of the nanomaterials are possible:

morphology: evaluation of the nanometric geometry and characteristics of the observed nanostructures.

homogeneity: determination of the statistical distribution of the various nanomaterials/ structures present in a sample.

dispersability: statistical determination of the quantity of nanostructures that form stable suspension and are found in the form of individual elements or in the form of bundles.

purity: determination, in each phase of the nanomaterials development, (synthesis, purification, integration, etc.) of the quantity of impurity particles and amorphous residues present in the sample. [90]

TEM microscopy

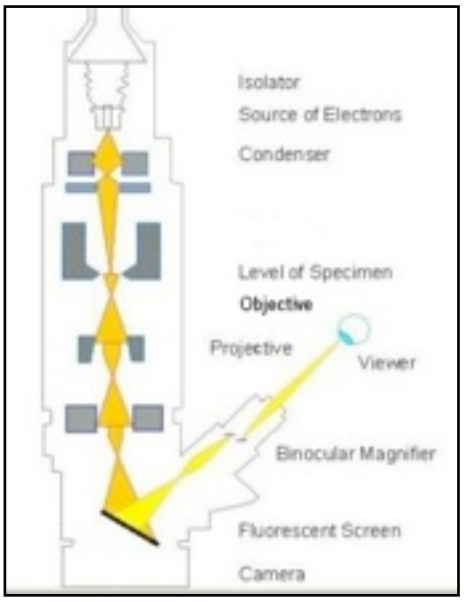

Fig. 36:Transmission Electron Microscope,

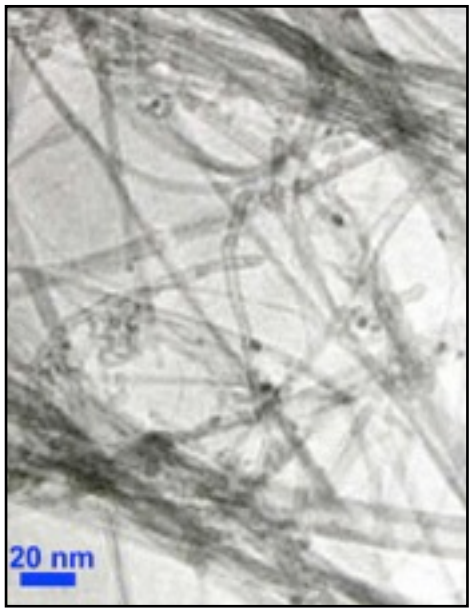

Fig. 37:TEM image of a nanotube sample

Transmission electron microscopy (TEM) is a microscopy technique where a highly focused monoenergetic beam of electrons is transmitted in vacuum through an ultra-thin specimen, interacting with the specimen as it passes through. An image is formed from the interaction of the electrons transmitted through the specimen; the image is magnified and focused onto an imaging device, such as a fluorescent screen, on a layer of

photographic film, or is detected by a sensor. A general scheme of the instrument is illustrated in figure 36.

TEM operates on the same basic principles as the light microscope but uses electrons instead of light. What you can see with a light microscope is limited by the wavelength of light. TEMs use electrons as "light source" and owing to their much lower de Broglie wavelength it is possible to get a resolution a thousand times higher than with a light microscope. This enables the instrument to be able to examine fine detail even as small as the atomic structure of the material in the sample, which is tens of thousands times smaller than the smallest resolvable object in a light microscope. TEM forms a major analysis method in a range of scientific fields, in both physical and biological sciences. TEMs find application in cancer research, virology, materials science as well as pollution and semiconductor research.

TEM is a key technique in the structural characterization of carbon nanotubes: it provides information on dispersibility, diameter, purity grade, presence of defects, length, and also functionalization of the nanotubes. However, TEM requires very thin samples, which are electron transparent. Therefore, for TEM analysis, nanotubes are typically deposited on commercial TEM grids. This procedure has two problems: in the deposition process the nanotubes can be damaged, and it does not work reliably if the nanotube density is too low.

SEM microscopy

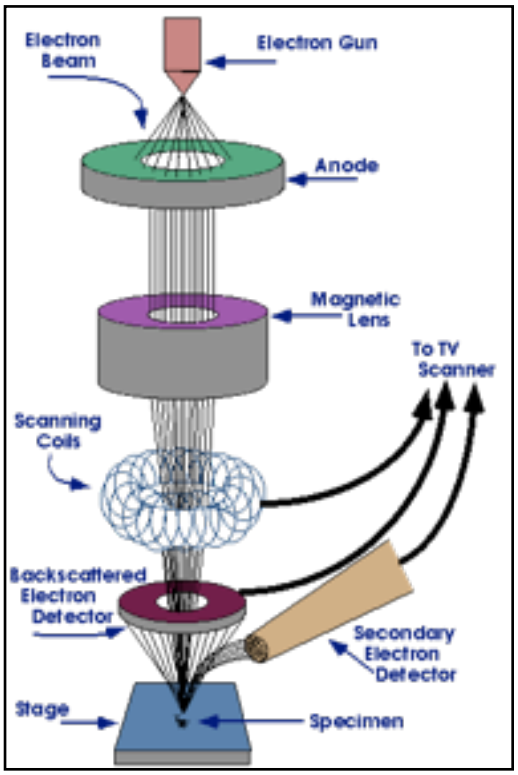

Fig. 38: Scanning Electron Microscope: general scheme

The scanning electron microscopy (SEM) is a type of electron microscopy that images the sample surface by scanning it with a high-energy beam of electrons in a raster scan pattern. The electrons interact with the atoms that make up the sample producing signals that contain information about the sample's surface topography, composition and other properties such as electrical conductivity. A general scheme of the instrument can be seen in figure 38. The SEM signals result from interactions of the electron beam with atoms at or near the surface of the sample. SEM can produce very high-resolution images of a sample surface, revealing details about less than 1 to 5 nm in size, yielding a characteristic three-dimensional image useful for understanding the surface morphology.

The morphology of CNTs, their dimension in diameter and length and their orientation can be easily revealed using SEM. The SEM microscopy has been extensively used to monitor the efficiency of the bulk- scale production of SWNTs by a variety of synthetic techniques analyzing the sample aspect in its complex. Due to its property of being a surface technique, it is particularly useful to analyze carbon nanotubes patterns in surfaces, getting a three dimensional picture of homogeneity, orientation and morphology of the tubes.

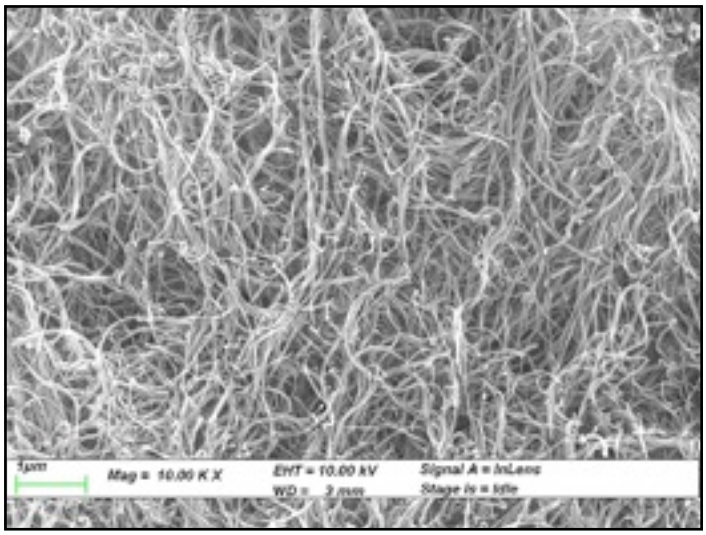

Fig. 39: SEM image of a nanotube sample

Thermogravimetric Analysis

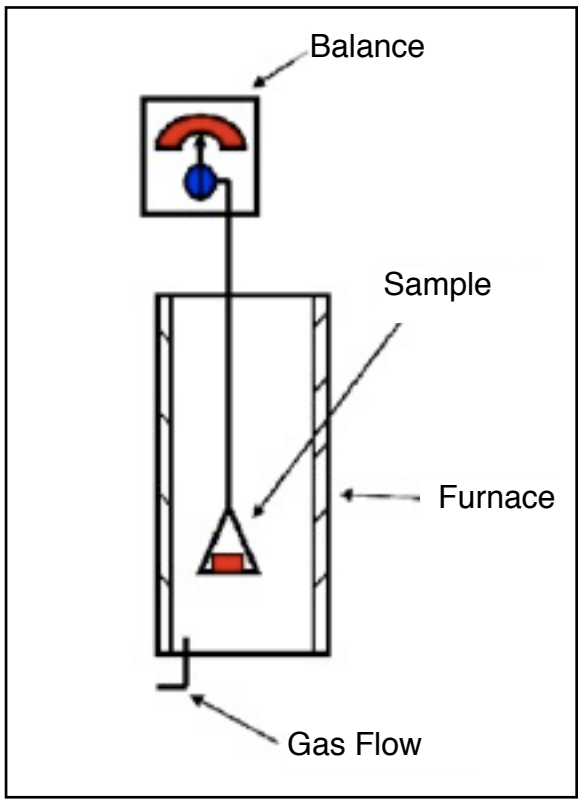

Fig. 40: TGA: general scheme

Thermogravimetric Analysis or TGA is a type of testing that is performed on samples to determine changes in weight in relation to change in temperature. Such analysis relies on three highly precise measurements: weight, temperature, and temperature change.

The analyzer consists of a high-precision balance with a pan (generally platinum) that is loaded with the sample. The pan is placed in an electrically heated oven with a thermocouple to accurately measure the temperature (see scheme in fig. 40). The atmosphere may be purged with an inert gas to prevent oxidation or other undesired reactions and to purify the environment from the gases originated by the sample decomposition. However, in some cases, an oxygen atmosphere may be required to study oxidation phenomena in the sample. A computer is used to control the instrument.

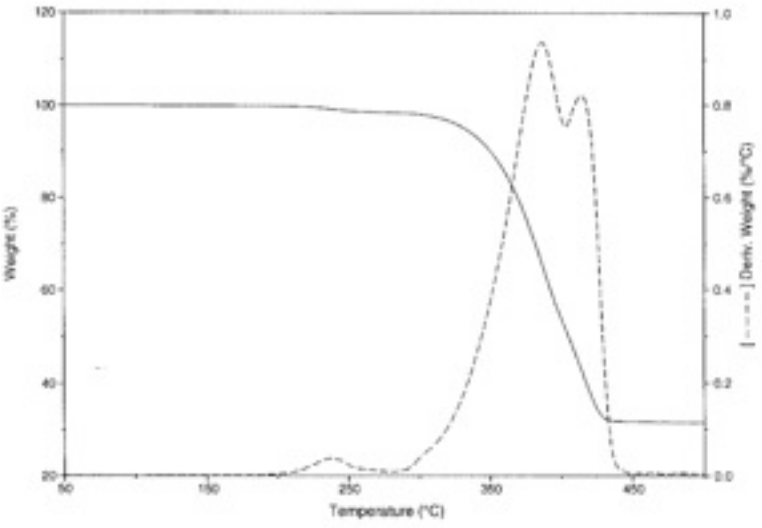

Fig 41: TGA profile of a SWCNT sample burned in air. The derivative of the curve shows two peaks the first one correspondant to the specifical combustion of amorphous carbon, the second one to CNT.

Analysis is carried out by raising the temperature gradually and plotting weight against temperature. The temperature in many testing methods routinely reaches 1000°C or greater. TGA is commonly employed in research to determine characteristics of materials, such as degradation temperatures, absorbed moisture content of metals, the level of inorganic and organic components in materials, decomposition points, and

solvent residues. Thermogravimetric analysis is a widely used analytical technique for the determination of the amount of metal catalyst in SWNT samples. If the carbon material is analyzed in oxidative atmosphere, combustion occurs and the residual weight can be associated to the metal catalysts present in the sample. The relative amount of different fractions (nanotubes, amorphous carbon and graphitic nanoparticles) in as-produced CNT can be identified if their combustion temperatures are well separated. It is imperative that proper homogenization is achieved to obtain representative test samples.[85] As in general the weight loss curves look similar, they require transformation before results may be interpreted. The derivative of the weight loss curve is generally used to tell the point at which weight loss is most apparent (fig. 41). The low temperature peak is generally associated with the amorphous carbon, while the high temperature peak is considered to originate from the CNT fraction. The fraction of metal catalyst is obtained by measuring the TGA residue after ramping of the sample temperature to 1000°C.
TGA is also an useful technique to determine the degree of derivatization in functionalized nanotubes: during the combustion of functionalized nanotubes the sample is heated in inert atmosphere, this allows the combustion of the organic functional groups and preserve the carbon structure, the weight loss corresponds to the percentage of organic material bonded to CNTs. From this data is possible to calculate the number of functional groups with respect to the number of carbon atoms and have a measure of the degree of functionalization of the tube.

1.8 Application of Carbon Nanotubes

Many potential industrial applications have been proposed for carbon nanotubes, including conductive and high-strength composites, energy storage and energy conversion devices, sensors, field emission displays and radiation sources, hydrogen storage media, and nanometer-sized semiconductor devices, probes, and interconnects (fig. 42). Some of these applications are now realized in products. Others are demonstrated in early to advanced devices or are surrounded by controversy. Nanotube cost, nanotube type, and limitations in processing and assembly methods are important barriers for some applications. [91] Here we propose a review on the main non-biological applications of CNTs, biological application of CNT will be reviewed in detail in the next paragraph.

Carbon Nanotube Composites

The first realized commercial application of CNT is their use as electrically conducting components in polymer composites. Depending on the polymer matrix, conductivity can be obtained for very low loading (5%). The low loading levels and the nanofiber morphology of the CNTs allow electronic conductivity to be achieved while avoiding or minimizing degradation of other performance aspects, such as mechanical properties. The

use of MWNTs rather than SWNTs is preferred for the lower cost, but unbundled SWNTs should enable lower percolation levels, reducing further the required loading levels.[92] Incorporation of nanotubes into plastics can potentially provide structural materials with dramatically increased modulus and strength. The critical challenges lie in uniformly dispersing the nanotubes, achieving nanotube-matrix adhesion that provides effective stress transfer.[93]

Electrochemical Devices

Because of the high electrochemically accessible surface area of porous nanotube arrays, combined with their high electronic conductivity and useful mechanical properties, these materials are attractive as electrodes for devices that use electrochemical double-layer charge injection. Examples include "supercapacitors," [94] which have giant capacities in comparison with those of ordinary dielectric-based capacitors, and electromechanical actuators, [95] that may eventually be used in robots. Supercapacitors with carbon nanotube electrodes can be used for applications that require much higher power capabilities than batteries and much higher storage capacities than ordinary capacitors. Nanotube electromechanical actuators function at a few volts, compared with the 100 V used for piezoelectric stacks and the 1000 V used for electrostrictive actuators. The success of actuator technology based on carbon nanotubes will depend on improvements in the mechanical properties of nanotube sheets and fibers with a high surface area by increasing nanotube alignment and the binding between nanotubes.

Field Emission Devices

Field emission devices have been extensively studied for technological applications such as flat panel displays, lamps, gas discharge tubes, X-ray and microwave generators. For this applications electronic materials should have the characteristic of being low field emitter and in the meantime they should be stable at high density currents. Industrial and academic research activity on electronic devices has focused mainly on using CNT as field emission electron sources [96] which are ideal candidate for their morphology, electrical properties and chemical stability. A potential applied between a carbon nanotube–coated surface and an anode produces high local fields, as a result of the small radius of the nanofiber tip and the length of the nanofiber. These local fields cause electrons to tunnel from the nanotube tip into the vacuum. Electric fields direct the field-emitted electrons toward the anode, where a phosphor produces light for the flat panel display application.

Molecular Nanoelectronics

Electronic circuits cannot continue to shrink by orders of magnitude and provide corresponding increases in computational power unless radically different device

materials architectures and assembly processes are developed. Recent dramatic advances have shown that CNT are useful for downsizing circuit dimension. For example current induced electromigration causes conventional metal wire interconnects to fail when the wire diameter becomes too small. The covalently bonded structure of carbon nanotubes militates against similar breakdown of nanotube wires, and because of ballistic transport, the intrinsic resistance of the nanotube should essentially vanish.

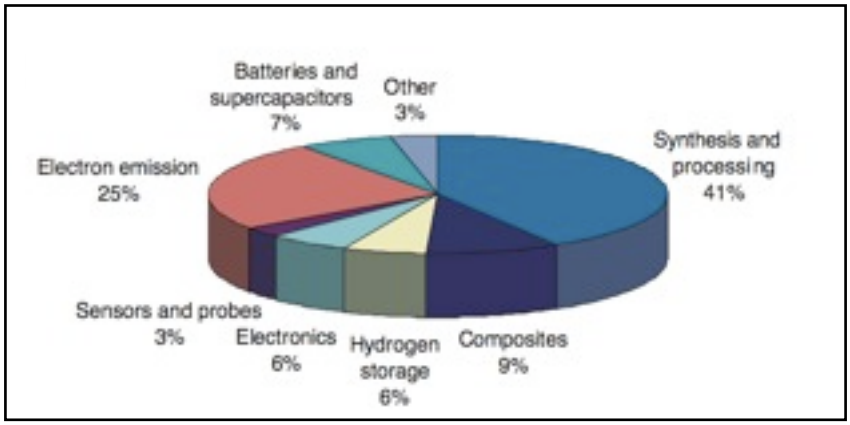

Fig. 42: Patent filligs in CNT research divided according to the main area of the invention.

1.9 Carbon Nanotubes for biological and biomedical applications

Ever since their discovery carbon nanotubes have been object of exploration of their potential in biology and medicine. [97] For biological and biomedical applications the lack of solubility of carbon nanotubes in aqueous media has been a major barrier. The recent expansion in methods to functionalize carbon nanotubes has made it possible to solubilize and disperse carbon nanotubes also in water, opening the path for their manipulation in physiological environments. Recently a huge expansion and availability of chemical modifications and bio-functionalization methods have made it possible to generate a class of "bio-active" nanotubes which are conjugated with proteins, carbohydrates or nucleic acids. The modification of a carbon nanotube on a molecular level using biological molecules is essentially an example of the bottom up fabrication principle of nanotechnology. The availability of these biomodified carbon nanotubes opens up an entire research direction in the field of chemical biology, finally aiming to target and to alter the cell's behavior at the subcellular or molecular level.

In the last years we have assisted at a noticeable development of the use of carbon nanotubes for functional biological nano-interfaces; a large number of methods for biomodification of carbon nanotubes; the development of hybrid systems of carbon nanotubes and biomolecules in the field of biosensing and bioelectronics and new

methods for carbon nanotubes as transporters for a specific delivery of peptides, genetic material and drugs to cells. All of these current research topics aim at translating these biotechnology modified nanotubes into potential novel therapeutic approaches.

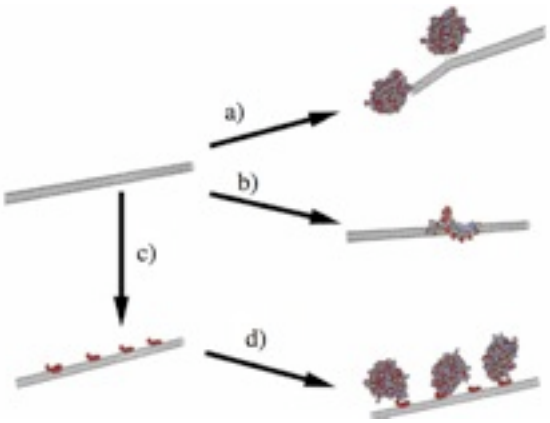

Fig. 43: the three main approaches for modifying carbon nanotubes with biomolecules: a)covalent approach; b) non covalent approach; c) hybrid approach.

With few exceptions the methods previously reviewed for the chemical functionalization of nanotubes, have been used for the indirect and direct modifications of carbon nanotubes with biomolecules. Biomolecules have been attached to the nanotubes covalently, non-covalently or by an hybrid approach which consists in linking the biomolecule of interest to a small anchor molecule which is then non-covalenty anchored to the tube. [97](fig. 43)

For example proteins can be covalently attached to nanotubes by reactions involving the amine (Lys residues and/or N-terminus residues) or thiol (Cys residues) groups. The reaction with the amine groups is more straightforward and can be performed, by the use of standard peptide coupling chemistry, between the protein and activated carboxylic groups exposed on oxidized nanotubes, or carboxylic groups exposed on a sidewall molecule previously attached to the nanotube.

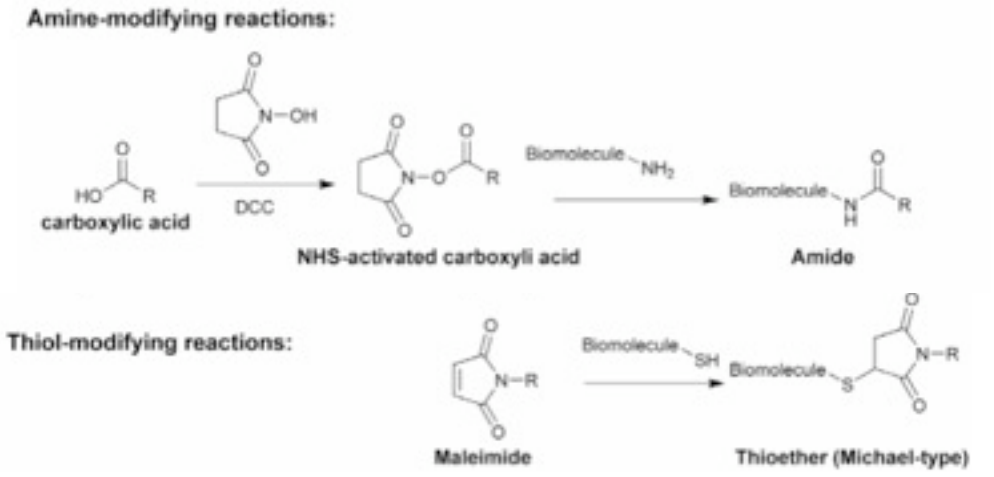

Fig. 44: the key methods for chemical attachment of biomolecules on nanotubes

While the first method of oxidizing nanotubes is the least specific and can also significantly influence the structure and properties of nanotubes, the side wall modification is much less damaging and also allows a higher specificity. The reaction with the thiol groups is more selective of that with the amino groups because usually proteins

have many lysine residues but only few possess one accessible cysteine residue available for functionalization. This reaction can take place by the introduction of a maleimide functionality on the surface of nanotubes (fig. 44).
DNA and RNA can be covalently attached to nanotubes in a similar fashion by the introduction of a short amine spacer or more frequently a thiol spacer at the 5' end of the DNA/RNA backbone.
The large aromatic hydrophobic surface of carbon nanotubes makes them ideal partners for non-covalent interactions that can take place either inside or outside the tube cavity. For example DNA has been transported through the nanotube cavity, but also the aromatic structure of the bases makes possible the non covalent interaction of the polymer with the external wall of the tube. Also other hydrophobic aromatic molecules and polymers that have a strong interaction with the tubes, can be used as a platform for the covalent attachment of variuos biomolecules, in the 'hybrid' approach. A major advantage of the non-covalent and 'hybrid' approach is that the carbon nanotube structure is not altered in any significant way. This makes it easier to compare properties such as conductivity before and after biomodification. The main disadvantages of these methods are the lack of specificity and, in some cases, denaturing of the target biomolecule upon adsorption.

Carbon nanotube based bio-electronics

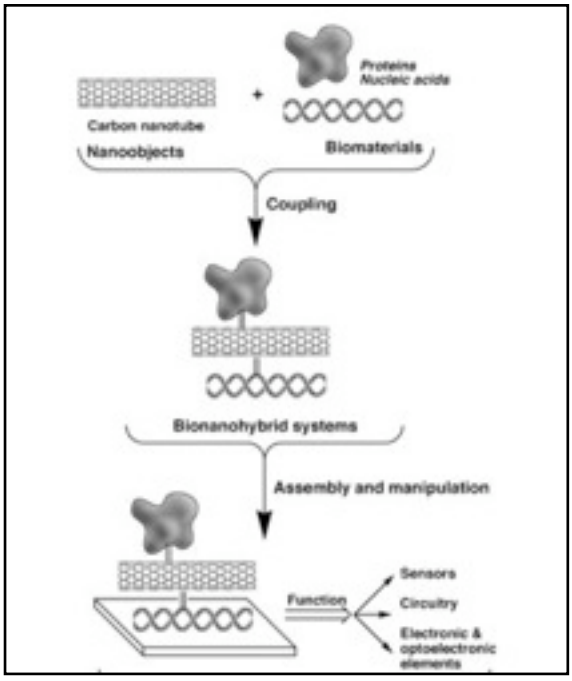

Fig. 45: The conceptual generation of biomolecule- CNT conjugates and their assembly to yield functional devices.

The integration of biomolecules with carbon nanotubes enables the use of new hybrid systems that combine the conductive or semiconductive properties of CNTs with the recognition or catalytic properties of the biomaterials (fig. 45). This may yield new bioelectronic systems (biosensors, field-effect-transistors) or templated nanocircuitry. The development of this research topic includes numerous challenging issues, such as the synthesis of site-specific and structurally-defined biomaterial-CNT hybrids, improved methods for the separation and characterization of conductive and semiconductive CNTs, the ordered and controlled assembly of addressable biomaterial-CNT systems on surfaces, and the development of microscopic imaging techniques to characterize the structures and functions of the nanoscale devices.[98] The conductive properties of CNTs suggest that they could mediate electron transfer reactions with electroactive species in solution when

used as the electrode material.[99] As electrode materials, carbon nanotubes show better behavior than traditional carbon electrodes, including a good conducting ability and high chemical stability.

It has been demonstrated that carbon nanotubes could promote electron-transfer with various redox active proteins, for example glucose oxidase.[100] For the use of carbon nanotubes in biosensing applications, however, the ability to immobilize biomolecules on the carbon nanotube structure without diminishing their bioactivity is indispensable. The device design and fabrication also play an important role in regulating their biosensing performance. For many electrochemical biosensing applications, randomly entangled carbon nanotubes have been physically coated onto conventional electrodes.[99] The use of vertically aligned carbon nanotubes [101], coupled with well-defined chemical functionalization, should offer additional advantages for facilitating the development of advanced biosensors with a high sensitivity and good selectivity.

Another promising direction for future transistor technology involves molecular electronics in which the active part of the device is composed of a single, or few molecules.[102] In 1998, Dekker and co-workers demonstrated the possibility of using an individual semiconducting SWCNT as a field-effect transistor. [103] Based on this transistor layout, several research groups started to construct SWCNT nanosensors, where the solid-state gate is replaced by nearby molecules that modulate the nanotube conductance. [104] Carbon nanotube field effect transistors have excellent operating characteristics, which are as good as, or better than, state-of-the-art silicon devices as an individual SWCNT operates as a quantum wire upon electron transfer, thus providing unique properties for its integration in field-effect transistors.

Biomedical application of carbon nanotubes

Due to the intriguing characteristics of nanotubes, there has been an increasing interest among biomedical scientists in exploring those properties for nanobiotechnology applications, such as the use of carbon nanotubes as a substrate for the growth of cells for tissue regeneration (topic that will be extensively reviewed in the next chapters), as a delivery system for a variety of diagnostic or therapeutic agents or as a vector for gene transfection.

CNT have been studied as a template for targeting bioactive peptides to the immune system. Among the many reviewed application in this field, it is worth to cite the work of Bianco et al. [105] that covalently attached the B-cell epitope of the foot-and-mouth disease virus to the amine groups present on CNTs, using a bifunctional linker. These peptide-modified CNT bioconstructs mimic the appropriate secondary structure for recognition by specific monoclonal and polyclonal antibodies. The immunogenic features of peptide-based CNT conjugates were subsequently studied *in vivo*. Immunization of mice with peptide–nanotube conjugates provided high antibody responses as compared with the free peptide. Further, the antibodies displayed virus-neutralizing ability.

Another exciting CNT research area is the study of nanotube-mediated oligonucleotide transport inside living cells. Dai and co-workers [106] demonstrated that SWNTs can be used as non-viral molecular transporters for the delivery of short interfering RNA (siRNA) into human
T cells and primary cells. The delivery ability and RNA interference efficiency of nanotubes far exceed those of several existing non-viral transfection agents, including various formulations of liposomes. It was suggested that nanotubes could be used as generic molecular transporters for various types of biologically important cells, from cancer cells to T cells and primary cells, with superior silencing effects over conventional liposome-based non-viral agents.
Biomodified CNTs can be easily labelled with a fluorescent agent and internalized into cells; the fluorescencent marker allows them to be tracked into the cytoplasm or the nucleus using epifluorescence and confocal microscopy. Kostarelos et al.[107] demonstrated that various types of functionalized carbon nanotubes exhibit a capacity to be taken up by a wide range of cells and could intracellularly traffic through different cellular barriers even under endocytosis-inhibiting conditions. Other mechanisms (such as phagocytosis), depending on cell type, size of nanotube, extent of bundling, may also be contributing to or be triggered by the ability of biomodified CNTs to penetrate the plasma membrane. The penetration of nanotubes into cells occurs by energy-independent mechanisms. The cylindrical shape and high aspect ratio of CNTs can allow their penetration through the plasma membrane, similar to a 'nanosyringe'. The use of CNTs as drug delivery system will be furtherly discussed in the appendix of this thesis.

1.10 Toxicity

The potential toxic effects of nanotubes have become an issue of strong concern for the environment and for health, which might delay the translation of appealing bench science data to relevant biomedical application in humans. Determining the toxicity of carbon nanotubes has been one of the most pressing questions in nanotechnology. Unfortunately such research has only just begun and the data is still fragmentary and subject to criticism; the difficulties in evaluating the toxicity lay in the heterogeneicity of the material. Available data clearly show that, under some conditions, nanotubes can cross membrane barriers, which suggests that if raw materials reach the organs they can induce harmful effects such as inflammatory and fibrotic reactions. [108]
A study led by A. Porter et al. shows that CNTs can enter human cells and accumulate in the cytoplasm, causing cell death. [109]
Results of studies on rodents collectively show that regardless of the process by which CNTs were synthesized and the types and amounts of metals they contained, CNTs were capable of producing inflammation, epithelioid granulomas (microscopic nodules), fibrosis, and biochemical/toxicological changes in the lungs. Comparative toxicity studies

in which mice were given equal weights of test materials showed that SWCNTs were more toxic than quartz, which is considered a serious occupational health hazard when chronically inhaled. As a control, ultrafine carbon black was shown to produce minimal lung responses.[110]

The needle-like fiber shape of CNTs, similar to asbestos fibers, raises fears that widespread use of carbon nanotubes may lead to mesothelioma, cancer of the lining of the lungs often caused by exposure to asbestos. A recently-published pilot study supports this prediction.[111] Scientists exposed the mesothelial lining of the body cavity of mice, as a surrogate for the mesothelial lining of the chest cavity, to long multiwalled carbon nanotubes and observed asbestos-like, length-dependent, pathogenic behavior which included inflammation and formation of lesions known as granulomas. According to co-author Dr. Andrew Maynard: "Although further research is required, results presented today clearly demonstrate that, under certain conditions, especially those involving chronic exposure, carbon nanotubes can pose a serious risk to human health."

1.11 References

(1) F. Henrich, C. Chan, V. Moore, M. Rolandi, M. O'Connell; "The element Carbon". *Carbon nanotubes - Properties and Applications*. New York, Taylor & Francis, **2006**.

(2) S. Subramoney; *Adv. Mater.* **1998**, *10,* 1157-1171.

(3) H. W. Kroto, J. R. Heath, S. C. O'Brien, R. F. Curl, R. E. Smalley; *Nature.* **1985**, *318,* 162-163.

(4) W. Krätschmer, L. D. Lamb, K. Fostiropoulos, D. R. Huffman; *Nature*. **1990**, *347*, 354-358.

(5) R. E. Haufler, J. Conceicao, L. P. F. Chibante, Y. Chai, N. E. Byrne, S. Flangan , M. M. Haley, S. C. O'Brien, C. Pan, Z. Xiao, W. E. Billups, M. A. Ciufolini, R. H. Hauge, J. L. Margrave, L. J. Wilson, R. F. Curl, R. E. Smalley; *J. Phys. Chem.* **1990** , *94*, 8634-8636.

(6) R. E. Smalley "Formation and properties of C_{60} and the fullerenes". National Institute of Standards and technology. 6-7/12/1990.

(7) S. IiJima; *Nature*. **1991**, *354*, 56-58.

(8) J. W. J. Wildoer, L. C. Venema, A. G. Rinzler, R. E. Smalley, C. Dekker; *Nature*. **1998**, *391*, 59-62.

(9) C. Journet, W. K. Maser, P. Bernier, A. Loiseau, M. Lamy de la Chapelle, S. Lefrant, P .Deniard, R. Lee, J. E. Fischer; *Nature*. **1997**, *388*, 756-758.

(10) S. Iijima, T. Ichihashi; *Nature*. **1993**, *363*, 603-605.

(11) D. S. Bethune, C. H. Kiang, M. S. de Vries, G. Gorman, R. Savoy, J. Vazquez, R. Beyers; *Nature*. **1993**, *363*, 605-607.

(12) X. Zhao, M. Ohkohchi, M. Wang, S. Iijima, T. Ichihashi, Y. Ando; *Carbon*. **1997**, *35*, 775 -781.

(13) C. Journet, P. Bernier; *Appl. Phys.* **1998**, *67*, 1-9.

(14) T. Guo, P. Nikolaev, A. Thess, D. T. Colbert, R. E. Smalley; *J. Phys. Chem.*, **1995**, *99*, 10694-10697. A. Thess, R. Lee, P. Nikolaev, H. Dai, P. Petit, J. Robert, C. Xu, Y. H. Lee, S. G. Kim, A. G. Rinzler, D. T. Colbert, G. E. Scuseria, D. Tomannek, S. E. Fischer, R. E. Smalley, *Science.* **1996**, *273*, 483-487.

(16) T. Guo, P. Nikolaev, A. G. Rinzler, D. Tomanek, D. T. Colbert, R. E. Smalley; *J. Phys. Chem.* **1995**, *99*, 10694-10697.

(17) T. Guo, P. Nikolaev, A. Thess, D. T. Colbert, R. E. Smalley; *Chem. Phys. Lett.* **1995**, *243*, 49-54.

(18) D. Laplaze, P. Bernier, W. K. Maser, G. Flamant, T. Guillard, A. Loiseau; *Carbon.* **1998**, *36*, 685-688.

(19) a) W. K. Hsu, J. P. Hare, M. Terrones, H. W. Kroto, D. R. M. Walton, P. J. F. Harris; *Nature.* **1995**, *377*, 687-689. b) W. K. Hsu, M. Terrones, J. P. Hare, H. Terrones, H. W. Kroto, D. R. M. Walton; *Chem. Phys. Lett*. **1996**, *262*, 161-166.

(20) M. J. Yacamàn, M. M. Yoshida, L. Rendon, J. G. Santiesteban; *Appl. Phys. Lett.* **1993**, *62*, 202-204.

(21) a) V. Ivanov, J. B. Nagy, Ph. Lambin, A. Lucas, X. B. Zhang, X. F. Zhang, D. Bernaerts, G. Van Tendeloo, S. Amelinckx, J. Van Landuyt; *Chem. Phys. Lett*. **1994**, *223*, 329-335. b) X.Y. Song, W. Cao, M.R. Ayers, A.J. Hunt; *J. Mater. Res*. **1994**, *10*, 251-254. c) N. M. Rodriguez, M. S. Kim, R. T. K. Baker; *J. Phys. Chem*. **1994,** *98*, 13108-13111.

(22) P. Nikolaev, M. J. Bronikowski, R. Kelley Bradley, F. Rohmund, D. T. Colbert, K. A. Smith, R. E. Smalley; *Chem. Phys. Lett*. **1999**, *313,* 91 – 97.

(23) H. Dai, A. G. Rinzler, P. Nikolaev, A. Thess, D. T. Colbert, R. E. Smalley; *Chem. Phys. Lett*. **1996**, *260*, 471-475.

(24) R. Khare, S. Bose; *Journal of Minerals & Materials Characterization & Engineering*. **2005**, *4*, 31-46.

(25) B. Q. Wei, R. Vajtai, P. M. Ajayan; *Appl. Phys. Lett*. **2001**, *79*, 1172-1174.

(26) S. Berber, Y. K. Kwon, D. Tomanek; *Phys. Rev. Lett*. **2000**, *84*, 4613–4616.

(27) D. H. Robertson, D. W. Brenner, J. W. Mintmire; *Phys. Rev. B*. **1992**, *45*, 12592-12595.

(28) A. Krishnan, E. Dujardin, T. W. Ebbesen, P. N. Yianilos, M. M. J. Treacy; *Phis. Rev. B*. **1998**, *58*, 14013-14019.

(29) A. J. Stone, D. J. Wales; *Chem. Phys. Lett*. **1986**, *128*, 501-503.

(30) S. Iijima; *Mrs Buletin*. **1994**, *19*, 43-49.

(31) D. Tasis, N. Tagmatarchis, A. Bianco, M. Prato; *Chem. Rev.* **2006**, *106* , 1105-1136.

(32) S. Niyogi, M. A. Hamon, H. Hu, B. Zhao, P. Bhowmik, R. Sen, M. E. Itkis, R. C. Haddon; *Acc. Chem. Res.* **2002**, *35*, 1105-1113.

(33) E. T. Mickelson, C. B. Huffman, A. G. Rinzler, R. E. Smalley, R. H. Hauge, J. L. Margrave; *Chem. Phys. Lett.* **1998**, *296*, 188-194.

(34) K. F. Kelly, I. W. Chiang, E. T. Mickelson, R. H. Hauge, J. L. Margrave, X. Wang, G. E. Scuseria, C. Radloff, N. J. Halas; *Chem. Phys. Lett*. **1999**, *313*, 445-450.

(35) E. T. Mickelson, I. W. Chiang, J. L. Zimmerman, P. Boul, J. Lozano, J. Liu, R. E. Smalley, R.H. Hauge, J. L. Margrave; *J. Phys. Chem. B.* **1999**, *103*, 4318-4322.

(36) V. N. Khabashesku, W. E. Billups, J. L. Margrave; *Acc. Chem. Res.* **2002**, *35*, 1087-1095.

(37) Y. Chen, R. C. Haddon, S. Fang, A. M. Rao, P. C. Eklund, W. H. Lee, E. C. Dickey, E. A. Grulke, J. C. Pendergrass, A. Chavan, B. E. Haley, R. E. Smalley; *J. Mater. Res.* **1998**, *13*, 2423-2431.

(38) A. Hirsch; *Angew. Chem., Int. Ed.* **2002**, *41*, 1853-1859.

(39) M. J. Moghaddam, S. Taylor, M. Gao, S. Huang, L. Dai, M. J. McCall; *Nano Lett.* **2004**, *4*, 89-93.

(40) a) V. Georgakilas, K. Kordatos, M. Prato, D. M. Guldi, M. Holzinger, A. J. Hirsch; *Am. Chem. Soc.* **2002**, *124*, 760-761. b) N. Tagmatarchis, M. Prato; *J. Mater. Chem.* **2004**, *14*, 437-440.

(41) M. Alvaro, P. Atienzar, P. de la Cruz, J. L. Delgado, H. Garcia, F. Langa; *J. Phys. Chem. B*. **2004**, *108*, 12691-12697.

(42) K. S. Coleman, S. R. Bailey, S. Fogden, M. L. H. Green; *J. Am. Chem. Soc.* **2003**, *125*, 8722-8723.

(43) B. Ni, S. B. Sinnott; *Phys. Rev. B.* **2000**, *61*, R16343-R16346.

(44) J. L. Bahr, J. Yang, D. V. Kosynkin, M. J. Bronikowski, R. E. Smalley, J. M. Tour, *J. Am. Chem. Soc.* **2001**, *123*, 6536-6542.

(45) a) M. S. Strano, C. A. Dyke, M. L. Usrey, P. W. Barone, M. J. Allen, H. Shan, C. Kittrell, R. H. Hauge, J. M. Tour, R. E. Smalley, *Science.* **2003**, *301*, 1519-1522. b) M. S. Strano; *J. Am. Chem. Soc.* **2003**, *125*, 16148-16153.

(46) J. L. Bahr, M. J. Tour; *Chem. Mater*. **2001**, *13*, 3823-3824.

(47) C. A. Dyke, M. J. Tour; *J. Am. Chem. Soc.* **2003**, *125*, 1156-1157.

(48) a) S. E. Kooi, U. Schlecht, M. Burghard, K. Kern; *Angew. Chem., Int. Ed.* **2002**, *41*, 1353-1355. b) K. Balasubramanian, M. Friedrich, C. Jiang, Y. Fan, A. Mews, M. Burghard, K. Kern; *Adv. Mater.* **2003**, *15*, 1515-1518. c) K. Balasubramanian, R. Sordan, M. Burghard, K. Kern; *Nano Lett.* **2004**, *4*, 827-830.

(49) S. Qin, D. Qin, W. T. Ford, D. E. Resasco, J. E. Herrera; *Macromolecules.* **2004**, *37*, 752-757.

(50) S. Qin, D. Qin, W. T. Ford, J. T. Herrera, D. E. Resasco, S. M. Bachilo, R. B. Weisman; *Macromolecules,* **2004**, *37*, 3965-3967.

(51) V. Ivanov, A. Fonseca, J. B. Nagy, A. Lucas, P. Lambin, D.Bernaerts, X. B. Zhang, *Carbon.* **1995**, *33*, 1727-1738.

(52) J. Chen, M. A. Hamon, H. Hu, Y. Chen, A. M. Rao, P. C. Eklund, R. C. Haddon; *Science.* **1998**, *282*, 95-98.

(53) M. A. Hamon, H. Hui, P. Bhowmik, H. M. E. Itkis, R. C. Haddon; *Appl. Phys. A.* **2002**, *74*, 333-338.

(54) a) Y. P. Sun, W. Huang, Y. Lin, K. Fu, A. Kitaygorodskiy, L. A. Riddle, Y. J. Yu, D. L. Carroll;. *Chem. Mater.* **2001**, *13*, 2864-2869. b) Y. P. Sun, B. Zhou, K. Henbest, K. F. Fu, W. J. Huang, Y. Lin, S. Taylor, D. L. Carroll; *Chem. Phys. Lett.* **2002**, *351*, 349-353.

(55) H. Li, R. B. Martin, B. A. Harruff, R. A. Carino, L. F. Allard, Y. P. Sun; *Adv. Mater.* **2004**, *16*, 896-900.

(56) a) W. Zhu, N. Minami, S. Kazaoui, Y. Kim; *J. Mater. Chem.* **2003**, *13*, 2196-2201. b) J. Zhang, G. Wang, Y. S. Shon, O. Zhou, R. Superfine, R. W. Murray; *J. Phys. Chem. B.* **2003**, *107*, 3726-3732. c) W. Zhu, N. Minami, S. Kazaoui, Y. Kim; *J. Mater. Chem.* **2004**, *14*, 1924-1926.

(57) M. G. Kahn, S. Banerjee, S. S. Wong; *Nano Lett.* **2002**, *2*, 1215-1218.

(58) C. Velasco-Santos, A. L. Martinez-Hernandez, M. Lozada-Cassou, A. Alvarez-Castillo, V. M. Castano; *Nanotechnology.* **2002**, *13*, 495-498.

(59) L. Liu, T. Wang, J. Li, Z. X. Guo, L. Dai, D. Zhang, D. Zhu; *Chem. Phys. Lett.* **2003**, *367*, 747-752.

(60) J. Liu, A. G. Rinzler, H. J. Dai, J. H. Hafner, R. K. Bradley, P. J. Boul, A. Lu, T. Iverson, K. Shelimov, C. B. Huffman, F. Rodriguez-Macias, Y. S. Shon, T. R. Lee, D. T. Colbert, R. E. Smalley; *Science.* **1998**, *280*, 1253-1256.

(61) a) P. W. Chiu, G. S. Duesberg, U. Dettlaff-Weglikowska, S. Roth; *Appl. Phys. Lett.* **2002**, *80*, 3811-3813. b) U. Dettlaff-Weglikowska, J. M. Benoit, P. W. Chiu, R. Graupner, R.; Lebedkin, S.; Roth; *Curr. Appl. Phys.* **2002**, *2*, 497-501.

(62) a) J. E. Riggs, Z. Guo, D. L. Carroll, Y. P. Sun; *J. Am. Chem. Soc.* **2000**, *122*, 5879-5880. b) R. Czerw, Z. Guo, P. M. Ajayan, Y. P. Sun, D. L. Carroll; *Nano Lett.* **2001**, *1*, 423-427.

(63) Y. Lin, S. Taylor, H. Li, K. A. S. Fernando, L. Qu, W. Wang, L. Gu, B. Zhou, Y. P. Sun; *J. Mater. Chem.* **2004**, *14*, 527-541.

(64) R. Andrews, M. C. Weisenberger; *Curr. Opin. Solid State Mater. Sci.* **2004**, *8*, 31-37.

(65) a) J. Zhu, M. Yudasaka, M. Zhang, D. Kasuya, S. Iijima; *Nano Lett.* **2003**, *3*, 1239-1243. b) J. Zhu, M. Yudasaka, M. Zhang, S. Iijima; *J. Phys. Chem. B.* **2004**, 108, 11317-11320.

(66) A. M. Rao, E. Richter, S. Bandow, B. Chase, P. C. Eklund, K. A. Williams, S. Fang, K. R. Subbaswamy, M. Menon, A. Thess, R. E. Smalley, G. Dresselhaus, M. S. Dresselhaus, *Science.* **1997**, *275*, 187-191.

(67) F. Balavoine, P. Schultz, C. Richard, V. Mallouh, T. W. Ebbesen, C. Mioskowski; *Angew. Chem., Int. Ed.* **1999**, 38, 1912-1915.

(68) B. F. Erlanger, B. X. Chen, M. Zhu, L. Brus; *Nano Lett.* **2001**, *1*, 465-467.

(69) R. J. Chen, Y. Zhang, D. Wang, H. Dai; *J. Am. Chem. Soc.* **2001**, *123*, 3838-3839.

(70) T. Takahashi, K. Tsunoda, H. Yajima, T. Ishii; *Chem. Lett.* **2002**, *31*, 690-691.

(71) C. Richard, F. Balavoine, P. Schultz, T. W. Ebbesen, C. Mioskowski; *Science.* **2003**, *300*, 775-778.

(72) a) M. Zheng, A. Jagota, E. D. Semke, B. A. Diner, R. S. McLean, S. R. Lustig, R. E. Richardson, N. G. Tassi; *Nat. Mater.* **2003**, *2*, 338-342. b) N. Nakashima, S. Okuzono, H. Murakami, T. Nakai, K. Yoshikawa; *Chem. Lett.* **2003**, 32, 456-457.

(73) M. Zheng, A. Jagota, M. S. Strano, A. P. Santos, P. Barone, S. Grace Chou, B. A. Diner, M. S. Dresselhaus, R. S. McLean, G. B. Onoa, G. G. Samsonidze, E. D. Semke, M. Usrey, D. J. Walls; *Science.* **2003**, 302, 1545-1548.

(74) a) B. W. Smith, M. Monthioux, D. E. Luzzi, *Nature.* **1998**, *296*, 323-324. (b) B. Burteaux, A. Claye, B. W. Smith, M. Monthioux, D. E. Luzzi, J. E. Fischer; *Chem. Phys. Lett.* **1999**, *310*, 21-24. c) B. W. Smith, M. Monthioux, D. E. Luzzi; *Chem. Phys. Lett.* **1999**, *315*, 31-36.

(75) a) B. W. Smith, D. E. Luzzi; *Chem. Phys. Lett.* **2000**, *321*, 169-174. b) K. Hirahara, K. Suenaga, S. Bandow, H. Kato, T. Okazaki, H. Shinohara, S. Iijima; *Phys. Rev. Lett.* **2000**, *85*, 5384-5387. c) K. Suenaga, M. Tence, C. Mory, C. Colliex, H. Kato, T. Okazaki, H. Shinohara, K. Hirahara, S. Bandow, S. Iijima; *Science.* **2000**, *290*, 2280-2282.

(76) G. H. Jeong, T. Hirata, R. Hatakeyama, K. Tohji, K. Motomija; *Carbon* **2002**, *40*, 2247-2253.

(77) K. Hirahara, S. Bandow, K. Suenaga, H. Kato, T. Okazaki, H. Shinohara, S. Iijima; *Phys. Rev. B.* **2001**, *64*, 115420/1-5.

(78) F. Stercel, N. M. Nemes, J. E. Fischer, D. E. Luzzi; *Mater. Res. Soc. Symp. Proc.* **2002**, *706*, 245-250.

(79) S. Joseph, R. J. Mashl, E. Jacobsson, N. R. Aluru; *Nano Lett.* **2003**, *3*, 1399-1403.

(80) a) S. C. Tsang, J. J. Davis, M. L. H. Green, H. A. O. Hill, Y. C. Leung, P. J. Sadler; *Chem. Commun.* **1995**, 1803-1804. b) J. J. Davis, M. l. H. Green, H. A. O. Hill, Y. C. Leung, P. J. Sadler, J. Sloan, A. V. Xavier, S. C. Tsang; *Inorg. Chim. Acta* **1998**, *272*, 261-266.

(81) I. C. Yeh, G. Hummer,; *Proc. Natl. Acad. Sci. U.S.A.* **2004**, *101*, 12177-12182.
(82) a) M. C. Gordillo, J. Marti; *Chem. Phys. Lett.* **2000**, *329*, 341-345. b) J. Marti, M.C. Gordillo; *Phys. Rev. B.* **2001**, *63*, 165430/1-5. c) J. Marti, M. C. Gordillo; *Phys. Rev. E.* **2001**, *64*, 021504/1-6.
(83) Y. Miyauchi, M. Oba, S. Maruyama; *Phys. Rev. B.* **2006**, *74*, 205440/1-6.

(84) H. Kataura, Y. Kumazawa, Y. Maniwa, I. Umezu, S. Suzuki, Y. Ohtsuka, Y. Achiba; *Synthetic Metals*, **1999**, *103*, 2555-2558.
(85) M. E. Itkis, D. E. Perea, R. Jung, S. Niyogi, R. C. Haddon. *J. Am. Chem. Soc.* **2004**, *127*, 3439-3448
(86) T. Belin, F. Epron; *Mat. Sci. Eng. B.* **2005**, *119,* 105-118.
(87) M. S. Dresselhaus, G. Dresselhaus, R. Saito, A. Jorio; *Phys. Rep.* **2005**, *409*, 47–99.
(88) A. Jorio, M. A. Pimenta, A. G. Souza, R. Saito, G. Dresselhaus, M. S. Dresselhaus; *New J. of Phys 5.* **2003**, *139*, 131-139.
(89) R. Graupner; *Journal of Raman Spectroscopy.* **2007**, *38*, 673-683.
(90) S. Bellucci, G. Gaggiotti, M. Marchetti, F. Micciulla, R. Mucciato, M. Regi; *Journal of Physics: Conference Series,* **2007**, *61*, 99-104.
(91) R. H. Baughman, A. A. Zakhidov, W. A. de Heer; Science. **2002**, *297*, 787-792.
(92) M. J. Biercuk M. C. Llaguno, M. Radosavljevic, J. K. Hyun, A. T. Johnson, J. E. Fischer; *Appl. Phys. Lett.* **2002**, *80*, 2767-2769.
(93) D. Qian, E. C. Dickey, R. Andrews, T. Rantell; *Appl. Phys. Lett.* **2000**, *76*, 2868-2870.
(94) C. Niu, E. K. Sickel, R. Hoch, D. Moy, H. Tennent; *Appl. Phys. Lett.* **1997**, *70*, 1480-1482.
(95) R. H. Baughman, C. Cui, A. A. Zakhidov, Z. Iqbal, J. N. Barisci, G. M. Spinks, G. G. Wallace, A. Mazzoldi, D. De Rossi, A. G. Rinzler, O. Jaschinski, S. Roth, M. Kertesz; *Science.* **1999**, *284*, 1340-1344.
(96) a) W. A. de Heer, A. Chatelain, D. Ugarte; *Science.* **1995**, *270*, 1179-1180. b) A. G. Rinzler, J. H. Hafner, P. Nikolaev, P. Nordlander, D. T. Colbert, R. E. Smalley, L. Lou, S. G. Kim, and D. Tománek; *Science.* **1995**, *269*, 1550-1553.
(97) W. Yang, P. Thodarson, J. J. Gooding, S.P. Ringer, F. Braet; *Nanotech.* **2007***, 18,* 412001+12.
(98) E. Katz, I. Willner; *Chem.Phys. Chem.* **2004**, *5*, 1084 - 1104.
(99) P. J . Britto, K. S. V. Santhanam, P. M. Ajayan, *Bioelectrochem. Bioenerg.* **1996**, *41*, 121-125.
(100) F. Patolsky, Y. Weizmann, I. Willner. *Angew. Chem. Int. Ed.*, **2004**, *43*, 2113-2117.
(101) L. Dai, A. Patil, X. Gong, Z. Guo, L. Liu, Y. Liu, D. Zhu, *Chem. Phys. Chem.*, **2003**, *4*, 1150-1169.
(102) C. Joachim, J. K. Gimzewski, A. Aviram; *Nature,* **2000**, *408*, 541-548.
(103) S. J. Tans, R. M. Verschueren, C. Dekker; *Nature* **1998**, *393*, 49-52.
(104) J. Kong, N. R. Franklin, C. W. Zhou, M. G. Chapline, S. Peng, K. Cho, H. J. Dai; *Science,* **2000**, *287*, 622-625.
(105) H. Dumortier, S. Lacotte, G. Pastorin, R. Marega, W. Wu, D. Bonifazi, J. P. Briand, M. Prato, S. Muller, A. Bianco; *Nano Lett.* **2006**, *6,* 1522–1528.
(106) Z. Liu, M. Winters, M. Holodniy, H. J. Dai; *Angew. Chem. Int. Edn,* **2007**, *46*, 2023–2027.
(107) K. Kostarelos, L. Lacerda, G. Pastorin, W. Wu, S. Wieckowski, J. Luangsivilay, S. Godefroy, D. Pantarotto, J. P. Briand, S. Muller, M. Prato, A. Bianco*; Nat. Nanotechnol.* **2007**, *2*, 108–113.
(108) J. Kolosnjaj, H. Szwarc, F. Moussa; *Adv Exp Med Biol.* **2007**, *620*, 181–204.
(109) A. Porter, M. Gass, K. Muller, J. N. Skepper, P. A. Midgley, M. Welland; *Nature Nanotech.* **2007**, *2*, 713-
(110) C. W. Lam, J. T. James, R. McCluskey, S. Arepalli, R. L. Hunter; *Crit Rev Toxicol.* **2006**, *36*, 189–217.
(111) C. A. Poland, R. Duffin, I. Kinloch, A. Maynard, W. A. H. Wallace, A. Seaton, V. Stone, S. Brown, W. MacNee, K. Donaldson; *Nature Nanotech.* **2008**, *3*, 423-428.

Chapter 2: Carbon Nanotubes for neural interfaces

2.1 Electrical Properties of Neurons

A cell in which the membrane response to depolarizations is non-linear, causing amplification and propagation of the depolarization itself, is called **excitable cell**. Neurons are the most common excitable cells. Apart from neurons, muscle cells are also excitable and electrical excitability can be observed in fertilized eggs, some plants and glandular tissue. In this introduction we will analyze the electrical properties that make neurons excitable cells, their characteristics, and the most common experimental methods in neurophysiology.

Membrane Potential

Each neuron has a cell membrane, made of a phospholipid bilayer. The cell membrane acts as a barrier which prevents the inside solution (intracellular fluid) from mixing with the outside solution (extracellular fluid). These two solutions have different concentrations of ions. Furthermore, this difference in concentrations leads to a difference in charge of the solutions. This creates a situation whereby one solution is more positive than the other. Therefore, positive ions will tend to gravitate towards the negative solution. Likewise, negative ions will tend to gravitate towards the positive solution. To quantify this property, the outside solution is set conventionally as the zero voltage. Then the difference between the inside voltage and the zero voltage is determined. This difference is what is commonly referred to as the **membrane potential** V_m which, for a neuron of the central nervous system, is set at -70 mV, which means that the inner part of the membrane has a lower voltage than the outside.
The membrane is nearly impermeable to ions. To transfer ions into and out of the neuron, the membrane provides two structures. **Ion pumps** use the cell's energy to continuously move ions in and out. They create concentration differences (between the inside and outside of the neuron) by transporting ions against their concentration gradients (from regions of low concentration to regions of high concentration). The **ion channels** then use this concentration difference to transport ions down their concentration gradients (from regions of high concentration to regions of low concentration). However, unlike the continuous transport by the ion pumps, the transport by the ion channels is non continuous. They only open and close in response to signals from their environment. This transport of ions through the ion channels then changes the voltage of the cell membrane.

Action Potential

An **action potential** is a transient alteration of the membrane potential across an excitable membrane in an excitable cell, such as a neuron, generated by the activity of voltage-gated ion channels embedded in the membrane [1]. Action potentials are most commonly initiated by excitatory postsynaptic potential from a presynaptic neuron. Typically, as a consequence of an electrical stimulation, neurotransmitter molecules are released by the presynaptic neurons. The arrival of the action potential opens **voltage-sensitive calcium channels** in the presynaptic membrane; the influx of calcium Ca^{++} causes vesicles filled with neurotransmitter to migrate to the cell's surface and release their contents into the synaptic cleft. These neurotransmitters then bind to receptors on the postsynaptic cell. This binding opens various types of ion channels on the postsynaptic neuron. This opening has the further effect of changing the local permeability of the cell membrane and thus the membrane potential. If the binding increases the voltage, (depolarizes the membrane), the synapse is excitatory. If, however, the binding decreases the voltage (hyperpolarizes the membrane), it is inhibitory. Whether the voltage is decreased or increased, the change propagates passively to nearby regions of the membrane. The amplitude of an action potential is independent of the amount of current which produced it. In other words, larger currents do not create larger action potentials. Therefore action potentials are said to be *all-or-none*, since they either occur fully or they do not occur at all. Instead, the frequency of action potentials is what encodes for the intensity of a stimulus.

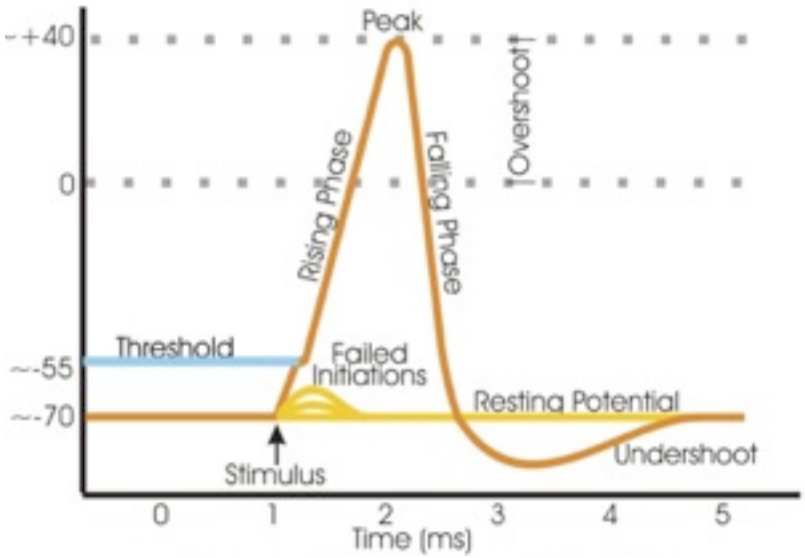

Fig.1: schematic rapresentation of the action potential

The course of the action potential can be divided into five parts: the **rising phase**, the **peak phase**, the **falling phase**, the **undershoot phase**, and finally the **refractory period** (fig. 1).

During the **rising phase** the membrane potential depolarizes (becomes more positive). This depolarization is often caused by the injection of extra sodium cations Na^+ into the cell. The initial membrane permeability to potassium K^+ is low, but much higher than that of other ions, making the resting potential close to $E_K \approx$ -70 mV. The depolarization opens both the sodium and potassium channels in the membrane, allowing the ions to flow into and out of the axon, respectively. If the depolarization is small, the outward potassium current overwhelms the inward sodium current and the membrane repolarizes back to its normal resting potential around −70 mV. However, if the depolarization is large enough, the inward sodium current increases more than the outward potassium current and a runaway condition called positive feedback results: the more inward current there is, the more *Vm* increases, which in turn further increases the inward current. A sufficiently strong depolarization causes the voltage-sensitive sodium channels to open; the increasing permeability to sodium drives *Vm* closer to the sodium equilibrium voltage $E_{Na} \approx +55$ mV. This positive feedback continues until the sodium channels are fully open.

The point at which depolarization stops is called the **peak phase**. At this stage, the membrane potential reaches a maximum. The positive feedback of the rising phase slows and comes to a halt as the sodium ion channels become maximally open. At the peak of the action potential, the sodium permeability is maximized and the membrane voltage *Vm* is nearly equal to the sodium equilibrium voltage E_{Na}. However, the same raised voltage that opened the sodium channels initially also slowly shuts them off, by closing their pores; the sodium channels become *inactivated*. This lowers the membrane's permeability to sodium, driving the membrane voltage back down. At the same time, the raised voltage opens voltage-sensitive potassium channels; the increase in the membrane's potassium permeability drives *Vm* towards E_K. Combined, these changes in sodium and potassium permeability cause *Vm* to drop quickly, repolarizing the membrane and producing the **falling phase** of the action potential.

During this stage the membrane potential **hyperpolarizes** (becomes more negative). The raised voltage opened many more potassium channels than usual, and these do not close right away when the membrane returns to its normal resting voltage. The potassium permeability of the membrane is transiently unusually high, driving the membrane voltage *Vm* even closer to the potassium equilibrium voltage E_K. Hence, there is an undershoot, a point during which the membrane potential becomes temporarily more negatively charged than when at rest, that persists until the membrane potassium permeability returns to its usual value.

Finally, the time during which a subsequent action potential is impossible or difficult to fire is called the **refractary period**, which can be divided into an *absolute refractory period*, during which it is impossible to evoke another action potential, and then a *relative refractory period*, during which a stronger-than-usual stimulus is required to provoke an action potential. These two refractory periods are caused by changes in the state of sodium and potassium channel molecules. When closing after an action potential, sodium

channels enter an inactivated state, in which they cannot be made to open regardless of the membrane potential—this gives rise to the absolute refractory period. Even after a sufficient number of sodium channels have transitioned back to their resting state, it frequently happens that a fraction of potassium channels remains open, making it difficult for the membrane potential to depolarize, and thereby giving rise to the relative refractory period.

Experimental Methods in Neurophysiology

The study of action potentials has required the development of new experimental methods.
The problem of developing fast, sensitive electronics was addressed with the development of the **voltage clamp**.[2]

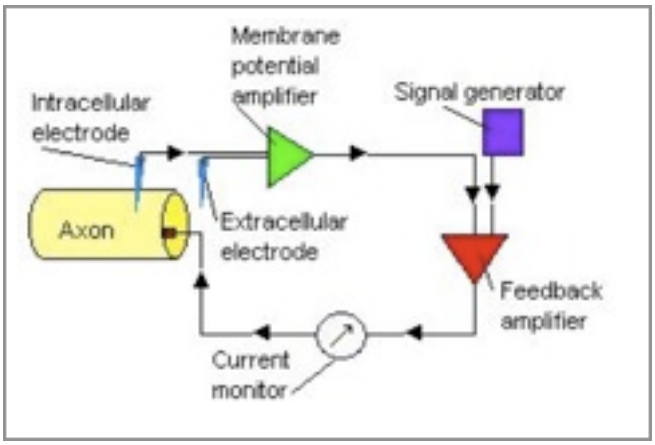

Fig 2: Scheme of the voltage clamp

The voltage clamp (fig. 2) is a current generator with two electrodes. Transmembrane voltage is recorded through a "voltage electrode", and a "current electrode" passes current into the cell. The experimenter sets a "command potential" $V_{command}$, and maintains the cell at this voltage. The electrodes are connected to an amplifier, which measures membrane potential V_m, subtracts the membrane potential from the command potential ($V_{command} - V_m$), and sends an output to the current electrode. Whenever the cell deviates from the holding voltage, the feedback circuit passes current into the cell to reduce the error signal to zero. Thus, the clamp circuit produces a current equal and opposite to the ionic current. This can be measured, giving an accurate reproduction of the currents flowing across the membrane.
Cole[2] developed the voltage clamp technique before the era of microelectrodes, so his two electrodes consisted of fine wires twisted around an insulating rod. Because this type of electrode could be inserted into only the largest cells, early electrophysiological experiments were conducted almost exclusively on **squid giant axons**. Squids squirt jets of water when they need to move quickly, as when escaping a predator. To make this escape as fast as possible, they have an axon that can reach 1 mm in diameter (signals propagate more quickly down large axons). The squid giant axon was the first preparation that could be used to voltage clamp a transmembrane current, and it was the basis of experiments on the properties of the action potential. The problem of obtaining electrodes small enough to record voltages within a single axon without perturbing it, was solved with the invention of the glass micropipette electrode,[3] which was

quicklyadopted by many researcher. Refinements of this method are able to produce electrode tips that are as fine as 100 Å, which also confers high input impedance.

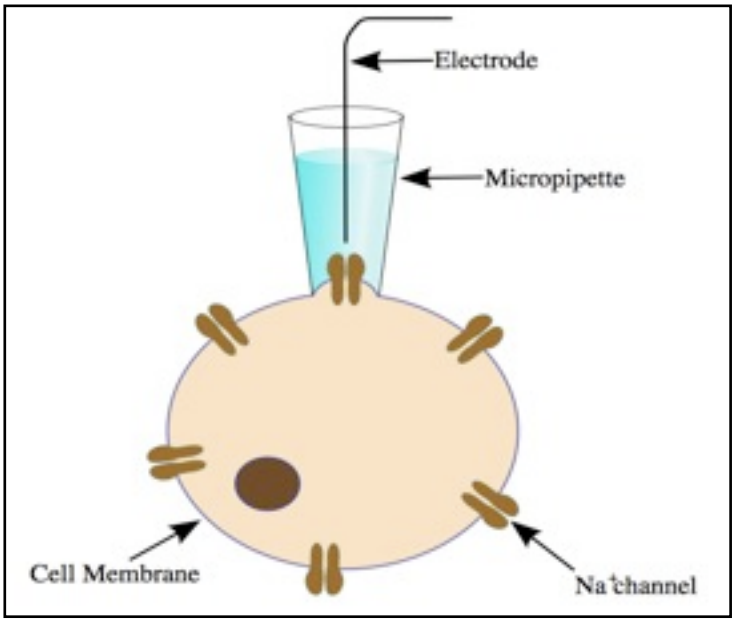

Fig. 3: Scheme of the patch clamp

The **patch clamp** technique (fig. 3) is a refinement of the voltage clamp developed by Neher and Sakmann in the late 1970s. They were awarded of the nobel prize in Physiology and Medicine in 1991 for this work.[4] This discovery made it possible to record the currents of single ion channels for the first time, proving their involvement in action potential conduction.

Patch clamp recording uses, as an electrode, a glass micropipette that has an open tip diameter of about one micrometre, a size enclosing a membrane surface area or "patch" that often contains just one or a few ion channel molecules. The interior of the pipette is filled with a solution matching the ionic composition of the bath solution, in the case of cell-attached recording, or the cytoplasm for whole-cell recording. A chlorided silver wire is placed in contact with this solution and conducts electrical current to the amplifier. The investigator can change the composition of this solution or add drugs to study the ion channels under different conditions. The micropipette is pressed against a cell membrane and suction is applied to assist in the formation of a high resistance seal between the glass and the cell membrane. The high resistance of this seal makes it possible to electronically isolate the currents measured across the membrane patch with little competing noise, as well as providing some mechanical stability to the recording. Unlike traditional two-electrode voltage clamp recordings, patch clamp recording uses a single electrode to record currents. Two different modes of recording can be used: **current clamp configuration** monitors variations in the membrane potential with the possibility of injecting currents to depolarize (positive current) o hyperpolarize (negative current) the cell; in this case spontaneous activity of neurons can be measured as a function of the number of action potentials over the time. In **voltage clamp configuration**, it is possible to record currents passing through channels present in cellular membrane at determined voltage.

2.2 Neuroscience and Nanotechnology

Nanomaterials can interact with biological systems at fundamental molecular levels with a high degree of specificity. By taking advantage of this unique molecular specificity nanotechnology can stimulate, respond to and interact with target cells and tissues in controlled ways to induce desired physiological responses.[5] An impressive space is given by current research to the application of nanotechnology in neuroscience, despite of the complexity and the difficulties associated with the study of neural cells, and this suggests the potential of the contributions that these technologies could make to neuroscience research.

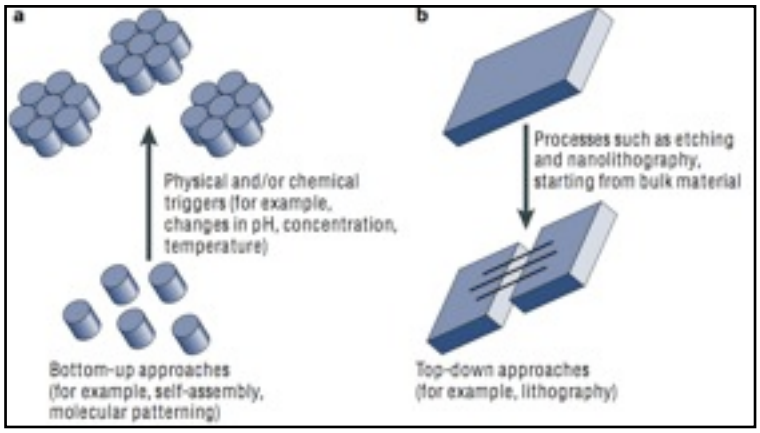

Fig. 4: a) bottom-up approach; b) top-down approach

Nanotechnology is the engineering of functional systems at the molecular scale (typically ranging from 1 to 100 nm). In its original sense, 'nanotechnology' refers to the projected ability to construct items from the **bottom up**, using techniques and tools to make complete, high performance products. This differs from the **top down** approach (fig.4) which relies essentially in breaking down a system to gain insight into its compositional sub-systems. This implies that some aspect of the material device can be manipulated and controlled by chemical and physical means at the nanometre resolution, which results in functional properties that are unique to the engineered technology and not shown by its constituent elements.

The junction between nanotechnology and neural tissues can be particularly worthy of scientific attention for several reasons: [6] first of all, neural cells are electro-active and the electronic properties of nanostructures can be tailored to match the charge transport requirements of electrical cellular interfacing. Secondly, the unique mechanical and chemical properties of nanomaterials are critical for integration with neural tissue as long-term implants, considering that solutions to many critical problems in neural biology/medicine are limited by the availability of specialized materials. For a medical scientist nanostructures represent the ideal candidate for an interface with the complex electrical properties and the nanoscale structural features of the neural tissue, because they have the potential to interact with the biological system on a molecular scale offering unprecedent levels of control. For a material scientist the rise of knowledge of the recent years on a large class of currently available nanomaterials, including nanoparticles, nanowires, multi and single walled carbon nanotubes, polymers, silicon elements and nanodevices, extensively studied and applied in other fields, such as electronics, optics

and structural composites, has already started contributing to a natural transition of their application from electronics to neural interfacing.

Current state of Neural Interface

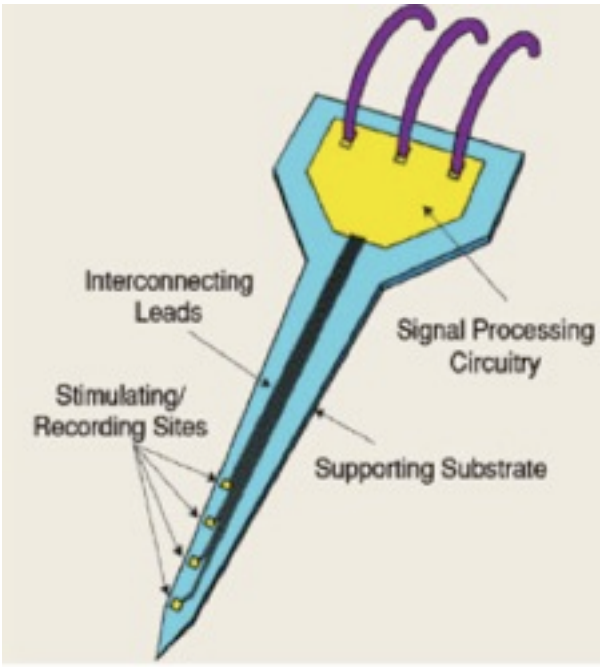

Fig.5: A neural stimulation electrode.

The history of biomedical use of electro-stimulation of neural tissues goes back in time and accompanies the process of discovery of electricity by mankind.
Nowadays diagnostic and therapeutic treatments and strategies for neural problems rely increasingly on electrical stimulation and recording techniques. There exists a wide range of health problems that can be treated by stimulation of the nervous system, including hearing loss, chronic pain, incontinence, obesity and diabetes. Some of these problems, such as paralysis or retinal degeneration, are exceptionally hard to treat. **Neural electrodes** (fig.5) have significantly improved the quality of life for an increasing number of people suffering from neurological disorder.
In order to evaluate nano-structured materials from the perspective of neural electrodes, it is necessary to give a brief overview of the actual electrical processes taking place at the neuron/electrode interface. The ability to interface with neural tissue is anchored in the movement of electrical charge between the electrode and the surrounding tissue. [7] The electrical processes taking place during stimulation and recording are almost identical, with the exception that the sequence of charge movements is reversed and magnitude of currents in the recording modality is smaller. For **stimulation**, charges are delivered **to the electrode** and induce the shift in the membrane potential of the neuron. For **recording**, the fluctuations of membrane potential cause the current to go **in and out from the electrode**. Having an effective interface is a prerequisite for both stimulation and recording although the amount of charge required for stimulation is orders of magnitude higher than what is recorded. The optimal **dimensions** of the electrode can also be quite different for stimulating and recording. For a safe stimulation, the electrode must deliver appropriate charge to the interface and tissue without inducing chemical redox reactions on the electrodes. The **material** selection for the electrode is, thus, a critical determinant for this process as the 'materials' structure can significantly impact the surface area. Electrical stimulation is typically carried out by a biphasic rectangular signal with equal cathodic and anodic charge distribution (net charge 0).[8] The **charge**

per phase and **charge density** are two parameters that commonly determine the threshold conditions for avoiding injury during electrical stimulation, thus stressing the importance of the **stimulation current magnitude and frequency**, as well as the **electrode size**, for safe and efficient stimulation. The **charge injection limit** is determined by the amount of charge that can be injected without causing electrode degradation or electrolysis of water. The **size** requirement for electrodes typically requires the electrode to be small enough to enable selective stimulation of a targeted population of neurons, with an area typically 2000 μm.[9] Several materials have already been identified as biocompatible, two of them are used most commonly in practical medicine: Pt and iridium oxide (IrO_x).

Anyway, there are practical and fundamental challenges related to the utilization and improvement of traditional neural electrodes: **reduction of the electrode size** without sacrificing the electrode ability to transfer charge is of a critical importance for the efficiency of the stimulation; most chronically implanted electrodes appear to be well tolerated initially but long-term electrode viability remains a significant problem.

It is desired that neural electrodes selectively excite or record from one neuron at a time. Reaching these capabilities will make possible fine-tuning of the curative effects, but also the reduction of the size of the electrode is intrinsically related to the reduction of injury to the tissue and scarring. The electrodes currently used in neurology are substantially larger than single cells having excitation/recording areas extending 70–150 mm in all directions from the electrode. This volume contains from dozens to hundreds of cells. The difficulties with further miniaturization are related to the limits of currently used materials in respect to charge storage capacity and impedance. Further reduction of electrode size requires the development of new materials.

From the long-term biocompatibility point of view there are some mechanical problems connected to the structure of the electrodes: many common neural electrodes are made by the deposition of a conductive and high charge capacity metal layer onto a lower performance substrate. This results in a sharp interface between the materials which generates mechanical stress between them, which is relieved only when one material becomes separated from the other. Mechanical properties of the material in contact with the cells have tremendous effect on their biological behavior.[10] Delamination of the conductive interfacial layer has been reported in many types of metal electrodes. Delamination results in the deposition of inflammatory tissues and proteins onto the electrode.[9] Another connected problem is the formation of a micro-scale gap between the device and the surrounding neural tissue. This gap causes significant reduction in the recording and charge injection capabilities over time and eventually leads to complete failure of the electrode.[11]

The functionality of currently used neural electrodes is limited due to the biological response that results from electrode implantation and their constant presence in the host tissue. [12] This chronic inflammation takes the form of glial scarring which results in replacement of neuronal cells with glial cells,[13] loss of electrode function due to encapsulation[12] and impediment to axonal re-growth.[14] Regarding the long-term (3–6 months) inflammatory response, various studies have reported astrocytic elements to

surround and encapsulate electrodes implanted in the CNS. This encapsulation causes an eventual increase in neural electrode impedance, even when systemic treatment with anti-inflammatory agents was used.[12] The size of implanted objects seems to make considerable difference in respect to activation of immune system and inflammation. Inflammation response is substantially reduced as the neural electrode become smaller.[15] Technologically, manufacturing of smaller electrodes is possible; however, the materials used do not provide sufficient charge injection capacity, interface impedance, or actual conductivity for successful reduction of neural electrodes dimensions.

Nanomaterials for neural interface

The use of nano-structured systems for neural interface brought significant success in all the directions previously mentioned such as improvement of the charge storage capacity, single neuron addressing, mitigation of inflammation.

Nanoscale **neural electrodes** have the potential to circumvent reactive biological responses by virtue of their small size and mechanical properties. For glial scarring due to chronic electrode presence, reasonably, decreased effects of electrode motion due to smaller electrode sizes and less disparity between mechanical properties of tissue and flexible nano-electrodes, should both contribute to a decreased reactive response to chronically implanted nano-electrodes.[16] Additionally, nanoscale probes have a unique potential to access neural tissue without interfering with normal physiological function. For example, nanowires probes could be introduced via catheter into the micro-vasculature of the brain, where their small dimensions would allow them to innocuously record surrounding electrical signals without interfering with blood flow or normal brain activity.[17]

A strategy that the use of nanomaterials brought as an useful tool in fighting the immune response around neural electrodes is the control of neural interfacing through nanoscale **chemical and physical patterning**. The former includes a variety of cell-adhesive and cell-repellent layers and makes possible the creation of sophisticated neural electrodes-live cell systems and unique neural devices.

A variety of surfaces have been designed to **reduce cell adhesion**, including those modified with self-assembled mono-layers (SAMs) presenting hydrocarbons,[18] mannitol, [19] PEG,[20] oligoethylene glycol (OEG),[21] and fluorinated hydrocarbons.[22] Non-polar surfaces that inhibit cell adhesion have the inconvenience of binding to hydrophobic domains of soluble proteins and thus the substrate may become less effective over time. Other surfaces, such as PEG, resist both cell and protein adhesion but can auto-oxidize in the presence of the transition metal ions at high concentration during cell culture.[21] Fluorinated hydrocarbons and OEG surfaces present an effective inert surface because they are among the most hydrophobic surfaces achievable by a SAM and are quite stable under culture conditions.[22]

Cell-adhesion coatings include factors such as poly(lysine),[23] poly(lysine) conjugated laminin,[24] fibronectin,[25] and collagen,[26] all of them adhesion proteins of the extracellular matrix. They can be patterned with nano and micro scale resolution using photolithography or microcontact printing.[27] Such patterned surfaces have been used to direct the attachment and confined growth of neurons maintaining the electrophysiological properties exhibited in bulk cultures. In a recent study,[23] sparsely plated neurons were cultured on patterned polylysine, with neurite growth guided along micropatterned lines, and it was noticed that several properties of neurons, such as the resting potential value, general electrophysiological properties, formation of functional synapses and presence of spontaneous postsynaptic currents, were similar to those of neurons grown in standard culture condition.

Physical patterning offers a potent means for the control of cell adhesion, migration, orientation, shape, and even gene expression.[28] Though surface topography and chemistry interact in a complex synergistic manner,[29] topographical cues alone are able to exert considerable influence over the cells they contact.[30] In the simplest case, nanotopography can be altered by randomly modulating a substrate's surface features (i.e.varying its roughness). Modulation of surface roughness is technically straightforward and has been applied to enhance the function of many biomedical materials, including silicon, silica, titanium, titania, stainless steel, iridium, iridium oxide and a variety of plastics used in neural medicine and neural electrodes.[31] A plausible mechanism by which nanoscale surface roughness promotes cellular adhesion is through increased contact area resulting from cell membranes conforming to fit the roughened surface.[32] An "average roughness" of 20-70 nm was found to be optimal for promoting neural adhesion and survival on etchant roughened Si. It should be noted, however, that roughness levels are difficult to define and quantify,[33] Neurons tend to attain an elongated shape within grooves due to surface-induced rearrangements of the cytoskeleton.[34] Neural growth cones are very sensitive to physical topography, even in the absence of specific biochemical cues, and this sensitivity can be exploited to achieve directed growth (fig.6). It was found that the majority of cells closely follow grooves and ridges, even over discontinuities.[28] It is interesting to compare the guidance effects of nanoscale topographical features with those exerted by chemical patterns.[29] When a range of groove depths from nanometric up to micrometric was used, it was found that the deeper the groove the more pronounced were the effects of the topography, so that at the greatest depths the nanoscale topographic groove effect dominated the chemical track effects.[29]

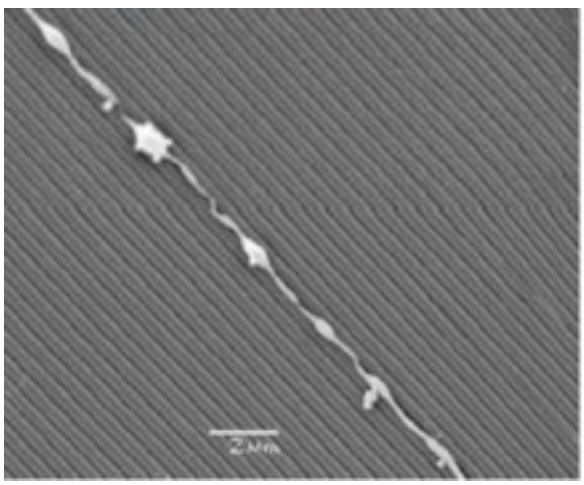

Fig. 6: Allignment of axons of adult mouse on horizontally inprinted pattern made by nanoscale contact printing.

2.3 Carbon Nanotubes for Neural Interfaces

As underlined before many challenges facing current neural electrodes are related to mechanical and electrical properties of the electrode materials. The extraordinary strength, toughness, electrical conductivity and surface area of CNTs make them excellent candidates for interfacing with neural systems for the development of biocompatible, durable, and robust neuroprosthetic devices. Mechanical compliance of highly conductive CNT composites with tissue can substantially reduce micromotions, suspected to activate fibrotic process in neural tissues, resulting in glial scarring. High surface area can drastically increase charge injection capacity [35] and decrease the interfacial impedance with neurons, which is exactly what further miniaturization of electrodes requires. Smaller size of neural electrodes will also reduce inflammatory response. Besides that, CNT coatings can also reduce delamination of electrodes from their underlying substrate. Additionally, the abundance of CNT bioactive derivatives involving biologically active components, such as peptides, proteins and DNA also allows one to consider them as a potential player in drug delivery and treatment of CNS disorders.[36]

In this section will be summarized the current state of the development of CNT/neural interface. In 2000, it was firstly suggested that CNTs could be used as substrates for neuronal growth.[37] Scanning electron microscopy (SEM) was used to identify the morphological changes of neurons brought about by MWNTs. The neuronal bodies were found to adhere to the CNT surface with neurites extending through the bed of CNT and elaborating into many branches. The neurons remained alive on the NTs for at least 11 days and it was shown that several chemical manipulations on the MWNT enhanced neurites growth and branching. After this first report, several groups developed methods of neuron culture on CNT films.[38] A similar study was carried out with living neurons on differently functionalized MWNTs films, monitored using traditional fluorescence techniques.[38a-b] The numbers of neurites were counted depending on the nature of the NT and their functionalization. The neuronal growth was systematically controlled on each chemically modified MWNT substrate and the morphological features of living neurons were characterized. It was found that neurons grown on positively charged MWNTs showed more growth cones together with more successful branching, thus simple variations in electrostatic charge on MWNT could manipulate neuronal growth patterns. A related question is whether CNTs, simply due to their intrinsic structure, can directly improve the functional rewiring of disconnected neuronal networks. The first steps toward utilization of both electrical and mechanical properties of SWNTs in neuroprosthetic devices were made with NTs films assembled using the LBL [38c-d] or other methods of making NT composite coatings with considerable adhesion to the substrate. The layering with polymers method allows one to control the structure of CNT–polymer composites and incorporate both high conductivity and high strength in one material.[39] It was demonstrated that cell cultures effectively grow and proliferate on these substrates.

Moreover, the number of neurites spun from individual cells exceeds those developed on traditional cell growth substrates.

Electrical recordings from neurons grown on carbon nanotubes substrates

The next advance in neuron–NT characterization came from the measurement of **spontaneous postsynaptic currents** (PSCs) from a single neuron which was firstly performed in our group in collaboration with Prof. Laura Ballerini.[40]
Even in absence of electrical stimulation, synapses have a certain probability of releasing neurotransmitters. This is reflected, in the electrophysiological recordings by the generation of spontaneous postsynaptic currents (PSCs). The appearance of PSCs provides clear evidence of functional synapse formation and is a widely accepted index of network efficacy.
Substrates covered with as produced MWNT (AP-MWNT) to exploit for culturing and studying the neural growth and behavior, were improved and substituted by the use of chemically modified CNT. First of all, the AP-MWNT did not adhere properly to glass, so that during the neurite growth, most of them kept floating around. Secondly, the use of a glass substrate covered with AP-MWNT was not reproducible in terms of neurite growth and elongation. AP-MWNTs also contain a number of impurities, such as amorphous carbon and especially metallic nanoparticles, which, apparently, help neither growth nor reproducibility. To obtain a homogeneous dispersion of more pure material, AP-MWTNs were functionalized using the 1,3-dipolar cycloaddition of azomethine ylides (see chapter 5, CNT1). The reaction generates MWNTs functionalized with pyrrolidine groups on the nanotube tips and sidewalls, which increase notably the solubility in organic solvents. Functionalized MWNTs (*f*-MWNT) were dissolved in dimethylformamide (DMF), and a small amount of the solution was deposited dropwise with the help of a micropipette on a glass coverslips. After evaporation of the solvent, the glass was placed in an oven at 350 °C under nitrogen atmosphere for 15 min. These conditions led to defunctionalization, leaving purified and non-functionalized MWNTs on the glass (see cap. 5, GS1)(fig. 7).

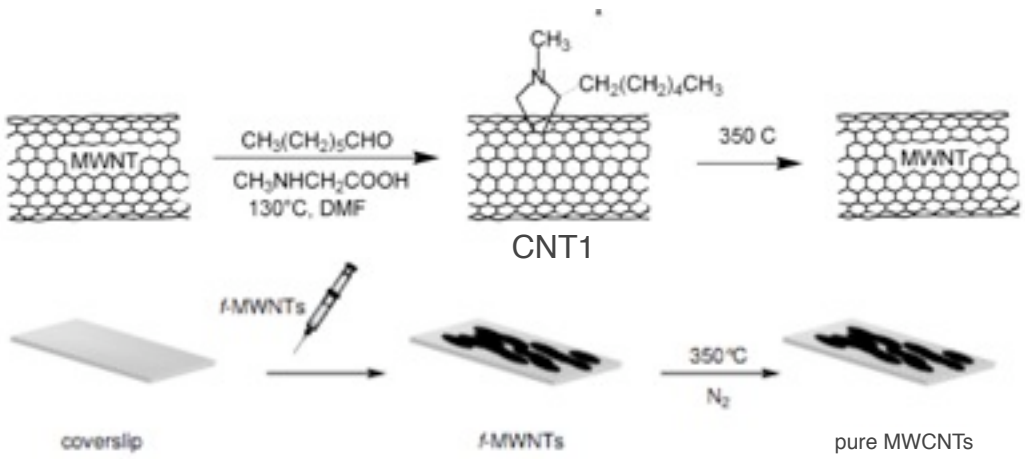

Fig 7: Scheme of the 1,3 dipolar cycloaddition reaction used to functionalize nanotubes and deposition of the functionalized nanotubes on glass coverslips. The last step at 350° provides defunctionalization.

This experimental conditions were succesfull for having a long term and stable retention of films of CNTs on glass (fig.8 A). Hippocampal neurons were seeded directly on glass coverslips, taken as control, or on a film of purified CNTs, directly layered on glass. Hippocampal neuron attachment and growth on the two different substrates were assessed first by using SEM examination after 8-10 days in vitro. As shown in Fig 8B-C, neurons grew attached to the purified CNTs and extended several neurites, which grew to various distances.

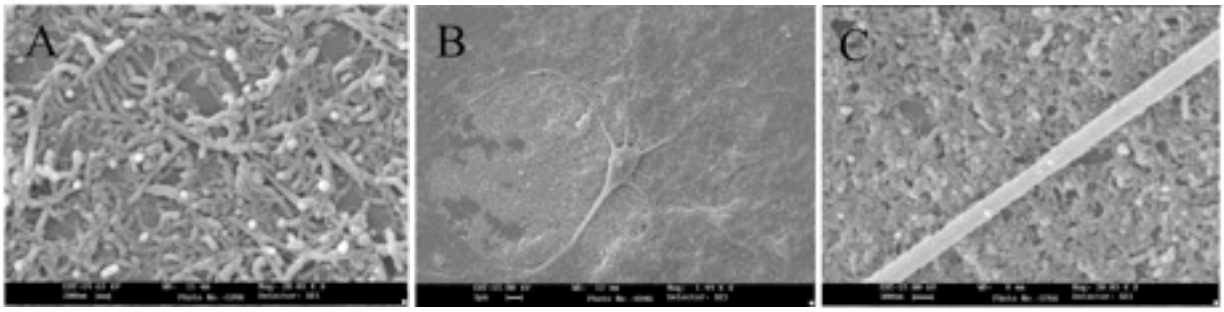

Fig.8: (A) SEM image showing the retention on glass of MWNT films after an 8-day test in culturing conditions. (B) Neonatal hippocampal neuron growing on dispersed MWNT after 8 days in culture. (C) A neurite is traveling in close contact to CNT.

To investigate neural network activity single-cell patch-clamp recording technique was used. It was monitored the occurrence of PSCs. The activity recorded from hippocampal neurons plated directly on borosilicate glass coverslips was represented by inward currents of fluctuating amplitude (fig.9) occurring at a frequency on average of 1.1 +- 0.2 Hz, in accordance to previously reported values.[41] Neurons deposited on CNTs displayed on average a 6-fold increase in the frequency of spontaneous PSCs 6.67+- 0.4 Hz. The majority of recorded hippocampal neurons possess spontaneous synaptic activity manifested as inward currents made up by a mixed population of inhibitory and excitatory PSCs.

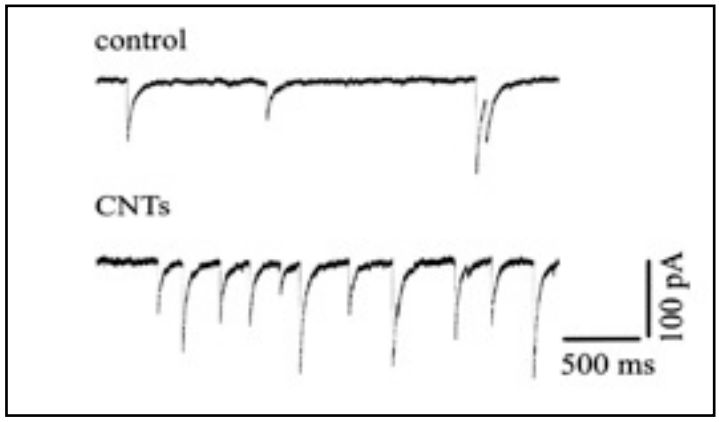

Fig 9:Spontaneous PSCs are shown in both control (top tracings) and in cultures grown on CNT substrate (bottom tracings). Note the increase in PSCs frequency under the latter condition.

The frequency of spontaneous PSCs generated by spontaneous action potential, as well as spontaneous quantal release, should mainly reflect random firing of local neurons and thus provide an index of how CNTs boosted neuronal networks function. In a group of neurons it was directly measured the spontaneous firing frequency at resting membrane potential by current clamp recordings (fig. 10). Also in this case, the CNT substrate strongly increased the average spontaneous action potential frequency of neurons from 0.22 +- 0.01 to 1.34 +- 0.69 Hz.

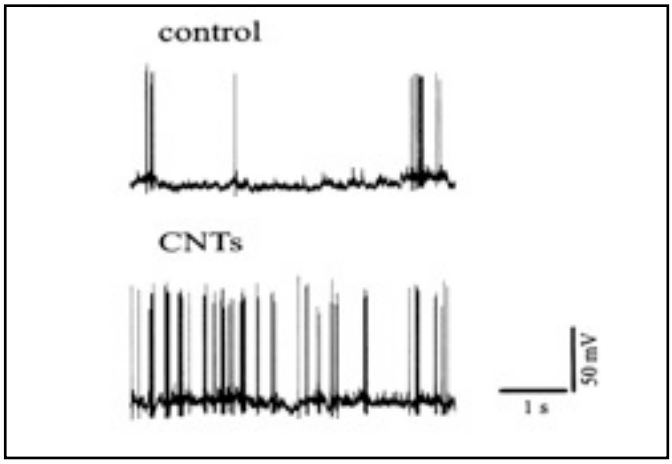

Fig 10:Current clamp recordings from cultured hippocampal neurons in control (top tracings) and CNT growth conditions (bottom tracings). Spontaneous firing activity is greatly boosted in the presence of CNT.

These results strongly suggest that growing neuronal circuits on a CNTs grid promoted a significant increase in network operation. Such an effect was not related to CNTs increasing the number of surviving neurons, suggesting that enhanced network activity was apparently related to a potentiated synaptic function more than an increase in the number of synapses. The morphology of neuronal cell grown on CNT substrates was analyzed by scanning electron microscopy (fig.11).[42] Scanning electron micrographs show that healthy hippocampal neurons adhered and grew on SWNT substrates displaying typical cell body morphology and size. Neuronal growth was accompanied by variable degree of neurite extension on the SWNT mat, similar to those observed for neurons grown on control glass surfaces. Detailed scanning electron microscopy analysis at higher magnifications of this and additional cultures suggested the presence of tight interactions between cell membranes and SWNTs at the level of neuronal processes and cell surfaces. High resolution micrographs were taken at subsequent magnifications to obtain details of a region in which a presumed afferent process contacted the neuronal cell body. By scanning the SWNT surface topography, we observed the stable retention of SWNT bundles. Such SWNT bundles appeared intermingled with neuronal membranes, and such a tight contact is potentially helpful in stabilizing electrical interfacing.

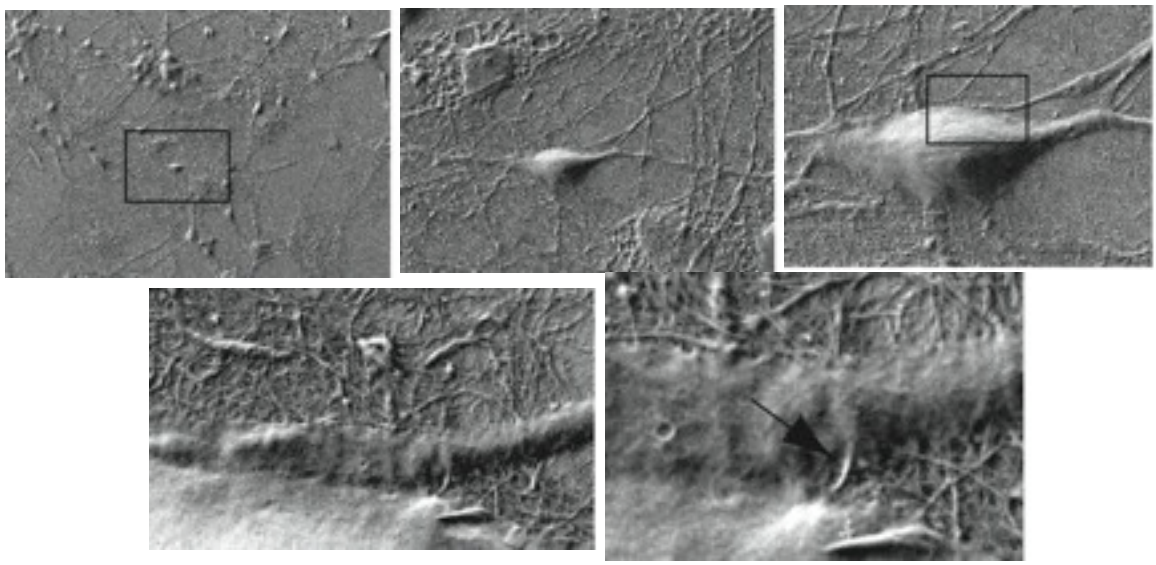

Fig.11: Subsequent micrograph at higher magnification of neurons grown on CNTs. At higher magnifications, the intimate contacts between bundles of SWNT and neuronal membrane are clearly shown.

To investigate neuronal responses to SWNT stimulations, current was delivered to neurons by patch-clamp recordings and also by delivering square-pulse voltage steps directly to the nanotubes by an Ag electrode coupled to the nanotube film. Voltage steps delivered via SWNT induced current changes as well as voltage steps of similar duration applied directly via the patch pipette. Under both stimulating conditions, large inward currents probably represent unclamped APs in distal processes. The similarity among extrinsic (via SWNT) and intrinsic (via patch pipette) stimulations is intriguing and opens several questions about the nature of the coupling between SWNT and neurons; in particular, it's important to know whether stimulating the SWNT layer effectively generates a steady current flow in the closely attached neurons. As a result of this study there is the new observation that neuronal circuits chronically grown on SWNT substrates can be effectively stimulated via the SWNT layers. This suggests that the intimate contact between the neurons and the CNT layer (fig. 11) might provide the physical substrate for neuron–CNT–neuron electrical coupling.
Indeed, the high conductivity of CNT is an interesting property in view of the extent of functional recovery in the CNS related to processes of neuronal learning, plasticity and adaptation. In this context, several important questions need to be addressed. Is the nanotube material able to transfer induced or spontaneous electrical signals generated by neurons? Can the design of the material be optimized to propagate electrical signals only in a chosen direction? What is the mechanism of the electrical interaction between CNT and neurons? If CNT are able to increase the rate of firing and of synaptic activity in a neural network, would they be suited for re-establishing communication in situations where neural communications are breaking down?

By single-cell electrophysiology in the most recent work in collaboration with Prof. Laura Ballerini,[43] we showed that direct nanotubes-substrate interactions with membranes of neurons can affect single cell activity. Neurons normally propagate action potentials down an axon. Action potentials might occasionally backpropagate to dendrites, that is against the direction flow. The interactions with nanotubes favour backpropagation of the action potential. The backpropagating current induces a voltage change that increases the concentration of Ca^{2+} in the dendrites: an event known as calcium electrogenesis; and can be measured through the presence of a slow membrane depolarization following repetitive action potentials.[44]
The experiments were conducted on the previously described glass coverslips covered by a mechanically stable film of pure, defunctionalized CNT of about 50-70 nm (cap.5: CNT1, GS1).
The effect of nanotubes on neuronal integrative properties was investigated by comparing the electrophysiology of rat hippocampal cells cultured on control substrates to those grown on a thin film of purified nanotubes for 8 to 12 days in terms of post-synaptic currents frequency, as shown previously. After this initial assessment, all recordings were conducted in the presence of 10 mM 6-cyano-7-nitroquinoxaline-2,3-dione (CNQX) and 5 mM gabazine (SR-95531), resulting in synaptic decoupling of individual neurons from each other. These chemical blockers selectively suppressed network activity while leaving

endogenous neuronal excitability unaffected, allowing us to investigate electrogenesis in isolated neurons.

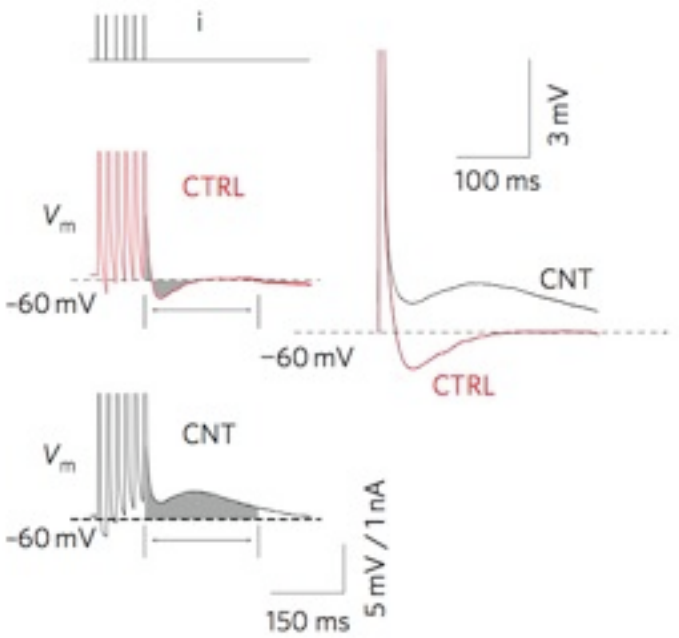

Fig.12: The nanotubes induced significantly larger after-potential depolarization (ADP) in neurons after a train of 6 subsequent action potentials. Current pulses evoke precisely timed action potentials in control (CTRL) and nanotubes (CNT). Averaged voltage trajectories V m are superimposed for comparison (right).

We studied the contribution of nanotubes to neuronal electrical regenerative properties by whole-cell current-clamp recordings from single neurons grown on nanotubes and control glass surfaces. In the first set of experiments injecting a brief current pulse into the soma, we forced the neuron to fire a regular train of six action potentials (fig. 12). The effects of the nanotubes on the integrative properties of the neurons has been recognized in the presence of additional somatic membrane depolarization after the last action potential of the train. Such an after-depolarization (ADP) represents an indirect effect of dendritic Ca^{2+} electrogenesis and is mediated by backpropagating action potentials. We computed the area under the trace in a 100 ms time window, starting at 50 ms after the last action potential of the train, taking the resting membrane potential as a reference. Note in fig. 12 the presence of the depolarizing after-potential in the presence of nanotubes.

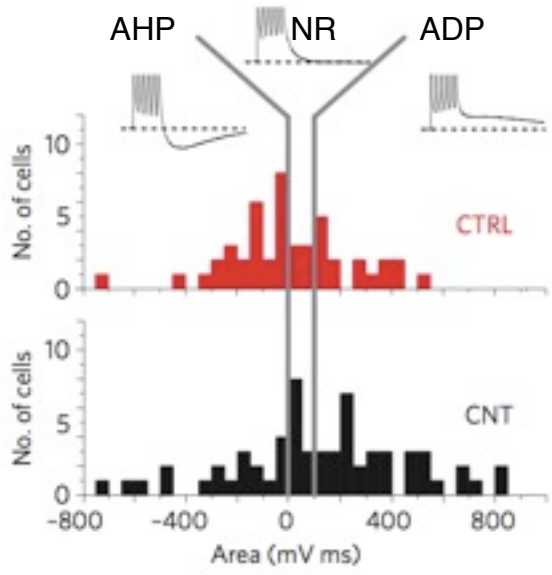

Fig. 13: Area distributions summary

Classifying the after-potential responses into three categories: after hyperpolarization (AHP), neutral response (NR) and after depolarization (ADP) we can notice that the majority (72%) of control neurons lying on glass substrates, when forced to fire action potentials trains, displayed either an AHP (47%) or NR (25%). Conversely, 54% of neurons grown on nanotubes displayed an ADP response (fig. 13) Such an ADP might reflect dendritic Ca^{2+} dependent electrogenesis.

Consistent with this hypothesis, ADP was abolished when bathed with 3 mM $CoCl_2$, a non-specific voltage-gated Ca^{2+} channel blocker. ADP could be blocked in part by 10 mM nifedipine and further abolished by co-application of 50 mM $NiCl_2$.(fig.14) These results indicated that the ADP was generated by both high and low voltage-activated Ca2+ channels. Applications of the same blockers in control neurons displaying AHP, highly increased the hyperpolarization.

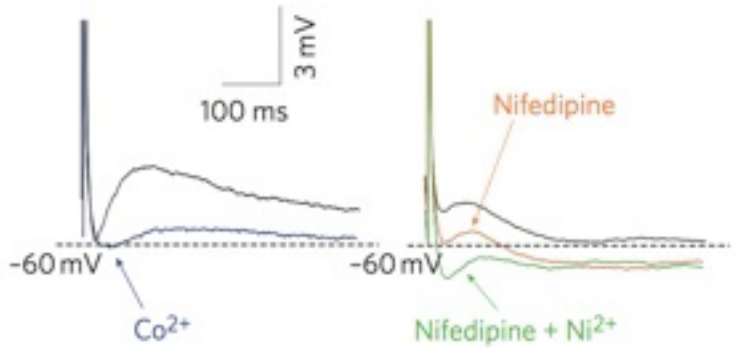

Fig. 14: Pharmacological blockade of calcium channels removed the ADP.

Action potentials, evoked by single current pulses, displayed comparable shape and amplitude in both groups (control and CNT). We observed no differences between the two groups in single action potential after-potentials, known to regulate intrinsic repetitive firing. We conclude that integration of a train of action potentials, not a single spike, is required for the ADP to appear. Testing the dendritic origin of the ADP, we also recorded responses to a train of action potentials in a different class of cultured neurons, the dorsal root ganglion cells. These neurons are considerably different from hippocampal neurons in that they have little to no dendritic arborization. Indeed, when ganglion neurons were tested they never displayed ADP at any of the spike frequencies tested.
Nanotubes substrates are electrically conductive and feature a nanoscale meshwork. In order to clarify whether both these physical properties are linked to ADP generation, hippocampal neurons were also cultured on two other substrate types: indium tin oxide (ITO), characterized by high electrical conductivity in the absence of surface nano-roughness and RADA16 (Ac – RADARADARADARADA – $COHN_2$) peptides characterized by the absence of conductivity in the presence of a clear nanoscale scaffold.

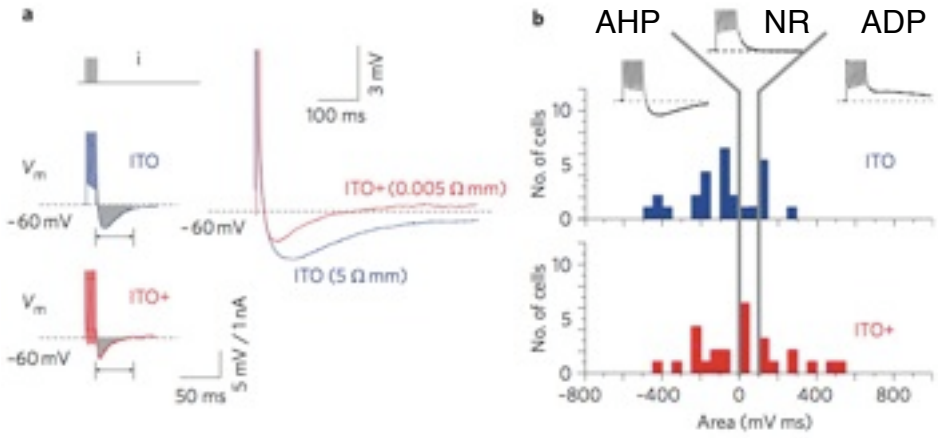

Fig. 15: ITO, sputtered on glass coverslips and used as a smooth growth substrate, did not induce ADP. a) Voltage trajectories after stimulation with a spike-train. Cells grown on ITO substrates with normal (red) and increased conductibility (blue) were similar to control. b) The ITO population summaries show significantly different distribution profiles compared to nanotubes.

We used two different types of ITO, one with resistivity similar to the nanotube substrates (blue track) and the other with a lower resistivity. Neurons attached and grew on ITO, similarly to controls on glass. The majority of ITO neurons displayed AHP or NR responses following stimulation, whereas only 21% of recorded cells underwent ADP. No correlation was observed with respect to the substrate resistance (fig.15).

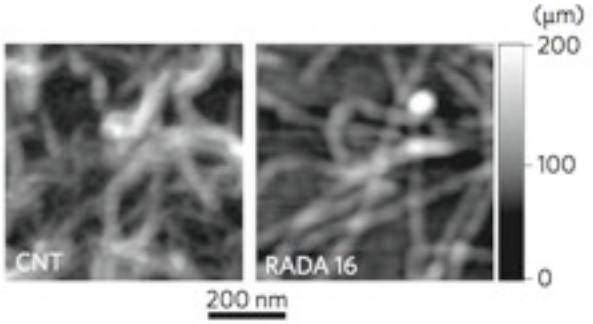

Fig. 16:AFM shows that RADA16 peptides form scaffolds similar to nanotubes

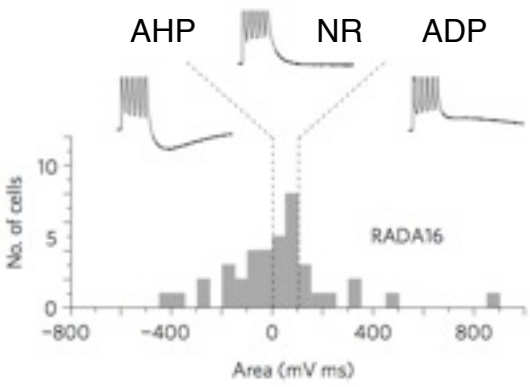

Fig.17: Population summary showed no significant difference compared to control.

RADA16 peptide substrates were layered on glass coverslips and self-assembled into nanofibres. Cultured neurons grew on the substrate, which had a local nano-meshwork similar to nanotube substrates (fig. 16) but without the conductive properties of the nanotubes. Neurons cultured on RADA16 displayed similar passive properties to those on control and nanotube substrates. When tested, RADA16 neurons replicated the control and ITO response profile, displaying in the majority of cases AHP or NR responses , with only 27.5% of neurons undergoing ADP (fig. 17). These results showed that the effects of nanotube layers on neuronal behaviour are specific and not simply reproducible by any substrate displaying either high conductivity or a clear nanostructure.

Theories to account for the increased effects of ADP might involve a potentiation of calcium-mediated currents occurring in neurons growing on nanotubes. Channels clustering, induced by mechanical interactions between nanotubes bundles and the cell cytoskeleton, might equally account for the observed ADP. Nevertheless, the formation of such 'hot-spots' for calcium currents should be limited to distal dendritic compartments, assuming that mechanical interactions between the nanotubes and the cytoskeleton might be more apparent at the small-diameter neuronal branches. Along these lines, one can also propose that both mechanical and electrical interactions of the nanotubes lead to the formation of calcium channel clusters for which the voltage gating is directly affected by the local electric field of the nanotubes.

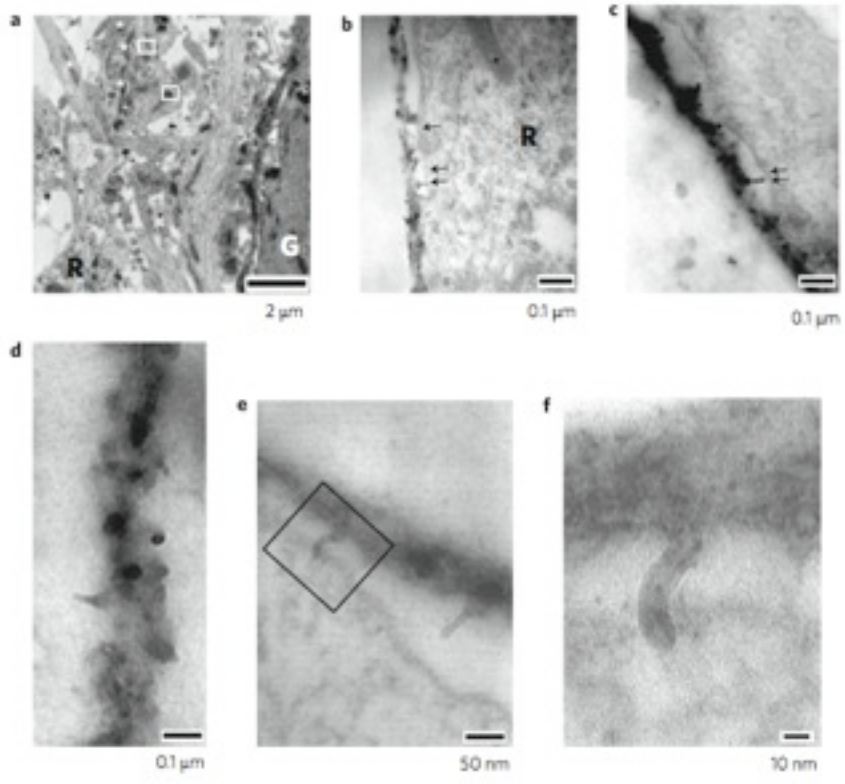

Fig. 18: a) TEM planar sections of neurons grown on nanotubes show a healthy organization of neuronal networks, with the presence of synaptic contacts (rectangular boxes). b-c) TEM sagittal sections illustrate multi-wall nanotubes – membrane contacts, indicated by arrows. d) Morphology of nanotubes. e-f) High-magnification micrographs from a section consecutive to those of b and c. The rectangular area in e is magnified in f. Note how nanotubes are 'pinching' neuronal membranes.

In fact, as a morphological evidence for this hypothesis, we investigated the presence of discontinuous and tight interactions between nanotubes and neuronal membrane by transmission electron microscopy (TEM).

Planar sections of the morphology and organization of hippocampal cells grown on nanotubes (fig 18-a) show the presence of synaptic contacts, mitochondria and ribosomes, together with clearly distinguishable longitudinal neurite sections containing bundles of microfilaments. In addition, in this section, a presumed glial cell is identified by the enhanced electron density of the cytoplasm (labelled G). All these features are indicative of healthy cultures. The same sample was further analysed in sagittal sections to visualize the zone of nanotubes – membrane contact (fig. 18 b-c). There is a recurrent, discontinuous and tight contact between the nanotubes and the neuronal membrane. Multi-wall nanotubes, in clear continuity with the nanotubes meshwork outside the neuron (fig. 18 c-e), are in intimate contact with a small area of the neuritic membranes (fig.18 c-e-f), supporting the hypothesis that intimate discontinuous interactions of nanotubes with neuronal membrane surfaces can induce specific changes in membrane electrical behaviour.

The results obtained from this work suggest that nanotubes re-engineer neuronal integrative properties in vitro. The precise mechanisms for the observed effect of nanotubes substrates in this study are not yet totally clear. TEM results suggest that one

mechanism might rely on the detected discontinuous and tight contact between nanotubes and membranes. The morphology of such contacts is indicative of the development of hybrid nanotubes – neuronal units which could be functionally different from other membrane areas. Despite all considerations on hypothetical mechanisms, the results reported indicate that nanotubes might affect neuronal information processing. It is tempting to speculate that gaining insights into the functioning of hybrid neuronal/ nanotubes networks might be relevant for the design of smart materials, triggering specific synaptic reorganization in a neuronal network.

Electrophisiology on couple of neurons

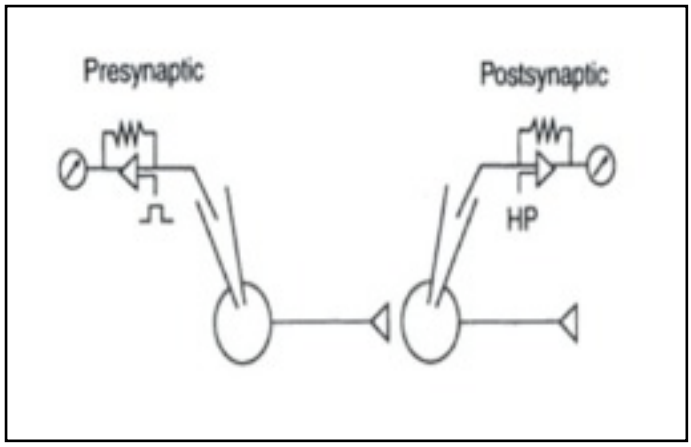

Fig. 19: Scheme of the experimental settings

With the aim to further assess and verify that neurons grown on carbon nanotubes patterns develop a higher number of synaptic connections and increase the efficacy of synaptic transmission we designed another experiment which consisted in performing pairs of neuron recordings.

In this type of experiment (fig. 19) the electrical activity of two neurons in close contact (150-200 μm) is recorded simultaneously. The first presynaptic cell is stimulated in a current clamp configuration to fire a regular train of 6 action potential of 20 Hz frequency. Contemporarily the activity of the second postsynaptic cell is recorded in voltage clamp configuration. The stimulation can lead to two different responses from the postsynaptic cell: if the cells are not synaptically coupled no electrical event will be recorded on the postynaptic cell. If, instead, the two neurons form a synapses every presynaptic action potential will start a correspondent PSC at the postsynaptic site so for each presynaptic action potential, will be present a deflection in the postsynaptic trace that represents an inward current due to the activation of postsynaptic receptors via

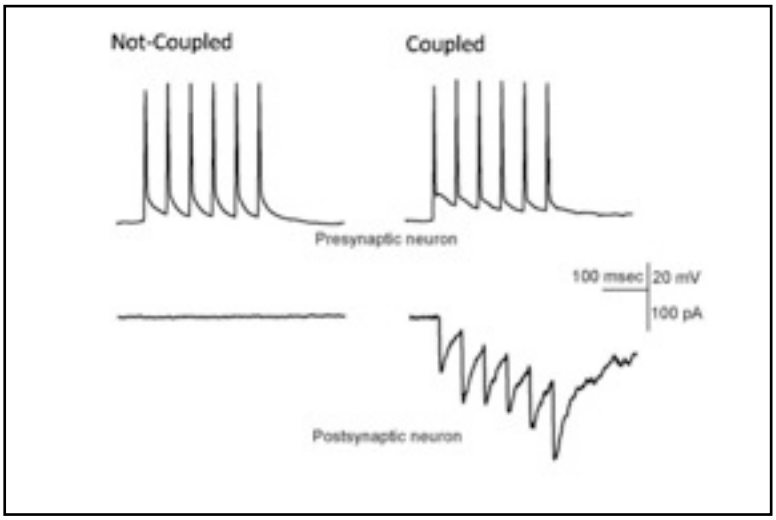

Fig.20: example of traces for couple of neurons

neurotrasmitters released at the presynaptic terminal (fig 20). As a first result, recording from a high number of couple of neurons grown on control glass substrates and on CNT substrates, we obtained that the probability to find a monosynaptic connection between the two neurons is increased in the presence of CNT (40% of neurons show synaptic connection on control substrates while 60% on CNT substrates) (fig.21). As a first observation, we can assess that neurons grown on CNT forms a larger network of functionally active contacts. This data is in accordance with the increase of the spontaneus postsynaptic activity firstly shown.[44]

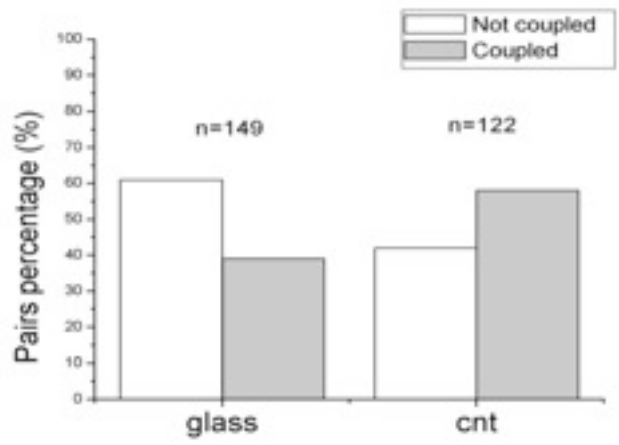

Fig. 21: statystical study on the probability to find synaptic connections between to neurons on ctrl condition and CNT

We then considered only the couple of neurons which established a synaptic contact. As mentioned, we fired in the presynaptic cell a series of 6 action potential of 20 Hz. We wanted to verify if there were differences in the trend of the postsynaptical responses of the second neuron, depending on the culture substrate (glass or CNT).

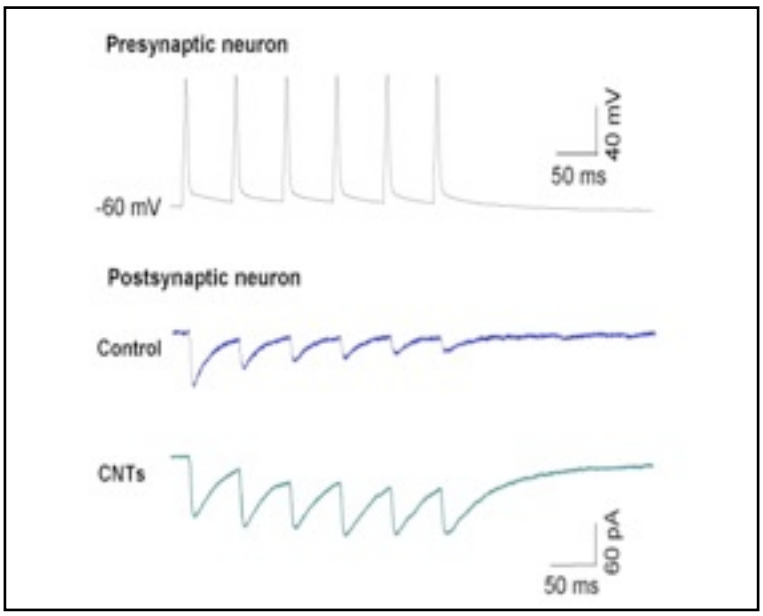

Fig.22: Difference of the postsynaptical response between neurons grown on control substrates and neurons grown on CNT

In most cases (70%), neurons grown on control substrates answer with a "depressed" trend where the subsequent responses become every time smaller in amplitude. Vice versa neurons grown on CNT show for the 40% of the cases "powered" postysynaptical responses which become every time larger in amplitude, while only 40% of them show a clear "depressed" trend (fig.22).
Even though these are still preliminary results we can already affirm that we are facing a mechanism of synaptic plasticity, where the presence of CNT strengthens and improves the communication between neurons. We are still investigating which is the real role played by CNTs in the modification of neuronal activity and thanks to this experiment we should be able to highlight whether morphological or electrical properties of CNT are determining the boosted activity of neural network.

2.4 References

(1) *D. Purves*, G. J. Augustine, D. Fitzpatrick, W. C. Hall, A. S. LaMantia, J. O. McNamara, L. E. White; *Neuroscience, 4th ed.* Sinauer Associates, **2008**.
(2) K. S. Cole; *Arch. Sci. Physiol.* **1949**, *3*, 253–258.
(3) G. Ling G, R. W. Gerard; *J. Cell. Comp. Physiol.* **1949**, *34*, 383–396.
(4) E. Neher, B. Sakmann, J. H. Steinbach; *Pflügers Archiv.* **1978**, *375*, 219–228.
(5) G.A. Silva; *Nature Rev*. **2006**, *7*, 65-74.
(6) N. A. Kotov, J. O. Winter, I. P. Clements, E. Jan, B. P. Timko, S. Campidelli, S. Pathak, A. Mazzatenta, C. M. Lieber, M. Prato, R. V. Bellamkonda, G. A. Silva, N. W. Shi Kam, F. Patolsky, L. Ballerini; *Adv. Materials*. **2009**, *21*, 1-35.
(7) D. Harnack, C. Winter, W. Meissner, T. Reum, A. Kupsch, R. Morgenstern; *J. Neurosci. Meth.* **2004**, *138*, 207-216.
(8) D. B. McCreery, W. F. Agnew, T. G. H. Yuen, L. Bullara; *IEEE Trans. Biomed. Eng.* **1990**, *37*, 996-1001.
(9) S. F. Cogan, A. A. Guzelian, W. F. Agnew, T. G. H. Yuen, D. B. McCreery; *J. Neurosci. Meth*. **2004**, *137*, 141-150.
(10) A. J. Engler, S. Sen, H. L. Sweeney, D. E. Discher; *Cell.* **2006**, *126*, 677-689.
(11) U. M. Twardoch; *J. Appl. Electrochem.* **1994**, *24*, 835-857.
(12) J. N. Turner, W. Shain, D. H. Szarowski, M. Andersen, S. Martins, M. Isaacson, H. Craighead; *Exp. Neurol*. **1999**, *156*, 33-49.
(13) R. Biran, D. C. Martin, P. A. Tresco; *Exp. Neurol.* **2005**, *195*, 115-126.
(14) S. J. A. Davies, M. T. Fitch, S. P. Memberg, A. K. Hall, G. Raisman, J. Silver; *Nature* **1997**, *390*, 680-683.
(15) Y.-T. Kim, R. W. Hitchcock, M. J. Bridge, P. A. Tresco; *Biomaterials* **2004**, *25*, 2229-2237.
(16) A. Beric, P. J. Kelly, A. Rezai, D. Sterio, A. Mogilner, M. Zonenshayn, B. Kopell; *Stereotact. Funct. Neurosurg.* **2001**, *77*, 73-78.
(17) R. R. Llinas, K. D. Walton, M. Nakao, I. Hunter, P. A. Anquetil; *J. Nanoparticle Res.* **2005**, *7*, 111-127.
(18) J. M. Corey, B. C. Wheeler, G. J. Brewer; *IEEE Trans. Biomed. Eng*. **1996**, *43*, 944-955.
(19) Y.-Y. Luk, M. Kato, M. Mrksich; *Langmuir* **2000**, *16*, 9604-9608.
(20) C. R. Jenney, J. M. Anderson; *J. Biomed. Mater. Res.* **1999**, *44*, 206-216.
(21) E. Ostuni, R. G. Chapman, R. E. Holmlin, S. Takayama, G. M. Whitesides; *Langmuir* **2001**, *17*, 5605-5620.
(22) J. B. Brzoska, I. B. Azouz, F. Rondelez; *Langmuir* **1994**, *10*, 4367-4373.
(23) C. Wyart, C. Ybert, L. Bourdieu, C. Herr, C. Prinz, D. Chatenay; *J. Neurosci. Methods* **2002**, *117*, 123-131.
(24) L. Kam, W. Shain, J. N. Turner, R. Bizios; *Biomaterials* **2001**, *22*, 1049-1054.

(25) K. K. Parker, A. L. Brock, C. Brangwynne, R. J. Mannix, N. Wang, E. Ostuni, N. A. Geisse, J. C. Adams, G. M. Whitesides, D. E. Ingber; *FASEB* **2002**, *16*, 1195-1204.
(26) S. Rohr, R. Fluckiger-Labrada, J. P. Kucera; *Eur. J. Physiol.* **2003**, *446*, 125-132.
(27) a)H. G. Craighead, S. W. Turner, R. C. Davies, C. James, A. M. Perez, P. M. St, John, M. Isaacson, W. Shain, J. N. Turner, G. J. Banker; *Biomed. Microdev.* **1998**, *1*, 49-64. b) B. Wojciak-Stothard, M. Denyer, M. Mishra, R. A. Brown; *InVitro Cell. Dev. Biol*. **1997**, *33*, 110-117.
(28) F. Johansson, P. Carlbergb, N. Danielsenc, L. Monteliusb, M. Kanjea; *Biomaterials* **2006**, *27*, 1251-1258.
(29) S. Britland, H. Morgan, B. WojiakStodart, M. Riehle, A. Curtis, C. Wilkinson; *Exp. Cell Res.* **1996**, *228*, 313-325.
(30) J. D. Foley, E. W. Grunwald, P. F. Nealey, C. J. Murphy; *Biomaterials* **2005**, *26*, 3639-3644.
(31) A. Nimmagadda, K. Thurston, M. U. Nollert, P. S. McFetridge; *J. Biomed. Mater. Res.* **2006**, *76*, 614-625.
(32) Y. W. Fan, F. Z. Cui, L. N. Chen, Y. Zhai, Q. Y. Xu, I. S. Lee; *Appl. Surf. Sci.* **2002**, *187*, 313-318.
(33) A. Curtis, C. Wilkinson; *Biomaterials* **1997**, *18*, 1573-1583.
(34) A. S. G. Curtis; *Eur. Cells Mater.* **2004**, *8*, 27-36.
(35) K. Wang, H. A. Fishman, H. Dai, J. S. Harris; *Nano Lett.* **2006**, *6*, 2043-2048
(36) S. Hampel, D. Kunze, D. Haase, K. Kaermer, M. Rauschenbach, M. Ritschel, A. Leonhardt, J. Thomas, S. Oswald, V. Hoffmann, B. Buechner; *Nanomedicine* **2008**, 3, 175-182.
(37) M. P. Mattson, R. C. Haddon, A. M. Rao; *J. Mol. Neurosci.* **2000**, *14*, 175-182.
(38) a)H. Hu, Y. Ni, V. Montana, R. C. Haddon, V. Parpura; *Nano Lett.* **2004**, *4*, 507-511. b)H. Hu, Y. Ni, S. K. Mandal, V. Montana, B. Zhao, R. C. Haddon, V. Parpura; *J. Phys. Chem. B* **2005**, *109*, 4285-4289. c) M. K. Gheith, V. A. Sinani, J. P. Wicksted, R. L. Matts, N. A. Kotov; *Adv. Mater.* **2005**, *17*, 2663-2670. d) M. K. Gheith, T. C. Pappas, A. V. Liopo, V. A. Sinani, B. S. Shim, M. Motamedi, J. P. Wicksted, N. A. Kotov; *Adv. Mater.* **2006**, *18*, 2975-2979. e) E. W. Keefer, B. R. Botternan, M. I. Romero, A. F. Rossi, G. W. Gross; *Nat. Nanotechnol.* **2008**, 3, 434-439.
(39) B. S. Shim, P. Podsiadlo, D. G. Lilly, A. Agarwal, J. Lee, Z. Tang, S. Ho, P. Ingle, D. Paterson, W. Lu, N. A. Kotov; *Nano Lett.* **2007**, 7, 3266-3273.
(40) V. Lovat, D. Pantarotto, L. Lagostena, B. Cacciari, M. Grandolfo, M. Righi, G. Spalluto, M. Prato, L. Ballerini; *Nano Lett.* **2005**, *5*, 1107-1110.
(41) J. Brask, K. Kristensson, R. H. Hill; *Eur. J. Neurosci.* **2004**, *19*, 3193-3201.
(42) A. Mazzatenta, M. Giugliano, S. Campidelli, L. Gambazzi, L. Businaro, H. Markram, M. Prato, L. Ballerini; *J.Neurosci.* **2007**, *27*, 6931– 6936.
(43) G.Cellot, E. Cilia, S. Cipollone, V. Rancic, A. Sucapane, S. Giordani, L. Gambazzi, H. Markram, M. Grandolfo, D. Scaini, F. Gelain, L. Casalis, M. Prato, M. Giugliano, L. Ballerini; *Nat. Nanotech.***2008**, *4*, 126-133.
(44) A.T. Schaefer, M. E. Larkum, B. Sakmann, A. Roth; *J. Neurophysiol*. **2003**, *89*, 3143 – 3154.

Chapter 3: Design of biocompatible surfaces based on Carbon Nanotubes

3.1 Introduction: micropatterned surface for control of cell shape, position and function

Interaction between abiotic surfaces and cells and tissue is inherent in the use of medical prosthetic implants. The ability to control the placement of cells in an organized pattern on a substrate has become increasingly important for the development of cellular biosensor technology and tissue engineering applications.[1] To directly monitor the status of sensor cells on a device requires that the cells be properly positioned on the circuit. Similarly, automation technologies to perturb and observe cells serially require that cells are positioned into addressable arrays. Finally, in aiding the process of tissue development the matrix plays a crucial role because it's responsible for defining the space that the engineered tissue occupies. Tissue engineering applications, indeed, require that cells can be specifically placed to generate organized structures, such as a neural network.
The methods to harness cells' natural affinity to specific surfaces are primarily based on chemical and topographical surface modification which alter the material surface and influence the attachment and growth of cells. In chemical modification the surface is patterned with heterogeneous regions with cell attracting and cell repelling chemistry.[2] For example, a method has been developed to fabricate "islands" of extracellular matrix (ECM) surrounded by nonadhesive regions, such that single cells would attach and spread only to the adhesive regions. This has been accomplished by microcontact printing patterns of various self-assembled monolayers (SAMs), which have been used to control the interactions of surfaces with proteins.[3]

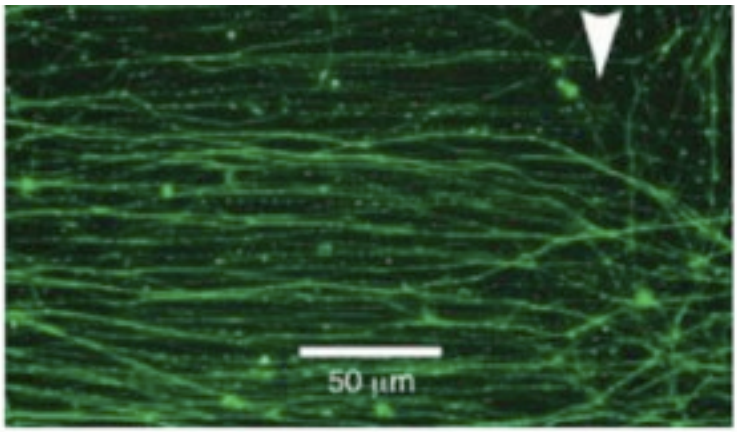

Fig.1: Alignment of axons of adult mouse sensory ganglia on horizontally imprinted pattern made by nanoscale contact printing with different topology.

Previous work has shown that, while hydrophobic SAMs rapidly and irreversibly adsorb proteins and promote cell adhesion, SAMs that present ethylene glycol moieties effectively resist protein adsorption and cell adhesion. [3] Thus, the pattern of these two SAMs presented on a substrate defines the pattern of ECM that adsorbs from solution onto the substrate, and an array of adhesive islands limits cell attachment to those islands.[1] In addition, recent work has shown that the size and geometry of these islands control cell shape,[4] enabling one to examine previously unapproachable questions regarding the mechanism by which ECM regulates cell function. More recently, nano-topography (fig. 1) was demonstrated as an alternative

effective method to control the attachment and growth of cells. Various studies have clearly demonstrated that surface texture at the scale of tens of nanometers to micrometers can influence the attachment of certain cells to surfaces and can be used as a mechanism to position cells at particular areas on a substrate.[5] It was shown that nano-scale textured silicon repelled transformed astrocytes cells, while attracting primary cortical astrocytes from neonatal rats. Both effects are attributed to the etched silicon surface. [6] The effectiveness of nano-surfaces for cell immobilization was attributed to topographical cues such as directional physical signals transmitted from adhesion to actin filaments. [7]

As already shown in chapter 2 for neural prostheses, stable external electrical stimulation of neuronal cells is a central objective for both basic studies and clinical therapies. In recent years, as shown in chapter 4, the introduction of microelectrode arrays (MEA) that conform to the spatial architecture of the particular region of interest has allowed more effective stimulation and recording.

From previous observation we have determined that carbon nanotube coated surfaces are biocompatible, provide an excellent surface for cell growth and offer high specific capacitance crucial in electrochemical applications.[8] Previous work have shown that carbon nanotube islands (in the order of 100 mm) grown on hydrophilic SiO_2 or quartz substrates form preferred surfaces for neuronal adhesion. Neuronal clusters are formed as the cells migrate on the low affinity substrate (quartz) towards high affinity, lithographically defined carbon nanotube templates on which they adhere and assemble. Subsequently, the gangliated neurons send neurites to form interconnected networks with pre-designed geometry and graph connectivity. This process is distinct from previously reported formation of clusterized neural networks.[2]

Cell Adhesion

Adhesion of tissue cells to bio-materials is an important prerequisite for the successful incorporation of implants. For **cell adhesion** we mean the binding of a cell to a surface, to the extracellular matrix or to another cell using cell adhesion molecules. *In vivo* we have specific adhesion proteins that rule the binding between cells and the interaction of cells with the extracellular matrix, such as selectins, integrins, and cadherins (fig.2).

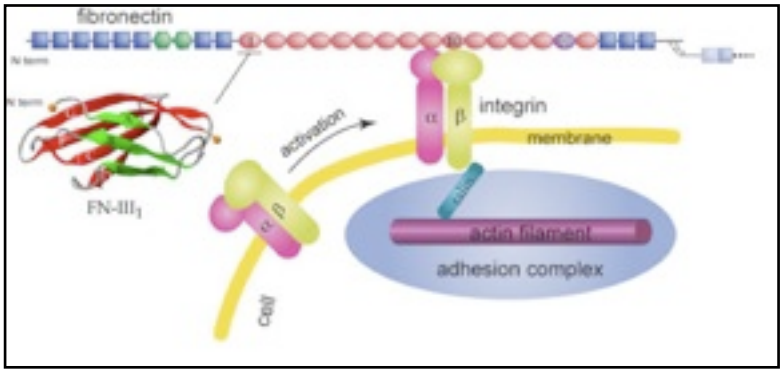

Fig 2: Mechanism of cell adhesion

These proteins are typically transmembrane receptors and are composed of three domains: an intracellular domain that interacts with the cytoskeleton, a transmembrane domain and an extracellular domain that interacts either with other adhesion proteins of the same kind (**homophilic** binding) or with other adhesion protein of the extracellular matrix (**heterophilic** binding).

Fibronectin is a typical adhesion protein that plays a major role in cell adhesion, growth, migration and differentiation, and it is important for processes such as wound healing and embryonic development.[9] **Laminin** is a glycoprotein that is an integral part of the structural scaffolding in almost every tissue of an organism. It is secreted and incorporated into cell-associated extracellular matrices. Laminin is vital for the maintenance and survival of tissues. Defective laminins can cause muscles to form improperly, leading to a form of muscular dystrophy, lethal skin blistering disease (junctional epidermolysis bullosa) and defects of the kidney filter (nephrotic syndrome).[10] In particular laminin has a role in neural development: it is a major substrate along which nerve axons will grow, both *in vivo* and *in vitro*.[11] For example, it lays down a path that developing retinal ganglion cells follow on their way from the retina to the tectum. It is also often used as a substrate in cell culture experiments. Interestingly, the presence of laminin can influence how the growth cone responds to other cues. For example, growth cones are repelled by netrin when grown on laminin, but are attracted to netrin when grown on fibronectin. This effect of laminin probably occurs through a lowering of intracellular cyclic AMP.

Considering the structural complexity and the difficult availability of the adhesion proteins, in spite of their pharmacological importance in the understanding of the cellular physiology development and also the mechanism of some diseases research has focused on developing RGD peptides that could mimic cell adhesion proteins and bind to integrins.

RGD peptides are amminoacidic chains of various length, starting from simple tripeptides, characterized by the presence within their structure of the Arginine - Glicine - Aspartic Acid peptide sequence (RGD represents the abbreviation of this three amminoacids). The RGD sequence is charactetristic of fibronectin and other components of the extracellular matrix so it allows the adhesion of particular cell lines by recognition of the sequence from the adhesion transmembrane proteins exposed on the cell surface. This amminoacidic sequence is throughly diffused in the body and is connected to many physiological functions. The diverse applications in pharmacological research for these peptides include inhibiting apoptosis, angiogenesis, and tumor formation, coating surfaces for use as biomaterials, enhancing drug delivery systems, and imaging for diagnostic purposes.

RGD peptides are attractive because they can mimic aspects of both the mechanical and biochemical properties of the extracellular matrix. In doing so, they can signal and induce very specific responses in neurons. So bioactive and biocompatible peptide-based self-assembling nanofibers that form self-supporting scaffold materials are being developed for neural regeneration applications.[12]

3.2 Aim of the work

In aiding the process of tissue development the matrix plays a crucial role because it's responsible for defining the space that the engineered tissue occupies. As a consequence of the previous observation with this work we intend to proceed in the study of the interaction between carbon nanotubes and neurons. If we want to reproduce as close as possible the *in vivo* tissue organization we must design substrates with a specific nano architecture that allow optimal structural support for axonal re-growth and affect cellular orientation. The recent development in nanotechnology has opened up novel frontiers in surface functionalization and characterization and to our aim it is highly desirable to prepare ordered micro-patterned CNT based surfaces so that the properties of individual nanotubes can be effectively probed for their possible incorporation into devices.
Also, adhesion of tissue cells to bio-materials is an important prerequisite for the successful incorporation of implants. *In vivo* we have specific adhesion proteins that rule the binding between cells and the interaction of cells with the extracellular matrix. To this issue CNT, not only are structural suitable material for tissue engineering, but more than that, can be functionalized by bioactive molecules to provide additional capabilities, for example adhesion peptides, which are currently used in neurobiology to rule the adhesion of cells when coltured on surfaces. Also they can be functionalized to release bioactive factors: it has been shown that such factors can be attached to nanotubes and still retain the enzymatic activity and control the cell growth.[13]
As far as we know neurons have been grown on several substrates designed with specific micro-architectures to allow optimal structural support and affect cellular orientation. Also, different bio-molecules have been anchored to such substrates with the purpose to understand how cells perceive information and respond. It is desirable to understand how implant surfaces should be composed to support the attachment, growth and function of cells. CNT have been demonstrated to be such a promising candidate as main constituent of neural prothesis in tissue engineering. Nevertheless, working with CNT presents many difficulties in current handling and characterization. In CNT samples we commonly deal with the presence of individual nanotubes of different length, diameter, chirality and electrical conductivity, thus it is not easy to correlate directly the enhancement of neural network activity with the concentration and composition of nanotubes. A step of fundamental importance to future development is to obtain an organized pattern of CNT to study neural communication and organization on surfaces. We believe that, in order to obtain a reproducible and as homogeneous as possible CNT-based substrate, it is necessary to use covalent chemistry. Self-assembling monolayers of organo-silanes have been successfully used to functionalize silicon oxide surfaces and they have been characterized to evaluate the effect of surface charge, wettabitlity and topography on cell behavior.[14] In our work we propose to use organo-silanes as an organic linker to attach covalently CNT on glass in order to dispose of covalent monolayers of CNT to be used and exploited for the study and characterization of neural cellular response. All the methods to chemically

functionalize carbon nanotubes can be used to attach directly or indirectly biomolecules to the carbon skeleton. The modification of a carbon nanotube on a molecular level using biological molecules is essentially an example of the 'bottom-up' fabrication principle of bionanotechnology. In this work we propose the double functionalization of carbon nanotubes, to exploit one functional moiety for the bond to the inorganic surface of glass by the use of silane coupling agents, and the other functional moiety to the bond with a biomolecule of interest, in this case RGD peptide, finally aiming to study the neural response and understand if the the cell's behaviour is in any way altered at the subcellular or molecular level.

3.3 Surface functionalization by CNT

Glass coverslips have been covalently functionalized by carbon nanotubes. The approach chosen to attach CNT on the surface was to create a SAM of a silane coupling agent on the glass surface.

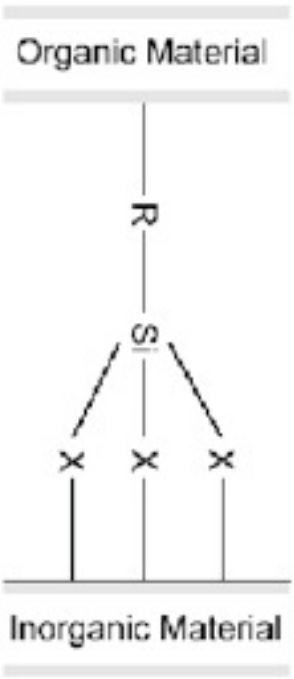

Fig. 3: General mechanism of surface functionalization by a silane coupling agent.

Silane coupling agents belong to a class of organosilane compounds having at least two reactive groups of different types bonded to the silicon atom in a molecule. They are commonly used to activate surfaces for subsequent immobilization of other molecules. The attachment is possible because the silane reagent activates the surfaces introducing a new reactive site as a location for subsequent attachments. One of the alkoxylic groups (ex. methoxy, ethoxy and silanolic hydroxy groups) is reactive with various inorganic materials such as glass, metals, silica sand and is able to form a chemical bond with the surface of the inorganic material while the other reactive groups (ex, vinyl, epoxy, methacryl, amino and mercapto groups) is reactive with various kinds of organic materials. The general structure of the molecule is a tetravalent silicon atom bearing three alkoxylic groups and as a fourth substituent an alkylic chain that bears a terminal organic moiety. The silane enables covalent linkage to a silanol-covered surface.[15] This is possible exploiting the different strength of the Si-C bond and the Si-O bond. In the presence of silanol groups the alkoxylic group is removed by hydrolysis and the silane molecule is attached to the silanol covered surface by the bond Si-O-Si, creating a network on the silanol-covered surface and leaving the alkylic chain exposed on the surface and free for subsequent functionalization. As a result of possessing these two types of reactive groups, silane coupling agents are capable of providing chemical bonding between an organic material

and an inorganic material (fig. 3). This unique property of silane coupling agents is utilized widely in surface chemistry for the treatment of glass fiber products, improvement of fiber-reinforced plastics, improvement of paints and adhesives, modification of surface properties of inorganic fillers, surface priming of various substrate materials, etc.

Functionalization of glass surfaces

Among a large variety of solid supports, glass surfaces were preferred because of ready availability, low cost, and easy surface modification techniques, but especially because all the morphological studies and recordings of neural substrates used an inverted microscope that needs transparent substrates to work. We first created a SAM of a long chain bromo-alkylsilane on the chosen surface following a standard procedure. The terminal bromide on the monolayer was easily converted to an azide group by substitution with sodium azide under usual conditions. This azide function was now ready for a 'click' cycloaddition reaction with a suitably functionalized nanotube (fig. 4).[16]

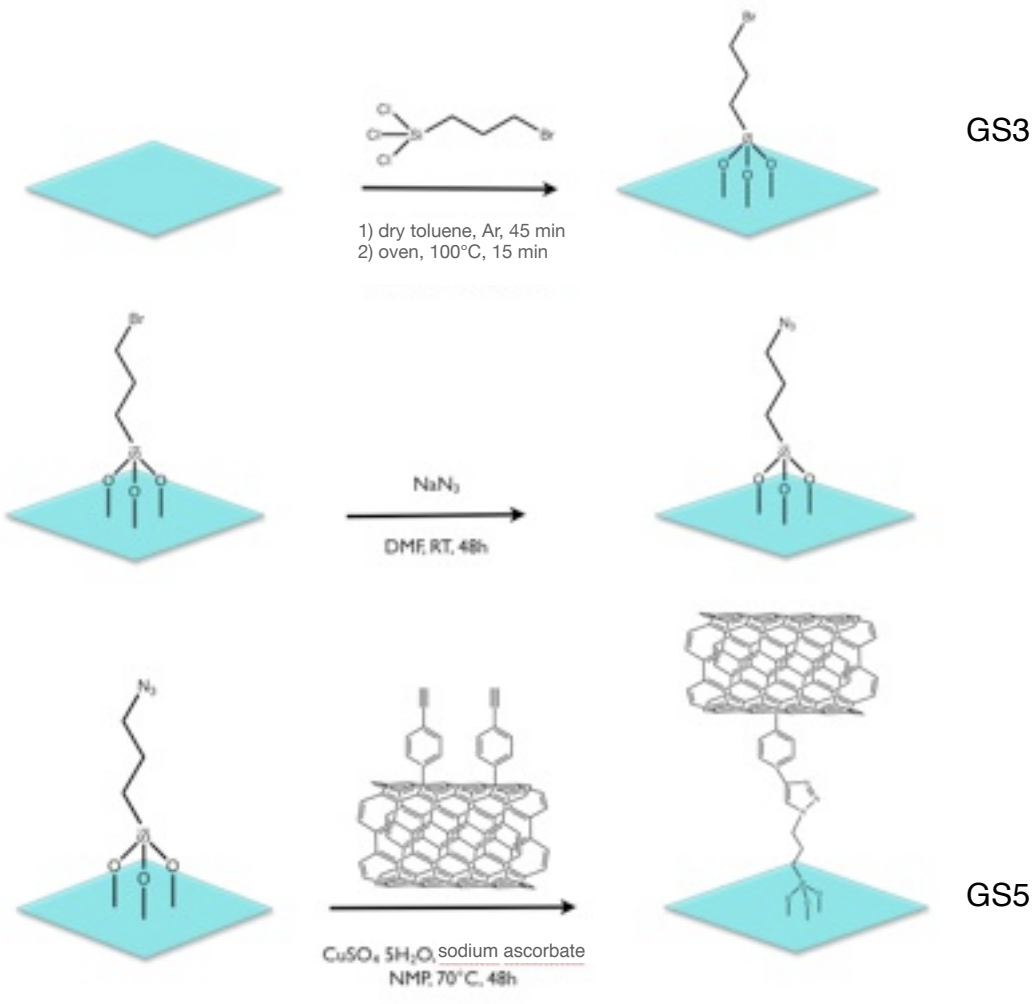

Fig. 4: general scheme reaction of glass functionalization

Click chemistry is a chemical philosophy introduced by K. B. Sharpless in 2001 and describes chemistry tailored to generate substances quickly and reliably by joining small units together.[17]

"Click reaction" is a common name with which we refer to one of the most popular reactions within the click chemistry philosophy that is the azide-alkyne Huisgen cycloaddition using a Cu catalyst at room temperature. This was an improvement over the same reaction first popularized by Rolf Huisgen in the 1970s, at elevated temperatures, in the absence of water and without a Cu catalyst. However, the azides and alkynes are both kinetically stable. The reaction is slow and thus requires high temperatures.

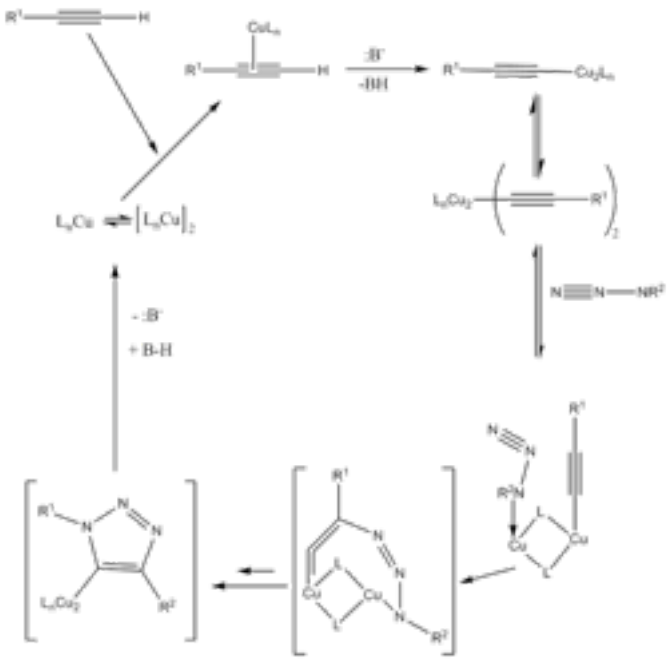

Fig 5: Mechanism of copper catalyzed click reaction.

Copper is the commonly used catalyst in the reaction. Copper catalysed click reactions work essentially on terminal alkynes. The Cu species undergo metal insertion reaction into the terminal alkynes. These Cu(I) species are typically generated in the reaction pot itself: a Cu compound (in which Copper is present in the +2 oxidation state) is added to the reaction in presence of a reducing agent which reduces the Cu from the (+2) to the (+1) oxidation state. The advantage of generating the Cu(I) species in this manner is that it eliminates the need of a base in the reaction. Also the presence of reducing agent makes up for any oxygen which may have gotten into the system. Oxygen oxidizes the Cu(I) to Cu(II) which impedes the reaction and results in low yields. One of the more commonly used Cu compounds is $CuSO_4$.

The Copper (I) species generated in situ forms a pi complex with the triple bond of a terminal alkyne. In the presence of a base, the terminal hydrogen, being the most acidic is deprotonated first to give a Cu acetylide. It has been suggested that the transition state involves two copper atoms. One Copper atom is bonded to the acetylide while the other Cu atom serves to activate the azide. The metal center coordinates with the electrons on the nitrogen atom. The azide and the acetylide are not coordinated to the same Cu atom. The azide displaces one ligand to generate a copper-azide-acetylide complex . At this point cyclization takes place. This is followed by protonation; the source of proton being the hydrogen which was pulled off from the terminal acetylene by the base. The product is formed by dissociation and the catalyst ligand complex is regenerated for further reaction cycles (fig.5). Commonly used solvents are polar aprotic solvents such as THF, DMSO, CH_3CN, DMF as well as in non-polar aprotic solvents such as toluene. [18]

Functionalization of Carbon Nanotubes

Fabrication of nanotube-based molecular assemblies is still limited because of the difficulty to incorporate highly engineered molecules on the nanotube surfaces. This issue can have mainly two origins: incompatibility between the functionality on the molecules and the conditions required for nanotube functionalization and/or the fact that nanotube functionalization requires a large excess of reagent which is difficult or impossible to recycle. There is a real need for simple and versatile reactions that can easily lead to nanotube-based functional materials.

"Click chemistry" can bring very elegant solutions to easily achieve nanotube-based functional materials, for the type of reaction, versatile and clean, with simple work-up and purification procedures.[19] In order to syntetize carbon nanotube derivatives with an alkyne moiety, that is complemental to the azide moiety exposed to the glass surfaces we chose to functionalize DWNTs with 4-ethynylaniline following the procedure developed by Tour and co-workers.[20]

Reaction of as produced DWCNT with 4-ethynylaniline in the presence of isoamyl nitrite in *N*-methylpyrrolidone (NMP) gave functionalized nanotubes (*f*-DWNTs) (fig. 6), that were then allowed to react with the azido modified glass surfaces in NMP in the presence of $CuSO_4$ and sodium ascorbate to give the nanotube-covered surface (fig.4).

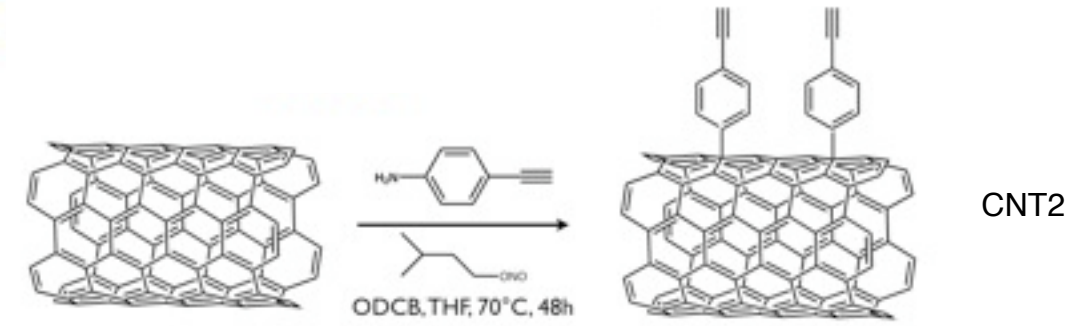

Fig. 6: Scheme of the Tour reaction on as produced CNTs

DWCNTS were chosen for their higher purity and for the relatively smaller amount of defects, with respect to commercial samples of SWCNTs. Also, Raman spectroscopy works on SWCNTs and DWCNTs, bust doesn't give significative information about the functionalization of MWCNTs. This is why DWCNTs were chosen. However, all the experiments were done also with MWCNTs, treated in the same way of DWCNT, because, since all the electrophysiology experiments on neuron's activity described in chapter 2 were conducted on MWCNTs substrates, to work on a covalently functionalized substrate of the same nanotubes would be the best way to compare the results and analyze the effect of the regular pattern on the activity on neurons. Here we will report the description of the experiments and the discussion of the results mainly for DWCNTs, reaction and characterization of MWCNTs, since very similar to those of

DWCNTS will be described in the experimental section (chapter 5).The one described above was the general procedure used for the functionalization of glass by CNT. As introduced in section 4.2 of this chapter, the aim of the thesis work has been the double functionalization of carbon nanotubes, to exploit one functional moiety for the bond to the glass surface, and the other functional moiety for the bond with a RGD peptide of interest.The decoration of carbon nanotubes with biological species such as peptides represents an effective approach for nanotechnology application in medicine. Here, we report the double functionalization of carbon nanotubes with radicalic Tour reaction for the introduction of the alkyne functionality to be exploited for the bond to the surface and with the RGD peptide H-Ser(tBut)-Asp(tBut)-Gly-Arg(Pbf)-OMe (furnished by Prof. B. Cacciari, University of Ferrara)(fig.7) for the preparation of nanotube-peptide conjugates.

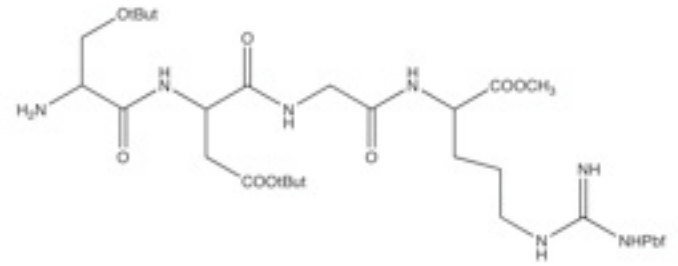

Fig. 7 : Structure of the H-Ser(tBut)-Asp(tBut)-Gly-Arg(Pbf)-OMe peptide

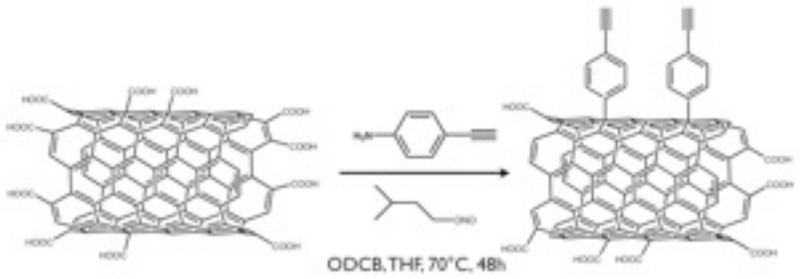

CNT3

Fig.8: Scheme of Tour reaction on oxidized CNTs

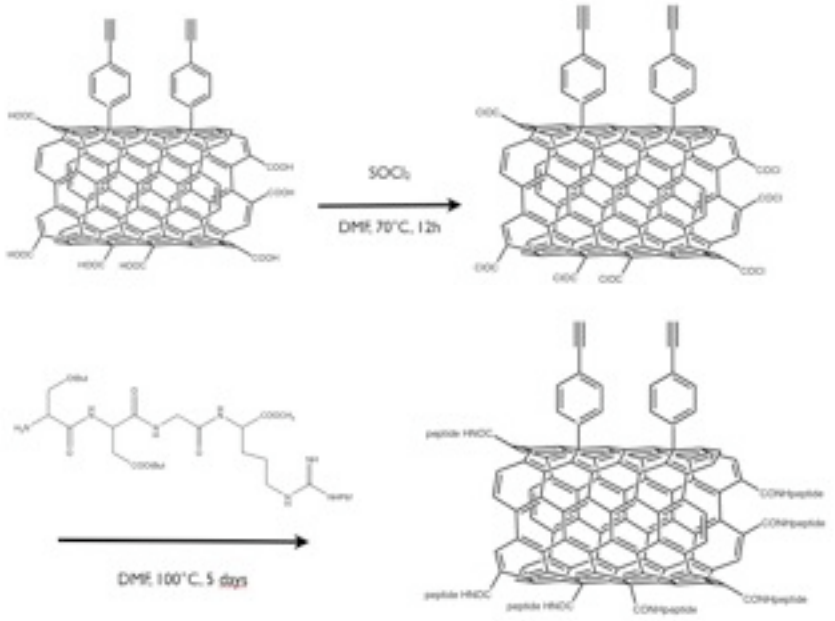

CNT4

Fig 9: Scheme of CNT functionalization by the RGD peptide

The functionalization is based on the activated amidation of oxidized nanotubes. Oxidized DWCNT expose carboxylic acid groups on the surface that alter and break the sp_2 network of the graphite sheet and introduce sp_3, more reactive, spots to be exploited for functionalization. These carboxylic acid groups usually occur predominantly at the more reactive (open) end or defect sides of single-walled and multi-walled carbon nanotubes, rather than the side walls, while the radicalic addition on the other end prefers the side walls. This is why steric hindrance can be avoided by this hybrid approach and the resulting product presents two functionalities. As produced, oxidized, DWCNT were functionalized with 4-ethynylaniline with the same procedure decribed above (fig. 8).
The carboxylic functionalities can be exploited for the reaction with the RGD peptide by amidic coupling. The coupling was preceded by the activation of the carboxylic functionalities by thionil chloride. The following reaction was performed by introducing the peptide in the reaction pot. The peptide, as is evident in the structure (fig.7), presents every single functionality protected by various protective groups except for the Serine NH_2 which is exploited for the amidic coupling (fig.9).
Also the bio-modified nanotubes have been used for reaction with the glass surface by the click reaction, that was mentioned above to obtain the final product reported in figure (fig. 10):

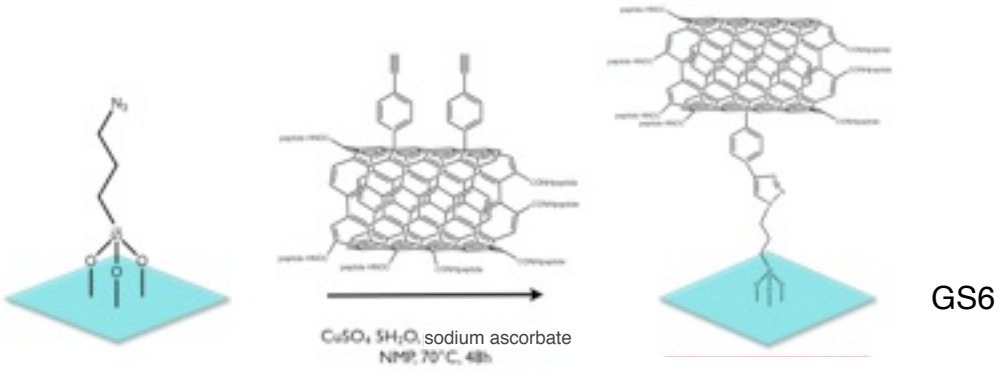

Fig. 10: Scheme reaction of glass functionalization by peptide-functionalized CNTs

Another important comparison that can be done is the effect on neuronal activity of the RGD peptide in absence of CNTs. To do so the glass surfaces were functionalized with the RGD peptide by the use of another silane coupling agent: 3-isocyanatopropyl triethoxy silane. The isocyanate terminal moiety can be exploited to establish a covalent bond with the free NH_2 group of the peptide creating a substituted urea (see chap.5, sec. 5.5.1)(fig. 11).

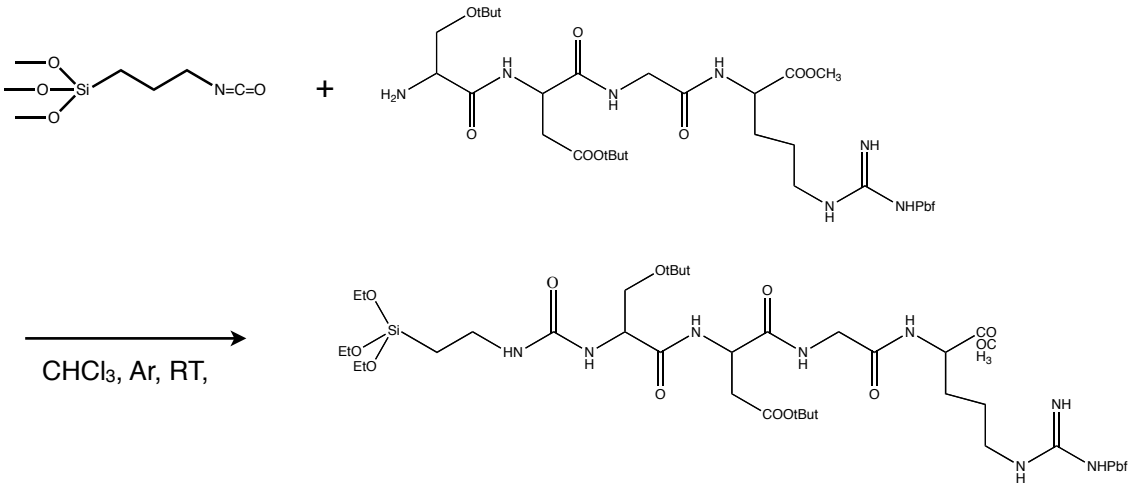

Fig. 11: scheme of the coupling between isocyanatepropyl triethoxysilane and the RGD peptide

Since the isocyanate group is very sensitive to moisture and immediately hydrolyzes, the strategy chosen in this case was to attach firstly the silane to the peptide, and then to introduce the glass slide in the same reaction environment keeping the inert atmosphere. All the protective groups of the peptide were removable in TFA, so washing the glass slides in TFA gave the resulting, deprotected, peptide functionalized, glass surface (fig. 12).

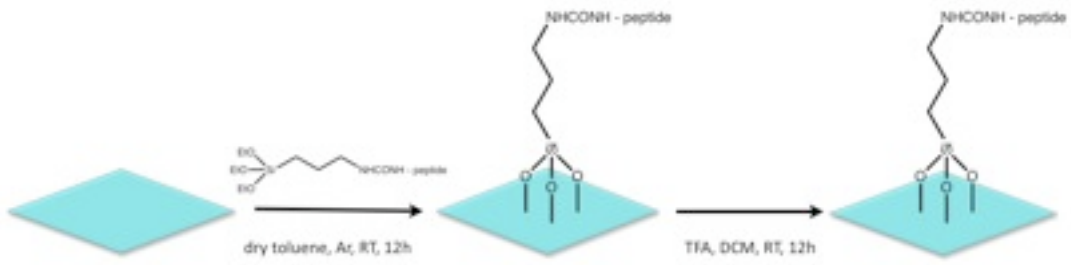

GS7

Fig. 12: Scheme reaction of glass functionalization by the RGD peptide

3.4 Characterization of functionalized CNT

The nanotube derivatives were characterized by standard analytical techniques such as Raman, thermogravimetric analysis (TGA) and TEM microscopy.

First of all, the Raman analysis of the alkyne functionalyzed DWCNTs **CNT2** (fig.13A - blue track) present an increased ratio between the intensity of the D and G band with respect to the pristine material (fig.13A - black track). This is a proof of the functionalization. The perturbation on the RBM zone in the functionalized nanotubes is

probably due to the formation of a polyaromatic multilayer on the nanotube surface. This effect usually happens at various degree when functionalizing nanotubes by Tour reaction because of the involvement of the reactive aryl radicals. [21]

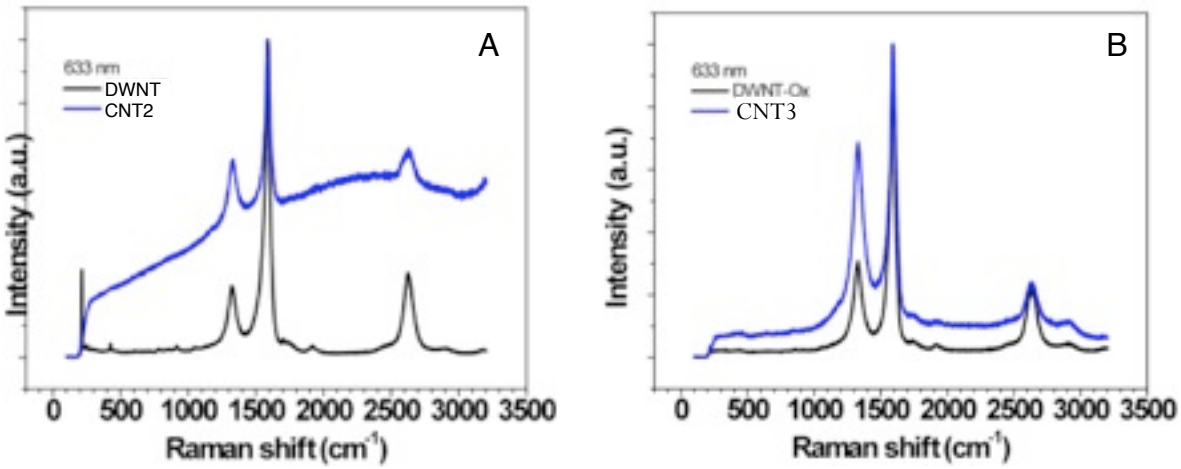

Fig.13: A) Raman spectra of pristine/Tour modified nanotubes; B) Raman spectra of oxidized/Tour modified nanotubes

The Raman analysis of the alkyne functionalized oxidized DWCNT **CNT3**, shows as well a very well defined increasing of the D/G ratio, that is proof of functionalization (fig. 13B).

The thermogravimetric analysis showed a loss of weight, taken at 500°C degree, of about 5% for alkyne-functionalized DWNTs **CNT2** (fig.14 black track, left graph), 7% for oxidized DWNTs (fig.14 black track, right graph), 10,5% for alkyne-functionalized oxidized DWCNTs **CNT3** (fig.14 red track, left graph), and 18,71% for peptide functionalized DWCNT **CNT4** (fig.14 blue track, left graph).

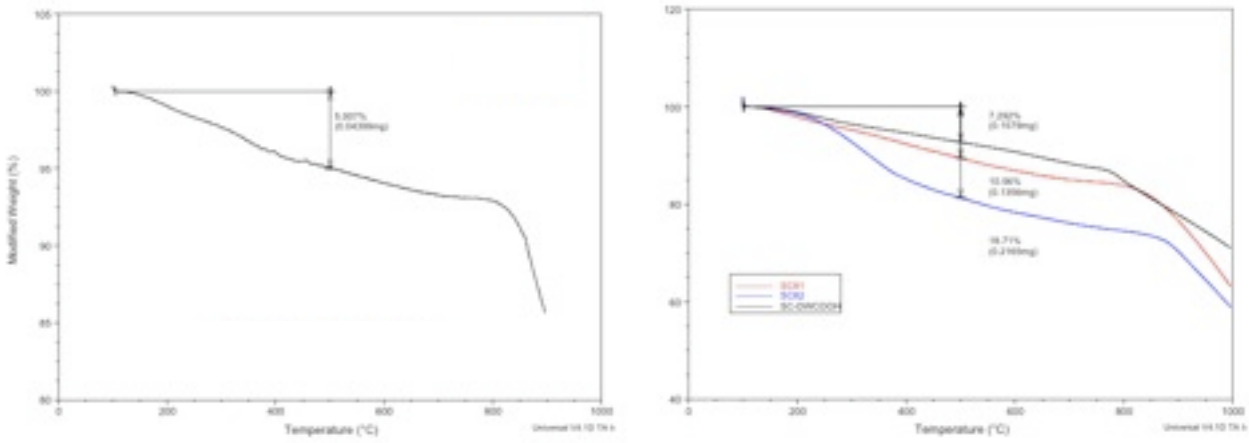

Fig. 14: TGA profiles

The TGA profiles correspond to the values of carbon atoms number per functional group reported in table 1:

sample	weight loss (500°C)	C atoms/*f*-groups
CNT2	5,01%	139
CNT3	10,56%	216
CNT4	18,71%	320

Table1: interpretation of TGA results

The carbon nanotube derivatives have been investigated by TEM microscopy. The TEM pictures of CNT2, CNT3 and CNT4 are reported below (fig. 15: 28000x, 16: 14000x, 17: 28000x). The images revealed the presence of individual or very thin bundles of nanotubes; the typical lengths of the objects are about 1,5 to 3 μm with diameters of about 1 to 3 nm.

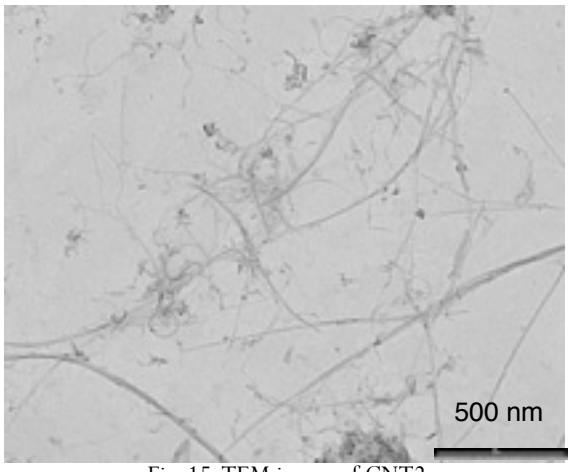

Fig. 15: TEM image of CNT2

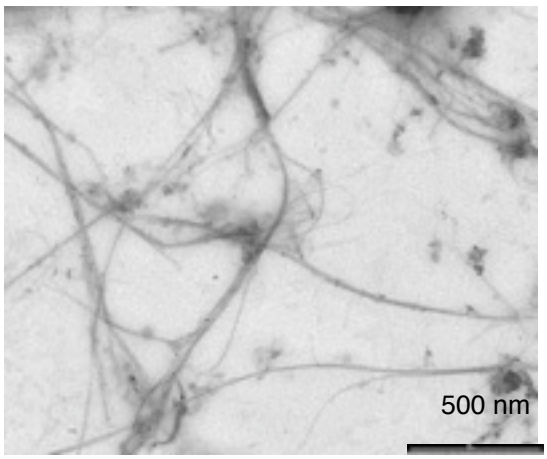

Fig. 16: TEM image of CNT3

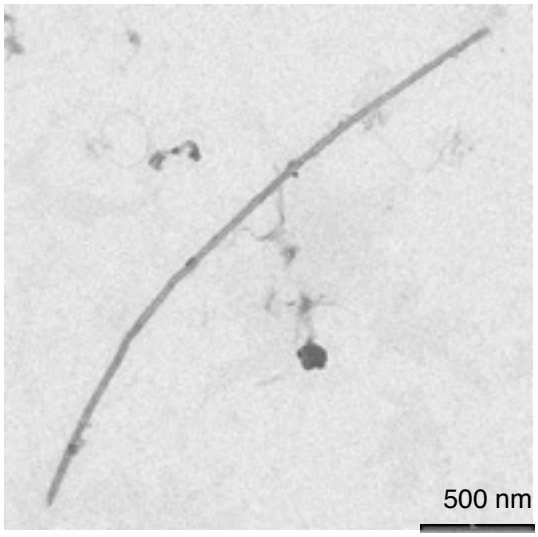

Fig. 17: TEM image of CNT4

Monitoring CNT functionalization by the use of Au nanoparticles

To characterize the peptide-functionalized CNT, a strategy was individuated in the use of gold nanoparticles, exploiting their optical properties that vary whenever the particle aggregates.

In nanotechnology, a particle is defined as a small object that behaves as a whole unit in terms of its transport and properties. It is further classified according to size: in terms of diameter, fine particles cover a range between 100 and 2500 nanometres, while ultrafine particles are sized between 1 and 100 nanometers. **Nanoparticles** are sized between 1 and 100 nanometers. Gold nanoparticles (AuNPs) are the most stable metal nanoparticles, and they present fascinating aspects such as their assembly of multiple types involving materials science, the behavior of the individual particles, size-related electronic, magnetic and optical properties (quantum size effect), and their applications to catalysis and biology. Their promises are in these fields as well as in the bottom-up approach of nanotechnology. [22]

The first studies concerning optical properties of colloidal gold were conducted in the XIX century. In 1857, Faraday reported the formation of deep-red solutions of colloidal gold by reduction of an aqueous solution of chloroaurate ($AuCl^{4-}$) using phosphorus in CS_2 (a two-phase system). He investigated the optical properties of thin films prepared from dried colloidal solutions and observed reversible color changes of the films upon mechanical compression (from bluish-purple to green upon pressurizing).[23]

The red ruby color of gold colloids is due to the absorbance of light in the UV/Vis region around 520 nm. This generates an intense band, known as *Surface Plasmon Band (SPB)*, that arises from the coherent oscillation of the conduction electrons, induced by the interaction with the electromagnetic field. The nature of the SPB was explained for the first time by Mie [24] in 1908. Mie associated SPB of spherical particles to the dipole oscillations of free electrons in the conduction band, which occupy the energy level immediately above the Fermi level. The intensity of the band decreases proportionally with the decrease of the size of the particle core. This is due to the *"quantum size effects"* which become important for particles with diameter < 3 nm and they cause also a blue shift. So, SPB is not found for particles with diameter < 2 nm, and so is not for bulk gold.

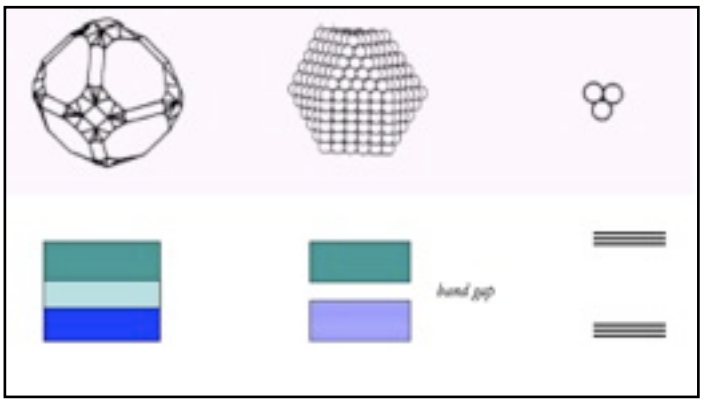

Fig. 18: Electronic states of a metal, depending on the dimension

"Quantum size effects" is the effect for which, if the dimension of the particle is reduced to few nanometer (1-10 nm), the chemical and physical properties of the clusters become different either from the properties of the

metallic bulk and as well from the properties of the molecular compounds. The continuos density of the electronic levels in the valence and the conduction band for the bulk metal is broken and it is adopted a structure of discrete energy levels. This causes a dramatic change in the electronic properties of the metal. In a bulk crystal the properties do not depend on the dimension but only on the chemical composition. In a nanometric scale the quantistic structure of the energetic levels causes the transition from continuos bands to become discrete and so the properties become dependent on the dimension and the shape of the clusters (fig.18).

Among the conventional methods of synthesis of AuNPs by reduction of gold(III) derivatives, the most popular one for a long time has been that using citrate reduction of $HAuCl_4$ in water, which was introduced by Turkevitch in 1951.[25] It leads to AuNPs of ca. 20 nm. In a more recent effort,[26] to obtain AuNPs of pre-chosen size (between 16 and 14 nm) via their controlled formation, a method was proposed where the ratio between the reducing/stabilizing agents (the trisodium citrate to gold ratio) was varied. This method is very often used even now when a rather loose shell of ligands is required around the gold core in order to prepare a precursor to valuable AuNP-based materials.

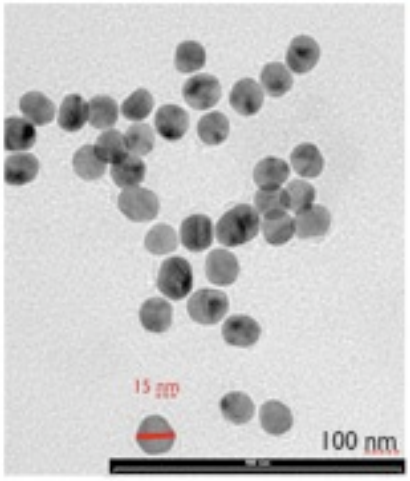

Fig.19: TEM micrograph of citrate stabilyzed gold nanoparticles

The nanoparticles used for this experiment were synthesized according to this technique. The method is based on simultaneous reduction of aqueous gold salt $HAuCl_4$ and stabilization of the formed gold nanocolloid with citrate. According to size analysis from transmission electron microscopy (TEM) micrographs, the resulting particle size was between 13 and 15 nm (fig. 19). The citrate stabilyzes AuNPs by creating a core of negative ions around the gold colloid. The nanoparticles are negatively charged and repulse each other. Their electronegativity is the medium by which they are able to establish electrostatic bonds with various charged polymers. [22] It has been observed that gold nanoparticles initiate protein aggregation at physiological pH, resulting in the formation of extended protein-nanoparticle assemblies, accompanied by large protein aggregates without embedded nanoparticles.[27]

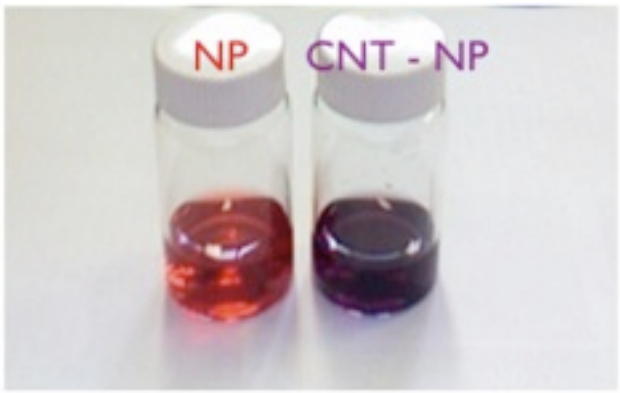

Fig. 20: change of color of AuNPs in the presence of CNT indicate the formation of aggregates.

As a consequence of this observation we hypotize that in the presence of peptide-functionalized CNT, depending on the pH of the solution wich determine the charge of the functional groups on the peptide surface, NP should aggregate on the surface of CNT in correspondence of the

spots were the peptide is bonded to the carbon structure. This should be monitored by TEM microscopy and also by UV spectroscopy by verifying the modification of the surface plasmon band, typical of gold colloids, whose intensity should decrease and shift at higher values of wave-length.
The peptide-functionalized CNT were added in a concentration of 0,125 mg/ml to a 0,5 mM solution of AuNPs in water. A first visible result is the drastic change of color of the solution which passes from ruby-red to violet in a range of time of less than an hour (fig. 20). It is important to notice that the nanotubes used for this experiment have been previously washed by acidic water for HCl, and then dried under vacuum, to protonate all the aminic and carboxylic functions. The same experiment conducted with nanotubes which were not washed in acidic water gave no result.
The UV/Vis spectra of the two solutions is reported below (fig. 21):

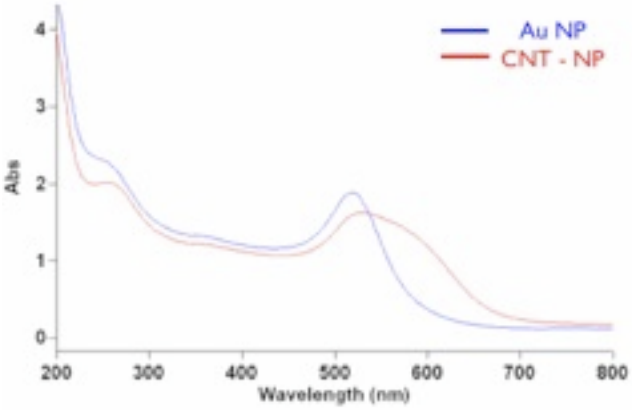

Fig. 21: UV/Vis spectra of AuNPs and CNT-AuNPs

It is evident the lower intensity and the red shift of the SPB as it is expected for aggregates of larger size.
The results were confirmed by the TEM micrograph, reported below, which shows the aggregation of AuNPs on the CNT surface in certain spots (fig.22). TEM images were recorded on CNT-NP samples which have been subjected to centrifugation in order to remove all the AuNPs in excess that are found in the supernatant.

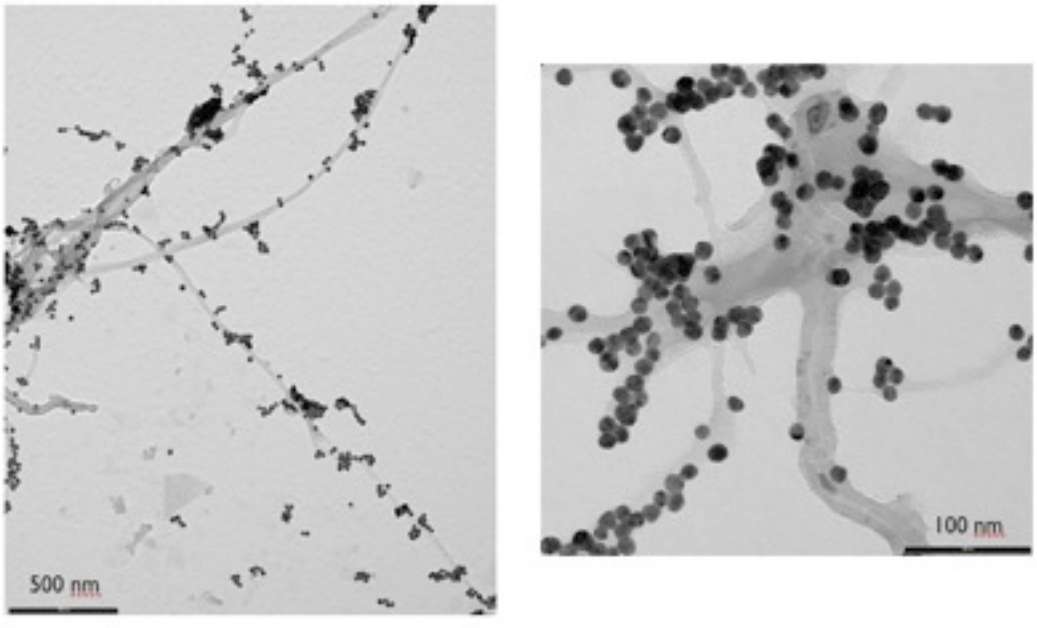

Fig.22: TEM micrograph of CNT-AuNPs: a) photo taken at 28000x; b) photo taken at 180000x.

3.5 Characterization of glass surfaces

The chemically modified surfaces were characterized by contact angle measurements. Values are reported in table 2:

surface	contact angle
starting material	57,82° ± 1,00
sample GS2	25,08° ± 1,00
sample GS3	83,30° ± 1,00
sample GS4	68,98° ± 1,00
sample GS5	91,86° ± 1,00
sample GS6	79,28° ± 1,00
sample GS7	29,72° ± 1,00

Table 2: contact angles values for the different glass surfaces

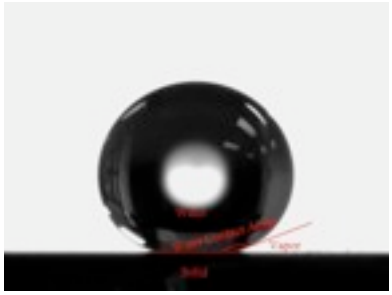

Fig. 23: contact angle measured in water

The **contact angle** is the angle at which the liquid/vapor interface meets the solid surface. The contact angle is specific for any given system and is determined by the interactions across the three interfaces (fig. 23). Contact angle measured in water gives a measure of the hydrophilicity of the surface, also called wettability. Higher contact angle are a proof of an hydrophobic surface and viceversa, lower contact angles of an hydrophilic surface. Contact angle measurements showed that the initial purification treatment of the original glass surface in pirana solution increases a lot the hydrophilicity of the surface by the oxidation of the silanol groups (from 57,82° to 25,08° for sample GS2). The number of oxydrilic groups exposed on the surface become significantly higher and this is propedeutic to the following silanization reaction. The addition of alkylic chain after the silanization reaction and the introduction of the bromine group decrease drastically the hydrophilicity in GS3, as expected (83,30°) but the addition of the azide group recovers a bit of the hydrophilicity in GS4 (68,98°). Introduction of nanotubes increases the hydrophobicity in GS5, as expected (91,86°), but peptide modified nanotubes are less hydrophobic systems as confirmed by the lower value of contact angle in GS6 (79,28°). Peptide modified surfaces GS7 are very hydrophilic with a value of contact angle of 29,72°.

For a first qualitative characterization of the functionalized glass surfaces FT-IR spectroscopy was performed to characterize the nature of the functional groups present in the samples. Especially this technique was useful for the detection of the azide moiety.

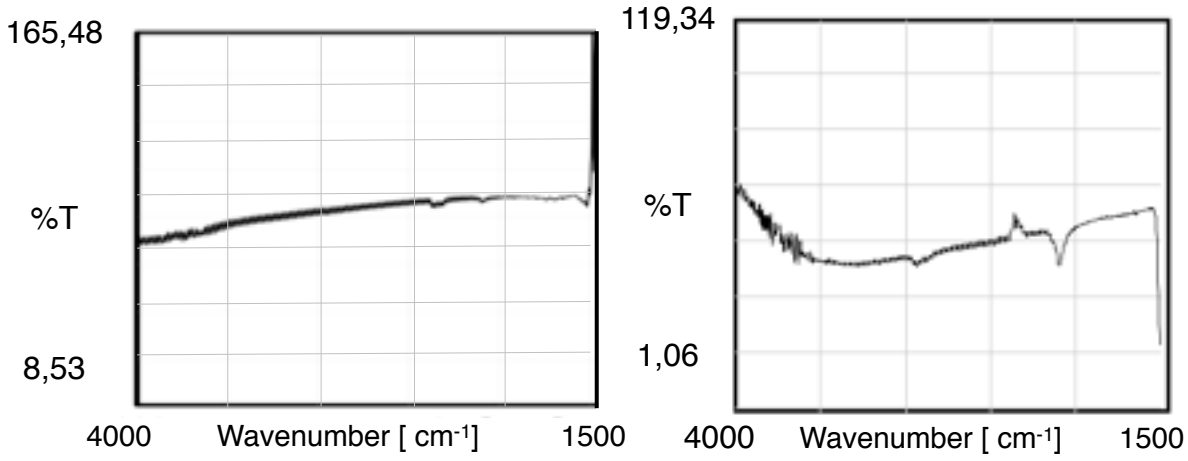

Fig. 24: FT-IR spectra of GS3 and GS4

After analyzing by FT-IR the sample GS4 the appearance of the characteristic azide peak at 2100 cm^{-1} indicated the successful formation of azide moieties after the first reaction step, since such a peak was not present in the original monolayer (fig. 24). However, FT-IR could not provide evidence of the quantitative conversion of bromine to azide.

The surfaces were also characterized by **XPS spectroscopy** in collaboration with Dr H. Traboulsi (FUNDP). X-ray photoelectron spectroscopy is a quantitative spectroscopic technique that measures the elemental composition, empirical formula, chemical state and electronic state of the elements that exist within a material. XPS spectra are obtained by irradiating a material with a beam of X-rays while simultaneously measuring the kinetic energy (KE) and number of electrons that escape from the top 1 to 10 nm of the material being analyzed. XPS requires ultra high vacuum (UHV) conditions. XPS is a surface chemical analysis technique that can be used to analyze the surface chemistry of a material in its "as received" state, or after some treatment.

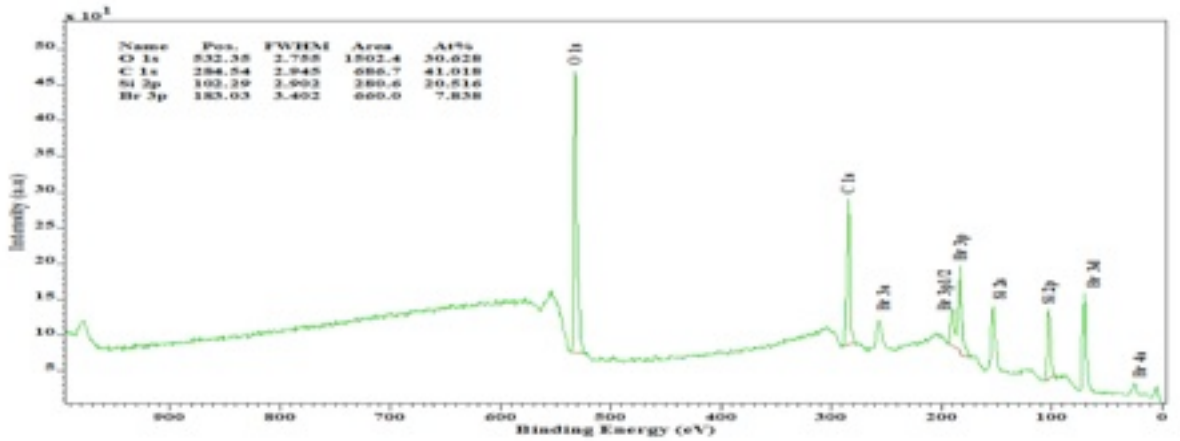

Fig. 25: XPS spectrum of the bromine terminated monolayer

XPS, among all the surface characterization techniques is the only one that can provide evidence of the quantitative conversion of bromine to azide and then of azide to triazole, after the click reaction. Therefore, high resolution XPS investigations were performed on all the fuctionalized glass surfaces. Special emphasis was placed on the investigation of the Br(3d) and N(1s) regions of the spectra in order to quantify the chemical functionalization steps. The XPS spectrum of the bromine-terminated precursor monolayer GS3 (fig.25) revealed a strong peak at 71 eV, which was assigned to the Br(3d) signal and other peripheral peaks associated to Br, and thus proved the presence of bromine in the layer.

After the conversion of bromine into azide, this peak almost completely disappeared (fig. 26), indicating the almost complete substitution of the bromine functions of the monolayer. The substitution reaction of bromine with sodium azide resulted in the observation of a signal in the N(1s) region of the XPS spectrum of the GS4 surface. Careful analysis showed the presence of a split peak with maxima at 401 and 405 eV (fig. 27). This peak splitting indicated the presence of two nitrogen species present in the azide-terminated monolayer and reflected the differently charged nitrogen atoms in the azide group. [28]

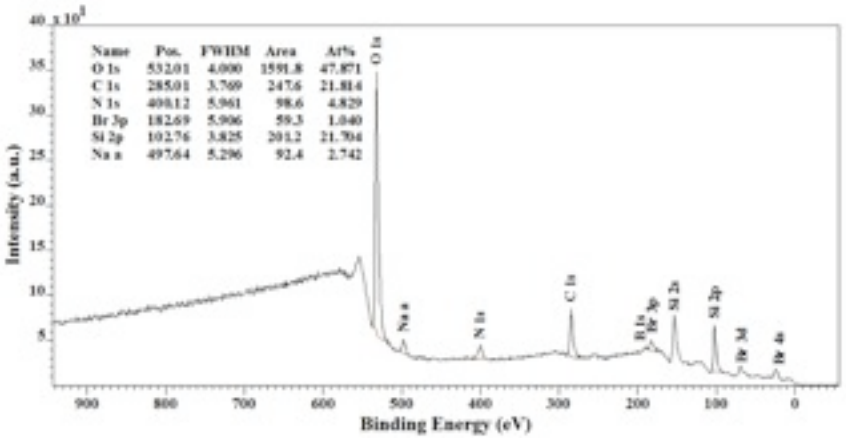

Fig. 26: XPS spectrum of the azide terminated monolayer

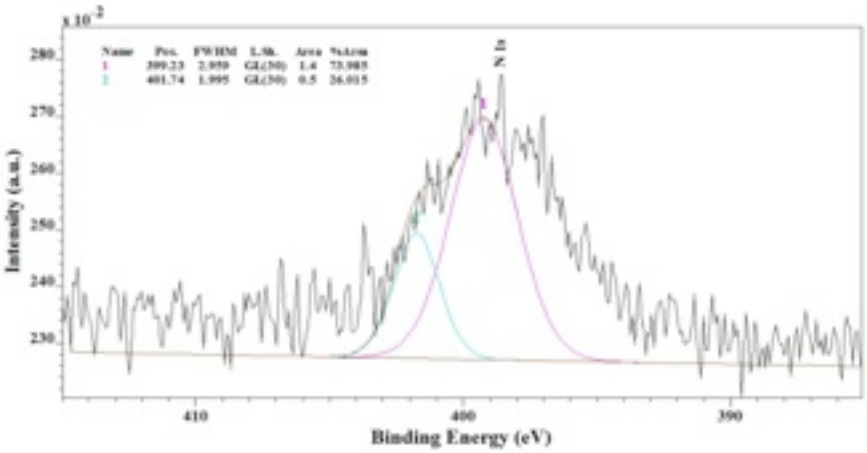

Fig. 27: high resolution XPS on the nitrogen region reveals the presence of the azide peak

A closer look at the XPS spectrum of the azide-terminated glass (fig.26) compared to the spectrum of the bromine terminated glass (fig.25) shows that the intensity of the nitrogen peak is much lower of the intensity of the bromine peak, even though the latter disappears almost completely after functionalization. This observation is most likely related to a faster degradation of the azide monolayer on glass because the extensive charging increases the decomposition of the azide which results in the diminution of the intensity of the signal.[29]

Such functionalized azide-terminated monolayers represented a substrate that could be employed in Huisgen cycloaddition reactions, reacting with terminal acetylene substituted nanotubes. The evidence of the 1,2,3-triazole formation on the azide-terminated monolayer GS5 was derived from XPS investigations of the N(1s) spectral region, which displayed only a single peak at 400 eV, thus confirming the conversion of the azide functions (fig. 28 - 29).

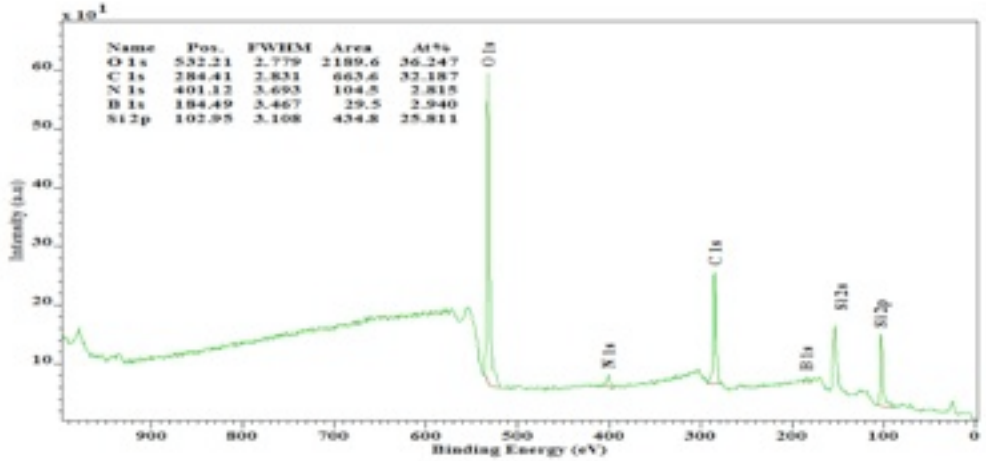

Fig. 28: XPS spectrum of the nanotube terminated monolayer

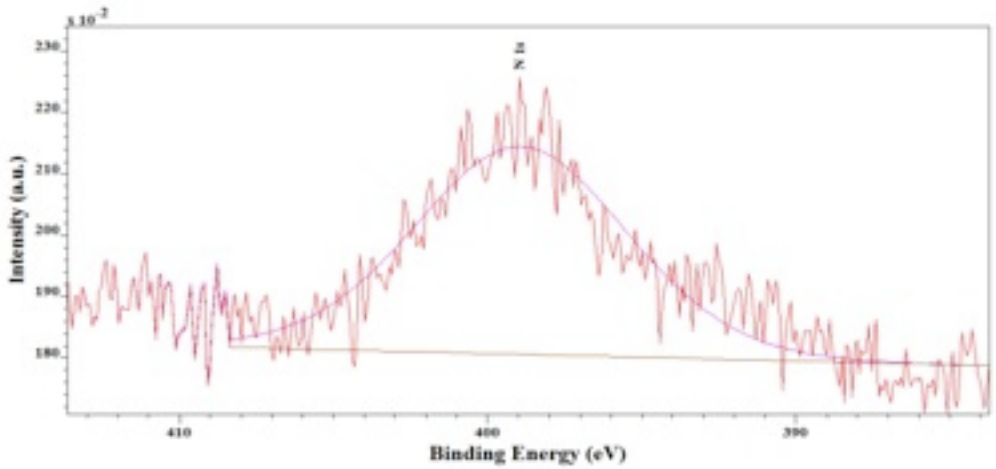

Fig. 29: high resolution XPS in the nitrogen region reveals the presence of the triazole peak

The surfaces functionalized by the peptide-nanotube conjugated GS6 were also characterized by XPS (fig.30). The only difference that is noticeable with the simple acetylene functionalized nanotubes is noticeable in the carbon region at 285 eV, where the

carbon peak appears broadened due to the presence of the many different carbon components reliable to the different bond that carbon establish with various ethero-atoms in the peptide structure (fig.31).

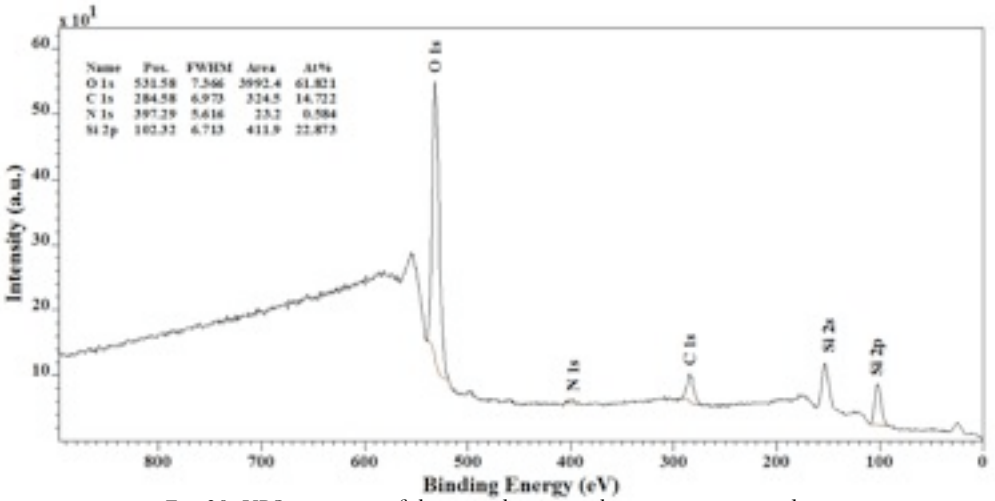

Fig. 30: XPS spectrum of the peptide- nanotube conjugates monolayer

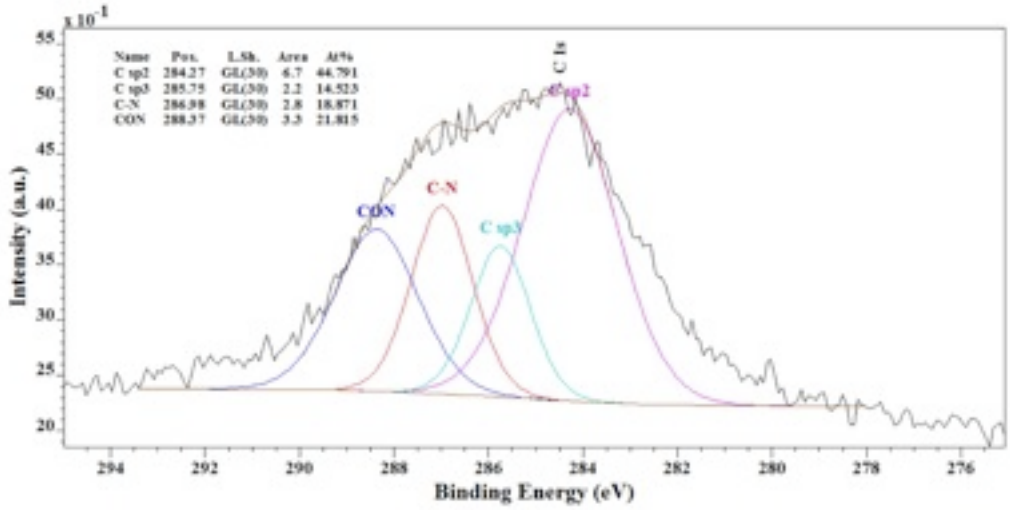

Fig. 31: high resolution XPS in the carbon region: carbon peaks appears broadened due to the presence of the peptide.

The same morpholgy of the carbon peak can be found in the XPS analysis of the peptide functionalized surfaces GS7 (see chap. 5, sec. 5.4.7).

The carbon nanotube functionalized surface have been investigated by SEM microscopy. In SEM pictures of DWCNT-functionalized surfaces (fig. 32-33), one can see the presence of nanotubes as spaghetti-like aggregates.

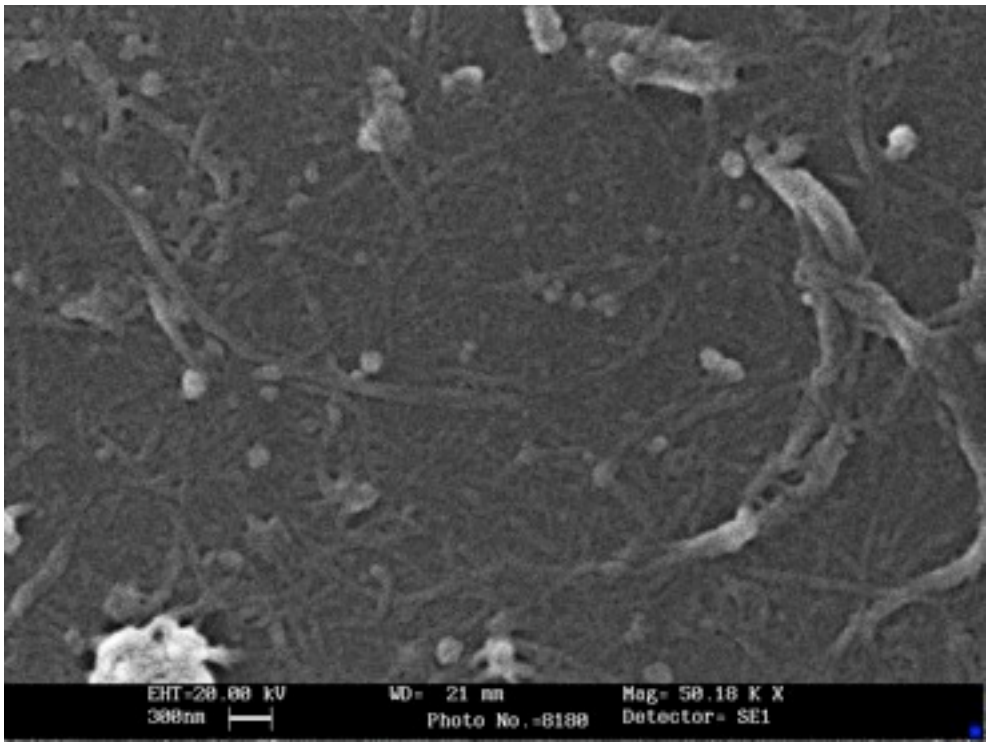

Fig. 32: SEM micrograph of the GS5 carbon nanotube functionalized surface

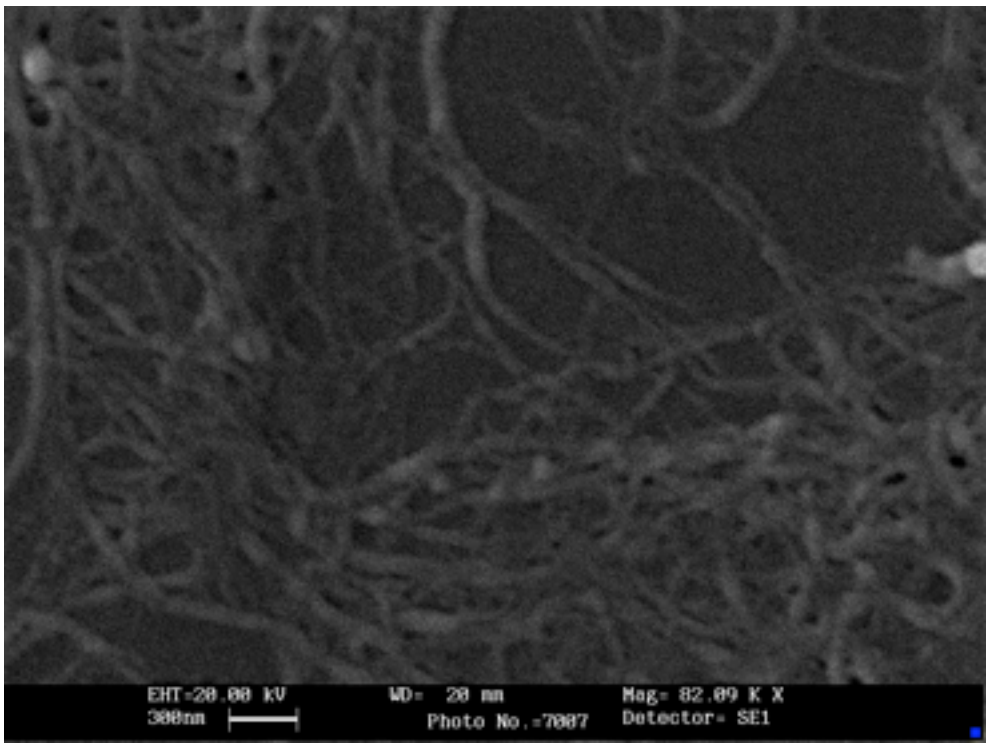

Fig. 33: SEM micrograph of the GS6 carbon nanotube-peptide conjugate functionalized surface

Conclusions

Here we have described the functionalization of carbon nanotubes with a 4-ethynylbenzene derivative and its subsequent attachment to glass using the Huisgen 1,3-dipolar cycloaddition. The nanotube derivatives were fully characterized by a combination of analytical techniques. We have demonstrated that click chemistry is an elegant method to functionalize carbon nanotubes and to easily achieve nanotube-based functional materials.

It was demonstrated the ability of 3-bromopropyl trichlorosilane to form a suitable precursor monolayer, which can be used to introduce tailor-made surface functionalities by means of chemical surface reactions. It was shown that such layers were stable enough to withstand the experimental conditions required for their functionalization with azide functions and further wet chemical processing to obtain the click reaction of alkyne functionalized nanotube. The modification sequence was investigated by FT-IR, XPS spectroscopies and SEM microscopy and the results displayed the successful attachment of nanotubes to the modified glass substrates. The conversion of the bromine moieties into azide units could be determined and XPS suggests a quantitative conversion (>95%). These results encourage further use of this reaction mechanism for the functionalization of micro and nanopatterned structures. Moreover, starting the introduced approach from a well-ordered, variable precursor unit is advantageous and click chemistry can provide a powerful tool for the functionalization of such structures.

We have also described and characterized an efficient methods to covalently attach a biomolecule of interest, in this case a RGD peptide, to carbon nanotubes via thionyl chloride-activated amidation. The method is important because may be used to introduce carbon nanotubes into other biologically and biomedically important systems.

3.6 References

(1) a) R. Singhvi, A. Kumar, G. Lopez, G. N. Stephanopoulos, D.I.C. Wang, G. M. Whitesides; *Science* **1994**, *264*, 696-698. b) K. E. Healy, B. Lom, P. E. Hockberger; *Biotechnol. Bioeng.* **1994**, *43*, 792-800.

(2) T. Gabay, E. Jakobs, E. Ben-Jacob, Y. Hanein; *Physica A.* **2005**, *250*, 611–621.

(3) K. L. Prime, G. M. Whitesides; *Science* **1991**, *252*, 1164-1167.

(4) C. S. Chen, M. Mrksich, S. Huang, G. M. Whitesides, D. E. Ingber; *Science,* **1997**, *276*, 1425-1428.

(5) H.G. Craighead; *Biomed. Microdev.* **1998**, *1*, 49–64.

(6) S. Turner, L. Kam, M. Isaacson, H.G. Craighead, W. Shain, J. Turner, J. Vac; *Sci. Technol. B.* **1997**, *15*, 2848–2854.

(7) B. Zhu, Q. Zhang, Q. Lu, Y. Xu, J. Yin, J. Hu, Z. Wang; *Biomaterials* **2004**, *25*, 4215–4223.

(8) J.H. Chen, W.Z. Li, D.Z. Wang, S.X. Yang, J.G. Wen, Z.F. Ren; *Carbon* **2002**, *40*, 1193–1197.

(9) R. Pankov, K. M. Yamada; *Journal of cell science* **2002**, *115*, 3861–3863.

(10) H. P. Erickson; *Journal of muscle research and cell motility* **2002**, *23*, 575–580.

(11) T. D. B. Nguyen-Vu, H. Chen, A. M. Cassell, R. Andrews, M. Meyyappan, J. Li; *Small* **2006**, *2*, 89-94.

(12) J. D. Hartgerink, E. Beniash, S. I. Stupp; *Science* **2001**, *294*, 1684-1688.

(13) K. Besteman, J. O. Lee F. G. Wiertz H. A. Heering C. Dekker; *Nano Lett.* **2003**, *3*, 727–730.

(14) N. Faucheux, R. Schweiss, K. Lutzow, C. Werner, T. Groth; *Biomat.* **2004**, *25*, 2721-2730.

(15) L. Henke, U. J. Krull, J. Can; *Anal. Sci. Spectrosc.* **1999**, *44*, 62–71.

(16) S. Sawoo, P. Dutta, A. Chakraborty, R. Mukhopadhyay, O. Bouloussa, A. Sarkar; *Chem. Comm.* **2008**, *45*, 5957-5959.

(17) H. C. Kolb, M. G. Finn, K. B. Sharpless; *Angew. Chem. Int. Ed.* **2001**, 2004–2021.

(18) V. D. Bock, H. Hiemstra, J. H. van Maarseveen; *Europ. Journ. of Org. Chem.* **2006**, ,51-68.

(19) H. Li, F. Cheng, A. M. Duft, A. Adronov; *J. Am. Chem. Soc.* **2005**, *127*, 14518-14524.

(20) C. A. Mitchell, J. L. Bahr, S. Arepalli, J. M. Tour, R. Krishnamoorti; *Macromolecules* **2002**, *35*, 8825-8830.

(21) J. L. Bahr, J. M. Tour; *Chem. Mater.* **2001**, *13*, 3823–3824.

(22) M. C. Daniel, D. Astruc; *Chem. Rev.* **2004**, *104*, 293−346.

(23) M. Faraday; *Philos. Trans.* **1857**, *147*, 145-181.

(24) G. Mie; *Ann. Phys.* **1908**, *25*, 377-445.

(25) J. Turkevitch, P.C. Stevenson, J. Hillier; *Discuss. Faraday Soc.* **1951**, *11*, 55-75.

(26) K. J. Watson, J. Zhu, S. B. T. Nguyen, C. A. Mirkin; *J. Am. Chem. Soc.* **1999**, 121, 462-463.

(27) D. Zhang, O. Neumann, H. Wang, V. M. Yuwono, A. Barhoumi, M. Perham, J. D. Hartgerink, P. Wittung-Stafshede, N. J. Halas; *Nano Lett.* **2009**, *9*, 666-671.

(28) M. T. Lee, G. S. Ferguson; *Langmuir* **2001**, *17*, 762-767.

(29) C. Haensch, S. Hoeppener, U. S Schubert; *Nanotechnology*, **2008**, *19,* 035703/1– 035703/7.

Chapter 4:
Carbon Nanotubes integration with MEA technology

4.1 Introduction: Micro Electrode Arrays

One of the most profound open challenges in modern science has to do with the emergence of a functioning brain from a collection of individual neurons. This question translates to how an assemblage of initially simple elements, namely neurons, self-organizes to form a new, extremely complex and highly coordinated functioning system: the neural network. Even at the level of a simple network, unraveling the underlying mechanisms involved in the complex activity of neural circuits has been, and still remains, a fundamental challenge. A common and well-accepted approach to study these issues is through the use of cultured neuronal networks on MEA systems. A microelectrode array (MEA) is an arrangement of several (typically 60) electrodes mounted on a glass support, offering the unique possibility of targeting several sites in parallel (as many as 60 recording sites) for non-invasive extracellular recording and stimulation (fig.1).

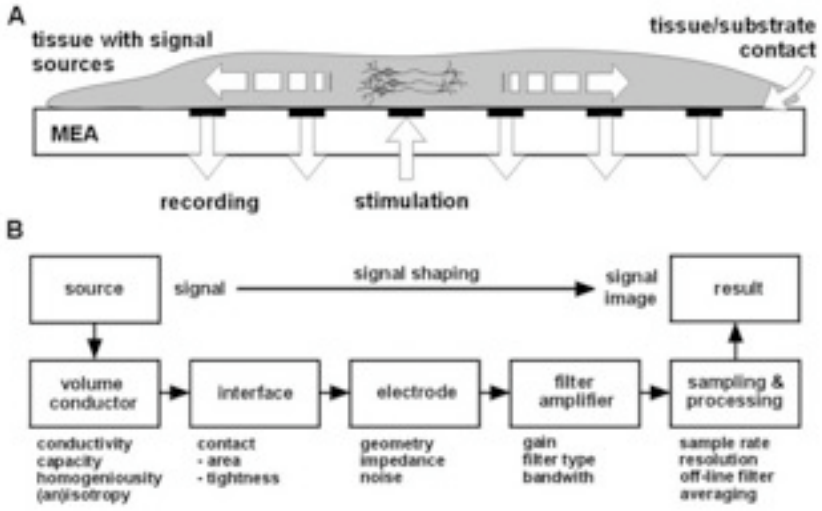

Fig. 1: Cell stimulation and recording by microelectrode arrays (MEA). A) A brain slice is attached to the planar surface of the MEA with its embedded electrodes, which can be used both for stimulation and recording. After stimulation a two-dimensional spread of evoked activity in the tissue occurs and can be recorded with high spatial and temporal resolution. Pre-requisite for reliable signal transmission is a close contact of the tissue to the substrate. B)The recorded, stored, and analyzed signal is an image of the original signal of the cellular sources shaped by several characteristic parameters of the components of the signal chain.

Since its introduction 30 years ago by Thomas and coworkers,[1] the MEA technology and the related colture methods for electrophysiological cell and tissue assays have been continually improved.[2] Since computer capacity has become large enough for online-processing of data streams generated by tens of electrodes, and measurement systems and microelectrode arrays have become commercially available, the technique now has found its way into many academic and industrial laboratories. The focus of MEA-related research over the last 10 years has been the development of high-quality arrays with novel

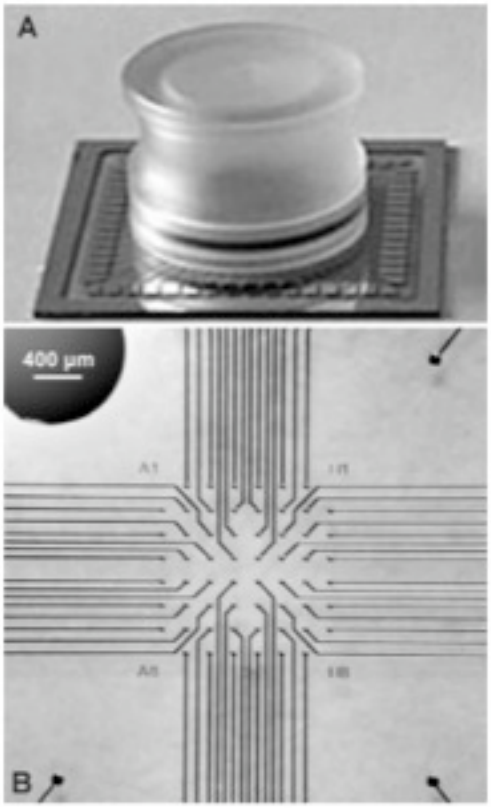

Fig. 2: The microelectrode array manufactured at the NMI Reutlingen. **A)** MEA with closed culture chamber enabling long-term recording from organotypic cell and tissue cultures under sterile conditions. **B)** Inner array of the MEA with 60 electrodes (diameter 10–50µm, spacing 100 or 200µm), a substrate-integrated reference electrode (*upper left corner*) and 3 additional stimulation electrodes (*other corners*). The connecting lanes are isolated by Si_3N_4.

electrodes (fig.2) suitable for long-term monitoring with sufficient signal-to-noise ratio,[3] the establishment of novel applications,[4] and the analysis of the data.[5] Recording experiments using MEAs can mostly be considered as following one or a combination of the following motivations:

I. to gain information about interactions between electrogenic cells at different locations in the same tissue, which may be used to analyze the spatio-temporal dynamics of activity or the representation of information in neuronal networks;

II. to reduce the time required for an experiment by simultaneously recording at several sites in parallel, and thus sample the distribution of electrophysiological behavior efficiently, which may include comparison of tissue properties at different locations;

III. to monitor changes of electrical activity over periods of time not accessible with individual conventional electrodes in *in vitro* experiments.

Furthermore, the exceptional stability of the recording situation when MEAs are used allows analyses that would otherwise not be feasible, for example, to compare activity at a precise raster of recording sites or to record from contracting cardiac myocytes without interfering with the cell.

The integration between biological cells and electronic chips such as MEAs is laden with challenges: biocompatibility, chip durability in a wet environment, packaging issues, electronic circuitry to accommodate data collection, and software to accommodate data analysis and compression.[6] Of the various challenges, achieving the right properties of the actual interface between the chip and the cells are of utmost importance. This interface is critical in ensuring both the viability of the cells and the effectiveness of the electrical interface. The desired properties of the interface between the chip and neurons depend on the transduction method used to convert the electro-physiological activity of the cells (i.e. ionic currents) to electrical signals (i.e. electronic voltage or current). When MEAs are in contact with ionic solution (i.e. biological medium), these electrodes can be regarded as electrochemical capacitors and the coupling between the electrodes and the cells is capacitive in nature.[7] Consequently, a fundamental requirement that these

interfaces have to accommodate is large electrode capacitance. This parameter defines the impedance of the electrode and determines its noise level, how well it can record electrical activity and, most importantly for implantable devices, its effectiveness in stimulating cell activity. On the other hand, to allow high specificity, the electrodes must be as small as possible. Thus, to optimize these two contradicting factors (small electrode projection and large effective area), electrodes with **high specific areas** are most desired. Additionally, since neuronal cells are far more particular than most cell types, **special surface treatment** prior to culturing is required to facilitate cell adhesion, proliferation, growth and proper activity. Commonly, these two requirements (proper electrical and biological coupling) are met separately, using two independent approaches. To achieve electrodes with **large specific area** various **roughening procedures** are used, and various chemical modification schemes are employed to mediate cell adhesion. Among the roughening procedures, electroplating is the most commonly used (in particular, platinum black electroplating,[8] but more recently the use of highly porous sputtered TiN has been demonstrated as a very effective scheme.[9] **Surface chemical modification** schemes to ensure cell adhesion and viability include various adhesion proteins and growth factors.[10] The deposition of the needed chemistry is typically straightforward, but its addition onto the electrode may affect the electrical performances of the electrode as well as its stability. Even though surface chemical modification is the most commonly used scheme to achieve cell adhesion in neurochip technology, a second alternative exists. A great deal of research has revealed the strong sensitivity of cells to the roughness of the surface.[11] In fact, it has been shown that by increasing the roughness of the surface to the nano-scale it is possible to achieve cell adhesive surfaces. With the use of lithographic methods to create heterogeneous surfaces containing flat and rough regions, it was possible to show that cells would preferentially adhere to the rough surface even if the chemistry of the rough and flat surfaces was identical. It should be noted that, despite the compelling evidence linking surface topography and surface roughness to cell adhesion, the origin of this link is not understood. The fact that rough surfaces can provide a good substrate for cell adhesion implies that a direct electrical interface between recording electrodes and cells can be obtained provided the surface of the electrode is both conducting and rough enough to allow direct cell attachment to the surface. The rough surface must also be very durable to avoid breakage.

4.2 CNT coated electrodes

An ideal material for these requirements is a carbon nanotube three-dimensional matrix. Being electrically conductive, CNTs are excellent electrochemical capacitors and have been investigated for super-capacitance applications with and without additional chemical treatments. CNTs are also a promising material in the realm of biomaterials, as we have discussed in chapter 1 and in particular for neurological applications, as highlighted in chapter 2. For all these reasons it is of a foundamental interest the development of a novel class of micro-electrodes coated with islands made of CNTs specifically designed as an

interface for neuronal systems. To develop a superior electro-chemical interface for neuronal recordings, it is of interest to allow the integration of CNT directly onto micro-electrodes. This has been achieved[12] by synthesizing (by a thermal chemical vapor deposition process) high density carbon nanotube islands on lithographically defined, passivated titanium nitride (TiN) conductors on a silicon dioxide substrate. The three dimensional nature of the CNT electrodes contributes to a very large surface area, and consequently to large electrode specific capacitance and low frequency dependence of the electrode impedance. Second, the roughness of the CNT surface is suitable for anchoring the cells to the electrode site. The interaction between the cells and the surface is so strong that it dramatically affects the overall arrangement of the cells on the surface, thus enabling network engineering. The use of CNT paper as a coating material for neuronal electrodes thus facilitates two fundamental capabilities. First, the electrodes act as anchoring points onto which cells can adhere and grow. Second, the electrodes can be used for high fidelity electrical recording and stimulation.

One of the most conspicuous effects observed when culturing neurons on CNT coated islands is the strong affinity of cells to these surfaces. In addition to the apparent cell affinity to the CNT surfaces, cells cultured on CNT electrodes also self-form ordered networks. This process typically occurs by bridging gaps between neighboring islands. The bridging consists of either an axon or bundles of axons and dendrites. The manner by which the cells move towards the CNT-coated surfaces and rearrange into a network is not obvious.

The success of the CNT electrodes in patterning and interfacing with neurons suggests the unique possibility to carry out investigations targeting basic questions related to the activity of small neuronal circuits. CNT electrodes facilitate the construction of the circuit as well as provide the means to perform the electrical recordings. Moreover, it is demonstrated that the CNT-MEAs are also suitable for interfacing with single cells at a very high level of fidelity. In these devices, one of the major challenges is the reactivity of the tissue with the electrode surface. In retinal implant devices, for example, one of the major problems is the weak coupling between the tissue and the electrodes, which results in very poor stimulation specificity. The cells are simply too far away from the electrode to allow stimulation at high efficacy, in terms of both charge injection and site specificity. On CNTs spontaneous bursts of neural impulses as well as slow oscillatory activity were routinely recorded, indicating the viability of these electrodes for recording from intact neural tissue. It is also important to note that the fabrication procedure currently used to produce the CNT-MEAs employs a relatively high temperature procedure, which restricts the range of substrates used while also increasing the fabrication cost relative to conventional MEA. This drawback may be overcome by developing alternative low-cost, low-temperature procedures.

4.3 CNTs electrode coating for ex vivo network-level electrophysiology

For the reasons illustrated above, CNTs represent an obvious choice for future neuroprosthetic devices, at the level of interfacing the neural tissue with "smart" electrodics. Along these motivations, we report a systematic study of hybrid MWCNTs-neuronal networks in vitro. We obtained thin-film depositions of MWCNTs over glass-substrate microelectrode arrays (MEAs), chronically coupled to cultured networks of postnatal hippocampal neurons. This allowed us for the first time to examine at the network-level, the way MWCTNs bidirectionally interacts with the spontaneous neuronal activity and its emergence ex vivo, as first observed at the single-cell level as described in chapter 2.

Two different CNT-coating techniques were considered and explored for MEA functionalization in order to address preliminary the relationship between the spatial extent of the deposition and the impact on spontaneous and evoked electrical activity. MEA devices where furnished by MultiChannel System, GmHb, Reutlingen, Germany. Commercially available MWCNTs were treated by cycloaddition reaction with epthanal and sarcosine as described elsewhere (see chap. 5 - CNT1). A solution containing the functionalized MWCNTs in DMF was prepared and few drops of it were manually deposited under visual control through a stereo-microscope according to two rough patterns: A) the full inner area of the MEA where substrate electrodes are located (i.e. a 2 cm x 2 cm square area centered over the inner MEA area); B) only half of such an area, leaving about half of the 60 electrodes uncovered. Further solvent evaporation through heating at 90°C, and later a treatment of 20 minutes at 350°C in nitrogen atmosphere completed the coating process leaving defunctionalized nanotubes stuck on the MEA surface. Although the deposition was performed manually, on all the MEA devices employed for experiments, there was a good level of deposition reproducibility.

The figure below (fig. 3) reports a glass-based commercial MEA device, with 8 x 8 planar TiN circular microelectrodes, each with a diameter of 30 μm and 200 μm inter-electrode spacing.

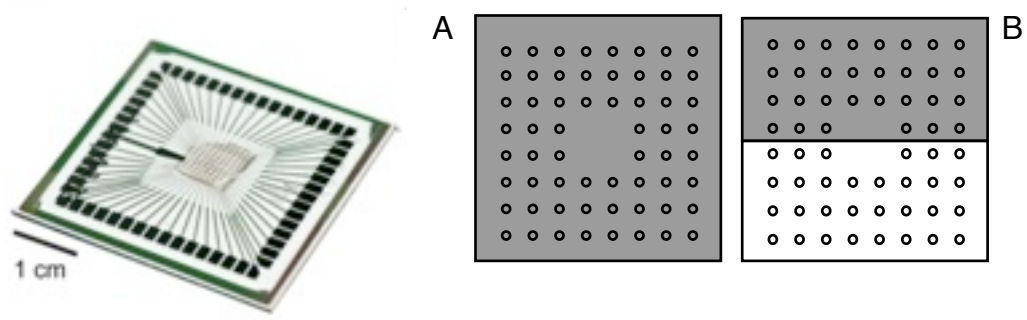

Fig.3: a MEA device covered by a CNT layer in the central area of the electrodes. A and B are the two different patterns used for the CNT deposition

Zooming into the inner area of the array reveal the layout and the actual CNT functionalized area that is represented in the draw on the right of figure 3.
As reported in the literature and routinely described in hippocampal and cortical dissociated neuronal cultures grown on substrate arrays of microelectrodes, [13] synaptic reorganization and maturation lead to the spontaneous emergence of synchronized network-bursts, after about 5-7 days in vitro. These spiking epoch consist in increased firing probability and in propagating waves throughout the cell culture. In addition these epochs are alternated to periods of asynchronous spiking activity, where the rate of spike emission is generally low (e.g. 0.5 - 2 Hz) and much lower than during a network burst (e.g. 10 - 50 Hz).
By means of conventional intracellular patch recordings, the occurrence of a network-burst is monitored in the postsynaptic membrane potentials as a membrane depolarization caused by the release of chemical neurotransmitters. These neurotransmitters are generally capable of eliciting a burst of spikes in the recorded cells which occurrence is synchronized throughout the network. Extracellular detection of the same spontaneous occurrence of network-wide synchronous events, results in quite different recorded waveforms. By definition of extracellular recordings, such waveforms conveys very poorly and give no information on the subthreshold temporal details of the transmembrane voltage trajectory. Information content is therefore generally limited to the firing times of the action potentials.
Previous attempts to interpret quantitatively a similar network-level ex vivo behavior and to related to single-cell and synaptic underlying properties [14] led to suggest that the boosting effect of CNTs on the frequency of occurrence of spontaneous network-burst may be related to synaptic hyper connectivity. This prediction was later verified experimentally by our work in collaboration with Prof. Laura Ballerini, described in chapter 2.

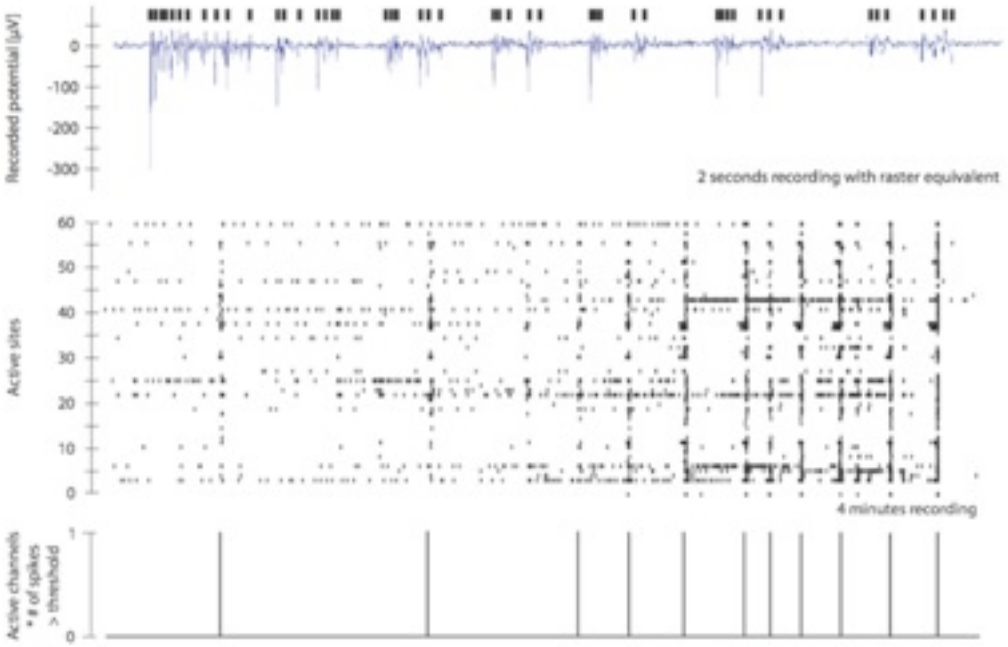

Fig. 4: raster diagram that represents the occurence of synchronous and asynchronous electrical events for each recording channel of the MEA.

Detection of Spike Efficiency

By standard methods of analysis of extracellularly detected multichannel data, it is possible to represent graphically the alternation between synchronous network-burst and asynchronous activity, in the form of a raster diagram (see fig. 4), where the occurrence of a single action potential is identified for each recording channels (for each MEA electrode or "site") and marked as a single time-stamp in a plot.
By a conventional definition, the occurrence of a population burst can be identified automatically, providing an indication on the number of individual spikes that compose it and on the time tags for the time of its ignition and of its end. [15]
Below in fig.5 we report another of such a raster-plot diagrams, expanding the horizontal scale during a network-burst and unveiling its composition in terms of actual synchronization of individual spike-trains.

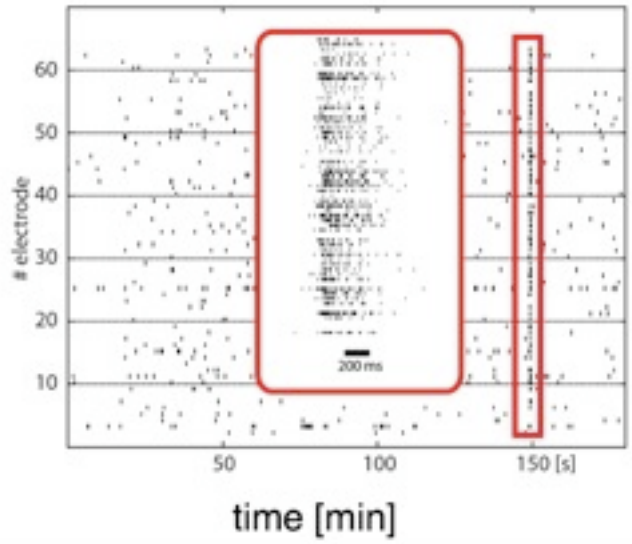

Fig. 5: raster diagram that represent the expansion, in the time scale, of a network burst event

Below in fig.6 we further report a 10 minutes sample recording obtained from a 16 days in vitro colture of hippocampal neurons grown on a MEA partly coated with CNT (see fig.3) consisting in a roughly 50:50 subdivision of the MEA electrodes in "coated" i.e. indicated in red) and "uncoated" (i.e. indicated in blue).
Results from a detailed analysis of the firing activity detected extracellularly in the partly coated CNT-MEA devices, and its comparison with activity detected from electrodes that were left unexposed, systematically revealed an uneven composition of the inter- and of the intra-burst firing. The average fraction of spikes during a network-burst (see the bar plot below), shows a ~50% increase in the network-burst composition, favoring the spike detected by CNT-coated electrodes. It is interesting to underline that the same increase percentage happens for both intra- and inter- burst epochs.

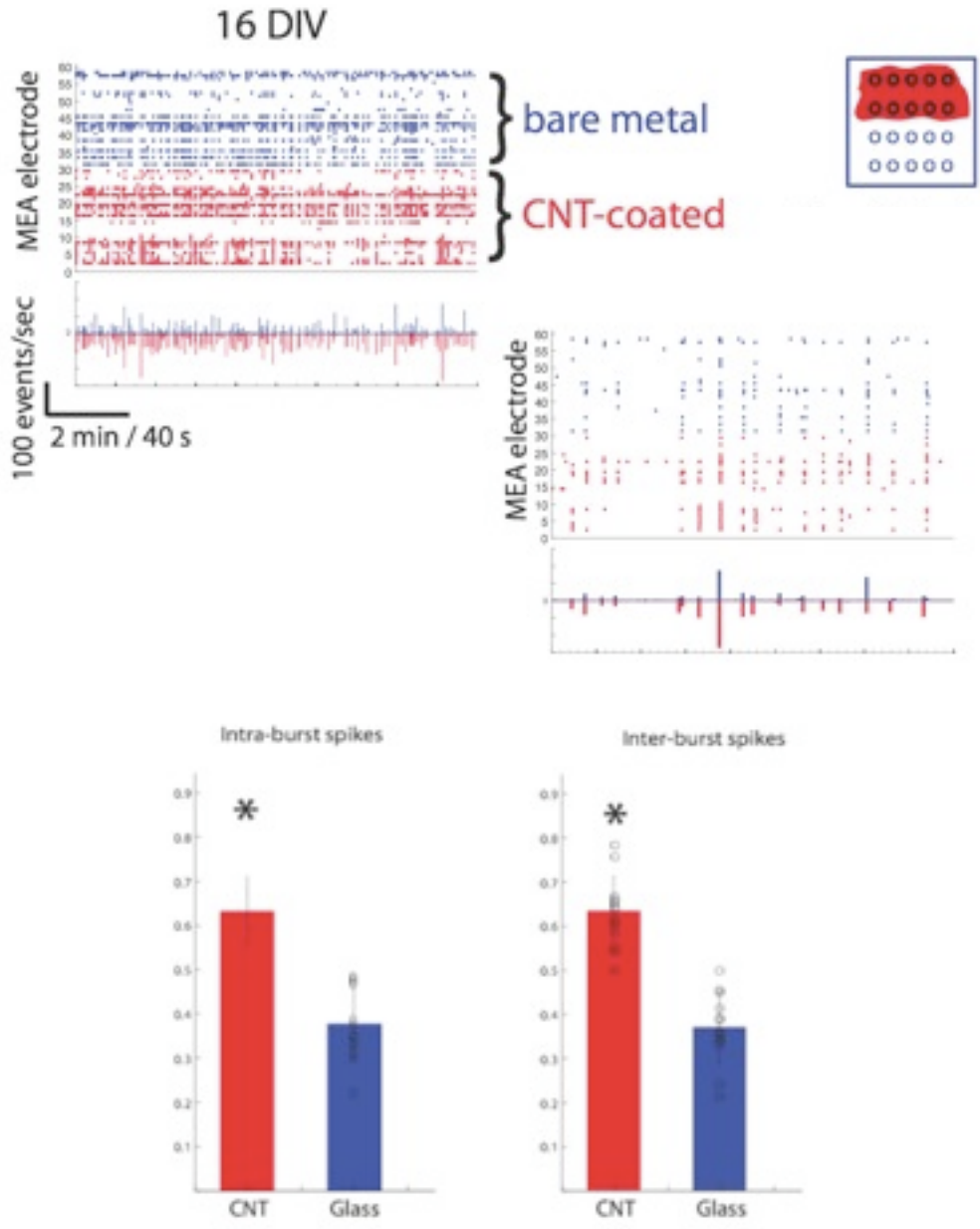

Fig. 6: In the upper part: 10 minutes sample recording obtained from a 16 days in vitro colture of hippocampal neurons grown on a MEA partly coated with CNT, and the relative enlargment in the time scale. In the lower part: histograms representing the fraction of intra- and inter- burst spikes detected by CNT-covered (red) and uncovered (blue) electrodes.

The simplest way to interpret the previous results is to assume that the effective electrical properties of extracellular sensitivity at the interface electrode-CNT-electrolyte were considerably increased, compared to the electrode-electrolyte: lower electrical impedance and higher capacitance. This is in agreement with the observations of Keefer et al.,[16] who found that covalently-attached CNTs on both MEA planar electrodes and metallic microelectrodes, are capable of a superior signal-to-noise ratio in virtue of a decrease in the electrode-electrolyte impedance, both *in vivo* and *in vitro*.

By the same color convention of the previous plots, in fig. 7 below we report an average of ~50% increase in the peak amplitude of extracellularly spikes, detected by CNT-coated electrodes compared to unexposed electrodes, after raw waveform processing.

Observe that the increment in the amplitude of detected raw spikes between the CNT coated and unexposed electrodes is correlated to the increment of the spike frequency.

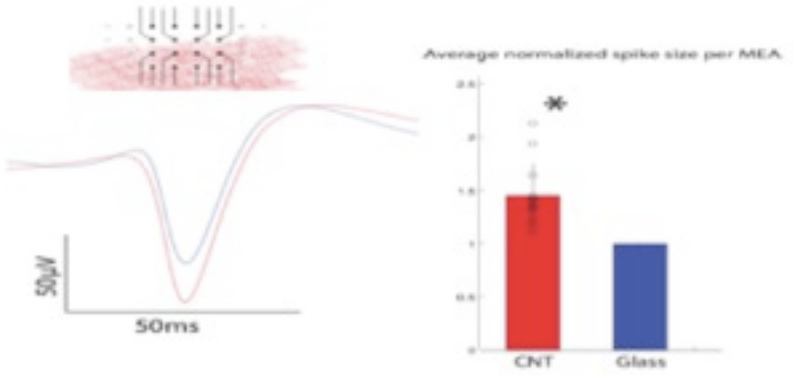

Fig. 7: Comparison of the peak amplitude for CNT-coated electrodes and unexposted electrodes.

In fig. 8 we have plotted the actual distributions of spike amplitudes. The comparison between the distributions for the CNT-coated and unexposed electrodes highlights the systematic increase of the spike amplitudes for the former case.

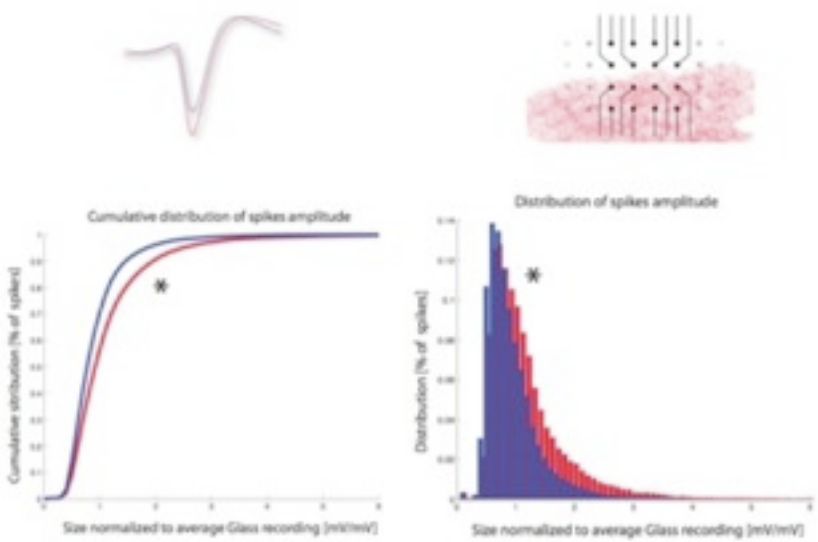

Fig. 8: cumulative distribution and distribution of spike amplitudes for CNT coated (red) and uncoated (blue)electrodes.

Burst shape analysis

We analyzed the average shape of network-bursts. To this aim, we computed the peristimulus time histogram (PSTH) of the times corresponding to each spike detected from MEA electrodes, employing first a very large bin size. In neurophysiology **peristimulus time histogram**, abbreviated **PSTH**, is an histogram of the time at

which neurons fire. This histogram is used to visualize the rate and timing of neuronal spike discharges in relation to an external stimulus or event. Threshold crossings of such a PSTH, once multiplied by the number of co-active electrodes in the corresponding time bin, allowed us to roughly localized each network-burst.[15] By recomputing the PSTH alone (i.e. ~ the global firing probability as a function of time, within a burst), through much finer time bins, we identified the local peak of the probability of firing that we have been estimating. Aligning all subsequent PSTHs to their peak value, we obtained the typical shape of a burst (see fig. 9).

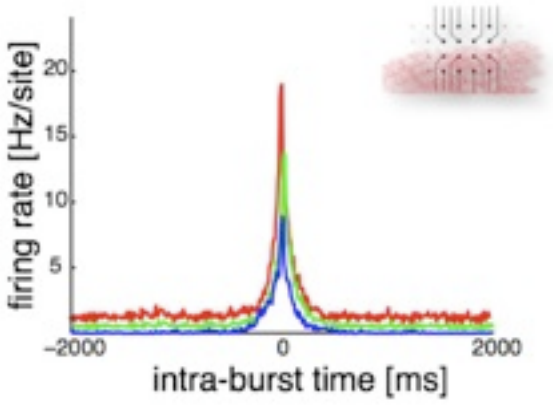

Fig. 9: average burst shape, for CNT coated electrodes (red), uncovered electrodes (blue), and all electrodes (green).

By selecting alternatively the two groups of ~30 MEA electrodes coated (red trace) or unexposed (blue trace), and as well selecting all electrodes (green trace), we obtain the average network-burst shape plotted above. In particular, the red trace is shifted upwards with respect to the blue trace, implying that the number of spikes both in the intra-burst and in the inter-burst epochs are more frequently detected by CNT-coated electrodes. When the average shapes of a network-burst identified on CNT-coated electrodes (red trace) and on unexposed electrodes (blue trace) are normalized to the same peak amplitude but aligned to a common threshold crossing, it is apparent that the rising phase of the red curve is slightly steeper than the one of the blue curve (see fig. 10).this might be indirectly linked to a hyper connectivity of the neurons growing on the CNT-coated areas, or to their stronger excitatory synaptic coupling.

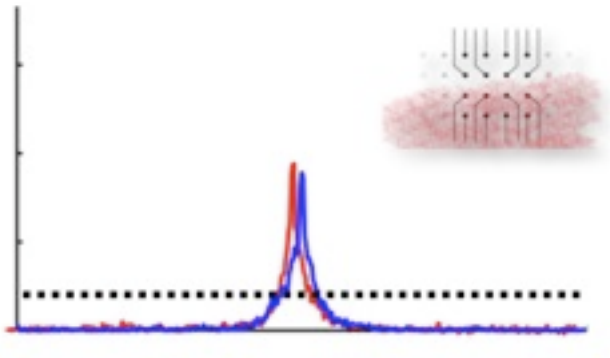

Fig. 10: average burst shape of a network of burst for CNT coated electrodes(red) and uncovered electrodes (blue) normalized in the same peak amplitude and aligned to a common threshold crossing

Pairwise cross-correlations between the timing of individual spikes, detected from pairs of MEA electrodes were computed by estimating the peak value of the spike-triggered cross - correlograms over a fixed time window (in the range 1 ms - 1s).
Spatially-extended CNT-substrates have been shown to increase synaptic connectivity in developing networks of cultured hippocampal neurons. Considering the partly coated MEA, an increase in the connectivity, although restricted to a 50% area of the network may not lead to a discriminable occurrence of spontaneous network-burst, as the two subnetworks are likely to be extremely densely interconnected to each other making any functional clustering of their activity impossible.
Nevertheless, the hyperconnectivity might be reflected into a higher level of spike-timing correlations, when computed from spike trains detected by pairs of CNT-coated electrodes. This was indeed the case, throughout all (n = 13) experiments, resulting into a 50% increase in the cross-correlation (see fig. 11), compared to levels of correlation between spike-trains detected at unexposed electrode pairs. The figure below reports the population summary for all the experiments, restricting the calculation of the cross-correlations to the intra-burst epochs. Although a higher correlation level was sometime observed during the asynchronous epochs, by definition there were too few spikes detected to allow for a reliable estimate of the cross-correlation. In addition, it is expected that such cross-correlation might lead to long-range functional connectivity between neurons.

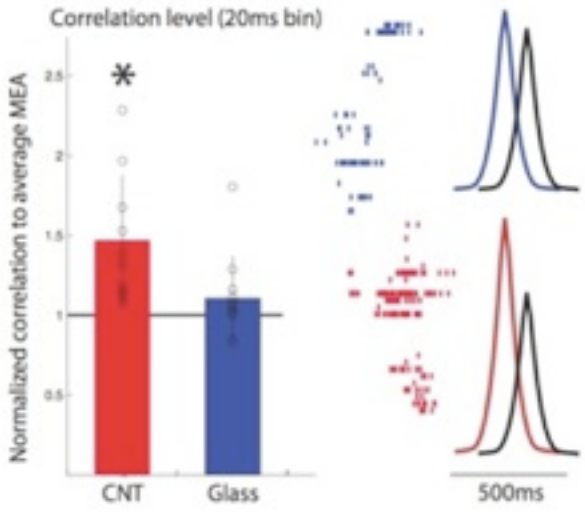

Fig. 11: pairwise cross-correlation between the timing of individual spikes for the intra-burst epochs

Extracellular stimulation through MEA+CNT

A set of 6 MEAs, completely coated by CNTs with a different coating density, were employed to investigate whether CNT coating and the consequent increase in the effective electrode capacitance, might be exploited for extracellular stimulation of neuronal activity. It was therefore possible to study the effect of electrical stimulations of increasing amplitudes and different spatial configuration, on neuronal electrical activity. This investigation considered 4 uncoated MEAs as a control, and six CNT-MEAs with increasing CNTs density. Electrical stimuli were delivered by means of a STG8000 (Multichannel Systems, Reutlingen) stimulus isolator. Stimuli waveforms were biphasic and voltage-controlled, consisting in symmetrical voltage-pulses of amplitude ranging from 0.8 to 1.8 V peak-to-peak, and with a pulse width of 400 μs. Pulses was delivered by means of a bipolar configuration, selecting random pairs of MEA electrodes of increasing distances (200, 600 and 1400 μm) where the pulsed transient voltage difference was applied. This stimulation paradigm has the advantage of producing a spatially restricted electrical field, since the force field lines do not disperse through the entire electrolyte as in the monopolar configuration (i.e. the stimulation electrical reference is set to the ground electrode) but are closed to the neighboring electrode of each pair. Because of the homogeneity of the responses, the results of these experiments have been mediated across the MEAs samples, composing each group (i.e. uncoated, low-density CNTs, high-density CNTs), and across the 6 distinct spatial configuration, the 6 different stimulus amplitudes, and the 20 repetition. Then, for each MEA a total of 720 evoked responses has been analyzed. Given a fixed electrical stimulation, it is clear that, for increasing CNT densities, neuronal responses are stronger.

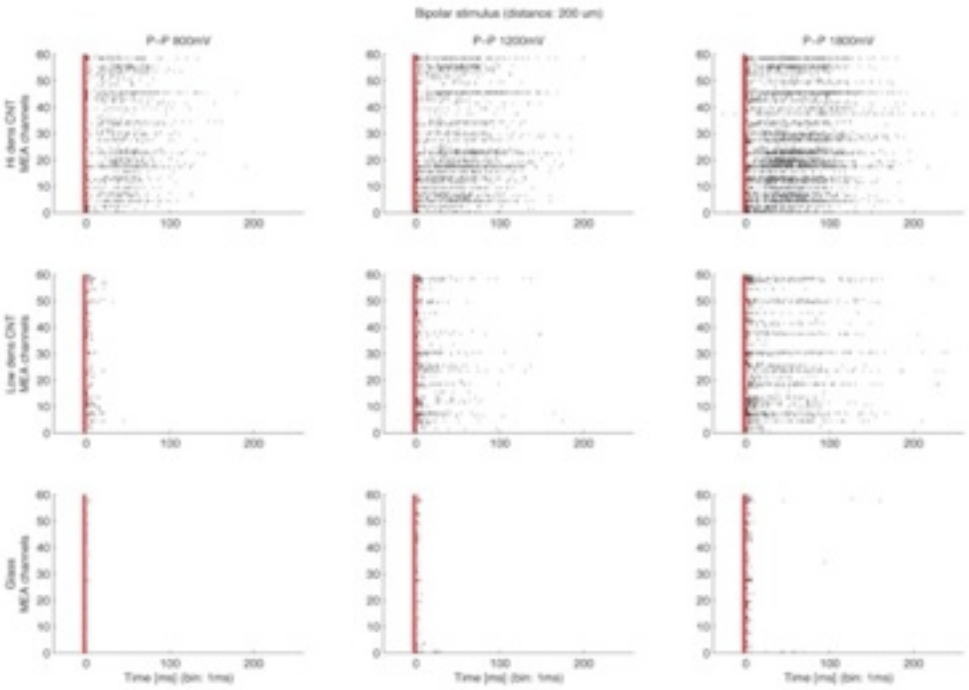

Fig. 12: raster diagrams for an inter-electrode distance of 200 um

Two sample raster diagrams (fig. 12 - 13), representing the temporal occurrence of spike activity at each of the 60 MEA electrodes, for each MEA type, are reported below. Moving from left to right, individual panels refer to increasing stimulation amplitude, while moving from the bottom to the top, they refer to increasing deposited CNTs-density.
Below, the very same raster diagram is reported when the inter-electrode distance was 600 instead of 200μm.

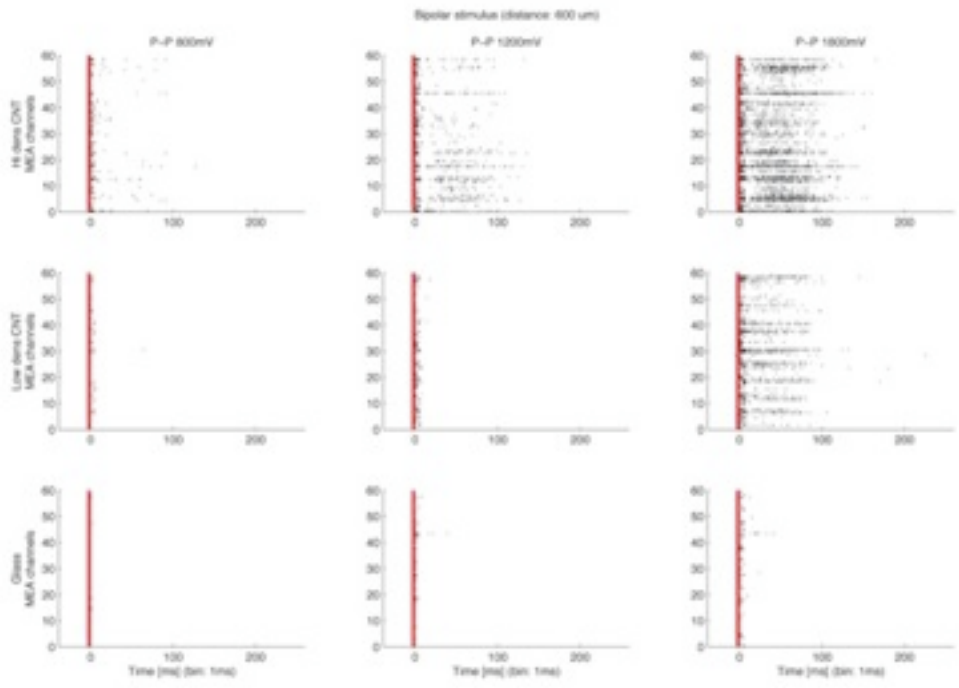

Fig. 13: raster diagrams for an inter-electrode distance of 600 um

As expected, the larger the distance the less the neuronal responsiveness due to a massive dispersion of the electrical stimulus, at the same stimulation intensity. The results of these experiments have been finally summarized in time histograms, triggered across several repetitions by the time of the delivered extracellular stimulation (see fig. 14). These activity histograms indicate by a different line color, the CNT density; light gray : control, gray: low CNTs density, black: high CNTs density. Different panels account for the effect of increasing stimulation intensity while the different rows outline the initial 60 msec of the population burst, evoked by the extracellular stimulation. As described extensively in the literature,[13] the evoked response is composed by a first phase, occurring over the first tens of msec that we defined a "feed-forward" response, and by a later phase, occurring over the subsequent hundreds of msec, that we defined a "recurrent" response. From the basis of the considerations of Giugliano et al.,[14a] the recurrent response is interpreted as an evoked population burst.

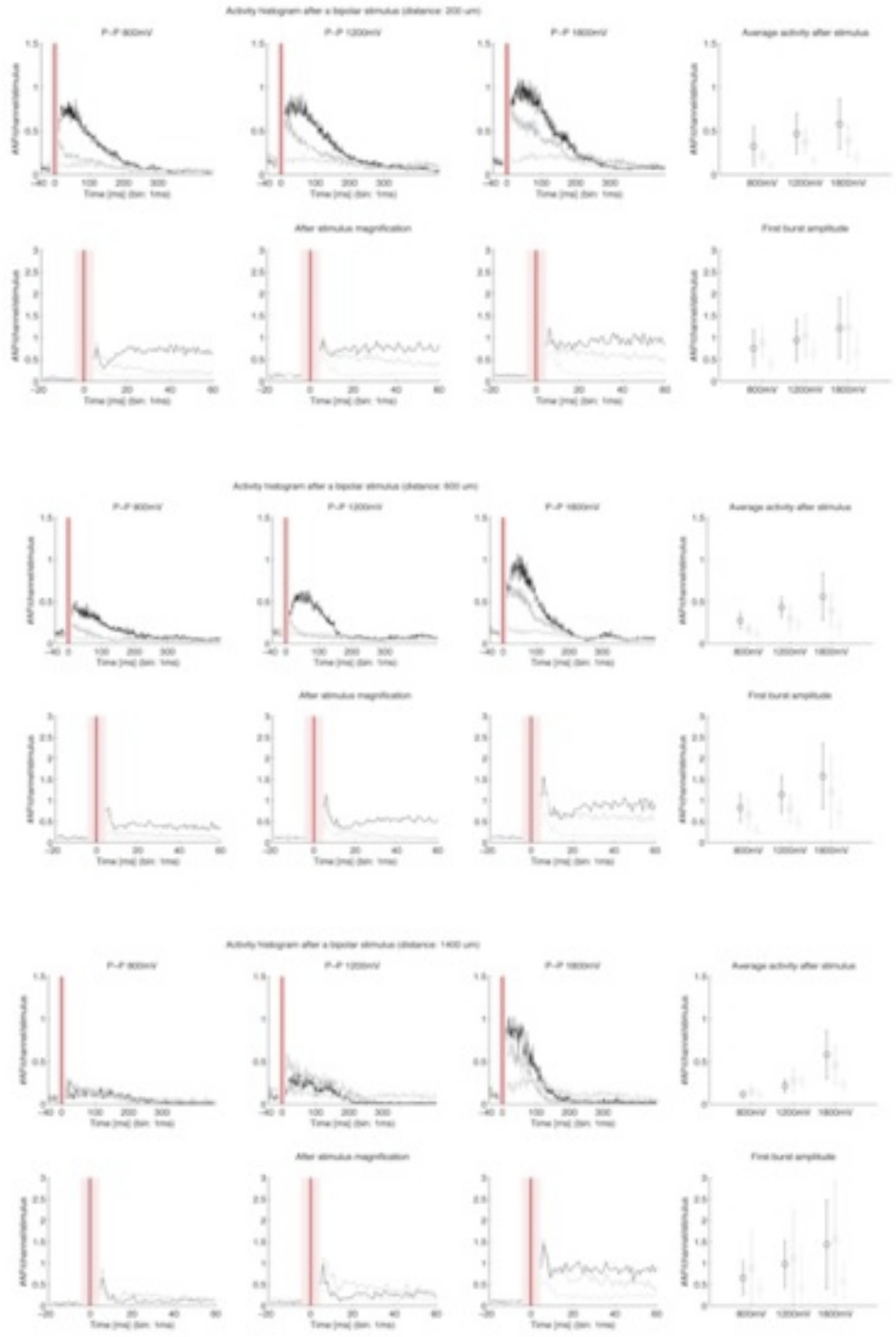

Fig. 14: Activity histograms after a bipolar stimulus of 200 um (first two rows), 600 um (third and fourth row), 1400 um (fifth and sixth row). Light gray represent the control uncovered MEA, dark grey the low density CNT covered MEA and black the high density CNT covered MEA. Different panels account for the effect of increasing stimulation

It is important to observe that the effect of CNT deposition is only reflected in a minor way in the peak amplitude of the "feed-forward" evoked response, among the different conditions (glass/ control, low density CNT, high density CNT). It is instead the area below the burst profile (the instantaneous evoked firing probability) that differs in a considerable manner between the three situations (glass/control, low density CNT, high density CNT). It can be intuitively appreciated how for decreasing stimulation amplitude or for increasing inter-electrode distances, both the elicited feed-forward and recurrent responses are inversely affected. All in all, these results support the observations that an extended CNT coating affects the overall network activity through the synaptic connectivity of the network and therefore modifies its susceptibility in firing a (stimulated vs spontaneous) population burst. From the data in our hand, the effect of the deposited CNT density on charge-injection capacity is much less dramatic, perhaps due to the specific geometry of deposition.

Conclusions

This work is focused on the recently described "endogenous" functional interactions arising when MWCNTs and neuronal networks are coupled. Beyond the expected improvements in terms of electrical impedance of MEA electrodes coated by MWCNTs, we explicitly addressed the impact on collective neuronal activity at the network-level, in the case of spatially extended MWCNTs thin-film depositions.
Our results confirm and extend to the network-level what is observable intracellularly, at the level of postsynaptic evoked/spontaneous responses.
In addition, these results set the ground for a mechanistic interpretation of the interaction between MWCNTs and neurons, potentially relevant for the future neuroengineering of neuronal tissue in direct contact to MWCNTs-based brain implants. We speculate that by the findings of on the apparent MWCNTs-mediated boosted calcium-electrogenesis (as reported in chapter 2), the larger spike-timing cross-correlations observed here closed self-consistently a conceptual loop: from long-lasting postsynaptic calcium-transients to increased spike co-occurrences, and from spike-timing correlations to reinforcement of synaptic connections.

4.4 References

(1) C. A. Thomas, P. A. Springer, G. E. Loeb, Y. Berwald-Netter , L. M. Okun; *Exp. Cell. Res.* **1972**, *74*, 61–66.
(2) S. M. Potter; *Prog. Brain. Res.* **2001**, *130*, 49–62.
(3) a) V. Bucher, M. Graf, M. Stelzle, W. Nisch; *Biosens Bioelectron* **1999**, *14*, 639–649. b) W. Nisch , J. Böck, H. Haemmerle, A. Mohr; *Biosens Bioelectron* **1994**, *9*, 737–741.
(4) U. Egert, B. Schlosshauer, S. Fennrich, W. Nisch, M. Fejtl, T. Knott, H. Haemmerle; *Brain Res Protoc* **1998**, *2*, 229–242.
(5) U. Egert , T. Knott, C. Schwarz, M. Nawrot, A. Brandt, S. Rotter, M.Diesmann; *J Neurosci Methods* **2002**, *117*, 33–42.
(6) E. Hulata, R. Segev, Y. Shapira, M. Benveniste and E. Ben-Jacob; *Phys. Rev. Lett.*, **2000**, *85*, 4637–4640.
(7) Y. Jimbo, A. Kawana; *Bioelectrochem. Bioenerg.*, **1992**, *29*, 193.
(8) C. D. James, A. J. H. Spence, N. M. Dowell-Mesfin, R. J. Hussain, K. L. Smith, H. G. Craighead; *Biomed. Eng.* **2004**, *51*, 1640–1645.
(9) M. Janders, U. Egert, M. Stelzle, W. Nisch; *Nano Lett.*, **1996**, *1*, 245–247.
(10) M. Matsuzawa, S. Tokumitsu, W. Knoll, H. Sasabe; *Langmuir* **1998**, *14*, 5133–5138.
(11) J. J. Pancrazio, S. A. Gray, Y. S. Subin, N. M. Dowell-Mesfin, M. A. Abdul-Karim, M. Turner, S. Schanz, H. G. Craighead, B. Roysam, J. N. Turner, W. Shain, *J. Neural Eng.*, **2004**, *1*, 78–90.
(12) E. Ben-Jacob, Y. Hanein; *J. Mater. Chem.* **2008**, *18*, 5181–5186.
(13) S. Marom, G. Shahaf; *Q Rev Biophys* **2002**, *35*, 63-87.
(14) a) M. Giugliano , P. Darbon, M. Arsiero, H. R. Luscher , J. Streit; *J Neurophysiol* **2004**, *92*, 977-999 b) M. Giugliano, G. La Camera, S. Fusi, W. Senn; *Biol Cybern* **2008**, *99*, 303-318.
(15)J. Van Pelt J, P. S. Wolters, M. A. Corner, W. L. Rutten , G. J. Ramakers; *IEEE Trans Biomed Eng* **2004**, *51*, 2051-2062.
(16) E. W. Keefer, B. R. Botterman, M. I. Romero, A. F. Rossi, G. W. Gross; *Nature Nanotech* **2008**, *3*, 434-439.

Chapter 5:
Experimental Section

5.1 Specific Instrumentation and Techniques

Nuclear magnetic resonance (NMR): 200 MHz ^{1}H-NMR and ^{13}C-NMR were obtained on a *Varian Gemini 200* spectrometer. Chemical shifts are reported in ppm using the solvent residual signal as an internal reference ($CDCl_3$: $\delta H = 7.26$ ppm, $\delta C = 77.16$ ppm, CD_3OD: $\delta H = 3.31$ ppm, $\delta C = 49.00$ ppm, Me_2SO-d6: $\delta H = 2.50$ ppm, $\delta C = 39.52$ ppm, C_5D_5N: $\delta H = 7.19, 7.55, 8.71$ ppm, $\delta C = 123.5, 135.5, 149.5$ ppm). Coupling constants (*J*) are given in Hz. The resonance multiplicity is described as *s* (singlet), *d* (doublet), *t* (triplet), *q* (quartet), *dd* (doublet of doublets), *m* (multiplet), *br* (broad signal).

Infrared Spectra (IR): were recorded on a FT-IS Shimazdu spectrometer operating in Fourier transformation mode.

UV-Vis-NIR Spectra: were recorded on a Jasco V-530 spectrometer in 1cm thick quartz cuvettes.

Fluorescence Spectra: were recorded on a F-4500 HITACHI spectrometer in 1 cm thick quartz cuvettes.

Raman Spectra: were recorded on a Reishaw System 1000 spectrometer with holographic filter super-Notch, with excitation wavelength of 633 and 488 nm.

Thermogravimetric analysis (TGA): TGA analysis were run on the instrument TGA Q500 using a N_2 gas flux and a heating ramp of 10°C per minute up to 1000° after isotherm at 100°C for 20 minutes. Measurements were taken 2 times per sample and the average value of weight loss was reported. Data were analyzed by evaluating the ratio between number of carbon atoms and functional groups obtained by the relation: ((100-A)/12)/(A/*B*); where A is the weight loss and B is the molecular weight of the functionalization.

Transmission electron microscopy (TEM): TEM images were taken on a Philips EM 208 electronic microscope operating at 100 kV. Sample were prepared suspending the compound in DMF, methanol or water and depositing a drop of the solution on copper grids covered by a carbon film of 3,00 mm. Solvent was dried overnight under vacuum.

Scanning electron microscopy (SEM): SEM images were taken on a Leica Stereoscan 430i microscope. CNT samples needed a previous metallization as they are not conductive substrates. Metallization was performed under vacuum with a conductive copper film by the Sputter Coater S150A (BOC Edwards, UK).

X-Ray Photoelectron Spectroscopy (XPS): XPS spectra were recorded on a ESCA Spectrometer SSX-100. The glass samples were fixed on the sample holder using double sided adhesive conductive carbon tap (SPI supplies). The sample holder was introduced to the first room of the apparatus under nitrogen flux, and then high vacuum was applied. After 40 minutes of pumping, the sample holder is transfered to the analysis room under a 10^{-8} torr vacuum. A flood gun was applied in order to minimize the charge effect. Survey spectra were taken after the accumulation of 10 scans, while high resolution spectra after the accumulation of 20 scans. EV/Step was fixed to 0.08 in the case of survey spectra and 0.8 for the high resolution spectra.

Contact Angle: were measured by a AB Lorentzen & Wettre (Stockholm) manual goniometer. Sample were analyzed by the "sessile drop method" using an optical system to capture the profile of a pure liquid on a solid substrate. The base b and the height h of the drop profile were evaluated and the contact angle α was given by the relation $tg(\alpha/2) = 2h/b$. All the values reported are an average on 10 samples, three measurements for each sample.

5.2 Materials

Chemicals were purchased from, *Aldrich*, *Fluka* and *Riedel* and used as received.

Solvents were purchased from *JTBaker* and *Aldrich*, and deuterated solvents from *Cambridge Isotope Laboratories*.

Carbon Nanotubes: MWCNT were produced by the CVD method and purchased from "Nanostructured & Amorphous Material Inc" (Los Alamos, USA). **SWCNT** were produced by the HiPCo method and purchased from "CNI Carbon Nanotechnologies Incorporated" (Houston, USA). **DWCNT** were produced by the CVD method and were purchased from "Nanocyl s.a." (Sambreville, Belgium).

Glass Coverslips were purchased from Kindler (Berlin). Dimensions were 12x24 mm, thickness 0,1 mm. Before depositing cells on glass coverslips they were treated in HCl 0.5 N for 24h, and washed in MIlliQ^R water for four times, absolute Ethanol for 1 time, and again MilliQ^R water for three times. Lastly they were treated in owen at 150°C for 12/24 hours.

MEA were purchased from "Multichannel Systems", GmHb, Reutinglen, Germany.

5.3 Modification and characterization of CNTs

5.3.1 Preparation of CNT1

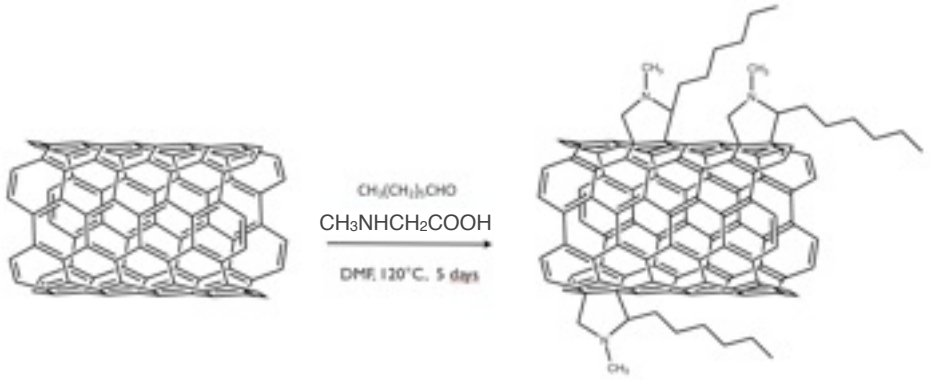

As produced MWNTs (100 mg), were suspended in 100 mL of DMF. The heterogeneous mixture was sonicated for 5 min. Sarcosine (300 mg) and heptaldehyde (130 µL, addition repeated every 24 h) were added and the reaction was stirred at 120°C for five days. The mixture was centrifuged and the supernatant was filtered using a 0.2 µm PTFE filter (Millipore, USA). The filter was washed and sonicated 5 times with DMF. The material recovered as functionalized MWNTs (60 mg) onto the filter was then extensively washed with DCM (100 mL), Methanol (100 mL) and Diethyl ether (100 mL) and dried under vacuum.

Characterization:

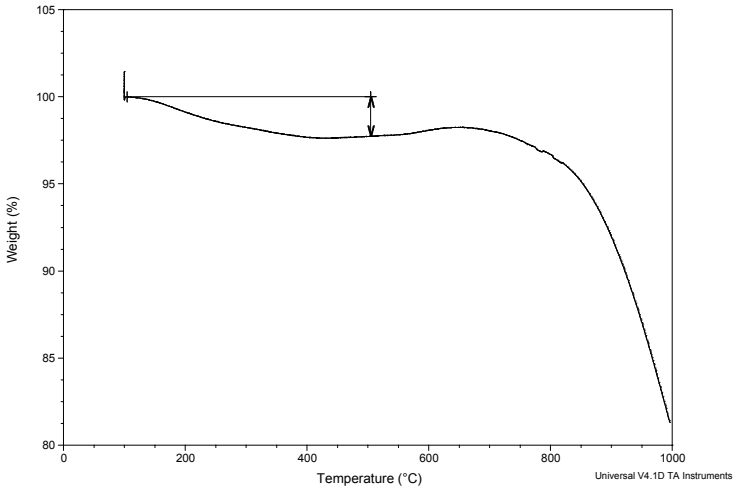

1) TGA

At the temperature of 500°C, which corresponds to a flex, and all the functionalization is burned, we register a weight loss of 2,3% which corresponds to one functional group every 480 carbon atoms, a normal value for multi-walled nanotubes.

2)TEM

Samples were prepared by dissolving the CNT1 in DMF. TEM micrograph show a sample very homogeneously dispersed (no bundles are present in the photos), particularly clean, and well purified. The two image below are taken at 44000x (left) and 22000x (right) magnification.

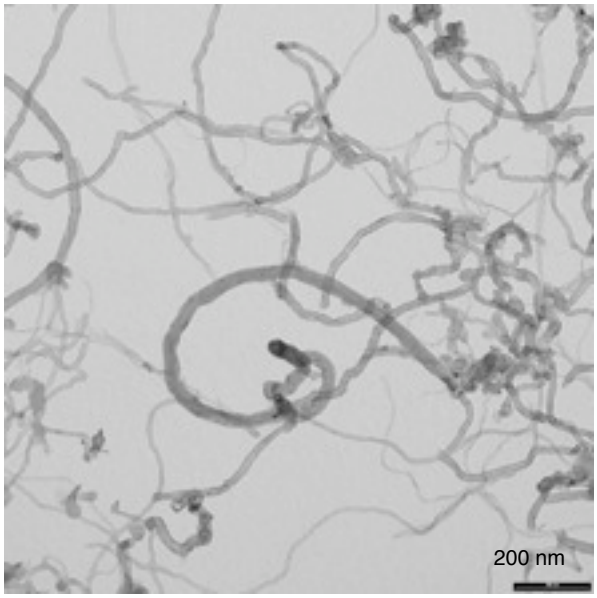

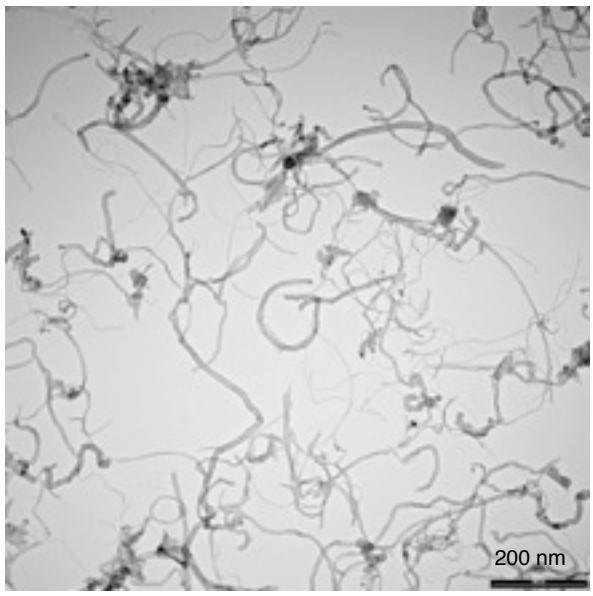

In the details individualized CNT are shown. This confirm the very good dispersion of the sample. Photos taken at 36000x.

5.3.2 Preparation of CNT2

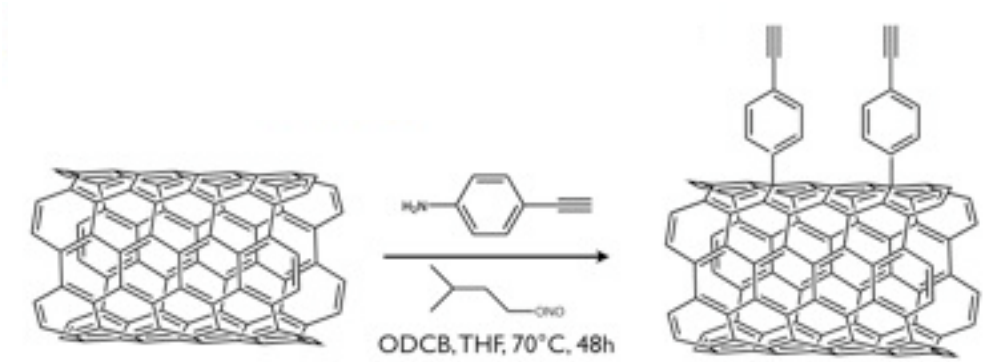

DWNTs (100 mg), were homogenized in a mixture of 150 mL of 1,2-dichlorobenzene and 30 mL of THF for a period of 20 min. The suspension was transferred to a 500 mL round-bottom flask equipped with a magnetic stir bar. The solution was sparged with nitrogen for 20 min, and 4-ethynil aniline (3.60 g, 12.5 mmol) was then added all at once. The flask was sealed and then evacuated and backfilled with nitrogen. Isoamyl nitrite (1.9 g, 16.6 mmol) was added by syringe. The contents were heated and stirred at an internal temperature of 55-60 °C for 48 h. Upon cooling of the reaction mixture, the suspension was diluted with 100 mL of DMF and then filtered over a PTFE membrane (0.45 μm). The filtrate was washed with an additional 50 mL portion of DMF, and homogenized for 20 min in 200 mL of fresh DMF. The suspension was again filtered, washed with 25 mL of DMF, and again subjected to homogenization in DMF. After a final filtration (the filtrate was clear at this point), the filtrate was washed with 40 mL of ethyl ether and kept wet. The resulting material was scraped off the filter and dried under vacuum to obtain a total of 117 mg.
The Raman, TGA and TEM characterization of this compound is reported in chap. 4, sec. 4.4

5.3.3 Preparation of CNT3

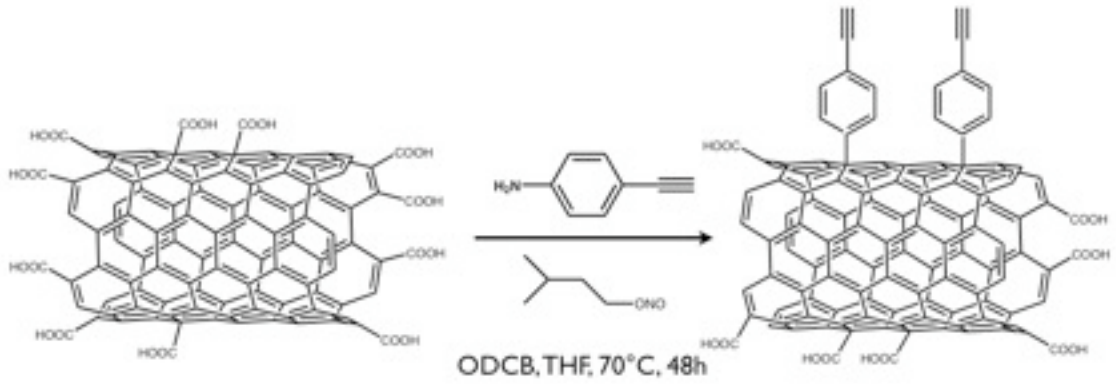

Oxidized DWNTs (100 mg), were treated by the radical Tour reaction with the same procedure described above for pristine DWCNTs. Using the same procedure, the same quantities and the same work-up, we obtained 104 mg of resulting material.

The Raman, TGA and TEM characterization of this compound is reported in chap. 4, sec. 4.4

5.3.4 Preparation of CNT4

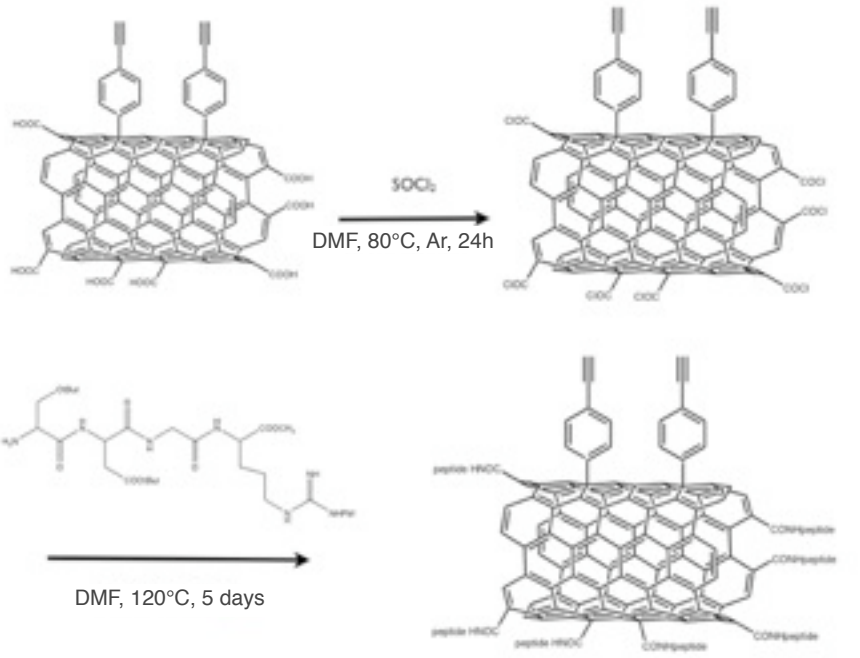

CNT3 (70 mg) were introduced in a 250 mL flask with a magnetic stirrer. The flask was put under anhydrous conditions and 50 mL of thionil chloride were added by siringe. The mixture was sonicated 20 min to homogenize the solution, and 10 mL of anhydrous DMF were added. The reaction was put under magnetic stirring at 80° C for 24 h, under Ar atmosphere.
At the end of the reaction time the flask was cooled at room temperature and solvent was dried under vacuum. Still under Ar flux, fresh DMF was added, the nanotubes were dispersed again by the use of a sonic bath, and 150 mg of the RGD peptide H-Ser(tBut)-Asp(tBut)-Gly-Arg(Pbf)-OMe were added. The reaction was left at 120°C for 5 days.
The flask was cooled at room temperature and the nanotubes were filtered on a PTFE membrane by a millipore filtration system. The nanotubes were washed by DMF and homogenized again in fresh DMF, and then washed and homogenized repeatedly in MeOH and CH_2Cl_2. After the final washing they were washed by diethyl ether, scraped off the filter and dried under vacuum overnight.
TGA and TEM characterization of this compound are reported in chap.4, sec. 4.4.

5.3.5 Preparation of CNT5

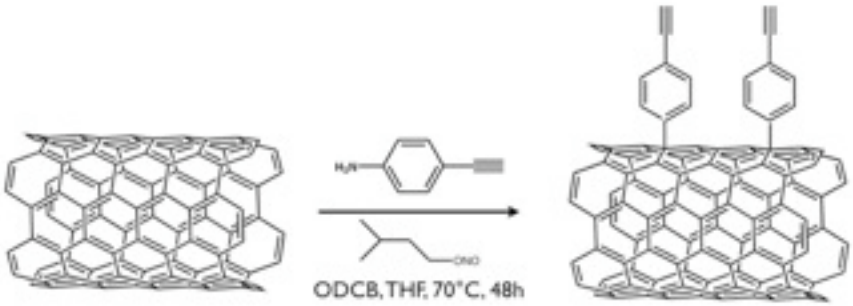

As produced MWNTs (100 mg), were treated by the radical Tour reaction with the same procedure described above for pristine DWCNTs (section 5.3.2). Using the same procedure, the same quantities and the same work-up, we obtained 97 mg of resulting material.

Characterization:

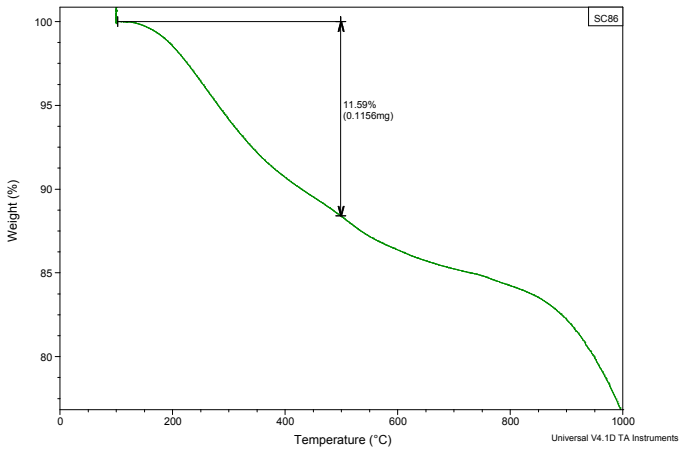

1)TGA

At the temperature of 500°C, which corresponds to the flex, and all the functionalization is burned, we register a weight loss of 11,7% which corresponds to one functional group every 66 carbon atoms, a very high value for multi-walled nanotubes.

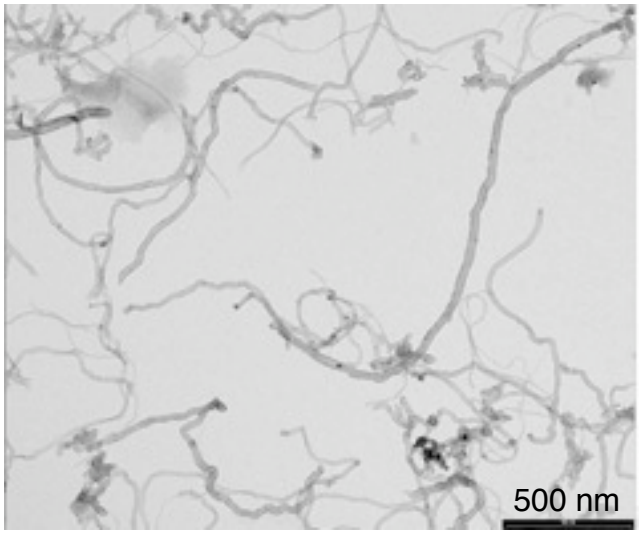

2)TEM

TEM images show a very clean sample and nanotubes appear very well dispersed and individualized.

5.3.6 Preparation of CNT6

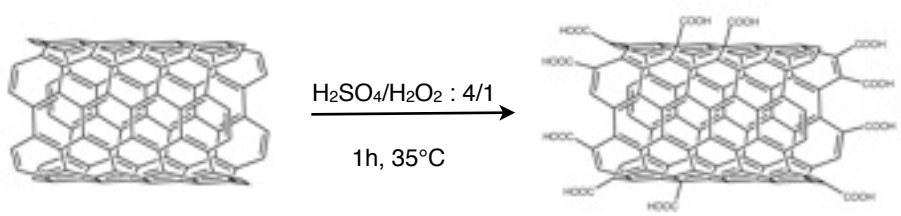

As produced MWNTs (100 mg), were dispersed in 100 mL of pirana solution (H_2SO_4/ H_2O_2: 4/1) and homogenized for few minutes. The mixture was heated at 35°C for 1h. The reaction mixture was diluted with water, cooled in a ice bath and pH was brought back to 7 by the use of NaOH and acetic acid. Once obtained neutrality the reaction mixture was filtered on a PTFE membrane by a millipore filtration system. The filtrate was washed several times by water and lastly methanol. Then the filtrate was scraped off the filter and dried under vacuum.

Characterization:

1)TGA

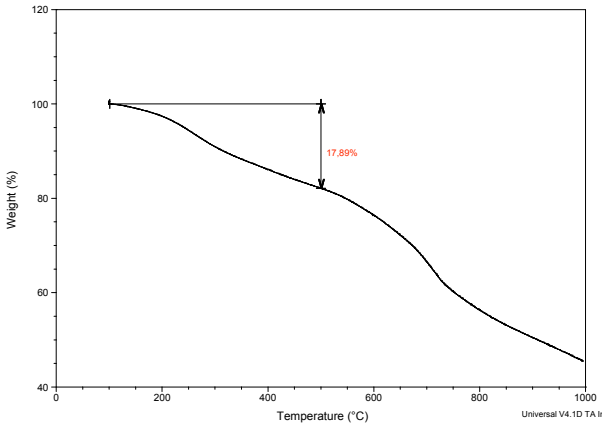

The TGA shows a weight loss of 17,89 % at the temperature of 500°C, which corresponds to one functional group every 17 carbon atoms, this corresponds to a very high oxidation of the tubes.

2)TEM

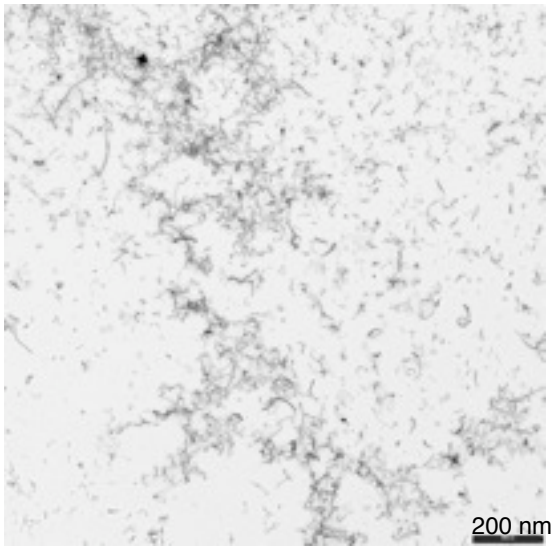

In the TEM micrographs (photos taken at 22000x) we notice that the tubes are considerably shortened after the cutting process.

5.3.7 Preparation of CNT7

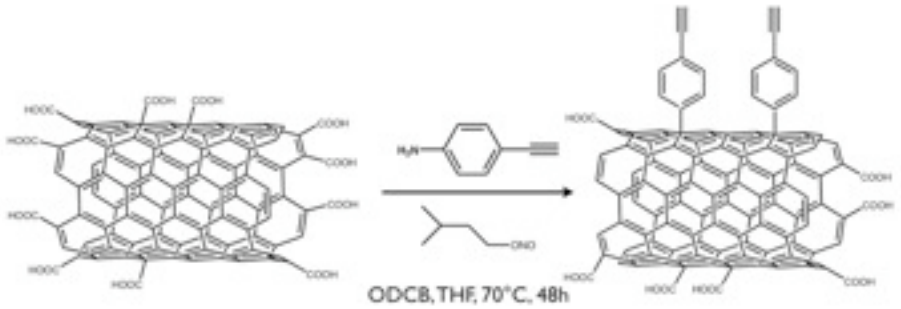

CNT6 (70 mg), were treated by the radical Tour reaction with the same procedure described above for pristine DWCNTs (section 5.3.2). Using the same procedure, the same molar proportions and the same work-up, we obtained 63 mg of resulting material.

Characterization:
1)TGA

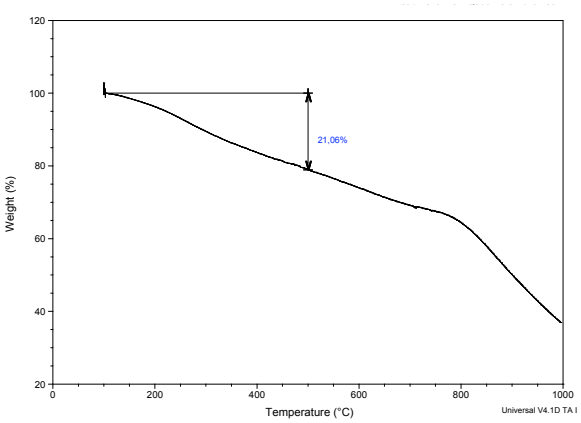

The TGA shows a weight loss of 21,06 % at the temperature of 500°C, which corresponds to one functional group every 201 carbon atoms, excluding the oxydrilic moieties: a normal value for multi-walled nanotubes.

2)TEM

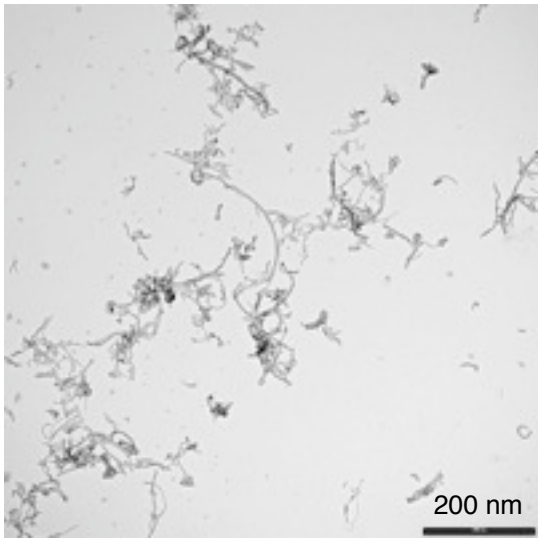

In the TEM we can notice that the structure of the tubes is preserved and that they are well dispersed. Photo is taken at 22000x.

5.3.8 Preparation of CNT8

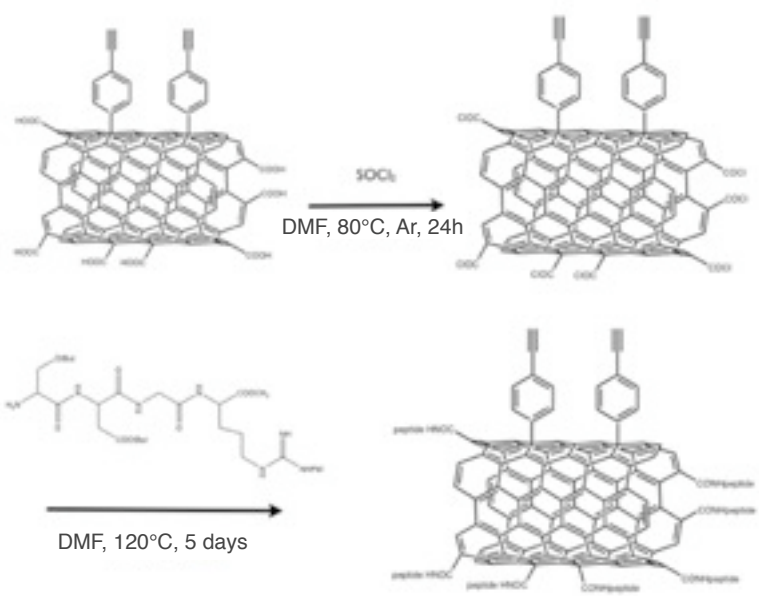

CNT7 (50 mg) were treated by the same procedure reported in section 5.3.4. Using the same procedure, the same molar proportions and the same work-up, we obtained 48 mg of resulting material.

Characterization:

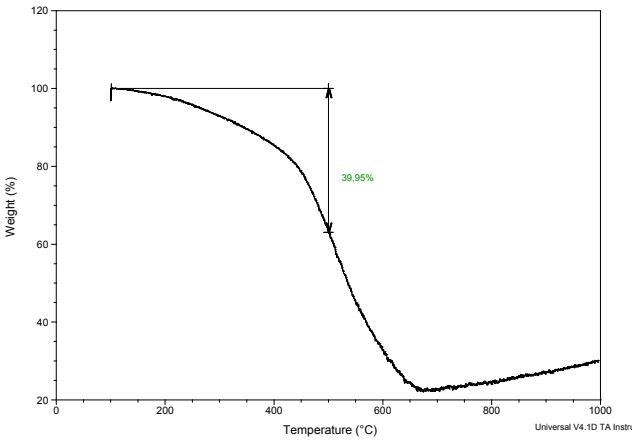

1) TGA

The TGA shows a weight loss of 39,95 % at the temperature of 500°C, which, excluding the oxydrilic functionalities and the alkyne functionalities corresponds to one functional group every 310 carbon atoms.

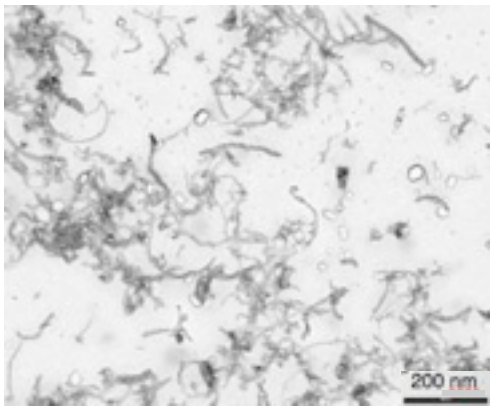

2)TEM

In the TEM we observe that the structure of the tube is preserved and the dispersion is good. We notice a few budles due probably to the high molecular weight of the functionalization. The photo is taken at 22000x

5.4 Preparation of the functionalized Glass Substrates

5.4.1 Preparation of GS1

200 µL of a DMF solution of functionalized MWNTs CNT1 (approximately 5 mg/mL) were deposited dropwise with a pipette onto the glass coverslips and the solvent removed by evaporation on a hot plate. The coverslips were kept in oven at 350°C under nitrogen atmosphere for 15 min, removed from the oven and used for electrophysiological experiments.

Characterization:

SEM

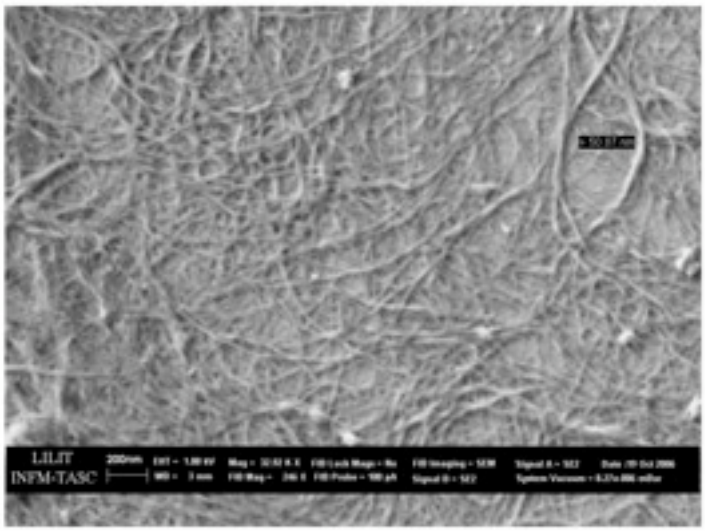

Glass substrates covered by nanotubes, analyzed by SEM microscopy, presented the general morphology of an homogeneously coated surface like reported in figure. The avarage thickness was extimated to be 50-70 nm.

5.4.2 Preparation of GS2

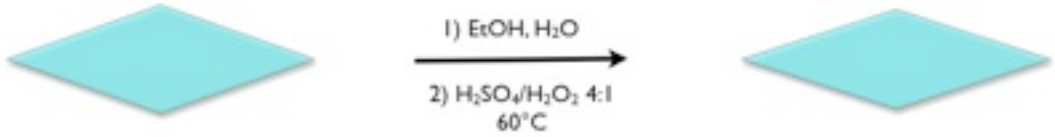

Glass slides were purified before functionalization by the following treatment: they were firstly washed in ethanol and water and exposed to an ultrasound bath. Afterwards they were treated by a mixture of sulfuric acid and hydrogen peroxide at the temperature of 60°C. They were then washed two times by water and dried under N_2 flux. This treatment should increase the hydrophilicity of the surface by the exposition of a larger amount of oxydrilic moieties on the surface. This is confirmed by the significantly lower value of the contact angle recorded after the purification.

Characterization

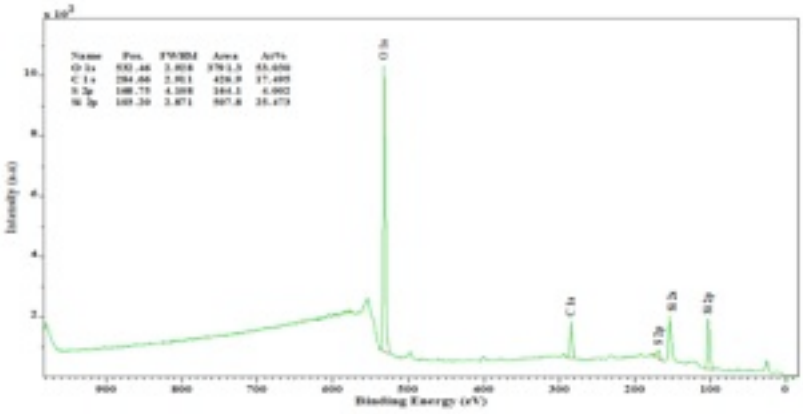

1) XPS

In the spectra we can notice the presence of the Si peak, of course due to the glass chemical composition and the carbon 1s peak. Traces of carbon are always present in every sample.

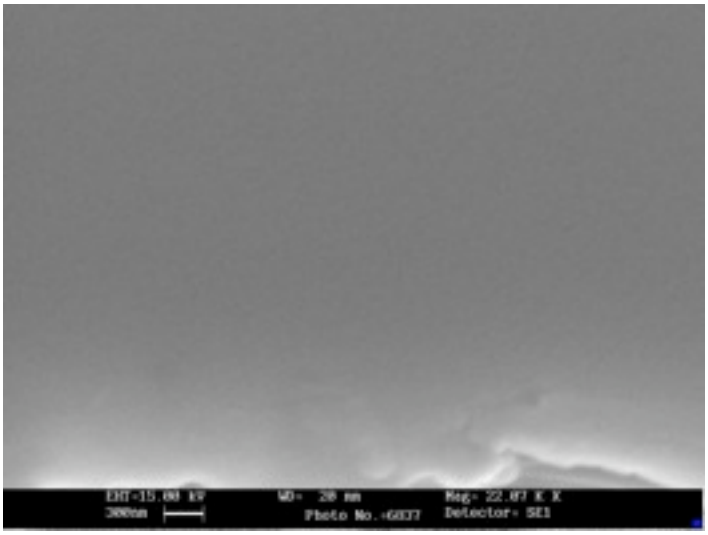

2) SEM

In the SEM micrograph we can notice the perfect and flat composition of the purified glass. No impurities are present in the surface before the treatment by the silane coupling agents.

5.4.3 Preparation of GS3

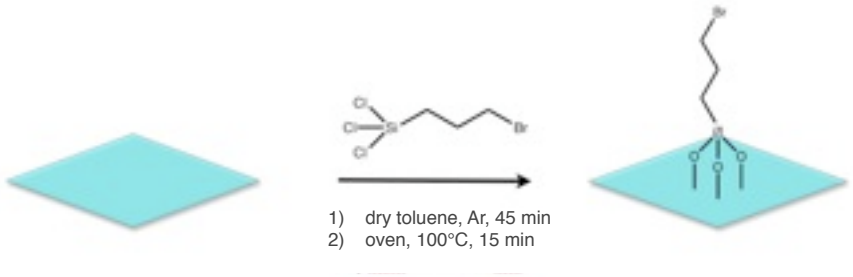

The purified glass slides GS1 were immersed in teflon test tubes containing a solution 1% v/v of 3-bromopropyl trichlorosilane in dry toluene (5 mL for every glass slides). The so obtained functionalized surfaces were extracted from the solution, washed in toluene and then in ethanol and lastly treated in oven at 100°C in order to create the silane network by thermal treatment.

Characterization:

Survey XPS spectrum and FT-IR characterization of this surface are reported in chap.4, sect. 4.5. Here we report the high resolution XPS spectra of the Br 3d peak and the C 1s peak.

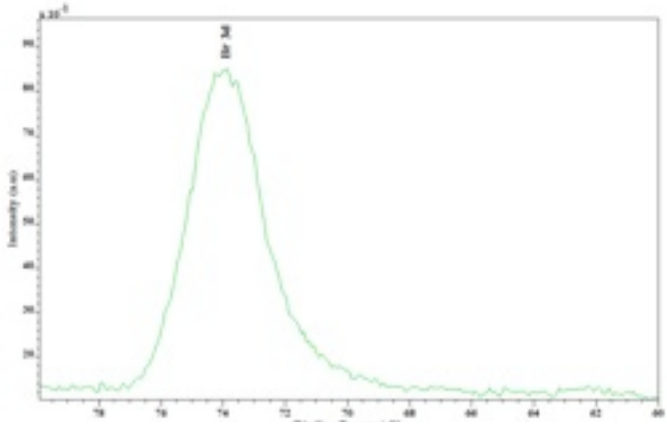

High resolution XPS

In the spectrum line appears the bromine peak. The peak has an high intensity.

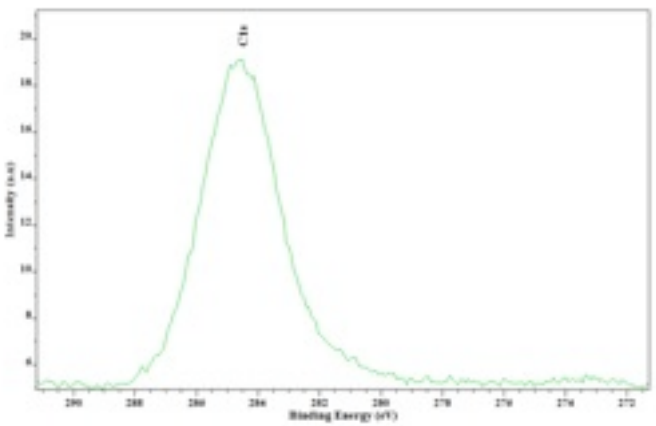

The C 1s peak wich was present also in the XPS survey spectra of the purified glass increases a lot in intensity, as you can see comparing the survey spectra of the pure glass and the survey spectra of the Br modified glass. (fig. chap. 4, sect. 4.5) This is obviusly due to the introduction of the alkyl chain of the 3-bromopropyl trichlorosilane.

5.4.4 Preparation of GS4

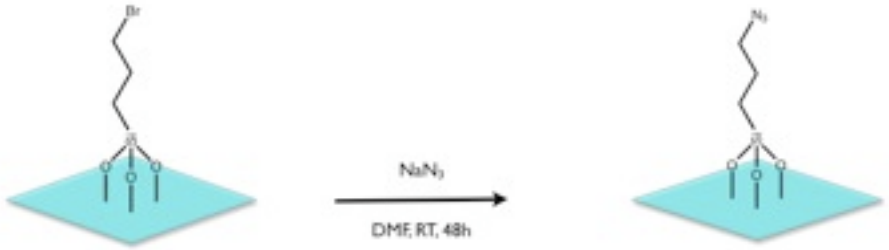

The modified glass slides GS3 were immersed in teflon test tubes containing a DMF solution with a large excess of sodium azide to obtain the complete sobstitution of bromine by the azide group. The solutions were stirred at room temperature by a micro magnet for 2 days. Afterwards they were washed in water two times and dried under a N_2 flux.

Characterization:
Survey XPS spectrum and high resolution XPS of the nitrogen peak together with FT-IR characterization of this surface are reported in chap.4 sect. 4.5. Here we report the high resolution XPS on the Br 3d region of the surface and the SEM micrograph:

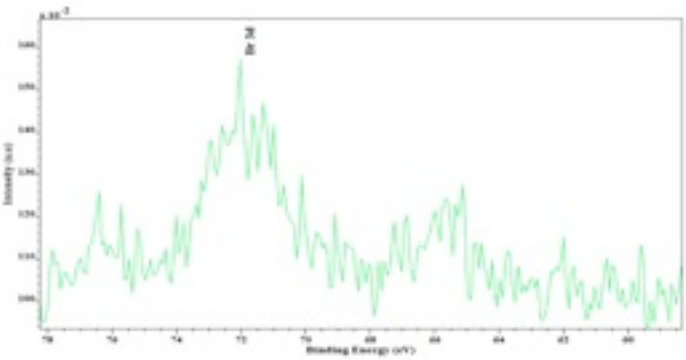

1) High resolution XPS

Notice the sensible reduction of the Br 3d peak that verifies the almost quantitative substitution of Br by the azide group.

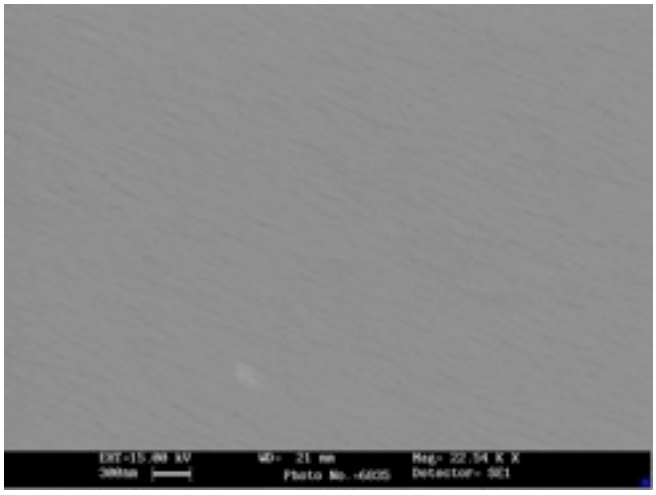

2) SEM

Comparing the SEM micrograph of the azido modified surface to the one of the purified glass we notice the different morphology, witnessed by the rugosity of the surface, when the silane is introduced.

5.4.5 Preparation of GS5

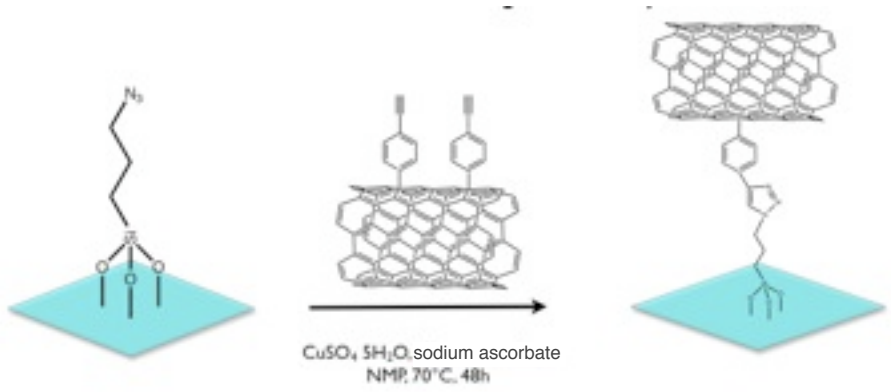

Alkyne modified carbon nanotubes CNT2 and CNT5 were used for functionalization of azide modified glass slides GS4 by immersion of the glass slides in a 5 mL NMP solution of CNT in the presence of $CuSO_4$ and sodium ascorbate. For 1 mg of CNT were added 0,16 mg of $CuSO_4$ and 1,24 mg of sodium ascorbate. The solutions were stirred at 70°C. After a reaction time of 2 days they were cooled at room temperature and the glass slides were extracted from the solution and washed in NMP and methanol. They were then dried under a N_2 flux and kept under vacuum.
XPS and SEM characterization of this surface are reported in chap.4, sect. 4.5.

5.4.6 Preparation of GS6

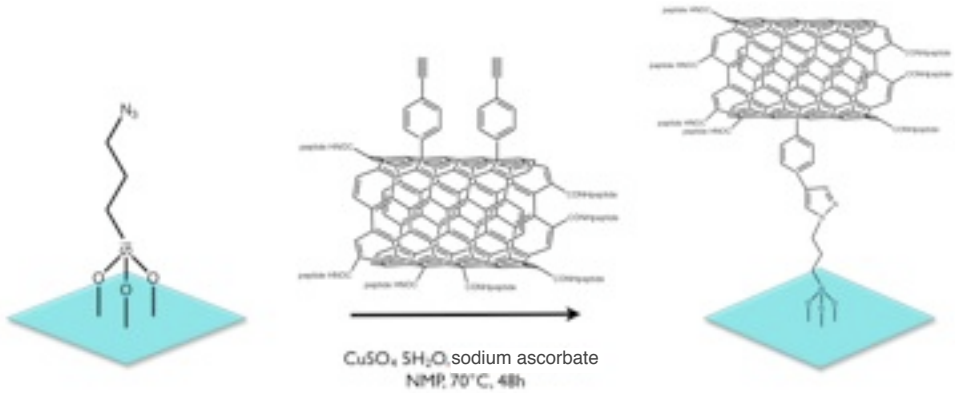

Alkyne-peptide modified carbon nanotubes CNT4 and CNT8 were used for functionalization of azide modified glass slides GS4 by the same procedure reported for GS5 in a NMP solution of CNT in the presence of $CuSO_4$ and sodium ascorbate. The quantity and the procedure adopted were the same in both cases.
As a last step the nanotube modified glass slide were left overnight in a solution of TFA in CH_2Cl_2 (1:2) at room temperature to deprotect all the functional groups of the peptide. They were again dried under a N_2 flux and kept under vacuum.
XPS and SEM characterization of this surface are reported in chap. 4, sect. 4.5.

5.4.7 Preparation of GS7

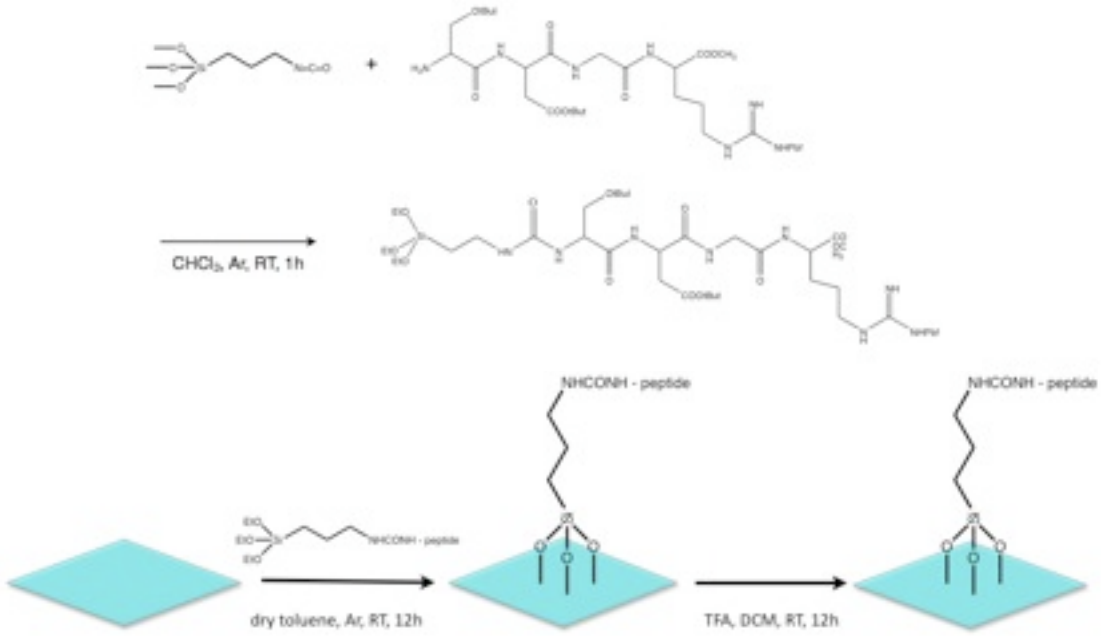

A solution of 9,56 mg of 3-isocyanatepropyl triethoxysilane in $CHCl_3$ was prepared by adding the reagent to 5 mL of the anhydrous solvent under Ar atmospere. The slvent was previously passed trough a allumine filter to eliminate every trace of acidity normally present in chloroform. 32 mg of the RGD peptide H-Ser(tBut)-Asp(tBut)-Gly-Arg(Pbf)-OMe were introduced under Argon in the solution and the reaction was stirred for 1 h at room temperature. The solvent was eliminated under vacuum and the resulting solid was collected.

The purified glass slides GS2 were immersed in a solution 1% v/v of the compound previously prepared. They were stirred at room temperature for 12 hours. The peptide-functionalized glass slides were extracted from the solution and washed in toluene and in methanol. They were dried under a N_2 flux and immersed in a solution of TFA in in CH_2Cl_2 (1:2) at room temperature to deprotect all the functional groups of the peptide. They were again dried under a N_2 flux and kept under vacuum.

Characterization:

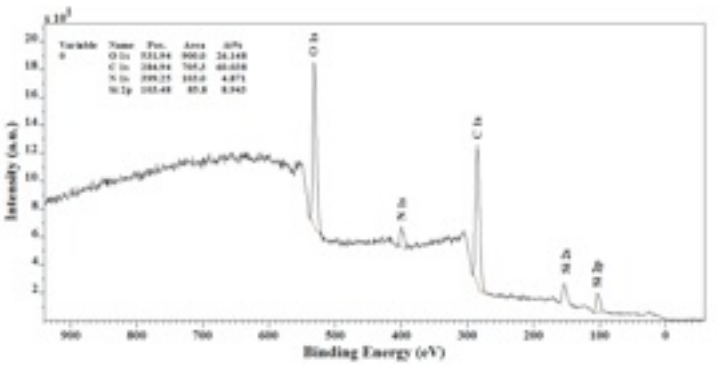

1) XPS

The survey XPS spectra shows a pattern in wich we can identify the nitrogen peak and the very intense carbon peak.

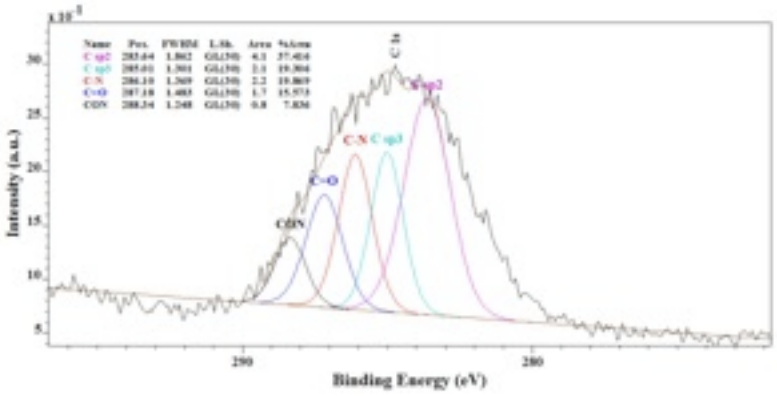

If we perform the high resolution XPS on the carbon area we notice that the carbon peak has many different components due to the many differents type of carbons that we find in the peptide structure.

2) FT IR

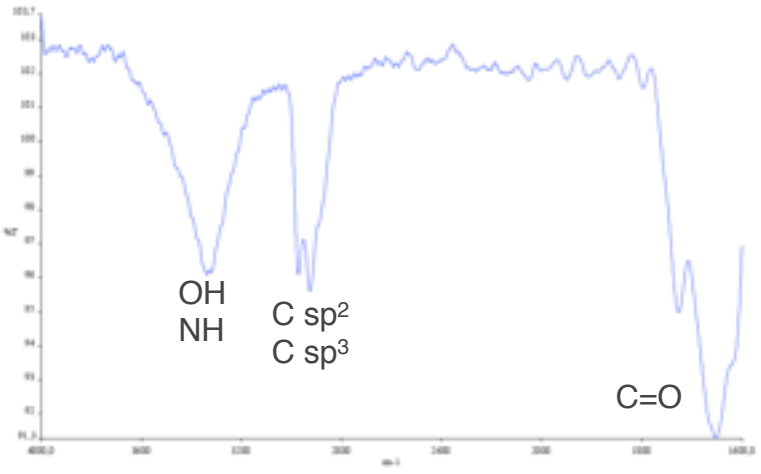

The FT-IR spectrum, performed directly on the glass slides indicate the presence of the peptide by showing the characteristic amide peak and carbonyl peak.

5.5 MEA coating by CNTs

1)

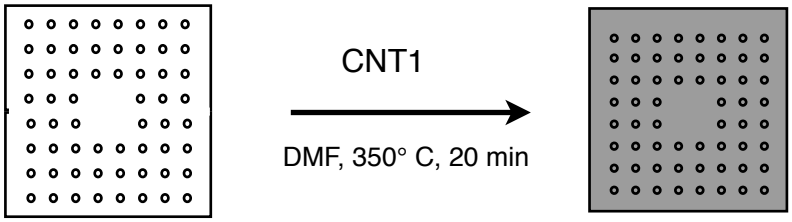

2)

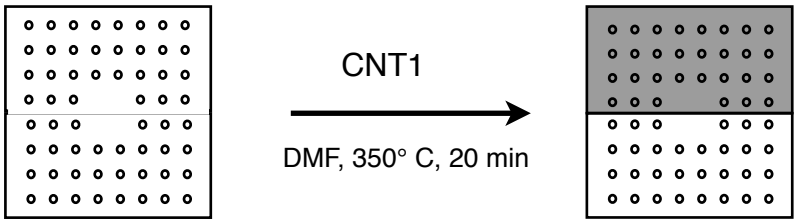

We have considered two methods for coating microelectrode arrays. Commercially available MWCNTs were treated under cycloaddition reaction condition (see CNT1, section 5.3.1). A stable dispersion 1mg/ml concentrated of the chemically modified and purified MWCNTs was prepared by sonicating them in DMF, and manually deposited on MEAs. Several drops of the solution were deposited with a pipette under stereo-microscope visual control, according to two rough patterns: 1) the entire inner area of the MEA, where substrate electrodes are located (i.e. a 2cm x 2cm square area, centered over the inner MEA layout); 2) half of such an area, leaving about half of the 60 electrodes unexposed . The same two patterns were repeated for different MEAs using the same quantity of the MWCNTs dispersion. Further solvent evaporation through heating at 80°C, and a thermal treatment at 350°C in nitrogen atmosphere for 20 minutes completed the coating process.

Appendix: Fluorescent labeling of CNTs for the study of their uptake and internalization in neural cells.

General Introduction

During the PhD a large part of work was dedicated to the fluorescent labeling of various type of CNTs and the study of their internalization in neural cells. Nevertheless, until now, there are only preliminary results on this subject. This work is important because the results are in a positive direction and because it gives a wider point of view in the understanding of the interaction between carbon nanotubes and neurons and, more in general, nanotechnology applications to neuroscience. Thus, this experiments and the few preliminary results are reported and described in this appendix.

The continuos discoveries in biology and medicine have allowed us to individualize with a high degree of detail the molecular basis of pathologies. This brought as well to the development of a crescent number of specific drug for every specific pathology. For a drug to be functional it is necessary to reach the target site, to carry out the requested function and, at the end, to be excreted. Chemical and physical characteristics of the drug are essential in defining the process of the drug uptake: the lipophilicity and hydrophilicity determine, for example, the attitude of the drug to cross, in the two directions, the biological membranes.

This issue is a subject of central importance in the case of pathologies related to the central nervous system because of the presence of the **blood brain barrier**. The blood-brain barrier (BBB) is a separation of circulating blood and cerebrospinal fluid in the central nervous system. It mainly has the function of restricting the diffusion of microscopic objects like bacteria and large or hydrophilic molecules into the CSF, while allowing the diffusion of small hydrophobic molecules (O_2, hormones, CO_2).

Due to the presence of the blood brain barrier there is an objective difficulty of delivering therapeutic agents to specific regions of the brain and this represents a major challenge to treatment of most brain disorders. In its neuroprotective role, the blood-brain barrier functions to hinder the delivery of many potentially important diagnostic and therapeutic agents to the brain, that might otherwise be effective in diagnosis and therapy.

A therapeutical approach in this sense could be the use of carrier molecules, that chemically linked to the drug, might allow it to pass the BBB and reach the target site. Molecules should posses some characteristics to be considered as potential carriers: it should be capable to cross membranes; it should not be toxic; the bond between the carrier and the drug should be breakable, *in vivo*, in a rapid scale of time.

The development of new and efficient drug delivery systems is of fundamental importance to improve the pharmacological profiles of many classes of therapeutic molecules. Nanotechnology may help in the transfer of drugs across the BBB.[1] Recently, researchers have been trying to build liposomes loaded with nanoparticles to gain access through the BBB. More research is needed to determine which strategies will be most effective and how they can be improved. Delivering drugs across the blood-brain barrier is one of the most promising applications of nanotechnology in clinical neuroscience. Nanoparticles could potentially carry out multiple tasks in a predefined sequence, which

is very important in the delivery of drugs across the blood-brain barrier.

Carbon Nanotubes as drug delivery systems

Within the family of nanomaterials, carbon nanotubes have emerged as a new alternative and efficient tool for transporting and translocating therapeutic molecules. CNT can be functionalised with bioactive peptides, proteins, nucleic acids and drugs, and used to deliver their cargos to cells and organs. Because functionalised CNT display low toxicity and are not immunogenic, such systems hold great potential in the field of nanobiotechnology and nanomedicine.

The use of carbon nanotubes in drug delivery has already been mentioned in the introduction (Chap.1, sect. 1.9). Solubilization and biological functionalization of carbon nanotubes have greatly increased the usage of carbon nanotubes in biomedical applications. Pantarotto et al.[2] were the first to demonstrate that peptide-functionalized carbon nanotubes are able to penetrate cell membranes and to accumulate inside living cells without causing apparent cytotoxicity. Functionalized SWNTs were conjugated with fluorescently labeled peptides. After a 60-min incubation of cells with functionalized CNTs, these conjugates were found to be distributed in the cytoplasm or even inside the nucleus. Based on this result, they further conjugated carbon nanotubes with plasmid DNA through electrostatic interaction between the amino groups of the functionalized CNTs and the phosphate groups of plasmid DNA.[3] After a 30-min incubation of cells with plasmid DNA–CNT conjugates, the gene encoded by the plasmid DNA began to be expressed, and then reached 10 times higher levels of gene expression than the incubation of cells with DNA alone after 3 h incubation. Owing to the low cytotoxicity caused by carbon nanotubes, they have demonstrated that carbon nanotubes can be used as a high-efficiency gene delivery system in various therapeutic applications.

In another study, Shi Kam et al.[4] demonstrated that large biomolecules such as streptavidin (MW approx 60 kDa) can be delivered into living cells by conjugating with biotin-functionalized carbon nanotubes within a short incubation period. They have proposed that the uptake mechanism of carbon nanotubes is through the endocytosis pathway driven by the nonspecific association between the non oxidized areas of the CNTs and the hydrophobic regions of the cell surface.

The development of efficient methodologies for the chemical modification of CNT has stimulated the preparation of soluble CNT that can be employed in several biological applications, among which drug delivery appears to be particularly promising.[5]

As already mentioned in chapter 1, two functionalization approaches are widely employed for modification of CNT. CNT can be oxidized using strong acids, resulting in the reduction of their length while generating carboxylic groups, which increase their dispersibility in aqueous solutions. Alternatively, addition reactions to the CNT external walls and tips make them soluble in water. Solubility under physiological conditions is a key prerequisite to make CNT biocompatible. In addition, functionalized carbon nanotubes can be linked to a wide variety of active molecules, including peptides, proteins, nucleic acids and other therapeutic agents (fig.1).

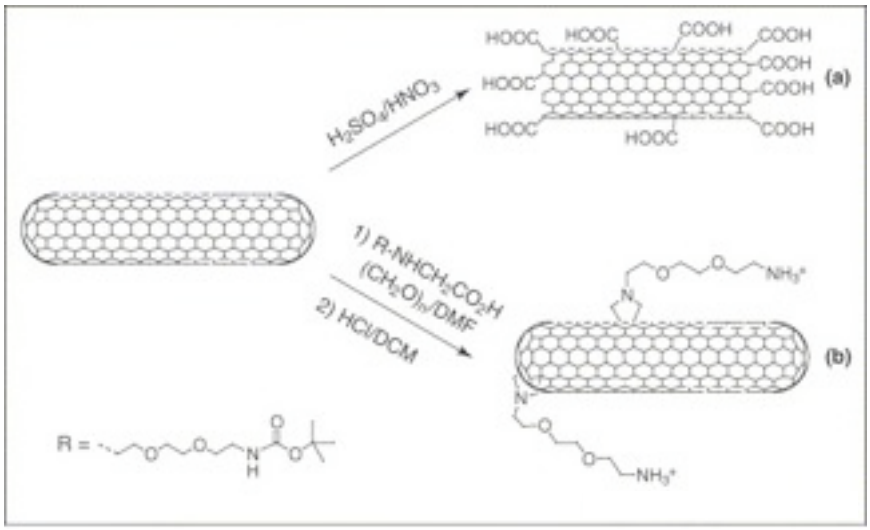

Fig.1 a) oxidative approach for the functionalization of CNT. b) sidewall functionalization of CNT by 1,3 dipolar cycloaddition.

By carefully choosing the reactants, it is possible to modulate solubility in organic solvents or aqueous solutions. CNT carrying ammonium groups are very soluble in water and have been exploited for their potential in the delivery of therapeutic molecules.

The search for new and effective drug delivery systems is a fundamental issue of continuous interest.[6] A drug delivery system is generally designed to improve the pharmacological and therapeutic profile of a drug molecule.[7] The ability of functionalized CNT to penetrate into the cells offers the potential of using functionalized CNT as vehicles for the delivery of small drug molecules.[2,4] However, the use of functionalized CNT for the delivery of anticancer, antibacterial or antiviral agents has not yet been fully ascertained. The development of delivery systems able to carry one or more therapeutic agents with recognition capacity, optical signals for imaging and/or specific targeting is of fundamental advantage. For this purpose, it is necessary a multiple functionalization of CNT with different types of molecules: a fluorescent probe for tracking the cellular uptake of the material and the active molecule having the therapeutic properties.

With this study we aim to demonstrate that water soluble SWNT derivatives, modified with a fluorescent probe, translocate across neural cell membranes. Since the functionalised CNTs appear to be non toxic for the cells, they can be considered as a new tool to deliver therapeutic organic molecules into the cells. Therefore, these systems can help to solve transport problems for pharmacologically relevant compounds that need to be internalised, and may have potential therapeutic applications. To determine whether CNTs can be used to deliver active molecules into the nerve cells, we have prepared fluorescein isothiocyanate (FITC) labeled single-walled and multi walled carbon nanotube derivative.

In spite of the already demonstrated capability of nanotubes to pass the cellular membrane nothing has already been said about the capability of nanotubes to pass the BBB, which could define the possibility for CNT to be used as drug carriers for the central nervous system. Further development of this study might investigate *in vivo* the

capability of functionalized CNT to pass the BBB and, therefore, individuate an important tool for the therapeutical applications that concern neural diseases.
In this appendix we will show the chemical procedure employed to chemically modify SWCNTs and MWCNTs by the fluorescent label and show some preliminary results, evidenced by confocal microscopy, of the cellular uptake and intracellular distribution into neural cells.

Experimental Section

Synthesis of compound OC1

2,2'-(ethilendioxy)bis-ethilammine (25 g; 169 mmol) was dissolved in THF (100 ml). The solution was stirred at 0° C in an ice bath. A solution of di-*tert*-butyl-dicarbonate (12,5 g; 57,3 mmol) in 30 mL of THF was added dropwise to the first solution. The reaction was stirred at room temperature overnight.
After eliminating the solvent under vacuum, the crude was diluted in water. The solid residue was filtered away and the filtrate was extracted in DCM.
The organic phase was dried over anhydrous Na_2SO_4. The solvent was removed under vacuum and the resulting compound was collected (15,7 g; 31,9 mmol; yield 37%)
$C_{11}H_{24}N_2O_4$, MW: 248,32 u.m.a.

^{1}H-NMR (200 MHz,$CDCl_3$): 5.1 (bs, 1H), 2.08-3.07 (m, 12H)1.69 (bs, 2H),1.39 (s, 9H).
^{13}C-NMR (50 MHz, $CDCl_3$): 28.27, 40.16, 41.51, 70.04, 73.14, 78.83, 155.92.
ES-MS (N_2) m/z: 271.17 [M $^+$ Na^+].

Synthesis of compound OC2

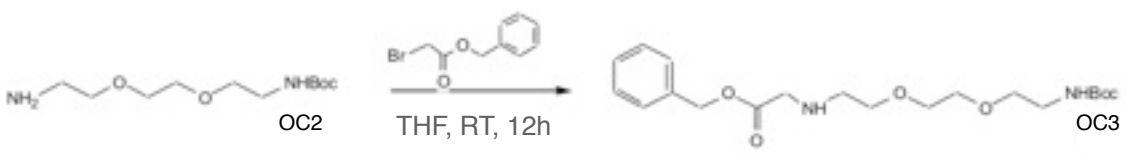

Compound OC1 (15,8 g; 64 mmol) was dissolved in THF (100 ml) with triethylammine (3,2 g; 32 mmol). The solution was stirred at 0°C in an ice bath. A solution of benzylbromoacetate (5.1 ml, 32 mmol) in THF (60 ml) was added dropwise. The reaction was stirred overnight.
Solvent was dried under vacuum and the crude was diluted in H_2O and extracted in CH_2Cl_2. Organic phases were collected and dried over anhydrous $NaSO_4$. Solvent was eliminated under vacuum. The crude was passed through a chromatographic column for purification (solvent: AcOEt/petroleum ether gradient). The compound OC2 was obtained as an oil (6 g; yield 84%)
$C_{20}H_{32}N_2O_6$, MW: 396,9 u.m.a.

^{1}H-NMR (200MHz, $CDCl_3$): δ 7.32 (m, 5H), 5.5 (bs, 1H), 5.1 (s, 2H), 2.7-3.6-3.46 (m, 14H), 2.1 (bs, 1H), 1.36 (s, 9H).
^{13}C-NMR (50 MHz, $CDCl_3$): δ 172.1, 155.9, 135.5, 128.5, 128.2, 128.20, 79.0, 70.6, 70.2, 70.1, 65.5, 50.8, 48.6, 40.4, 40.3, 28.5.
FT-IR (NaCl): cm^{-1} 3347, 2871, 1712, 1512, 1458, 1368, 1248, 1175, 966, 865, 747, 701.
EI-MS: m/z 396 (M^+, 20%), 205, 161, 91.

Synthesis of Compound OC3

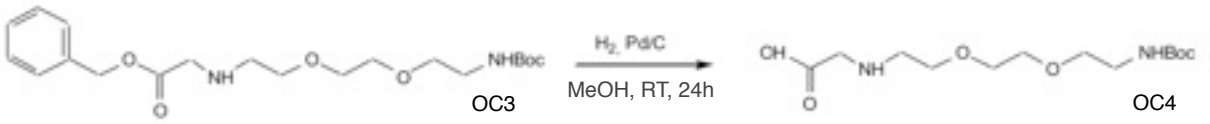

Compound OC2 (6 g; 20 mmol) was dissolved in MeOH. Pd/C was added to this solution under magnetic stirring (10% w/w), after bubbling N_2 in the solvent for 20 minutes in order to remove O_2. Reaction was satured by H_2 and left in H_2 atmosphere for 24 hours at room temperature. The reaction mixture is filtered over celite, washed with MeOH and dried under vacuum. The amino acid OC3 was obtained as a white solid. (4,3 g; yield 100%)
$C_{13}H_{26}N_2O_6$, MW: 306 u.m.a.

^{1} H-NMR (200 MHz, $CDCl_3$): 10.6 (s, 1 H), 7.8 (bs, 1H), 3.2-3.8 (m, 14 H), 1.7 (bs, 2H), 1.4 (s, 9 H).
^{13} C-NMR: δ 170.5, 156.2, 79.1, 70.4, 70.3, 70.1, 66.6, 49.8, 46.8, 40.4, 28.6.
IR-DRIFT: cm-1 3250, 2970, 1706, 1620, 1540, 1365, 1115, 686, 590, 480.
EI-MS: m/z 306 (M^+).

Preparation of CNT9

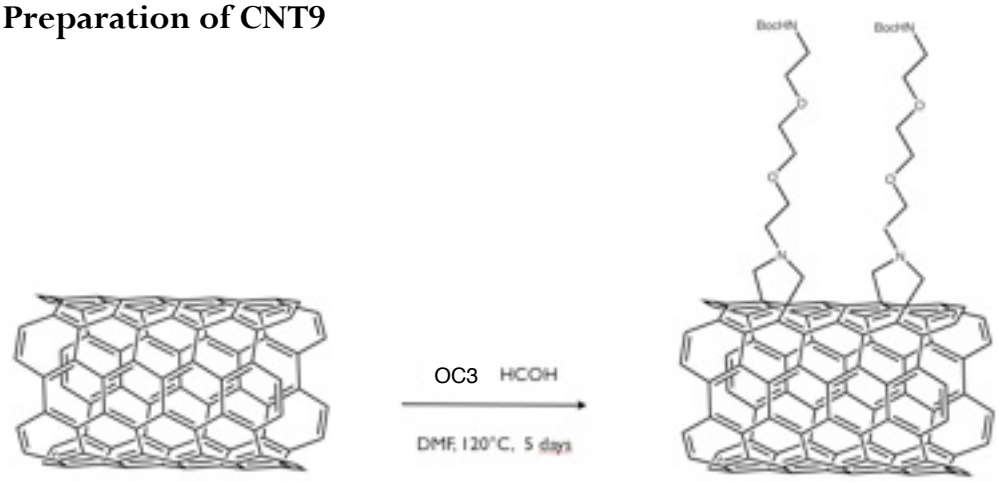

As produced MWNTs (100 mg), were suspended in 100 mL of DMF. The heterogeneous mixture was sonicated for 5 min. The aminoacid OC3 (80 mg) and *p*-formaldehyde (80 mg, addition repeated every 24 h) were added and the reaction was stirred at 120°C for five days. The mixture was centrifuged and the supernatant was filtered using a 0.2 μm PTFE filter (Millipore, USA). The filter was washed and sonicated 5 times with DMF. The material recovered as functionalized MWNTs (60 mg) onto the filter was then extensively washed with DCM (100 mL), Methanol (100 mL) and Diethyl ether (100 mL) and dried under vacuum.

deprotection:

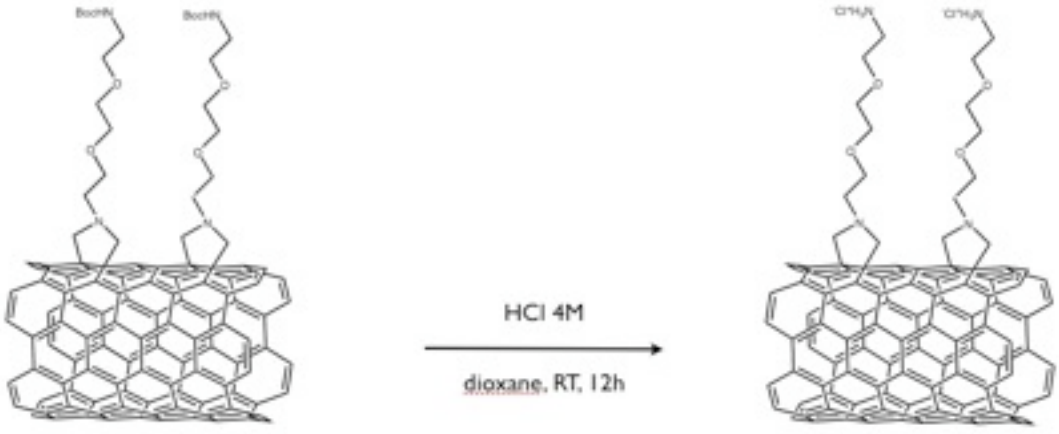

50 mg of the cycloadditionated compound were dispersed in a solution of HCl 4 M in dioxane (50 mL). The reaction mixture was stirred overnight at room temperature. The mixture was filtered on a PTFE membrane. The black solid was washed in MeOH and Et_2O. The product CNT9 was dried under vacuum. We obtained 50 mg of material.

Preparation of CNT10

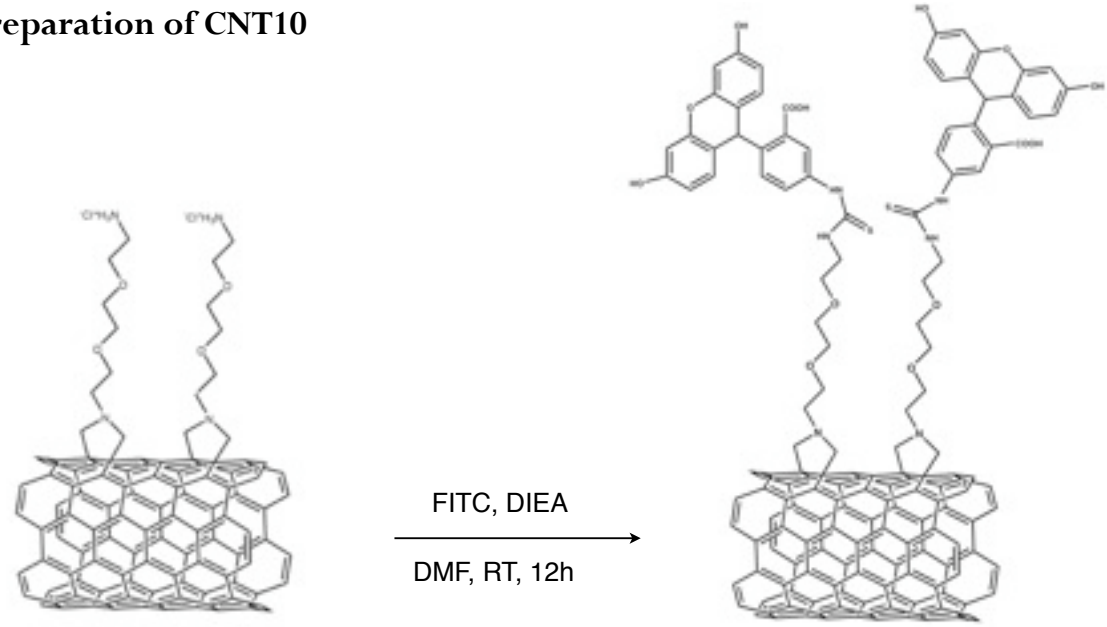

25 mg of CNT9 were dispersed in 25 ml di DMF by sonicating for 10 minutes. FITC in defect (60%) with respect to the mole of amino groups determined by Kaiser test on CNT9 was added to the mixture (1,28 g; 3,2 mmol)and then an excess of DIEA (3 ml; 2,28 g; 8,7 mmol). The reaction mixture was stirred at room temperature overnight. The mixture was filtered over a PTFE membrane (0,2 µm diameter). The black solid was kept on the filter and washed with DMF, MeOH and finally in Et_2O, until FITC was completely eliminated and the filtrate was clean. We obtained 23 mg of CNT10

Characterization

1)TGA

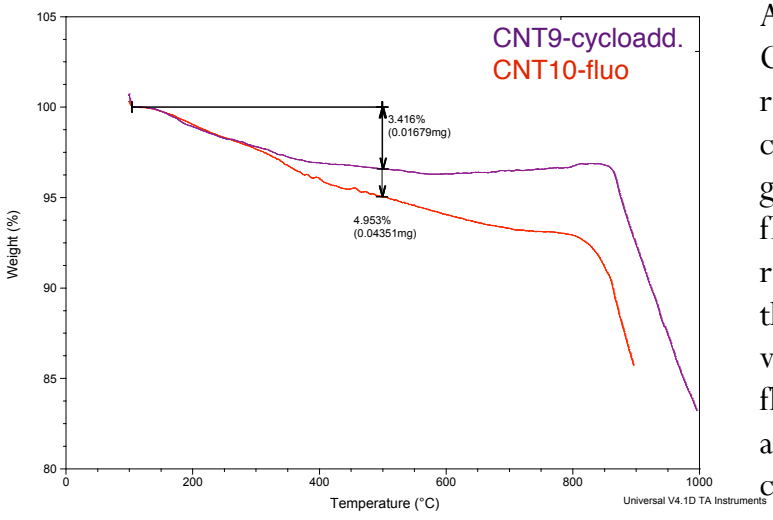

At the temperature of 500°C the CNT9 cycloadditionated sample registered a weight loss of 3,4% correspondent to one functional group every 366 C atoms, while the fluoresceinated CNT10 sample registered a weight loss of 4,9 % that, subtracted to the previous value, corresponds to one fluorescein functionalitiy every 1,6 amino groups (60%). Every value is confirmed by the kaiser test results.

2)Kaiser test

sample	K.T. value
CNT 9 (depr.)	219 μmol/g
CNT10	85,6 μmol/g

3)TEM

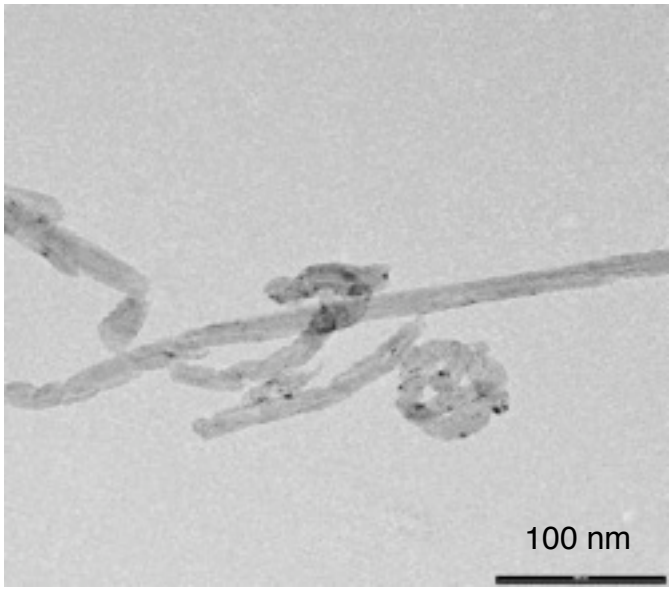

The TEM micrograph of the CNT10 sample, prepared in water, shows that the nanotubes are very well dispersed and individualized. This is guaranteed because of the partial functionalization by fluorescein. The presence of free amino groups along the tube sidewalls assures the solubilization. The photo at the left is taken at 180000x

4)fluorescence

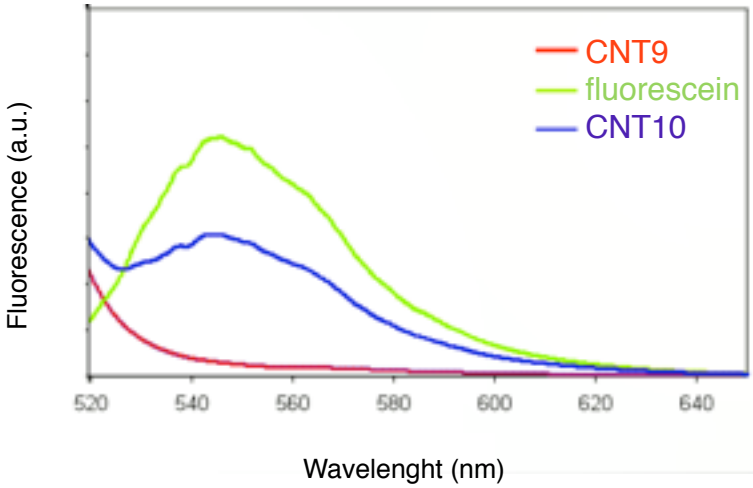

Fluorescence spectra of the samples CNT9 and CNT10, compared to the fluorescence spectra of fluorescein show that fluorescent CNT10 have a maximum of fluorescence emission at c.a. 570 nm. This value is typical of fluoresceine. The same peak is absent in the non fluorescent CNT9. The spectra were taken at the excitation wavelenght of 488 nm.

Preparation of CNT11

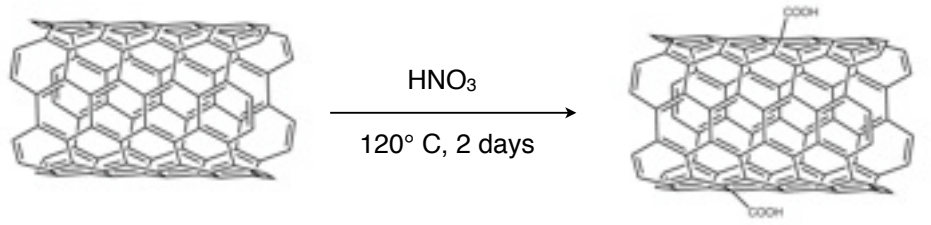

100 mg of SWCNT were dispersed in 100 ml di HNO_3 2,6 N and stirred at 120°C for two days. Temperature was brought to 0°C with an ice bath and the pH of the mixture was adjusted to neutrality, adding 66 ml of NaOH 4 M .The mixture was filtered over a PFTE membrane and the solid was washed many times with H_2O. The yellow filtrate was eliminated. The black solid over the filter was kept and washed again with MeOH and Et_2O. The solid was collected and dried under vacuum. We obtained 87 mg of material.

Preparation of CNT12

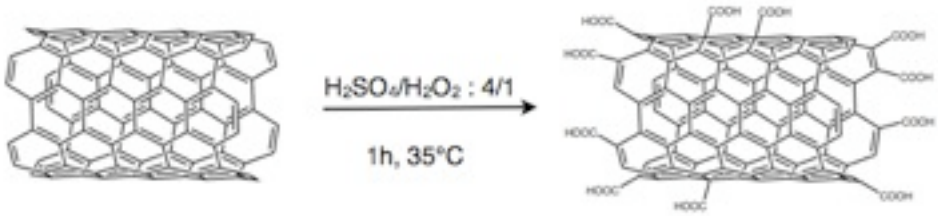

Purified SWNTs CNT11 (80 mg), were dispersed in 80 mL of pirana solution (H_2SO_4/ H_2O_2: 4/1) and homogenized for few minutes. The mixture was heated at 35°C for 1h. The reaction mixture was diluted with water, cooled in a ice bath and pH was brought back to 7 by the use of NaOH and acetic acid. Once obtained neutrality the reaction mixture was filtered on a PTFE membrane by a millipore filtration system. The filtrate was washed several times by water and lastly methanol. Then the filtrate was scraped off the filter and dried under vacuum. We obtained 71 mg of material

Preparation of CNT13

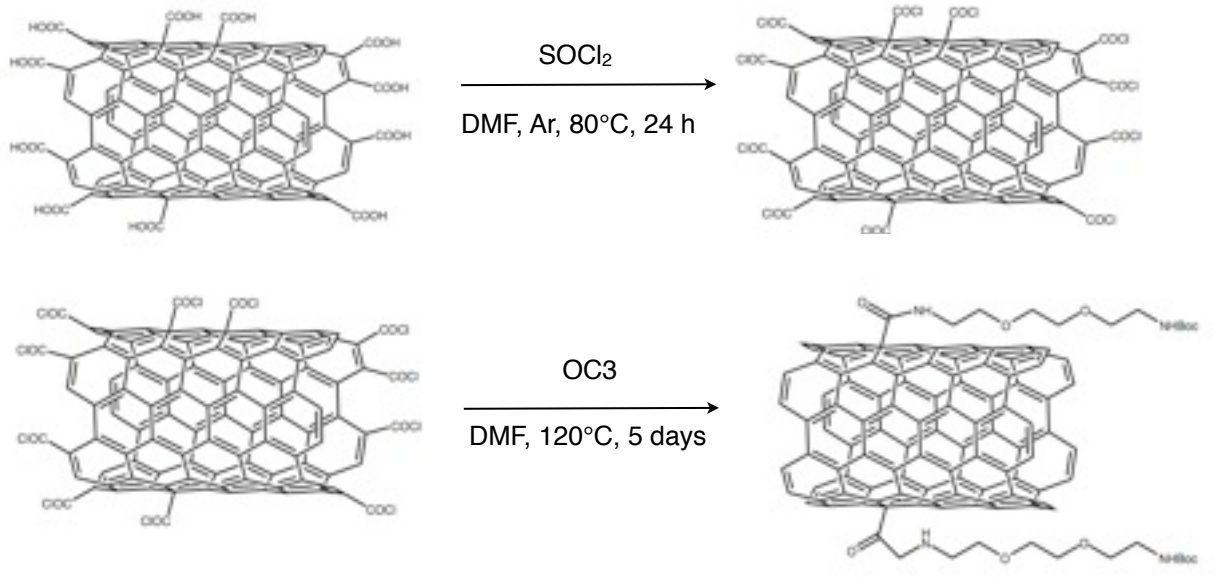

CNT12 (60 mg) were introduced in a 250 mL flask with a magnetic stirrer. The flask was put under anhydrous conditions and 50 mL of thionil chloride were added by siringe. The mixture was sonicated 20 min to homogenize the solution, and 10 mL of anhydrous DMF were added. The reaction was put under magnetic stirring at 80° C for 24 h, under Ar atmosphere.

At the end of the reaction time the flask was cooled at room temperature and solvent was dried under vacuum. Still under Ar flux, fresh DMF was added, the nanotubes were dispersed again by the use of a sonic bath, and 150 mg of the aminoacid OC3 were added. The reaction was left at 120°C for 5 days.

The flask was cooled at room temperature and the nanotubes were filtered on a PTFE membrane by a millipore filtration system. The nanotubes were washed by DMF and homogenized again in fresh DMF, and then washed and homogenized repeatedly in MeOH and CH_2Cl_2. After the final washing they were washed by diethyl ether, scraped off the filter and dried under vacuum overnight.

Deprotection:

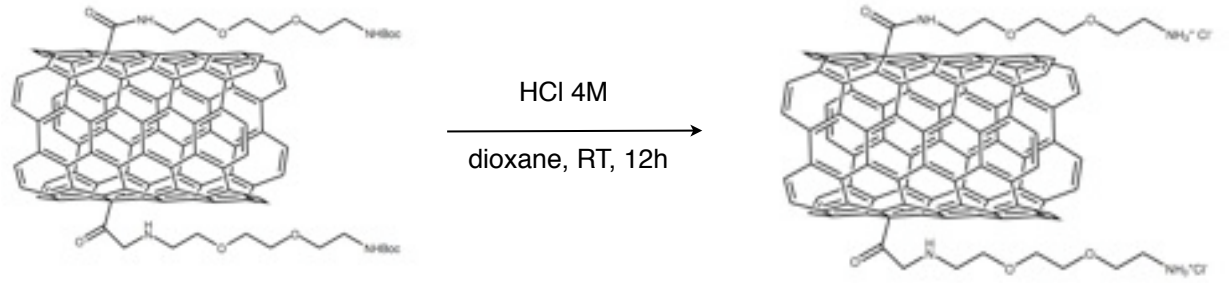

50 mg of the Boc-protected compound were dispersed in a solution of HCl 4 M in dioxane (50 mL).The reaction mixture was stirred overnight at room temperature. The mixture was filtered on a PTFE membrane. The black solid was washed in MeOH and Et_2O. The product CNT13 was dried under vacuum. We obtained 50 mg of material.

Preparation of CNT 14

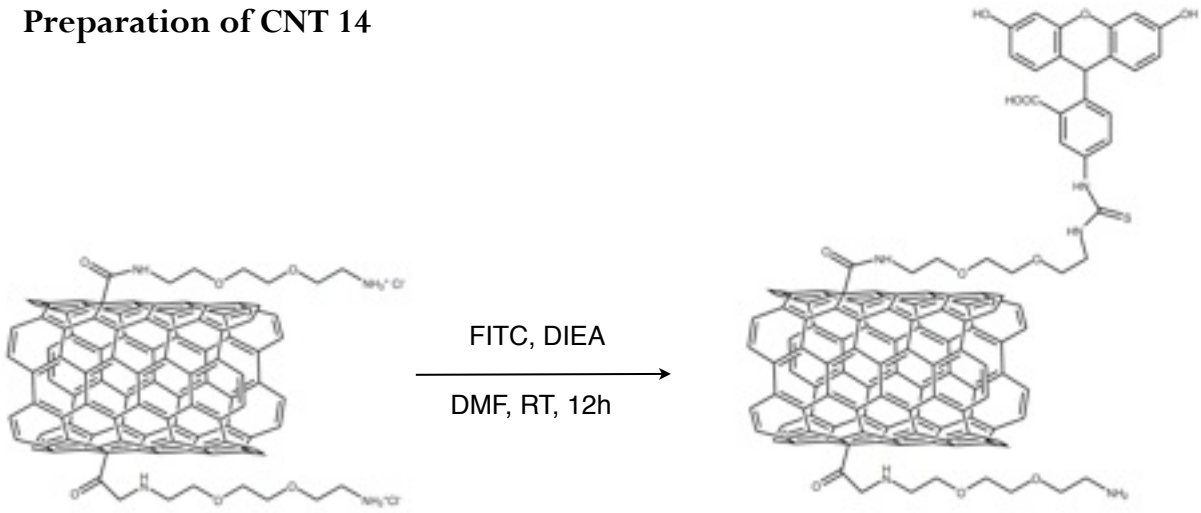

25 mg of CNT13 were dispersed in 25 ml di DMF by sonicating for 10 minutes. FITC in defect (60%) with respect to the mole of amino groups determined by Kaiser test on CNT13 was added to the mixture (1,5 g; 4 mmol). DIEA was added in excess (3 ml; 2,28 g; 8,7 mmol). The reaction mixture was stirred at room temperature overnight. The mixture was filtered over a PTFE membrane (0,2 µm diameter). The black solid was kept on the filter and washed with DMF, MeOH and finally in Et_2O, until FITC was completely eliminated and the filtrate was clean. We obtained 23 mg of CNT14

Characterization:

1) Raman

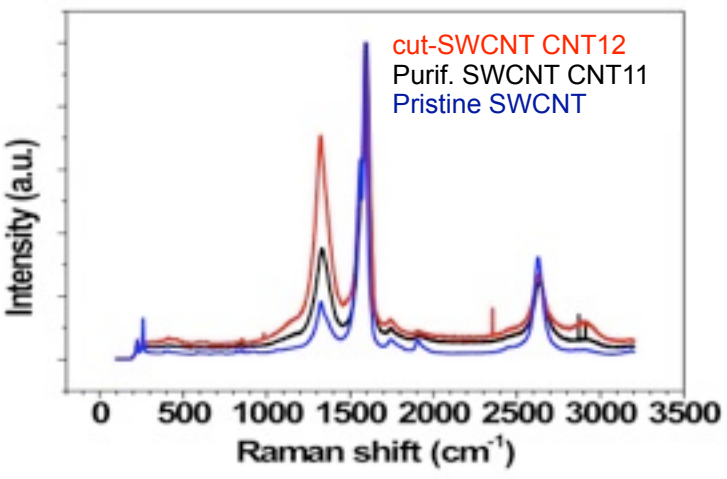

The Raman overlay shows that the G band increases after the purification and after the cutting of the pristine SWCNTS. This is due to the introduction of defects and of carboxylic functionalities, that corresponds to the break of the sp^2 network and the introduction of many sp^3 carbons.

2) TGA

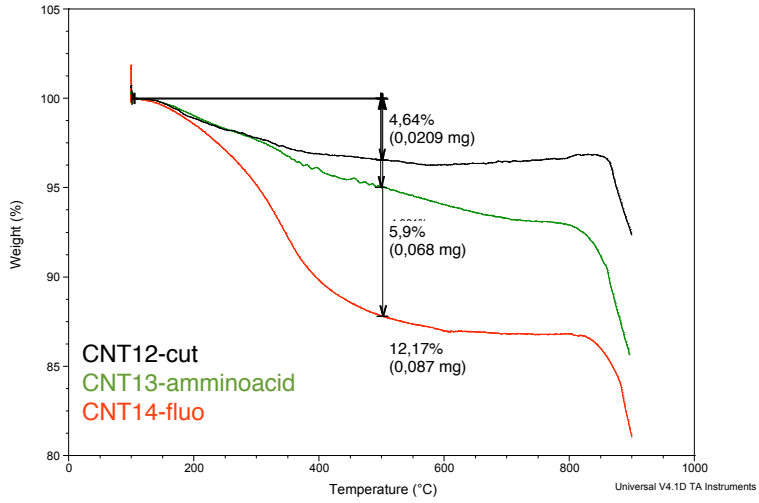

At the temperature of 500°C the CNT12 sample of cut nanotubes registered a weight loss of 4,64%, while the aminoacid-coupled CNT13 sample registered a weight loss of 5,9 % that corresponds to one functionalization every 24 C atoms. The fluoresceinated CNT14 nanotubes registered a weight loss of 12,17% that subtracted to the previous value, corresponds to one fluorescein functionalitiy every 1,79 amino groups (60%). Every value is confirmed by the kaiser test results.

3) Kaiser test

sample	K.T. value
CNT13 (depr.)	298 μmol/g
CNT14	162 μmol/g

4)Fluorescence

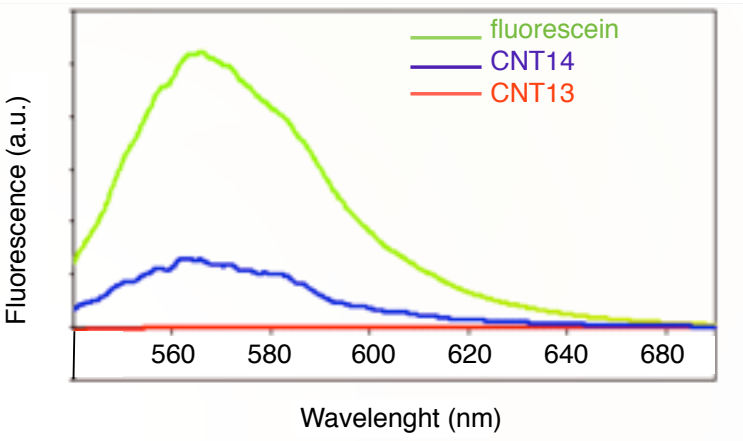

Fluorescence spectra of the samples CNT13 and CNT14,taken in the same conditions of CNT9 and 10, compared to the fluorescence spectra of fluorescein, show that fluorescent CNT14, like in the case of MWCNTs CNT10, have a maximum of fluorescence emission at c.a. 570 nm. This value is typical of fluoresceine. The same peak is absent in the non fluorescent CNT13.

5) TEM

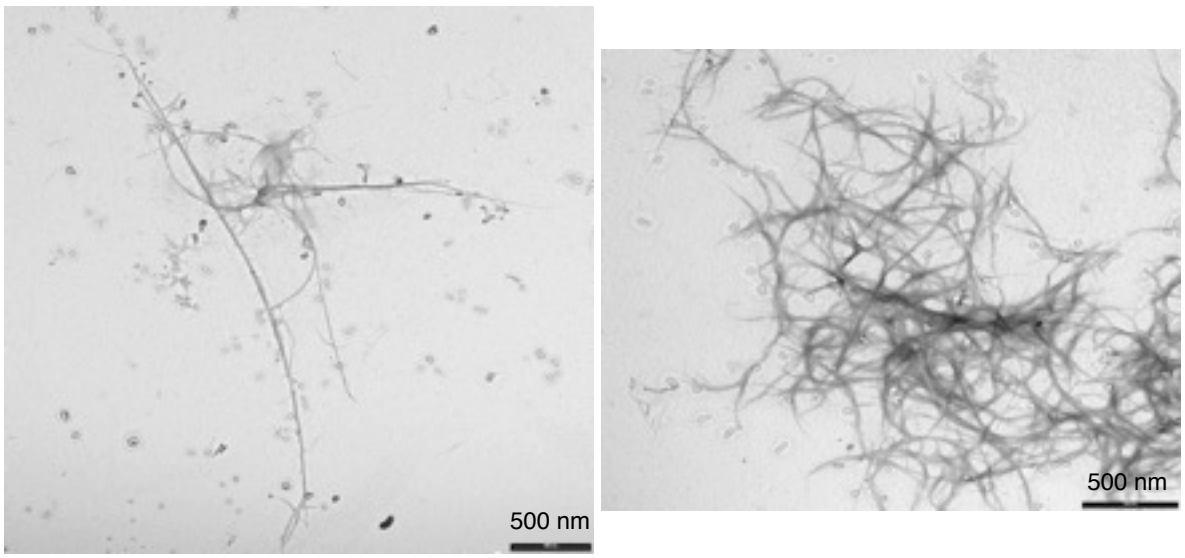

The TEM images of the sampe CNT14, prepared in water, evidenced that the dispersibility of the sampe was good and the sample was very clean. Small bundles were present in the sample. The structure of the nanotubes, that were previously oxidized and cutted, appears shorter even though few unshortened individual tubes are still present in the sample. The photos were taken at 22000 x.

Description of the procedure for Kaiser test

The Kaiser test [8] is a qualitative and quantitative test that verifies the presence or absence of free primary amino groups in a compound, and it can be a useful indication about the completeness of a coupling step. The test is based on the reaction of ninhydrin with primary amines (fig.2), which gives a characteristic dark blue color.

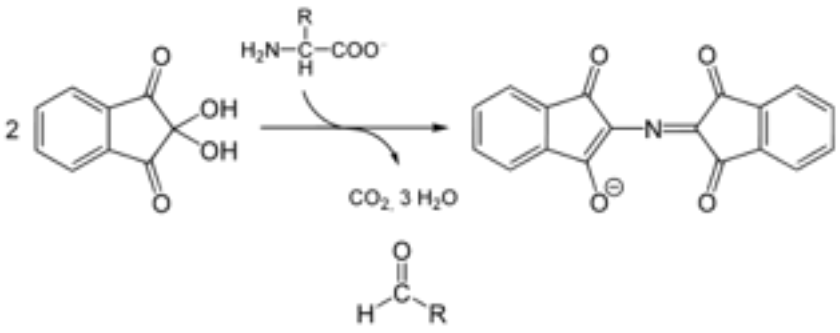

Fig.2: Reaction of ninhydrin with primary amines

Every kaiser test was performed as follows using the following three solutions:

- solution 1: 80 g of phenol in 20 ml of ethanol
- solution 2: 2 ml of KCN 1 mM in H_2O in 98 ml of pyridine
- solution 3: 1 g of ninhydrin in 20 ml of ethanol

1 mg of amino-functionalizad nanotubes is weighted on an analytic balance. 75 µl of solution 1, 100 µl of solution 2 and 75 µl of solution 3 are added in this order. The mixture is heated at 100°C for 7 minutes. At the end is diluted with ethanol 60% in water, up to 5 ml of final volume. Test is positive if the solution turns dark blue/violet. For the quantitative determination of the free amino groups on the surface of nanotubes the absorbance of the solution at 570 nm is recorded, and the absorbance of a blank solution is subtracted to this value. The following relation gives the ratio between the moles of the amine moiety and the weight of the sample:

$$\frac{\mu mol}{g} = \frac{[Abs_{sample} - Abs_{blank}]*dil*10^6}{E*B}$$

where Abs_{sample} is the absorbance of the sampe at 570 nm; Abs_{blank} is the absorbance of the blank solution at 570 nm; dil is the dilution (5 mL); E is the estinction coefficient (15000 $M^{-1}cm^{-1}$) and B is the weight of the CNTs (mg).

Discussion

The SWCNTs and MWCNTs were functionalized with two different synthetic approaches in nanotube chemistry (see fig.1). In both cases it was chosen the highly soluble aminoacid OC3 in order to obtain wires with free amino groups uniformly distributed around their side-walls. This create the substrate for further functionalization of CNT and the possibility to couple the amine functionalities to other molecules. In this case they were coupled with fluorescein isothiocyanate creating a thiourea bond with the fluorescent probe. The amount of NH_2 after the functionalization was monitored by Kaiser test. Knowing the moles of amino groups present in the sample we decided to proceed to the subsequent coupling using a defect of reagent to preserve the solubility of the nanotubes in water, that is due to the amino groups. Fluorescein isothiocyanate is a large, hydrophobic molecules with an aromatic backbone that interacts naturally with the tubes with p-p stacking forces. For this reason the covalent attachment of this molecule to the tubes could not be univocally performed even if the TGA characterization showed weight loss. For this reason is important to proceed carefully in the work-up of the coupling reaction in order to be sure to eliminate every trace of fluorescein not covalently bonded.

After the coupling with fluorescein both SWCNTs CNT14 and MWCNTs CNT10 are very soluble in water and at the high dilution required for the biological tests they do not aggregate. The capacity of the fluorescent-labeled CNTs 10 and 14 to penetrate into the cells was studied by epifluorescence and confocal microscopy.
To verify if nanotubes are able to pass the cell membrane, coltures of hippocampal neurons were incubated for two hours at 37°C with a 2,5 μg/mL solution of CNT10 in water. Subsequently, the cells were carefully rinsed with a buffer, fixed with paraformaldehyde, mounted on a microscope glass with an antifade agent and observed under the microscope.

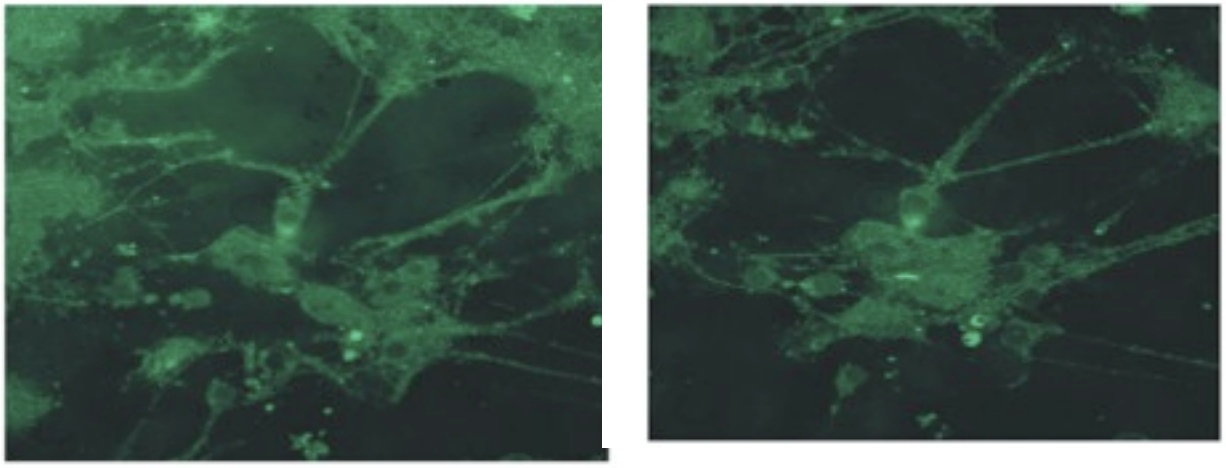

Fig.3: Confocal microscope photos of dissociated coltures of rat hippocampal treated in vitro with fluorescent MWCNT CNT10 for two hours. The images were taken to different focal planes, distant 1,5 μm from each other. Fluorescence registered in the different focal planes reveals that CNT are able to pass the membrane and distribute homogeneusly into the cells, not penetrating into the nucleus.

Fig.3 shows confocal microscopy images of hippocampal neurons incubate with fluorescent MWCNT. We can notice that the fluorescent signal of fluorescein (emission at 545 nm - green fluorescence) is localized inside the cells. The images were taken at different focal planes and this allow us to exclude that nanotubes could only be stuck to the cellular surface, but they effectively penetrated the cell membrane. The internalized nanotubes are distributed in the cytoplasm, but not in the nucleus.

With the aim to go further in the understanding of the nanotube distribution inside the cells, dissociated coltures of hippocampal tissue were incubated with fluorescent nanotubes and then with specific antibodies for the various cellular type: GFAP for glial cells and MAP2 for neurons. In the picture above (fig.4) is possible to see that fluorescent MWCNT are internalized in both cellular type and in both cases they are found in the cellular body and in the terminal processes, but never in the nucleus.

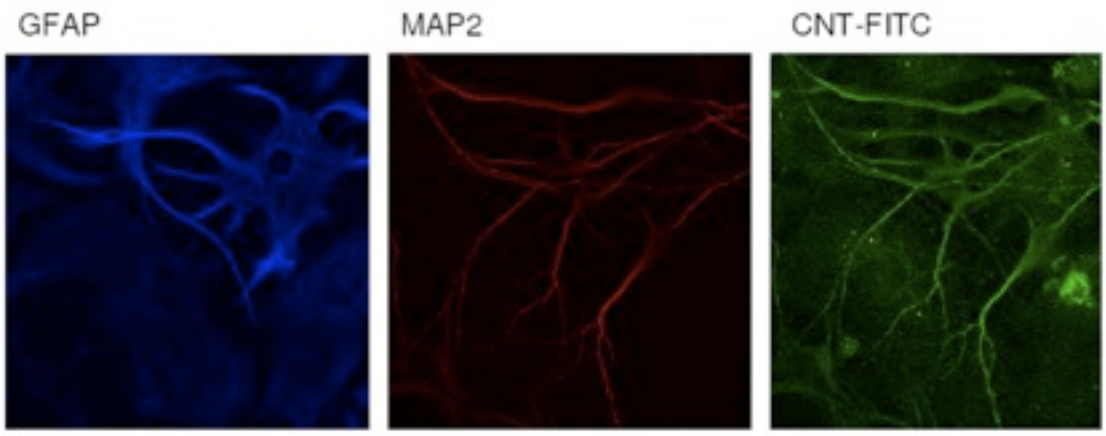

Fig. 4: Confocal microscope photos of dissociated coltures of rat hippocampal treated in vitro with fluorescent MWCNT CNT10 for two hours. Using specifical antibodies for glial cells (GFAP, blue) and for neurons (MAP2, red), it is possible to see that CNT are able to pass the membrane and distribute at the intracellular level in the different cell types.

In conclusion we demonstrated that MWNTs can penetrate the cellular membrane of neural cells and localize homogeneously in the cytoplasm.
To assess if neurons can represent an innovative drug delivery system for the central nervous system more valuable proof are needed. As a future development of this work we could verify by electrophysiological recordings if nanotubes alter in a significant way the membrane properties of neurons and so verify their citotoxicity.
Further studies could be performed to verify if effectively carbon nanotubes are able to pass the BBB and penetrate neural cells *in vivo*.

References

(1) G. A. Silva; *BMC Neuroscience* **2008**, *9*, 1-4.
(2) D. Pantarotto, J. P. Briand, M. Prato, A. Bianco; *Chem. Comm.* **2004**, *1*, 16-17.
(3) D. Pantarotto, R. Singh, D. McCarthy, M. Erhardt, J. P. Briand, M. Prato, K. Kostarelos, A. Bianco; *Angew. Chem. Int. Ed.* **2004**, *43*, 5242-5246.
(4) N. W. Shi Kam, T. C. Jessop, P. A. Wender, H. Dai; *J. Am. Chem. Soc.* **2004**, *126*, 6850-6851.
(5) Y. Lin, S. Taylor, H. Li, K.A. Fernando, L. Qu, W. Wang, L. Gu, B. Zhou and Y.P. Sun; *J. Mater. Chem.* **2004**, *14*, 527–541.
(6) T.M. Allen and P.R. Cullis; *Science* **2004**, *303*, 1818–1822.
(7) K. Kostarelos; *Adv. Colloid Interface Sci.* **2003**, *106*, 147–168.
(8) E. Kaiser, R. L. Colescot, C. D. Bossinge, P. I. Cook; *Anal. Biochem.* **1970**, *34*, 595-598.